Targeting the gut microbiota to investigate the role of secondary bile acids in colorectal cancer

Von der Fakultät für Mathematik, Informatik und Naturwissenschaften der RWTH Aachen University zur Erlangung des akademischen Grades einer Doktorin der Naturwissenschaften genehmigte Dissertation

vorgelegt von

Esther Wortmann, M.Sc.

aus Wattwil, Schweiz

Berichter: Universitätsprofessor Dr. rer. nat. Thomas Clavel
Universitätsprofessor Dr. rer. nat. Mathias Hornef
Universitätsprofessor Dr. rer. nat. Lars Blank

Tag der mündlichen Prüfung: 14.12.2023

Diese Dissertation ist auf den Internetseiten der Universitätsbibliothek online verfügbar.

Abstract

Colorectal cancer (CRC) is one of the most fatal cancer types worldwide. The production of secondary bile acids (SBAs) by gut bacteria has been linked to CRC. However, proof of causality and mechanistic insights *in vivo* are scarce. We used several animal models, microbiota-targeted approaches, and multi-omics techniques to address these points. First, we performed faecal microbiota transplants from $APC^{1311/+}$ pigs to germfree $Apc^{1638N/+}$ mice to investigate if a CRC phenotype can be transferred by the microbiota. The microbiota of mice colonised with stool from the pigs that were fed a diet high in red meat and lard (RL) clustered separately from that of recipient mice that received the control (CTRL) microbiota. Microbiota structure of CTRL recipients was more affected by the cholic acid supplemented diet compared to RL recipients, suggesting that the RL microbiota was more resistant to bile acid (BA) stress. Most lesions were found in the small intestine of $Apc^{1638N/+}$ mice, with no significant differences due to colonisation type. Second, germfree wild type mice fed a high-fat diet were colonised with a synthetic community with or without the bacterial species *Extibacter muris*, which produces SBAs by 7α-dehydroxylation. Carcinogenesis was induced by AOM/DSS treatment. Mice with *E. muris* had significantly more tumours compared to those mice without *E. muris*. Third, to assess host responses to SBAs in the gut, we tested the effects of *E. muris* on the colonic epithelium in gnotobiotic $Apc^{1638N/+}$ mice colonised with the minimal microbial consortium OMM12, using single-cell RNA sequencing. Colonisation with *E. muris* (OMM12+E) was associated with a higher fraction of absorptive enterocytes, characterised by high expression of multiple BA transporters and receptors, and a lower fraction of cell clusters classified as goblet cells. PROGENy analysis revealed upregulation of hypoxia, NFκB, and the tumor suppressor p53 pathway in OMM12+E mice. Finally, we tested whether the BA scavenger colestyramine (COL) could improve disease by reducing the bacterial production of SBAs when added to the diet of $APC^{1311/+}$ pigs. RL diet feeding lead to enhanced cell proliferation and lower goblet cell numbers in the distal colon, and to increased T cell infiltration in the proximal colon. These effects were counteracted by COL supplementation in the diet. COL also counteracted the following effects of the RL diet on the microbiota: lower Shannon effective counts in the caecum, high relative abundance of *Bacillota* and a low fraction of *Bacteroidota*, and increased levels of *Lactobacillus johnsonii* (SOTU1). Additionally, the COL diet also lead to significantly higher levels of conjugated primary BAs and SBAs, especially in the caecum and colon, while levels of individual SBA species were not significantly affected. We conclude that physiological levels of microbially produced SBA, especially DCA, promote early events of tumorigenesis under high fat diet conditions, potentially by affecting epithelial cells types and gene expression. Our results highlight the complex interactions between diet, microbiota, and the host in CRC development and point at the importance of consuming diets that limit microbial SBA production.

Zusammenfassung

Kolorektalkrebs ist eine der tödlichsten Krebsarten weltweit. Die Produktion von sekundären Gallensäuren durch Darmbakterien wurde mit Kolorektalkrebs in Verbindung gesetzt, allerdings wurde noch keine Kausalität bewiesen und *in vivo* Mechanismen sind unklar. Wir nutzten mehrere Tiermodelle, Mikrobiota-orientierte Vorgehen und "multi-omics" Methoden, um diese Punkte zu adressieren. Als Erstes führten wir eine fäkale Mikrobiota-Transplantation (FMT) von $APC^{1311/+}$ Schweinen in keimfreie $Apc^{1638N/+}$ Mäusen durch, um zu untersuchen, ob Kolorektalkrebs durch die Mikrobiota transferiert werden kann. Die Mikrobiota von Mäusen, die mit Stuhl von Schweinen kolonisiert wurden, welche mit einer Diät reich an rotem Fleisch und Schmalz (RL) gefüttert worden waren, unterschied sich von der Mikrobiota von Mäusen, die mit der Kontroll-Mikrobiota (CTRL) kolonisiert wurden. Die Mikrobiota-Struktur von CTRL-Empfängermäusen war dabei stärker beeinflusst durch den Zusatz von Cholsäure in der Diät als RL-Empfängermäuse, was darauf hinweist, dass die RL-Mikrobiota resistenter gegen Gallensäurestress ist. Die meisten Läsionen wurden im Dünndarm der $Apc^{1638N/+}$ Mäuse gefunden, wobei es keine signifikanten Unterschiede zwischen den Kolonisierungsgruppen gab. Als Zweites wurden keimfreie Wildtyp-Mäuse, die eine fettreiche Diät erhielten, mit einem synthetischen Konsortium mit oder ohne der Bakterienspezies *Extibacter muris* kolonisiert, welche sekundäre Gallensäuren durch 7α-Dehydroxylierung produziert. Karzinogenese wurde durch AOM/DSS Behandlung induziert. Mäuse mit *E. muris* entwickelten signifikant mehr Tumore im Vergleich zu Mäusen ohne *E. muris*. Als Drittes testeten wir den Effekt von *E. muris* auf das Dickdarmepithel durch RNA-Sequenzierung einzelner Zellen in Mäusen, die mit dem Minimalkonsortium OMM12 kolonisiert wurden, um die Wirts-Reaktion auf sekundäre Gallensäuren zu evaluieren. Die zusätzliche Kolonisierung mit *E. muris* (OMM12+E) war dabei mit einem höheren Anteil an resorptiven Enterozyten assoziiert, gekennzeichnet durch hohe Expression von Gallensäure-Transportern und -Rezeptoren, und einem geringeren Anteil an Becherzellen. Analyse mit PROGENy zeigte eine Hochregulierung von verschiedenen Signalwegen in OMM12+E Mäusen: Hypoxie, NFκB, und dem Tumorsuppressor-Signalweg p53. Als letztes testeten wir, ob die Zugabe des Gallensäuren-bindenden Colestyramin (COL) zur Diät das Krankheitsbild durch Reduktion bakterieller sekundärer Gallensäureproduktion verbessern könnte. Die RL Diät führte zu höherer Zellproliferation und weniger Becherzellen im distalen Kolon, sowie höherer T Zell-Infiltration im proximalen Kolon. Diese Effekte wurden durch COL-Supplementierung in der Diät verhindert. Des Weiteren wurden folgende Effekte der RL Diät auf die Mikrobiota durch COL verhindert: tiefere Shannon effective Zahlen im Zäkum, hohe relative Abundanz an *Bacillota* und ein tiefer Anteil an *Bacteroidota*, sowie erhöhte Abundanz von *Lactobacillus johnsonii* (SOTU1). Die COL Diät führte auch zu signifikant höheren Mengen an konjugierten primären und sekundären Gallensäuren, besonders im Zäkum und

Kolon, wobei die Mengen von individuellen Gallensäuren nicht signifikant beeinflusst wurden. Wir schließen daraus, dass physiologische Mengen an mikrobiell produzierten sekundären Gallensäuren, besonders DCA, bei einer Diät reich an Fett frühe Ereignisse in der Tumorgenese fördern. Dies geschieht möglicherweise durch die Beeinflussung von Epithel-Zelltypen sowie deren Genexpression. Unsere Ergebnisse betonen die komplexe Interaktion zwischen Diät, Mikrobiota und Wirt in der Entstehung von Kolorektalkrebs und zeigen die Bedeutung einer Diät auf, welche die mikrobielle sekundäre Gallensäureproduktion begrenzt.

Acknowledgments

I would like to acknowledge that this PhD project was funded by the German Research Foundation (DFG): project no. 395357507, SFB1371. It was very inspiring to be part of such a large research consortium.

I would like express my sincere gratitude to my supervisor Tom Clavel for the outstanding guidance and support throughout this project. I am very grateful to have had so many great current and former colleagues within AG Clavel: Afrizal, Alina Viehof, Amy Coates, Andrea Martinez Aguirre, Atscharah Panyot, Charlie Pauvert, David Wylensek, Nicole Treichel, Ntana Kousetzi, Maja Magel, Marko Baloh, Johanna Bosch, Johannes Masson, Selina Nüchtern, Soheila Razavi, Susan Jennings, Theresa Streidl, and Tom Hitch. A special thank you goes to David, Susan, Atscharah and Alina for their invaluable support and help for the mouse and pig experiments, sometimes also very early in the mornings, late in the evenings, or on weekends. Thank you also to other people of the Institute of Medical Microbiology: Aline Dupont and Johannes Schöneich, for their support for the scRNA-Seq experiment.

Furthermore, I would like to thank all external collaborators: Annika Osswald, Soeren Ocvirk, Krzysztof Flisikowski, Wei Liang, Tatiana Flisikowska, Angelika Schnieke, Viola and Steffen Loebnitz, Anika Sander, Thomas Winogrodzky, Gerhard Liebisch, Silke Matysik, Colin Volet, Michael Gigl, Karin Kleigrewe.

Last but not least, I want to thank my family, friends, and boyfriend for their support outside of the lab and office.

Contributions

All contributions by collaborators are summarised in Table 1 and indicated again in the respective method sections. Part of this work was supported by the Genomics and FACS Core facilities of the Interdisciplinary Center for Clinical Research (IZKF) Aachen within the Faculty of Medicine at RWTH Aachen University.

Table 1: Contributions for each chapter.

Contributor	Type of contribution	Contribution	Chapter
David Wylsensek	Provided faecal microbiota stocks for colonisation of germfree mice. Assisted with sampling of *Apc*$^{1638N/+}$ mice and *APC*$^{1311/+}$ pigs.	50%	3.1 and 3.4
Atscharah Panyot	Helped for gavaging and sampling gnotobiotic mice	10%	3.1 and 3.3
Alina Viehof	Helped for gavaging and sampling gnotobiotic mice	10%	3.1 and 3.3
Susan Jennings	Breeding of germfree *Apc*$^{1638N/+}$ mice	25%	3.1
Nicole Treichel	16S rRNA gene amplicon sequencing of faecal samples and gut content	20%	3.1, 3.2, 3.3, 3.4
Ntana Kousetzi	DNA extraction, 16S rRNA gene amplicon sequencing of faecal samples and gut content	20%	3.1, 3.2, 3.3, 3.4
Klaus-Peter Janssen	Histological analysis of intestinal lesions	20%	3.1
Sören Ocvirk	Provided experimental facilities, mice, and sampled AOM/DSS mice; performed FACS analysis	90%	3.2
Annika Osswald	Colonised mice, applied AOM injections, maintained mice during the experiment, sampled mice, performed FACS analysis	90%	3.2
Colin Volet	Sample preparation and bile acid measurements	30%	3.2 and 3.3
Aline Dupont	Provided expertise and help for epithelial cell isolation and library preparation for scRNA-Seq experiment	10%	3.3
Johannes Schöneich	Prepared sequencing data, merged samples, provided quality control, pathway analysis; shared expert knowledge for data analysis	40%	3.3
Krzysztof Flisikowski	Planned experiment, provided pigs, carried out colonoscopies, analysis of tumour numbers	50%	3.4
Wei Liang	Sampling, immunostaining of tissue sections	30%	3.4
Karin Kleigrewe	Bile acid measurements	10%	3.4
Michael Gigl	Bile acid measurements	10%	3.4
Silke Matysik	Sterol/stanol measurements	20%	3.4
Gerhard Liebisch	Fatty acid measurements	20%	3.4

Eidesstattliche Erklärung

Ich, Esther Wortmann, erkläre hiermit, daß diese Dissertation und die darin dargelegten Inhalte die eigenen sind und selbstständig, als Ergebnis der eigenen originären Forschung, genereiert wurden.

Hiermit erkläre ich an Eides statt

1. Diese Arbeit wurde vollständig oder größtenteils in der Phase als Doktorand dieser Fakultät und Universität angefertigt;
2. Sofern irgendein Bestandteil dieser Dissertation zuvor für einen akademischen Abschluss oder eine andere Qualifikation an dieser oder einer anderen Institution verwendet wurde, wurde dies klar angezeigt;
3. Wenn immer andere eigene- oder Veröffentlichungen Dritter herangezogen wurden, wurden diese klar benannt;
4. Wenn aus anderen eigenen- oder Veröffentlichungen Dritter zitiert wurde, wurde stets die Quelle hierfür angegeben. Diese Dissertation ist vollständig meine eigene Arbeit, mit der Ausnahme solcher Zitate;
5. Alle wesentlichen Quellen von Unterstützung wurden benannt;
6. Wenn immer ein Teil dieser Dissertation auf der Zusammenarbeit mit anderen basiert, wurde von mir klar gekennzeichnet, was von anderen und was von mir selbst erarbeitet wurde;
7. Ein Teil oder Teile dieser Arbeit wurden zuvor veröffentlicht und zwar in:

Wortmann, E., Osswald, A., Wylensek, D., Liang, W., Treichel, N., Schumacher, F., ... & Clavel, T. Secondary bile acid production by gut bacteria promotes Western diet-associated colorectal cancer. *bioRxiv*, 2023.

Aachen, January 29, 2024 _____

(Esther Wortmann)

List of Figures

List of Tables

Glossary

7αDH	7α-dehydroxylating
AB-PAS	Alcian blue-periodic acid Schiff (staining)
Acaa1b	acetyl-Coenzyme A acyltransferase 1
AKT	also known as PKB, protein kinase B
AOM	azoxymethane
apc	adenomatous polyposis coli
Aqp4	aquaporin-4
ASBT	apical sodium dependent bile acid transporter
ATF6	activating transcription factor 6
BA	bile acid (a comprehensive list of BAs is given in Table 1.3)
BACOMI	bile acid converting microbiota
bai	bile acid inducible
BCFA	branched chain fatty acid
BFT	*Bacteroides fragilis* toxin
BSH	bile salt hydrolase
CD	control diet (mouse diet)
CIMP	Cpg island methylation pathway
Clca4a	chloride channel accessory 4a
CMS	consensus molecular subtype
COL	colestyramine (pig diet)
CRC	colorectal cancer
CTRL	control (pig diet)
DC	dendritic cell
DCA	deoxycholic acid
DE	differentially expressed
DNA	deoxyribonucleic acid
DSI	distal small intestine
DSS	dextrane sodium sulfate
EPEC	enteropathogenic *E. coli*
ERK	extracellular signal-related kinase
ETBF	enterotoxigenic *Bacteroides fragilis*
FA	fatty acid
Fabp2	fatty acid-binding protein 2
FACS	fluorescence-activated cell sorting
FAME	fatty acid methyl ester
FAP	familial adenomatous polyposis coli
Fcgbp	Fc Gamma Binding Protein

FGF	fibroblast growth factor
fl	floxed
FMT	faecal microbiota transplant
FOB	faecal occult blood test
FOXP3	forkhead box P3
FXR	farnesoid x receptor
Gal3st2c	galactose-3-O-sulfotransferase 2C
GC-MS	gas chromatography coupled to mass spectrometry
GLP-1	glucagon-like peptide-1
GPBAR1	G protein-coupled bile acid receptor 1 (synonym for TGR5)
HE	hematoxylin and eosin (staining)
Hopx	homeodomain-only protein homeobox
HSDH	hydroxysteroid dehydrogenase
IBABP	ileal bile acid binding protein
IBD	irritable bowel disease
IEC	intestinal epithelial cell
IgG	immunoglobulin G
ILN	iliac lymph node
iNOS	inducible nitric oxide synthase
ISTD	internal standard
JAK-STAT	Janus kinase - signal transducer and activator of transcription
KEGG	Kyoto encyclopedia of genes and genomes
Kras	Kirsten rat sarcoma viral oncogene homologue
Lgr5	leucine-rich repeat-containing G-protein coupled receptor 5
LOH	loss of heterozygocity
MAPK	mitogen-activated protein kinase
MDS	multidimensional scaling
MLN	mesenteric lymph node
MMR	mismatch repair
MP	multiple polypoid adenomas with low-grade dysplasia
MRP	multidrug resistance-associated protein
MSI	microsatelite instability
mTor	mechanistic target of rapamycin
MUFA	mono-unsaturated fatty acid
NMDS	nonmetric multidimensional scaling
Olfm4	olfactomedin 4
OMM	oligo mouse microbiota
OST	organic solute transporter
OTU	operational taxonomic unit
PAR	periampullary region
PBA	primary bile acid
PBS	phosphate buffered saline
PC/LPC	phosphatidylcholine/lysophosphatidylcholine
PCR	polymerase chain reaction
Pdk4	pyruvate dehydrogenase kinase 4
Pi3K	phosphoinositide 3-kinase

PROGENy	pathway responsive genes (analysis)
PROM1	prominin 1
PSI	proximal small intestine
PUFA	poly-unsaturated fatty acid
PXR	pregnane x receptor
RBC	red blood cells
Reg4	regenerating family member 4
RL	red meat and lard (pig diet)
RNA	ribonucleic acid
RORγt	retinoid-related orphan receptor-γt
ROS	reactive oxygen species
RT	room temperature
SAFA	saturated fatty acid
SBA	secondary bile acid
SCFA	short chain fatty acid
scRNA-Seq	single cell RNA sequencing
SHP	small heterodimer protein
sIgA	secretory immunoglobulin A
SNP	single nucleotide polymorphism
SOTU	sub-OTU
Sox4	SRY-box transcription factor 4
Sox9	SRY-box transcription factor 9
SPF	specific pathogen free
Sprr2a3	small proline-rich protein 2A3
SRC	steroid receptor coactivator
TAM	tumour-associated macrophage
Tff3	trefoil factor 3
tg	transgenic
TGFβ	transforming growth factor β
TGR5	Takeda G-protein-coupled receptor 5
TH	T helper cell
TNF	tumor necrosis factor
TRAIL	TNF-related apoptosis-inducing ligand
Treg	regulatory T cell
UC	ulcerative colitis
VDR	vitamin D receptor
YAP	yes-associated protein

Table of contents

CHAPTER 1

Introduction

Colorectal cancer (CRC) is one of the most fatal cancer types, accounting for 9.4% of all cancer deaths worldwide (Sung et al., 2021). Incidence is high in countries with a high Human Development Index, and it is predicted to further increase until 2040 (Sung et al., 2021). This makes CRC a relevant public health problem, and research about its causes and cures is still ongoing.

1.1 Colorectal cancer

The majority of CRC is associated with sporadic factors (Keum and Giovannucci, 2019; Jasperson et al., 2010). While 25% of CRC cases are associated with family history, only a small proportion (3-5%) of CRC is known to be caused by inherited mutations (Peters et al., 2015; Keum and Giovannucci, 2019), e.g. in the tumour suppressor gene *adenomatous polyposis coli* (*APC*), which predisposes for familial adenomatous polyposis (FAP), or in mismatch repair (MMR) genes (Lynch syndrome) (Peters et al., 2015). A small proportion (<2% of all CRC) is associated with inflammation (Keum and Giovannucci, 2019). The development of CRC results from a sequence of several genetic and epigenetic events as well as a dysregulated immune response, eventually leading to aberrant cell growth and tissue infiltration (Janney et al., 2020). These events happen over the course of several decades, and can be divided into different stages, as depicted in Figure 1.1 **a**: tumour initiation, tumour progression, and carcinoma with possible metastasis formation (Carethers and Jung, 2015). Based on the genetic mutations at different stages of progression, CRC has been categorised into different molecular pathways and subtypes.

The main molecular pathways comprise chromosomal instability, CpG island methylation, and microsatellite instability (MSI) (Mundade et al., 2014; Schmitt and Greten, 2021). The chromosomal instability pathway (CIMP), also called the classic pathway, involves aneuploidy (abnormal number of chromosomes) and loss of heterozygosity (LOH) at loci of tumour suppressor genes (Figure 1.1 **b**). Mutations cause loss of function of tumour suppressor genes like *APC*, *SMAD4*, or *TP53*, or activate proto-oncogenes like *KRAS* and *PIK3CA* (Schmitt and Greten, 2021). Tumours developing through the CIMP can be divided into $CIMP^{low}$ tumours with *KRAS* mutations and $CIMP^{high}$ tumours, with activating mutations of *BRAF* and methylation of *MLH1* (Schmitt and Greten, 2021; Shen et al., 2007). The MSI pathway also starts with inactivation of the *APC* gene, in combination with failure of MMR genes, e.g. *MLH1*, mostly by hypermethylation of the respective promoters (Mundade

et al., 2014). Further, apoptosis-inducing genes like *BAX* fail (Figure 1.1 **b**), eventually leading to carcinoma formation (Mundade et al., 2014; Alzahrani et al., 2021).

Apart from these three molecular pathways of sporadic CRC, the colitis-associated pathway (>2% of all CRC) is mainly associated with patients suffering from inflammatory bowel disease (IBD), especially ulcerative colitis (UC) (Keum and Giovannucci, 2019; Itzkowitz and Yio, 2004). Colitis-associated CRC does not develop the typical visible lesions found in sporadic CRC, but rather develops with a flat morphology through neoplastic transformations in large areas of inflamed mucosa (Shah and Itzkowitz, 2022). Therefore, more elaborate detection methods like chromoendoscopy or high-definition endoscopy are used (Buchner and Lichtenstein, 2016). The sequence of genetic mutations for this type of cancer is different from sporadic cancer, with *TP53* mutations occurring as an early event (Figure 1.1 **b**), whereas *APC* mutations are only found at later stages at the transition to carcinoma (Shah and Itzkowitz, 2022).

Besides the different molecular pathways, tumours have also been categorised into four consensus molecular subtypes (CMS1-4), which, however, do not completely match with the different pathways for sporadic CRC (Guinney et al., 2015; Schmitt and Greten, 2021) (Figure 1.1 **b**). Knowing the molecular characteristics of cancer development and different cancer stages, however, provides useful opportunities for the development of CRC treatment (Dienstmann et al., 2017). Tumours of CMS1 are characterised by MSI, CIMP, hypermethylation, *BRAF* mutation and immune cell infiltration and activation (Guinney et al., 2015). CMS1 patients show infiltration of (T_H1) helper cells, natural killer cells, and cytotoxic T cells, in specific activated CD8+ cells (Becht et al., 2016; Braumüller et al., 2022). The other subtypes (CMS2-4) are characterised by higher chromosomal instability. The CMS2 (canonic subtype) is characterised by higher copy numbers of oncogenes (and therefore Wnt and Myc activation) and less copy numbers of tumour suppressor genes. *KRAS* mutations and metabolic deregulation are characteristic for CMS3, also called metabolic subtype (Guinney et al., 2015). Miller et al. (2021a) found higher expression of goblet cell marker genes in CMS3 tumours in CRC. Lastly, CMS4, the mesenchymal subtype, has high somatic copy number alterations, transforming growth factor-β (TGF-β) activation, angiogenesis, and high levels of infiltrating cytotoxic T cells, macrophages, and stromal cells (Guinney et al., 2015; Becht et al., 2016). The classification of CRC into different cancer molecular subtypes is not exclusive, with around 14% of the analysed tumours being mixed or intermediate tumours as well as of non-consensus type (Guinney et al., 2015). Joanito et al. (2022) refined the CMS classification based on a combination of intrinsic epithelial subtype, MSI status, and fibrosis, resulting in 5 different subtypes. This emphasises that CRC research is still ongoing and even existing consensus are challenged. Having appropriate experimental models is important to study CRC development as well as possible treatment options. Whilst *in vitro* experiments (e.g. using cell cultures or organoids) are suitable to test specific effects and mechanisms and are thus an important tool in CRC research, studying long term effects of potential risk factors, spatial distribution of tumours, or metastasis formation require living organisms. However, the complexity and heterogeneity of disease and the long time for CRC to develop still pose a difficulty for studies in humans, but also in animals.

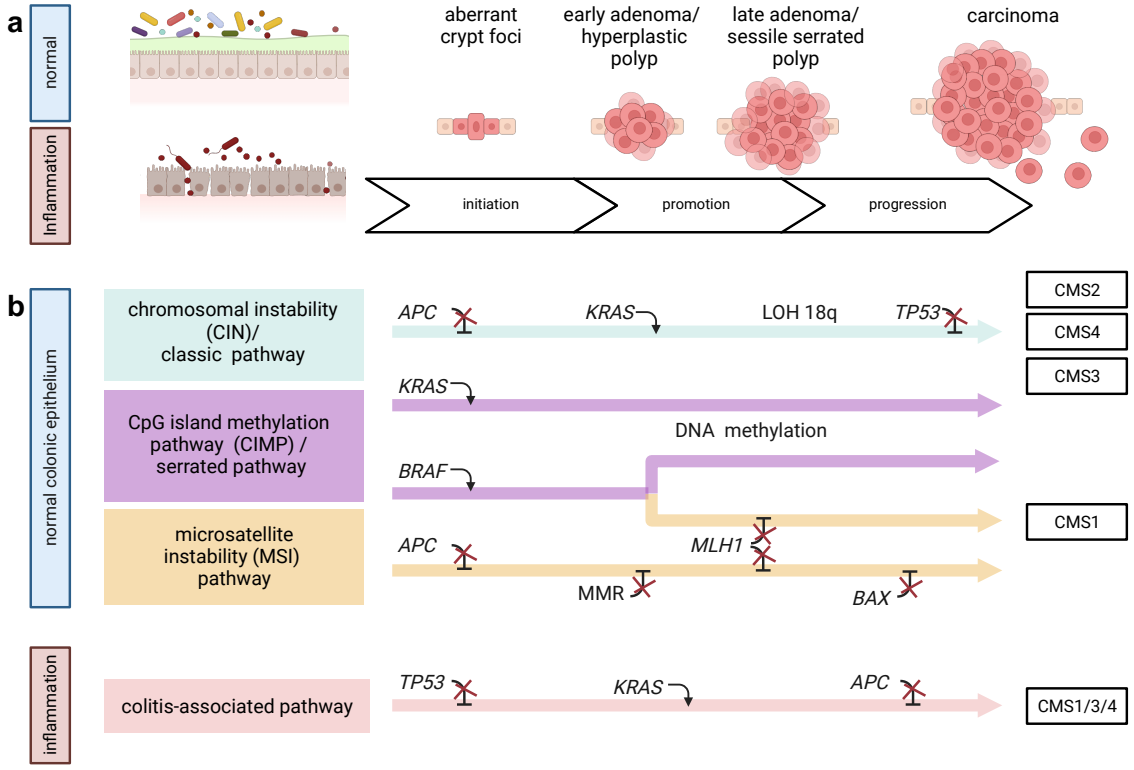

Figure 1.1: Development of CRC over time. **a** Different stages of CRC: tumour initiation, tumour progression, and carcinoma with possible metastasis formation. **b** Most CRC cases develop via the classic pathway, which is initiated by loss of function mutation of the *APC* gene and followed by activating mutations of proto-oncogenes, LOH of chromosome 18 (LOH 18q) and mutation of tumour suppressor *TP53*. The serrated pathway develops either via *KRAS* mutation and aberrant methylation, or via *BRAF* mutation, which can also involve MSI. The MSI involves fail of MMR genes, e.g. *MLH1*, as well as inactivation of the tumour suppressor *BAX*. The inflammatory pathway is initiated by *TP53* mutation, followed by mutations in *KRAS* and *APC*. This figures shows only a fraction of genetic and epigenetic events that can happen during CRC development. Categories of molecular pathways and CMS do not completely match, as depicted by the CMS categories on the right hand side. Failing of tumour suppressors is indicated by red crosses. This figure was created with BioRender.com, based on Schmitt and Greten (2021); Alzahrani et al. (2021); Shah and Itzkowitz (2022); Mundade et al. (2014); Carethers and Jung (2015).

The use of animal models in CRC research started with rats, but with the availability of genetic information and genetically engineered animals, mice have become the major model organism (De Robertis et al., 2011). Several approaches have been used to generate models for CRC (Table 1.1). Chemically induced models can be used to study the effect of dietary carcinogens like heterocyclic aromatic amines or also colitis-associated cancer and application of the chemicals can be by feeding, oral gavage, or injection (Bürtin et al., 2020; De Robertis et al., 2011). Nakagama et al. (2002) for example found that PhIP (a heterocyclic aromatic amine) treatement induced colon cancer in rats. A commonly used chemically induced CRC mouse model to study colitis associated cancer is the combined application of the carcinogenic azoxymethane (AOM) as a tumour inducer and proinflammatory dextran sulfate sodium (DSS) in drinking water as a tumour promoter (De Robertis et al., 2011). There are different protocols for AOM/DSS treatment, and susceptibility to AOM/DSS treatment is differ-

ent between mouse strains, which affects the observed phenotypes (Suzuki et al., 2005; De Robertis et al., 2011). An advantage of this model is that it reflects the CRC pattern observed in humans, with a high tumour frequency in the distal colon (De Robertis et al., 2011). CRC can also be introduced by transplanting cancer grafts, tumour cells, organoids or tumour tissue into animals (Bürtin et al., 2020). This transplant can even happen from patients into mice (xenogeneic graft) (Bürtin et al., 2020). Intrarectal injection of tumours was found to lead to colonic primary tumour growth with a low mortality and development of liver and lung metastases in mice (Hite et al., 2018).

A large number of mouse models has been generated with modifications or mutations in the *Apc* gene (Smits et al., 1997). Inherited mutations of this gene are the cause of FAP (Peters et al., 2015) and also sporadic cancer development can be initiated by mutations in this gene (Dow et al., 2015). One of the first but still widely used mouse models with a mutation in the *Apc* gene is the $Apc^{Min/+}$ mouse model. These mice, however, show tumour formation primarily in the small intestine and also develop lesions in other tissues, e.g. desmoid tumours or mammary tumours (Moser et al., 1995). $Apc^{Min/+}$ mice show a strong pathology, as they develop more than 50 intestinal adenomas and have a short lifespan, rarely surviving longer than 120 days (Moser et al., 1990). The $Apc^{1638N/+}$ mouse model was developed by introducing a neomycin cassette at codon 1638, leading to a chain-termination mutation (Fodde et al., 1994). While Apc^{1638} homozygotic animals do not survive the embryonic stage, around 70% of Apc^{1638} heterozygotic mice survive up to 1 year (Fodde et al., 1994). This model also develops adenomas and adeno-carcinomas mainly in the small intestine, but also in the stomach, and forms liver metastases (Smits et al., 1997; Fodde and Smits, 2001; Fodde et al., 1994). Next to mouse models, also a pig model with a mutation in the *APC* gene was created. As opposed to *Apc* mutant mice, which mainly develop tumours in the small intestine, the $APC^{1311/+}$ pig model develops low- and high-grade dysplastic adenomas in the large intestine (Flisikowska et al., 2012). Pig models are very useful in translational research, since they are similar to humans in terms of metabolism and intestinal physiology, and they are omnivores (Gonzalez et al., 2015).

Table 1.1: Overview of a selection of different CRC animal models.

Animal	Model for	Example	Main tumour site	Reference
rat	dietary carcinogen	PhIP	colon	Nakagama et al. (2002)
mouse	colitis-associated cancer	AOM/DSS treatment	distal colon	De Robertis et al. (2011)
mouse	FAP	germline mutation: $Apc^{Min/+}$	small intestine	Moser et al. (1995)
mouse	FAP	germline mutation: $Apc^{1638N/+}$	small intestine	Smits et al. (1997)
mouse	colitis-associated & sporadic CRC	somatic mutation: nATF6 Vil-$Cre^{ERT2\ Tg}$	colon	Coleman et al. (2018)
mouse	CRC	xenograft transplant	rectum	Bürtin et al. (2020)
pig	FAP	germline mutation: $Apc^{1311/+}$	colon	Flisikowska et al. (2012)

The *Cre-loxP* system has been developed for tissue-specific mutations of genes (Lakso et al., 1992). The use of transgenic (tg) mice with a tamoxifen-dependent Cre recombinase under the control of the villin promoter (vil-Cre-ER^{T2}) even allows a timely control of somatic recombinations in epithelial cells (El Marjou et al., 2004). This method has been used to generate a large variety of different mouse models (Bürtin et al., 2020). For example, Coleman et al. (2018) found that tamoxifen-induced intestinal epithelial cell (IEC) specific expression of activating transcription factor 6 (ATF6) lead to

100% tumour incidence in nATF6 Vil-Cre$^{ERT2\ tg}$ mice 16 weeks after activation. Interestingly, microbiota was essential for tumour development in transgenic homozygous nATF6$^{IEC\ tg/tg}$ mice (Coleman et al., 2018). Furthermore, tg/tg mice showed a shift in microbiota structure (β-diversity) as well as lower Shannon effective counts compared to heterozygous mice (one transgene and one wild type gene: tg/wt) or mice without transgene expression (floxed/floxed: fl/fl) (Coleman et al., 2018). Colonising germfree mice with the dysbiotic microbiota from specific pathogen free (SPF) tg/tg mice lead to reduced survival and higher tumour incidence compared to mice colonised with microbiota from fl/fl SPF donor mice (Coleman et al., 2018). These findings point towards the importance of the microbiome in CRC, also in humans, as addressed in the following sections.

1.2 The gut microbiome

The human body is colonised by approximately the same number of microbial cells as own eukaryotic cells and the large intestine is most densely populated, harboring around $4x10^{13}$ cells (Sender et al., 2016). Since the early 2000s, research about gut microbes has expanded substantially, with over 13'500 publications in 2022 on PubMed (research string: "gut microbiome" OR "intestinal microbiome" OR "gut microbiota" OR "intestinal microbiota" OR "intestinal flora" OR "gut flora"). With increasing knowledge, the research community has deviated from the formerly used term "gut flora" to more elaborated definitions. The term microbiota is used for all populations of microorganisms in a defined habitat, e.g. the gut, including bacteria, phages, archaea, fungi (Marchesi, 2011). Metagenome describes the compilation of genomes and genes from the microbiota members in that habitat, whilst the term microbiome is used to describe the entire ecosystem, including both the microorganisms (microbiota) and their genomes (metagenome), as well as the surrounding environmental factors (Marchesi, 2011).

The host (habitat) and its microbes are tightly interconnected. The term holobiont has been used to describe the complex and interactive network between a host (e.g. human subject) and the microbes that colonise it (Zilber-Rosenberg and Rosenberg, 2008; Gordon et al., 2013). Intrinsic (host) factors that shape the microbial composition in different areas of the gastrointestinal tract are e.g. pH, oxygen, mucus composition, antimicrobial peptides, and secretory Immunoglobulin A (sIgA) (Simrén et al., 2013). The different regions of the intestine provide a variety of niches for microbes. The colon is the most anaerobic region, providing an optimal environment for strict anaerobic bacteria (Walter and Ley, 2011; Simrén et al., 2013). Even though the host largely profits from the presence of a microbiota, e.g. short-chain fatty acids (SCFA) are important nutrients for intestinal epithelial cells, it also keeps bacteria at distance via e.g. sIgA or antimicrobial peptide production (Macpherson and Uhr, 2004; Sekirov et al., 2010). Also the residing gut microbiota prevents pathogen invasion by saturating functional niches and by producing antimicrobial substances (O'Shea et al., 2012).

Gut microbiota composition is, besides the aforementioned intrinsic factors, greatly affected by environmental factors from birth on, starting with the mode of delivery due to the transmission of microbes from the mother to the infant (Dominguez-Bello et al., 2010). Approximately half of the shared bac-

terial species between mother and infants were found to be the same strains (Valles-Colomer et al., 2023). With age and the influence of additional environmental cues, the gut microbiota gains complexity and richness reaches a maximum, but its composition and functions continue to evolve (Martino et al., 2022; Sekirov et al., 2010). In fact, it has been found that environmental factors have much more impact on the human gut microbiota composition than genetic factors (Rothschild et al., 2018). Such exogenous factors could be exposure to xenobiotics like antibiotics, infections, circadian rhythm or diet (Lynch and Pedersen, 2016; Asnicar et al., 2021).

1.3 Microbiome signatures in diseases

Microbiota composition is highly variable between individuals and depends on many different factors. However, there is a conserved group of microbes and genes that are shared between (human) individuals, referred to as the core microbiome (Tremaroli and Bäckhed, 2012; Malard et al., 2021). The symbiosis between host and microbes is well balanced in a healthy state, but once this balance is disrupted due to multiple genetic and environmental factors, the gut microbiota can contribute to the development of diseases (Sekirov et al., 2010). Gut microbiota features can be positively or negatively associated with disease. For example, Arrieta et al. (2016) found that four bacterial genera (*Faecalibacterium*, *Lachnospira*, *Veillonella*, and *Rothia*) play a causal role in the prevention of childhood asthma. IBD has been associated with low species diversity (Manichanh et al., 2012), but increased relative (rel.) abundance of the phyla *Bacillota* (formerly Firmicutes), *Pseudomonadota* (formerly Proteobacteria) and the genera *Fusobacterium* and *Streptococcus* as well as the species *Escherichia coli*(Metwaly et al., 2022). Patients with IBD have also an increased risk for colitis-associated CRC (Shah and Itzkowitz, 2022).

Metagenomic studies have identified several microbial signatures for CRC across different human cohorts (Table 1.2): *Fusobacterium nucleatum* (Zeller et al., 2014; Thomas et al., 2019; Lee et al., 2023; Yachida et al., 2019; Yu et al., 2017; Dai et al., 2018), *Peptostreptococcus stomatis* (Zeller et al., 2014; Yachida et al., 2019; Thomas et al., 2019; Yu et al., 2017), *Parvimonas micra* (Thomas et al., 2019; Yachida et al., 2019; Yu et al., 2017; Dai et al., 2018), *Porphyromonas asaccharolytica* (Zeller et al., 2014; Thomas et al., 2019; Dai et al., 2018), *Solobacterium moorei* (Thomas et al., 2019; Yu et al., 2017), *Streptococcus gallolyticus* (Lee et al., 2023; Thomas et al., 2019), and *Bilophila wadsworthia* (Ai et al., 2019; Yachida et al., 2019; Lee et al., 2023). Besides associations based on metagenomic studies, some causal relationships between specific bacterial species, their metabolites, and CRC have been identified (Table 1.2). Colibactin is produced by *pks*$^+$ *E. coli* and was found to induce distinct mutations in human organoids (Pleguezuelos-Manzano et al., 2020). *F. nucleatum*, which is normally a coloniser of the oral cavity but can engraft in the distal gut under specific conditions that remain to be determined, produces *F. nucleatum* adhesin A (FadA) that can bind to E-cadherin in colonic epithelial cells and activate the β-catenin pathway (Rubinstein et al., 2013). Enterotoxigenic *Bacteroides fragilis* (ETBF) produces the *B. fragilis* toxin (BFT), which cleaves E-cadherin and leads to the release of β-catenin (Wu et al., 1998, 2003). Wirbel et al. (2019) searched for these microbial fea-

tures and found that the *pks* gene cluster, *FadA*, and the the bile acid (BA) inducible (*bai*) gene cluster were also significantly enriched in CRC metagenomes, whereas the *bft* gene was not significantly different between CRC and control metagenomes. In line with this, *B. fragilis* was only enriched in CRC in 2 out of 4 cohorts analysed by Dai et al. (2018), while Wirbel et al. (2019) found enrichment of *Clostridium hylemonae* and *Clostridium scindens*, which contributed to the enrichment of the *bai* operon. Zeller et al. (2014) identified a collective of 22 bacterial species associated with CRC, among which they also found *C. hylemonae* and *C. scindens*.

Table 1.2: Bacterial species and characteristics found in CRC.

Species	**Enriched in CRC faecal metagenomes**	**Metabolite/ toxin**	**References**
Fusobacterium nucleatum	species, *fadA*	FadA	Zeller et al. (2014); Yu et al. (2017); Dai et al. (2018); Yachida et al. (2019); Thomas et al. (2019); Lee et al. (2023)
Peptostreptococcus stomatis	species	NA	Zeller et al. (2014); Yu et al. (2017); Yachida et al. (2019); Thomas et al. (2019)
Parvimonas micra	species	NA	Yu et al. (2017); Dai et al. (2018); Yachida et al. (2019); Thomas et al. (2019)
Porphyromonas asaccharolytica	species	NA	Zeller et al. (2014); Dai et al. (2018); Thomas et al. (2019)
Solobacterium moorei	species	NA	Thomas et al. (2019); Yu et al. (2017)
Streptococcus gallolyticus	species	NA	Lee et al. (2023); Thomas et al. (2019)
Bilophila wadsworthia	species	H_2S	Attene-Ramos et al. (2006); Ai et al. (2019); Yachida et al. (2019); Lee et al. (2023)
pks+ *Escherichia coli*	*pks*	colibactin	Pleguezuelos-Manzano et al. (2020); Wirbel et al. (2019)
Enterotoxigenic *Bacteroides fragilis* (ETBF)	species, *bft*	BFT	Wu et al. (1998, 2003); Dai et al. (2018)
Clostridium hylemonae *Clostridium scindens*	species and *bai* operon	DCA	Wirbel et al. (2019); Kawano et al. (2010); Wu et al. (2021)

Besides microbes that have been directly associated with cancer, other microbes or their metabolites may promote cancer progression indirectly as "complicits" by having immunomodulatory functions, or causing inflammation or dysfunctional immunosurveillance (Sepich-Poore et al., 2021). One example is p53, a tumour suppressor that is often mutated in human cancer (Freed-Pastor and Prives, 2012). Kadosh et al. (2020) showed that that a mutant p53 was tumour-suppressive in the proximal intestine and in the absence of microbes in organoids, while it was tumour-promoting in the colon of in Casein kinase α 1 (*Csnk1a1*)-deficient and $Apc^{Min/+}$ mice. Interestingly, a single gut microbial metabolite - gallic acid, produced by *Lactiplantibacillus plantarum* (formerly *Lactobacillus plantarum*) and *Bacillus subtilis* - was shown to be sufficient to induce these oncogenic effects (Kadosh et al., 2020).

The absence of certain dominant gut microbiota members might also contribute to the development of CRC over time, as some species were found depleted in early stages of CRC, e.g. *Eubacterium rectale, Eubacterium eligens*, or *Streptococcus salivarius* (Zeller et al., 2014; Yachida et al., 2019). Some of these species (*E. rectale* or *E. eligens*) produce butyrate, which was found to have anti-tumorigenic effects, e.g. by promoting differentiation of anti-inflammatory T cells and apoptosis of IECs (Louis et al., 2014; Janney et al., 2020). However, depending on genetic events and tumour progression state, butyrate seems to play a pro- or anti-tumorigenic role in CRC, as butyrate lead to IEC hyperproliferation and an increase in reactive oxygen species (ROS) in mice without a mismatch repair apparatus (Janney et al., 2020). Certain types of CRC tumours have even been associated with SCFA

producing gut microbiota members, e.g. *Ruminococcus lactaris*, *Eubacterium ventriosum*, *Odoribacter splanchnicus*, *Anaerostipes hadrus*, and *Alistipes shahii* (Lee et al., 2023). A meta-analysis of different metagenomic studies revealed more positive than negative microbiota-CRC associations, indicating that microbiota members rather benefit from or contribute to tumorigenesis (Wirbel et al., 2019).

Besides disease development, also cancer therapy is influenced by the gut microbiome (Hitch et al., 2022b; Zhao et al., 2023). One example is immune checkpoint inhibitor therapy, e.g. CTLA-4 blockade, which is mediated by *B. fragilis*, *Bacteroides thetaiotaomicron* and *Burkholderiales* (Vétizou et al., 2015). Also *Bifidobacterium pseudolongum* improved anti-CTLA-4 immunotherapy response in a mouse model of CRC by the production of inosine in a T cell dependent manner (Mager et al., 2020). Several bacterial species, among them *Bifidobacterium longum*, *Collinsella aerofaciens*, and *Enterococcus faecium*, were more abundant in patients that responded to Anti-PD-1-based immunotherapy than in so called non-responders (Matson et al., 2018). Lee et al. (2022) found that *Bifidobacterium pseudocatenulatum*, *Roseburia* spp., and *Akkermansia muciniphila* were associated with immune checkpoint inhibitors, but identified no species as a fully consistent biomarker between all cohorts.

The aforementioned studies substantiate the potential of gut microbiome research for CRC development and treatment. Therefore, it is also important to understand how the microbiome is shaped, e.g. by dietary habits.

1.4 Effect of diet on CRC and the gut microbiome

There is good evidence that lifestyle factors such as physical activity, nutrition, or body composition (fat) influence the risk for CRC (Clinton et al., 2020). Intake of a "Western diet" was found to be associated with higher colon cancer risk (Slattery et al., 1998). The term Western diet is used to describe the eating pattern that prevails in the Western world and it is commonly defined by high fat and refined sugar content as well as high amounts of processed food and low fibre intake (So et al., 2023). Processed meat was even classified as a Group 1 carcinogen ("carcinogenic to humans") (Bouvard et al., 2015), due to formation of carcinogenic compounds like *n*-nitroso-compounds, polycyclic aromatic hydrocarbons, and heterocyclic aromatic amines. Next to possible direct action of dietary compounds as carcinogens, diet is also a major factor that influences the gut microbiota, and specific dietary compounds have been shown to induce shifts in bacterial genera (Singh et al., 2017). Several gut bacterial species were found to be associated with dietary patterns or even specific diet compounds in humans and these diet-driven changes in the gut microbiota can occur within a days (Asnicar et al., 2021; Johnson et al., 2019; O'Keefe et al., 2015).

In humans, a switch from a prudent, low-fat, plant polysaccharide-rich diet to a high-fat, high-sugar Western-style diet lead to fast adaption of the composition and gene expression of the microbiome (Turnbaugh et al., 2009). In another study with humans, the short-term consumption (4 days) of

an animal-based diet lead to an increase in bile-tolerant bacteria like *Alistipes*, *Bilophila*, and *Bacteroides*, whereas the occurrence of *Bacillota*, *E. rectale*, and *Ruminococcus bromii* levels decreased (David et al., 2014). Furthermore, RNA-seq analysis revealed that the animal-based diet lead to higher expression of genes within pathways for vitamin biosynthesis, β-lactamase, and degradation of carcinogenic polycyclic aromatic hydrocarbons, and bile salt hydrolases (BSH) (David et al., 2014). The animal-based diet also lead to significantly lower levels of acetate and butyrate, but significantly higher faecal levels of the branched-chain fatty acids isovalerate and isobutyrate and of total BAs, including DCA (David et al., 2014). In contrast, a switch from a diet low in fruits and vegetable to an isocaloric Mediterranean diet for 8 weeks caused changes in the faecal microbiome and metabolome, including increased gene richness and butyrate-producing *Faecalibacterium prausnitzii*, lower plasma and urine carnitine levels, as well as reduced inflammation (Meslier et al., 2020). Donohoe et al. (2014) showed that dietary fibre significantly reduced tumour multiplicity in AOM/DSS treated mice in presence of the butyrate-producing bacterial strain *Butyrivibrio fibrisolvens*. In contrast, the switch from a high-fibre, low-fat diet to a low-fibre, high-fat diet lead to an increase in mucosal biomarkers of CRC risk as well as changes in the microbiota and metabolome in rural South Africans (O'Keefe et al., 2015).

Another randomised, controlled dietary intervention trial in humans over a period of 6 months showed that higher fat content in the diet lead to increased levels of *Alistipes* and *Bacteroides* and decreased *Faecalibacterium* and SCFA levels, whereas a low-fat diet was associated with increased α-diversity, *Blautia*, and *Faecalibacterium* (Wan et al., 2019). Furthermore, subjects on the high-fat diet showed higher levels of proinflammatory factors in the plasma after intervention, namely high sensitivity C-reactive protein and thromboxane B_2 (Wan et al., 2019). Faecal metagenomic analysis revealed associations between functional changes such as enrichment of protein and mucin catabolism and reduced carbohydrate degradation genes, and CRC in humans (Wirbel et al., 2019). In mice, a high-fat, Western diet was associated with obesity and greater weight of orthotopic tumours compared to low-fat Western diet fed mice (O'Neill et al., 2016), indicating that high fat content of the Western diet plays an important role in tumorigenesis. Interestingly, tumour numbers and sizes of AOM/DSS-treated mice were suppressed by ketogenic diets with increasing fat-to-carbohydrate ratios, which was associated with the ketone body β-hydroxybutyrate (Dmitrieva-Posocco et al., 2022). Higher fat content of the diet leads to higher excretion of BAs into the intestine (Reddy, 1981). Already in 1973, it was found that North Americans who consumed a high-fat, Western diet had increased levels of the secondary BAs (SBAs) deoxycholic acid (DCA), lithocholic acid (LCA), 12-keto lithocholic aicd (12-KLCA) and cholesterol metabolites (coprostanol, coprostanone) in faeces (Reddy and Wynder, 1973). These findings suggest that a high-fat diet influences CRC risk and also affects bacterial BA metabolism.

1.5 Bile acids

Primary BAs (PBAs) are synthesised from cholesterol in the liver via two pathways. The classic pathway starts with the rate-limiting cytochrome P450 enzyme CYP7A1, which finally leads to formation of cholic acid (CA). The alternative pathway involves the enzyme CYP27A1, resulting in chenodeoxycholic acid (CDCA) formation (Figure 1.2). The majority of BAs is produced via the classical pathway. However, environmental factors like cold exposure or high-fat/high-cholesterol diet can induce BA production via the alternative pathway (Worthmann et al., 2017; Yetti et al., 2018; Perino et al., 2021). The human liver only produces CA and CDCA, whereas mice additionally produce α-muricholic acid (αMCA), βMCA, and ursodeoxycholic acid (UDCA), which have an additional hydroxy group at the C6 atom and are considered PBAs in mice (Honda et al., 2020; Takahashi et al., 2016). UDCA also occurs in humans, but is then considered to be a SBA produced by gut bacteria from CDCA through epimerisation (Takahashi et al., 2016; Perino and Schoonjans, 2015). In pigs, CDCA and hyocholic acid (HCA) were found to be the main PBAs (Lin et al., 2019; Hofmann et al., 2010)

As a final biosynthesis step in the liver, BAs are conjugated to amino acids to make them more hydrophilic and thus soluble (Begley et al., 2005). In humans, the ratio of glycine to taurine conjugated BAs is 3:1, whereas in mice most BAs are conjugated to taurine (Begley et al., 2005; Li and Dawson, 2019). Alternative conjugations are sulfonation, glucuronidation, and N-acetylglucosamination (Hofmann and Hagey, 2008). The hydroxy groups as well as the presence of an amino acid moiety (glycine or taurine) increase hydrophilicity of BAs and influence their biological functions (Perino et al., 2021). BAs are collected in the bile canaliculi, secreted into the bile duct and stored in the gallbladder until they are released into the small intestine upon ingestion of a meal (Perino et al., 2021). Conjugated BAs have detergent-like properties and form micelles with dietary lipids and fat-soluble vitamins, helping with their absorption (Perino et al., 2021).

In the small intestine, BAs undergo microbial deconjugation by bacteria expressing a BSH, resulting in the release of unconjugated BAs (Figure 1.2). This deconjugation may provide a metabolic advantage for the strains that can utilise glycine or taurine for example as an electron acceptor (Begley et al., 2005). Alternatively, deconjugation might enable the incorporation of BAs into the bacterial membrane, or it could be a detoxification mechanism (Begley et al., 2005). PBAs can be further transformed by members of the gut microbiota, who carry out secondary transformations like 7α-dehydroxylation (7αDH), epimerisation, or oxidation (Perino et al., 2021). These multi-step transformations result in a variety of different SBAs with different properties and different affinities to BA receptors Ridlon et al. (2014). The transformation of BAs by 7αDH is carried out by bacterial species harboring the *bai* gene cluster and might provide an advantage for these bacteria to use BAs as electron acceptors (Ridlon et al., 2006). An overview of the different BAs and their chemical structures is given in Figure 1.3 and Table 1.3.

Only 5% of the intestinal BAs are excreted via faeces, while the rest is recycled via enterohepatic circulation (Ridlon et al., 2006). In the distal ileum, BAs are transported into the epithelial cells via the apical sodium-dependent BA transporter (ASBT) (Perino et al., 2021). Inside epithelial cells, the ileal BA-binding protein (IBABP) facilitates BA transport through the cell from the apical to the basolateral membrane (Figure 1.2). There, they are secreted into the portal vein via the multidrug-resistance protein 3 (MRP3) or the organic solute transporters OSTα-OSTβ and transported back to the liver for re-conjugation (Dawson, 2011; Perino et al., 2021). In rodents, SBAs like DCA can be re-hydroxylated in the liver, whereas in humans, this reaction does not take place and DCA accumulates in the system over time (Ridlon et al., 2006). Conjugated as well as deconjugated BAs are actively re-absorbed in the terminal ileum, while in the colon, BAs are mostly passively absorbed (Figure 1.2). In the nucleus, they can bind to nuclear receptors (pregnane X receptor, PXR; farnesoid X receptor, FXR; or vitamin D receptor, VDR) and activate the transcription of certain genes and lead to several feedback mechanisms (Perino et al., 2021). Liver- and intestine-specific FXR knockout mice showed increased BA pool sizes (Kim et al., 2007), with intestinal FXR being required for CYP7A1 repression in the liver. One FXR target gene is the small heterodimer protein (SHP), which inhibits BA uptake by ASBT (Kuipers et al., 2014). Additionally, both FXR and VDR induce the fibroblast growth factor FGF19 (FGF15 in mice), which is transported to the liver via the portal vein (Kuipers et al., 2014). In the liver, FGF15/19 inhibits CYP7A1 and consequently the synthesis of new BAs from cholesterol (Figure 1.2).

An important membrane-bound BA receptor is the G protein-coupled bile acid receptor 1 (GPBAR1, also called TGR5). Binding of BAs to TGR5 on enteroendocrine cells leads to the release of glucagon-like peptide-1 (GLP1), an important molecule for glycemic homeostasis (Thomas et al., 2009). It has been suggested that TGR5 agonists, in particular ursocholic acid (UCA), are anti-inflammatory and reduce flow or uptake of BAs and could act by activation of epithelial cells or FXR (Lin et al., 2019). Recently, it was shown that BAs binding to TGR5 in intestinal stem cells promote regeneration of the intestinal epithelium upon injury via activation of yes associated protein 1 (YAP1) and the proto-oncogene protein-tyrosine kinase (SRC) (Sorrentino et al., 2020). Furthermore, it was shown that binding of BAs to TGR5 can activate mitogen-activated protein kinase (MAPK) signalling via several pathways like extracellular signal-regulated kinases (ERK1/2), SRC, and the mechanistic target of rapamycin (mTor) (Perino et al., 2021).

Figure 1.2 (Next page.): Schematic overview of BA metabolism and signalling: BA production and conjugation in the liver, bacterial transformations in the intestine, and BA signalling in intestinal epithelial and enteroendocrine cells, enterohepatic circulation and feedback mechanisms in hepatocytes. For clarity, HCA, which is a PBA in pigs (Zheng et al., 2021) is not shown as such. Sulf-BA: sulfated BA Gluc-BA: glucuronidated BA. Figure compiled and adapted with information from Perino et al. (2021); Kuipers et al. (2014); Dawson (2011); Studer et al. (2016); Burrin et al. (2013); Sorrentino et al. (2020); Huang et al. (2023); Sato et al. (2021); Trabelsi et al. (2015); Heinken et al. (2019); Bunnett (2014) and created with BioRender.com.

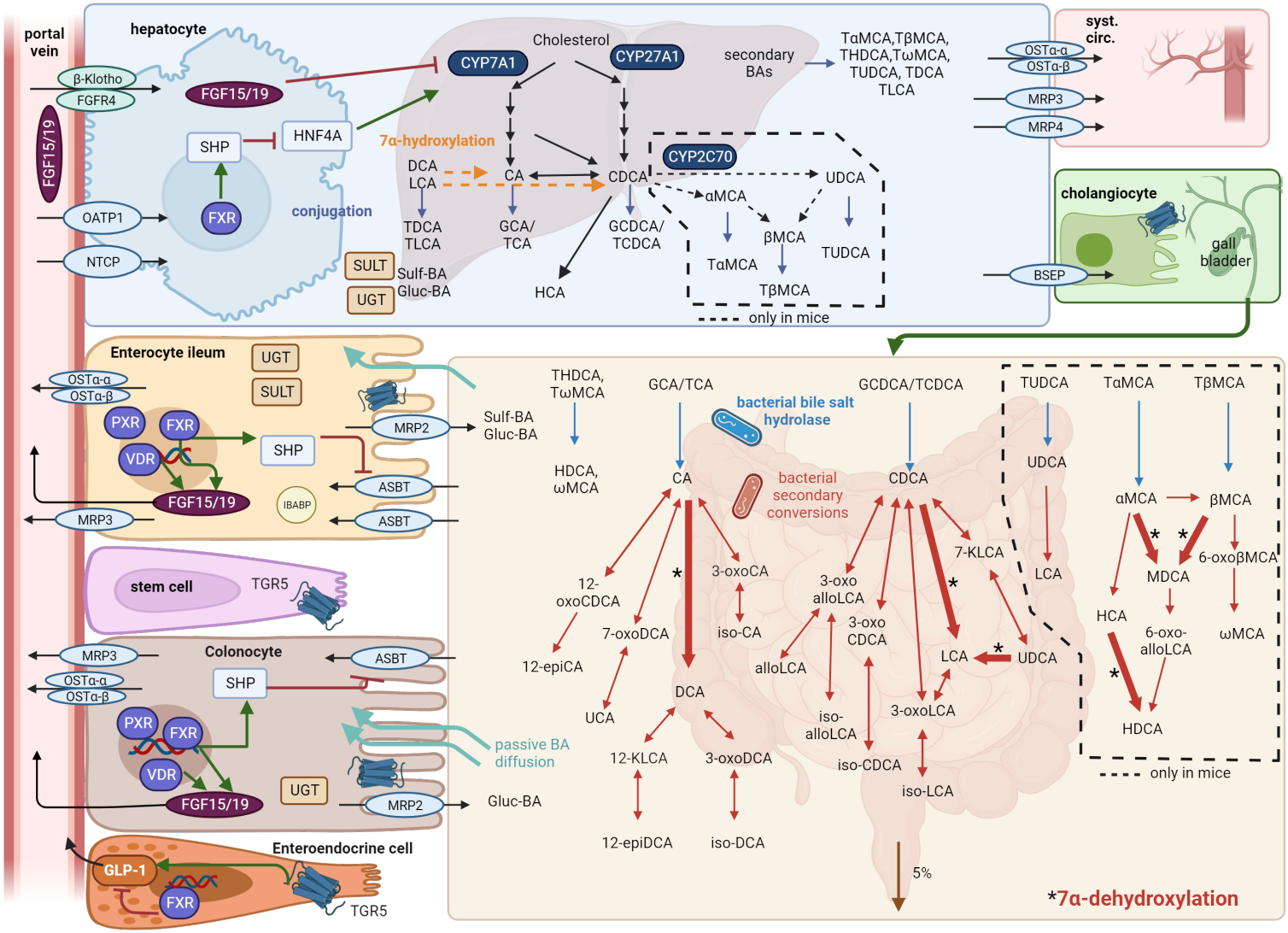

Figure 1.2: Caption on previous page.

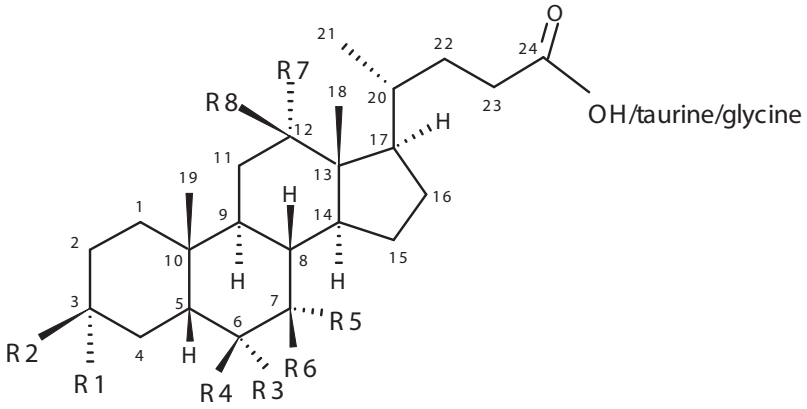

Figure 1.3: Chemical backbone of all BAs conjugated with taurine or glycine. They can be deconjugated by gut bacteria expressing BSH. R1-R8 as well as the position of the H atom at the C9 position determine the different BAs and is further specified in Table1.3.

Table 1.3: Molecular structure of BAs. Based on Zhang et al. (2012); Sato et al. (2021); Zheng et al. (2021). * only in rodents, ** PBA in rodents, SBA in humans, *** PBA in pigs.

BA	**alternative name**	**abbreviation**	**R1**	**R2**	**R3**	**R4**	**R5**	**R6**	**R7**	**R8**	**H**		**primary (P) /**
			3α	3β	6α	6β	7α	7β	12α	12β	5β	5α	**secondary (S)**
cholic acid		CA	-OH				-OH		-OH		-H		P
chenodeoxycholic acid		CDCA	-OH				-OH				-H		P
α-muricholic acid*		αMCA	-OH			-OH	-OH				-H		P
β-muricholic acid*		βMCA	-OH			-OH		-OH			-H		P
ursodeoxycholic acid**		UDCA	-OH					-OH			-H		P/S
deoxycholic acid		DCA	-OH						-OH		-H		S
lithocholic acid		LCA	-OH								-H		S
murideoxycholic acid		MDCA	-OH			-OH					-H		S
hycholic acid***	γ-muricholic acid	HCA	-OH		-OH		-OH				-H		P/S
ω-muricholic acid		ωMCA	-OH		-OH			-OH			-H		S
hyodeoxycholic acid		HDCA	-OH		-OH						-H		S
ursocholic acid		UCA	-OH					-OH	-OH		-H		S
iso-cholic acid		isoCA		-OH			-OH		-OH		-H		S
iso-deoxycholic acid		isoDCA		-OH					-OH		-H		S
iso-chenodeoxycholic acid		isoCDCA		-OH			-OH				-H		S
iso-lithocholic acid		isoLCA		-OH							-H		S
3-oxo-cholic acid	3-dehydro cholic acid	3-oxoCA	=O				-OH		-OH		-H		S
3-oxo-deoxycholic acid	3-dehydro deoxycholic acid	3-oxoDCA	=O						-OH		-H		S
3-oxo-chenodeoxycholic aicd	3-dehydro chenodeoxycholic aicd	3-oxoCDCA	=O				-OH				-H		S
3-oxo-lithocholic aicd	3- dehydro-lithocholic acid	3-oxoLCA	=O								-H		S
3-oxo-allo-lithocholic acid		3-oxo-alloLCA	=O									-H	S
6-oxo-lithocholic aicd	6-oxomurideoxycholic acid	6-oxoLCA	-OH		=O						-H		S
6-oxo-βmuricholic acid	6-oxo-ursodeoxycholic acid	6-oxo-βMCA	-OH		=O			-OH			-H		S
7-oxo-lithocholic acid	7-ketolithocholic aicd	7-KLCA	-OH				=O				-H		S
7-oxo-deoxycholic acid		7-oxoDCA	-OH				=O		-OH		-H		S
12-epi-cholic acid		12-epiCA	-OH				-OH			-OH	-H		S
12-epi-deoxycholic acid		12-epiDCA	-OH							-OH	-H		S
12-oxo-chenodeoxycholic acid	12-ketochenodeoxycholic acid	12-oxoCDCA	-OH				-OH		=O		-H		S
12-oxo-lithocholic acid	12-ketolithocholic acid	12-KLCA	-OH						=O		-H		S
allo-lithocholic acid		alloLCA	-OH									-H	S
iso-allo-lithocholic acid		iso-alloLCA	-OH	-OH								-H	S

BAs are influenced by gut bacterial metabolism, but they in turn also affect the gut microbiota. For instance, vancomycin-resistant *Enterococcus* species undergo a morphotype switch when exposed to LCA, resulting in diplococci instead of long chains. This reduces their ability to form biofilms and enhances their antibiotic susceptibility (McKenney et al., 2019). It was also shown that the hydrophobic SBA tauro-DCA (TDCA) and DCA were able to inhibit bacterial growth significantly more than the hydrophilic tauro-CA (TCA), CDCA and tauro-UDCA (TUDCA) (Sung et al., 1993). DCA production by *C. scindens* was shown to decrease *Clostridium difficile* load and pathogenesis in the colon of gnotobiotic mice. Sato et al. (2021) found that iso-alloLCA had a negative effect on Gram-positive pathogens. Not only bacteria are affected by BAs, but also immune cells.

1.6 Bile acids and the immune system

Macrophages and monocytes e.g. carry the BA receptor TGR5, and its activation leads to anti-inflammatory effects by reduced chemokine and inflammatory cytokine expression and macrophage migration (Perino and Schoonjans, 2015). Opposingly, Wang et al. (2020) found that a high-fat diet lead to increased faecal DCA levels and infiltration of pro-inflammatory nitric oxide synthase positive (iNOS+) macrophages in the colon, which could be prevented with vancomycin treatment. Furthermore, intraperitoneal DCA injection promoted again pro-inflammatory macrophage infiltration and pro-inflammatory cytokine production in vancomycin-treated, high-fat diet-fed mice (Wang et al., 2020). *In vitro*, Wang et al. (2020) found a dose-dependent effect of DCA on inflammatory macrophage signature genes like iNOS, tumour necrosis factor α (TNF-α), and interleukin 6 (IL-6). Campbell et al. (2020) showed that isoDCA lead to induction of forkhead box P3 (FOXP3) by reducing the immunostimulatory properties of dendritic cells (DCs). This effect was dependent on the nuclear BA receptor FXR in the DCs. Iso-alloLCA was shown to increase regulatory T cell (T_{reg} cell) differentiation via production of mitochondrial ROS and consequent FOXP3 expression (Hang et al., 2019). Li et al. (2021) identified that the LCA derivative 3-oxoLCA inhibits T_H17 cells differentiation by binding to RAR-related orphan receptor gamma (RORγt) (Hang et al., 2019). Imbalance between T_{reg} cells and T_H17 cells can cause excessive activation of the immune system, autoimmune responses or even metabolic syndrome (Zhang et al., 2021b). Also CRC, especially CSM1 is characterised by infiltration of cytotoxic T cells, natural killer cells and T_H1 cells, while T_{reg} cell activation was under-enriched in this molecular subtype (Guinney et al., 2015). Next to influencing the immune system and therefore certain types of CRC, BAs might also affect CRC development directly.

1.7 Bile acids and CRC

Several studies found elevated levels of faecal SBAs in CRC patients (Imray et al., 1992; Kawano et al., 2010), or associated with CRC risk markers (Ou et al., 2013). Bayerdörffer et al. (1995) found a positive association between DCA concentration in serum and colorectal adenoma. Yachida et al. (2019) reported elevated DCA levels at the stage of multiple polypoid adenomas with low-grade dysplasia, an early stage in CRC development. Furthermore, DCA and LCA could induce cancer stem cell markers in normal human colonic epithelial cells, which was dependent on M3R signalling (Farhana et al., 2016). Payne et al. (2007) showed that DCA could induce oxidative stress in mitochondria of HCT 116 colon cancer cells and activate nuclear factor kappa-light-chain-enhancer of activated B cells (NFκB). Other experiments with this cancer cell line found that 0.3 mmol/L DCA increased ROS and genomic DNA fragmentation, increased the tumour-promoting ERK1/2 pathway, but inhibited activation of tumour suppressor retinoblastoma protein (Zeng et al., 2015).

In *Apc*$^{Min/+}$ mice, a diet supplementation with CA (0.4% w/w, 12 weeks) lead to more and larger intestinal tumors compared to the control diet (Wang et al., 2019). Interestingly, microbiota depletion with antibiotics reduced the tumour-promoting effect of CA supplementation, emphasising the importance of microbial conversions for the detrimental effect of BAs (Wang et al., 2019). This study however lacked a control group with antibiotics treatment as well as deuterium labelled standards for BA measurements, which hampers the comparability of their measurements (Wang et al., 2019). Another study with wild type mice showed that diet supplementation with DCA (0.2% w/w for 8-10 months) led to more tumours in the proximal colon (Bernstein et al., 2011). In AOM-treated Wistar rats, 0.3% DCA in feed lead to a significant increase in colonic tumours as well as a significant increase in Kirsten rat sarcoma viral oncogene homologue (*Kras*) point mutations in these tumours (Narahara et al., 2000). Treatment of *Apc*$^{Min/+}$ mice with DCA (0.2 % in drinking water, 12 weeks) lead to tumour progression, higher tumour numbers and significantly higher cell proliferation (Cao et al., 2017). However, final colonic or faecal DCA levels were not reported. In the same study, faecal microbiota transfer from DCA-treated mice to microbiota-depleted *Apc*$^{Min/+}$ mice on control diet increased DCA levels transiently and lead to significantly higher intestinal tumour numbers compared to mice that received microbiota from control mice without oral DCA treatment (Cao et al., 2017).

The existing studies using different animal models point towards a detrimental effect of DCA in CRC, but a few caveats have to be considered when interpreting the results. It has to be assumed that direct DCA supplementation in mice results in higher amounts of DCA in the small intestine than they would normally encounter through enterohepatic circulation. This could result in disturbance of the small intestinal microbiota and abnormal bacterial metabolism in the proximal intestine. Additionally, the commonly used *Apc*$^{Min/+}$ mouse model develops tumours predominantly in the small intestine instead of the colon (Moser et al., 1995). Furthermore, BA pools differ significantly between different vertebrate orders (Hofmann and Hagey, 2014). As shown in Figure 1.2, there are 3 more PBAs in mice compared to humans. Finally, the use of complex microbiota in *in vivo* experiments is linked to a wide range of uncontrolled BA modifications and other confounding factors.

1.8 Hypothesis and aims of this thesis

Even though literature work has revealed a correlation between SBAs and CRC, the causal role of SBA-producing gut bacteria on cancer development *in vivo* still remains to be elucidated. Different diets, complex microbiota, different BA pool compositions as well as the interactions of these three factors with the host make it difficult to prove causality. We hypothesised that intestinal bacteria can promote CRC development by SBA production, especially under detrimental conditions like those induced by a Western diet. In this context, we sought to elucidate the complex effects of SBAs in CRC by using different animal models of CRC and a combination of approaches targeting the microbiota. In the first part of this thesis, the influence of pig-derived microbiota shaped by a Western diet on CRC development was tested by conducting FMT in the $Apc^{1638N/+}$ mouse model for intestinal cancer under gnotobiotic conditions. In the second part, the microbial complexity was reduced by using a gnotobiotic setting. The tumour-promoting effect of a SBA-producing bacterial strain added to a background synthetic community was tested under experimental CRC conditions (AOM/DSS treatment in combination with a high-fat diet). Next, the effect of this bacterial strain on the colonic epithelium was tested at the single cell level, revealing possible mechanisms of actions of SBAs. The last section presents the results of a feeding trial in $APC^{1311/+}$ pigs that tested the effects of the BA-scavenging drug colestyramine on CRC development.

CHAPTER 2

Material and methods

This material and methods section is structured according to the different animal trials in the same order as they appear in the results. At the end of each sub-section, the detailed contributions of collaborators are described.

2.1 Faecal microbiota transplant in germfree *Apc*$^{1638N/+}$ mice

Based on a previous feeding trial in *APC*$^{1311/+}$ pigs (Wortmann et al., 2023), a faecal microbiota transplant (FMT) into germfree *Apc*$^{1638N/+}$ mice was performed to test whether the phenotype observed in pigs, i.e. worsening of disease due to red-meat and lard (RL) diet, could be transferred via the microbiota. Three pigs from each the control diet (CTRL) and RL diet group were selected based on changes in tumour development and faecal levels of SBAs (especially DCA) during the feeding period: increased polyp numbers and DCA levels for RL donor samples vs. decreased polyp numbers and lower DCA increase for CTRL donors (Figure 2.1 **a** and **b**). Pigs with substantially divergent microbiota profiles after the dietary intervention were excluded to avoid results being driven by extreme microbiota states (Figure 2.1 **c**).

2.1.1 Breeding and genotyping of germfree mice

Apc$^{1638N/+}$mice (B6/J.129-(Apc1638N)tm) were obtained from Dr. Marijana Basic and Prof. André Bleich (Hannover Medical School) and bred in germfree isolators (flexible film isolator type 2D, NKPisotec) in our own gnotobiotic unit (University Hospital of RWTH Aachen, Germany). Earpunches were used for genotyping. Shortly, DNA was extracted overnight by using 400 µL tail extraction buffer (1 M Tris, pH 8; 0.5 M EDTA; 5 M NaCl; 20 % SDS) and 10 µL proteinase K (Carl Roth, Germany, cat. nr. 7528.1) while shaking at 55 °C. After vortexing, 200 µL supernatant was collected and DNA was precipitated by adding 200 µL isopropanol (Carl Roth, Germany, cat. nr. 6752.1), followed by centrifugation (10 min, 9,600 g, RT). The DNA pellet was dissolved in 200 µL TE buffer (pH 7.5), shaking overnight at 55 °C. Genotypes were determined by PCR using one forward primer (5'-CAGCCATGCCAACAAAGT) and two reverse primers (5'-GGAAAAGTTTATAGGTGTCCCTTCT for wild type, 5'-GCCAGCTCATTCCTCCACTC for mutant) and the 2X One Taq Mastermix (New England Biolabs, cat. nr. M0482). The PCR was run with 94 °C (60 s) initial denaturation, followed by 30 cycles of denaturation (94 °C, 20 s), annealing (58

°C, 20 s), extension (68 °C, 20 s), and a final extension (68 °C, 60 s). Only heterozygous *Apc*$^{1638N/+}$ mice were used for the experiment.

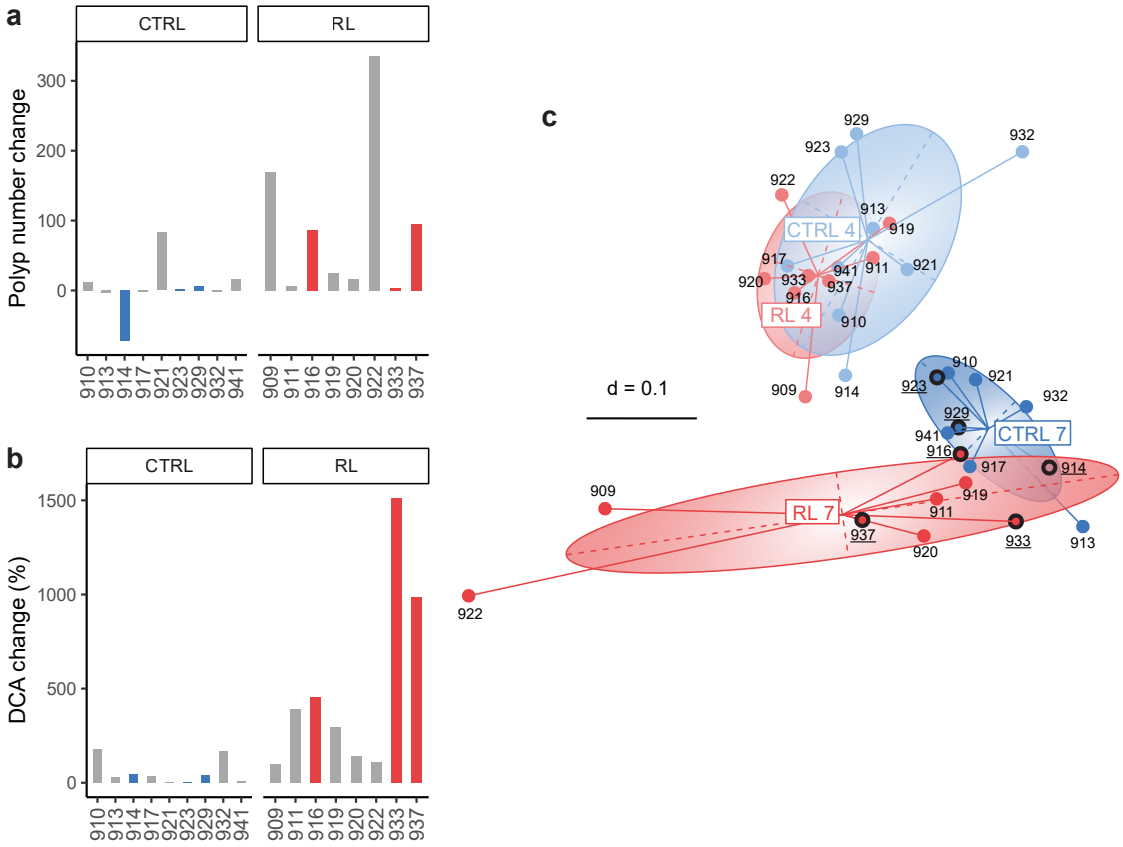

Figure 2.1: Selection of the donor pigs for FMT was based on **a** change in polyp number, **b** DCA levels in faeces over the course of the experiment, and **c** microbiota profiles. Selected pigs are marked in colours (**a** and **b**) or with underscore and a black circle (**c**).

2.1.2 Animal experiment

This animal experiment was performed under LANUV ethical approval nr. 81-02.04.2018.A425 in accordance with EU directive 2010/62/EU. Germfree *Apc*$^{1638N/+}$ mice (B6/J.129-(Apc1638N)tm) were colonised with faecal microbiota from pigs. The mice were allocated to the colonisation and diet groups by paying attention to spread littermates across different cages and groups, as depicted in Figure 2.2. All mice were initially housed in cages of at least two mice, but male mice that started fighting had to be separated into different cages. The experimental setup is depicted in Figure 2.3. Germfree mice were removed from the breeding isolator at 4 weeks of age and colonised with 150 µL or max. 10% (v/w) of body weight of faecal microbiota cryostocks (20% v/v glycerol by oral gavage. Gavage was done twice, with two days in between. For the following two weeks, mice were housed in cages of the ISOcage P-Bioexclusion System (ISO30P, Tecniplast, Italy), and supplied with autoclaved (121 °C, 20 min) standard chow diet (ssniff Spezialdiäten GmbH, cat. nr. V1534-300) and autoclaved tap water *ad libitum*. After this 2-week period to reach a stable colonisation, mice were transferred into filter top cages (GM500, Tecniplast, Italy). After one more week of adjustment to

the new environment, the diet was changed to either an experimental control diet (CD diet, ssniff Spezialdiäten GmbH, cat. nr. S5745-E902) or the same diet supplemented with 0.2% (w/w) of the PBA CA (BA diet, ssniff Spezialdiäten GmbH, cat. nr. S5745-E903), both of which were sterilised by irradiation (2 x 25 kGy). The feed composition can be found in Appendix Table A.1. Mice were scored daily for body-conditioning, general state of health, behaviour and Bristol stool type. Faecal sample collection and weighing were done weekly. Faecal pellets were stored at -80 °C or used directly for a faecal occult blood check using a guaiac test as described in section 2.1.4. If mice reached a total score of 10, the observation interval was increased to twice a day. If a score of 20 or higher was reached, mice were culled. All other mice were sampled at 30 weeks of age (see section 2.1.3).

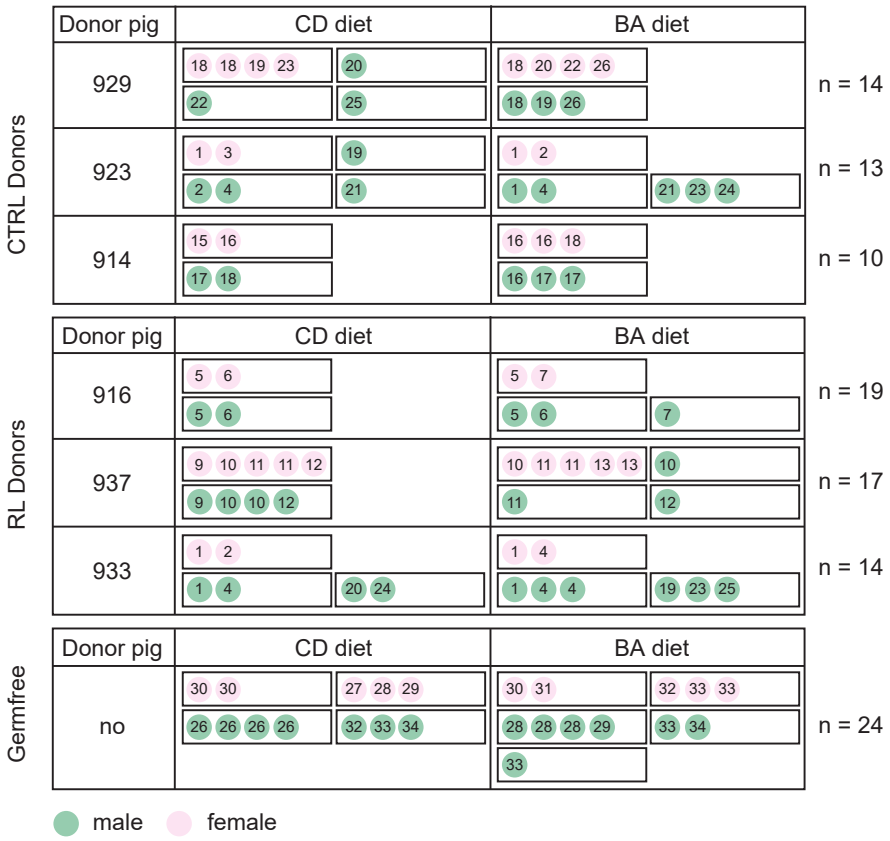

Figure 2.2: Each circle represents one mouse and each small box stands for one cage. Genders are indicated by colour and litters are indicated by number. The final cage distribution after separating male mice that started fighting is shown.

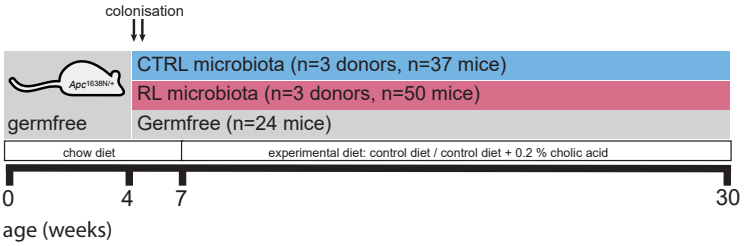

Figure 2.3: Germfree *Apc*$^{1638N/+}$ mice were colonised at 5 weeks of age with one of three selected CTRL or RL microbiota from pig donors. Mice from each microbiota group were divided into two groups and fed with either a control diet (CD diet) or the same diet supplemented with 0.2% CA (BA diet).

2.1.3 Sampling procedure

Mice were weighed and faecal samples were collected under a laminar flow cabinet. Mice were then culled by an overdose of Isofluran (Abbvie, cat. nr. 10182054). Death was verified by checking of reflexes before drawing cardiac blood with a syringe (1010 Sterican, 27G x 0.5 inch, 0.4 x 12mm, Braun), flushed with EDTA (6 g/mL, Merck, cat. nr. 8421), of which 10 µL were diluted in 1990 µL NaCl for red blood cell (RBC) count. The number of RBC was counted with a Neubauer improved counting chamber (0.02 mm depth). The peritoneum was opened, examined for desmoids or other abnormalities (e.g. intussuceptions), and the gastrointestinal tract, starting from the stomach, was removed carefully. Small and large intestinal length were measured. The intestine was then divided into duodenum, jejunum, ileum, caecum, and colon (Figure 2.4), and each part was put in a separate well of a 6-well plate (cat. nr. 6657160, Greiner Bio-One, Germany) filled with sterile, ice-cold PBS (D8537, Sigma-Aldrich). Caecum weight was recorded and all other intestinal sections were cut open longitudinally and content was collected and snap frozen. The intestine was screened under a binocular and any malformations, abnormalities, and lesions were noted. If lesions were found, their size was measured at the longest diameter and they were either fixed in 4% buffered formaldehyde for 24h and paraffin embedded, or snap frozen. Since pathological and histological assessment was done only for a subset of the possible polyps or tumours, they are referred to as lesions in the results section. A subset of the intestinal lesions was stained with hematoxylin and eosin (HE) and analysed by Prof. Klaus-Peter Janssen (Klinikum rechts der Isar, Technical University of Munich, Germany).

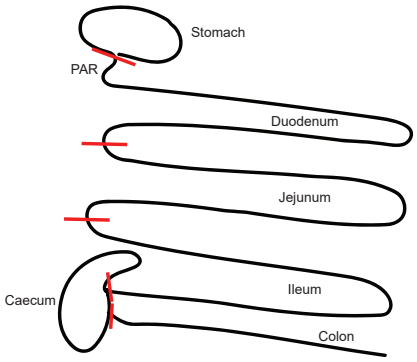

Figure 2.4: Sampling scheme for the intestine of *Apc*$^{1638N/+}$ mice from the FMT trial. The intestine was divided into the different regions: duodenum with the periampullary region (PAR), jejunum, ileum, caecum, and colon.

2.1.4 Faecal occult blood test

The guaiac faecal occult blood test is a stool test commonly used for CRC screening in humans (Li and Yuan, 2019). This test detects heme in faeces, which reacts with hydrogen peroxide to oxidise guaiac and turns blue. Shortly, a fresh faecal sample was smeared onto three fields of one 2-hole slide test (hemoCARE, CARE diagnostica Laborreagenzien GmbH, cat. nr. 005031-E/D). Once the sample was dried, 1-2 drops of the developer solution were applied and the result was observed visually after ca. 1 min. Positive samples turned blue, whereas the colour did not change in the case of negative samples. Depending on the colour intensity, an arbitrary score from 1-3 was given (Figure 2.5).

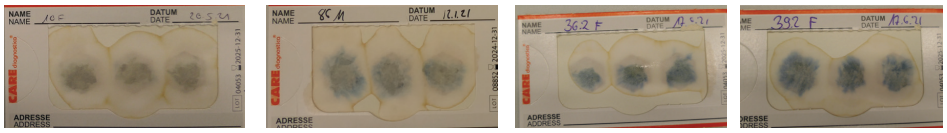

Figure 2.5: Example pictures of different scores of faecal occult blood tests.

2.1.5 High-throughput 16S rRNA gene amplicon analysis

Metagenomic DNA was isolated from caecal content as described previously (Just et al., 2018). Briefly, the DNA was purified using columns (Macherey-Nagel, Germany) after mechanical lysis by bead beating. The V3-V4 regions of 16S rRNA genes was then amplified and sequenced as described before (Afrizal et al., 2022). Raw sequencing reads were processed using IMNGS (Lagkouvardos et al., 2016), a UPARSE (Edgar, 2013) based pipeline (`https://www.imngs.org/`). The analysis settings for the pipeline were: number of allowed mismatches in the barcode: 1; minimum fastq quality score for trimming of unpaired reads: 20; length for single reads or amplicons for paired sequences: minimum 350, maximum 500; max. rate of expected errors in paired sequences: 0.005; maximum mismatches during merging of reads allowed 50; minimum %id of alignment during scoring merge: 70; length of trimming at forward and reverse side of the sequences: 20; minimum rel. abundance cutoff: 0.0025. Pairing, quality filtering and operational taxonomic unit (OTU) clustering at 97% identity was done using USEARCH version 11.0 (Edgar, 2010). Non-16S sequences were removed with SortMeRNA v4.2 (Kopylova et al., 2012). Sequences were aligned and taxonomically classified using SINA version 1.6.1 and SILVA release 128 (Pruesse et al., 2012). A maximum likelihood approximation tree was calculated with Fasttree. Samples <2000 reads (n = 9) were removed and the analysis was repeated.

After the filtering step to remove molecular species of low rel. abundance, samples with 5,484 ±2,609 reads (mice and FMT donor samples) were analysed in R (R Core Team, 2022) using Rhea (`https://github.com/Lagkouvardos/Rhea`; Lagkouvardos et al. 2017). The rel. abundance cut-off was set to 0.25%, all values below were replaced with NA. For statistical group comparisons, a prevalence cut-off of 80% was selected. For heatmaps, NAs were considered as zeroes for mean calculation and in the colour scale. Presence/absence testing with the Fisher Exact-test was done in R using the Rhea script (Lagkouvardos et al., 2017). Multiple comparisons were done with

non-parametric tests and Benjamini-Hochberg corrections for multiple comparisons using the rstatix package (Kassambara, 2023).

2.1.6 Screening for 7α-dehydroxylating species

Sequences of all single molecular species (SOTUs) were blasted against a list of published 7α-dehydroxylating (7αDH+) strains (Table 2.1). A threshold of 97% sequence identity was used as an identity cut-off.

Table 2.1: Bacterial species, strain designation, and accession numbers used to search for 7αDH+ species in 16S rRNA gene amplicon data.

Species	Strain	Accession number	Reference
Clostridium scindens	ATCC35704	ABFY02000057	Doerner et al. (1997)
Clostridium hylemonae	TN-271	AB023972	Ridlon et al. (2010)
Clostridium leptum	DSM753	ABCB02000019	Doerner et al. (1997)
Clostridium sordellii	ATCC9714	NR_112173.1	Takamine and Imamura (1995)
Peptacetobcter hiranonis	TO-931	AB023970	Wells and Hylemon (2000); Kitahara et al. (2001)
Proteocatella sphenisci	PPP2	AF450134	Kim et al. (2022)
Extibacter muris	DSM8650^T	KR364761	Streidl et al. (2021)

2.1.7 Contributions

DNA extraction, 16S rRNA gene amplicon sequencing, and raw reads file pre-processing (remultiplexing) were done by Ntana Kousetzi and Dr. Nicole Treichel (AG Clavel, University Hospital of RWTH Aachen, Germany). Several colleagues helped during the experiment and on sampling days: David Wylensek, Alina Viehof, Atscharah Panyot, Susan Jennings (AG Clavel, University Hospital of RWTH Aachen, Germany). I conducted the animal experiment, analysed all metadata and did the downstream analyses of remultiplexed sequences from 16S rRNA gene amplicon sequencing.

2.2 Effect of DCA-producing *E. muris* on disease in a gnotobiotic mouse model of CRC

This experiment was carried out at the German Institute of Human Nutrition (DIfE) in Potsdam-Rehbrücke (Nuthetal, Germany). It was approved by the Ministry of Social Affairs, Health, Integration and Consumer Protection of the state Brandenburg (permit no. 2347-15-2021).

BACOMI (bile acid-converting microbiota) is a synthetic microbial consortium (Wortmann et al., 2023) based on a previously published minimal consortium (Ridlon et al., 2020), from which the original 7αDH+ strains were removed. A short description of the members of this consortium follows. *Bacteroides uniformis* DSM 6597, *Phocaeicola vulgatus* DSM 1447 and *Parabacteroides distasonis* DSM 20701 express BSH. *B. wadsworthia* DSM 11045 can metabolise taurine released by

BSH activity into H_2S. *Blautia producta* DSM 2950 was added due to being a dominant human gut bacterium that is H_2-consuming, acetogenic, able to isomerise BAs and therefore increases variability of the BA pool (Ridlon et al., 2020). *Extibacter muris* DSM 28560^T is a SBA-producing species from the mouse intestine known to produce DCA from CA by 7αDH (Streidl et al., 2019). Two versions of the BACOMI consortium were created: BACOMI(7αDH-) without the capacity to produce DCA by 7αDH, and BACOMI(7αDH+), which produces DCA due to addition of *E. muris*.

2.2.1 Animal experiment

Germfree BALB/cJ mice were kept in positive-pressure isolators with a 12 h light-dark cycle at 22 ± 2 °C and 55 ± 5 % humidity. One week before colonisation, mice were put on a high-fat diet (Appendix Table A.2). Mice (n = 10 per group) were then colonised either with BACOMI(7αDH+) or BACOMI(7αDH-) by gavage of bacterial culture (10^8 cells per strain in 100 µL medium; 50 µL orally and 50 µL rectally, at day 0 and 2). Starting at week 2 after colonisation, mice received three intraperitoneal injections of AOM (5 mg/kg body weight) in the interval of one week (Figure2.6). This was followed by 3 cycles of DSS treatment, consisting of 5 days of 1.5 % DSS in drinking water and 16 days of normal drinking water. Colonisation was checked by 16S rRNA gene amplicon analysis before the start of the AOM intervention and at the end of the experiment (see section 2.1.5). Two female mice dropped out in the BACOMI(7αDH+) group after the first DSS cycle. After 18 weeks, all other mice were sampled.

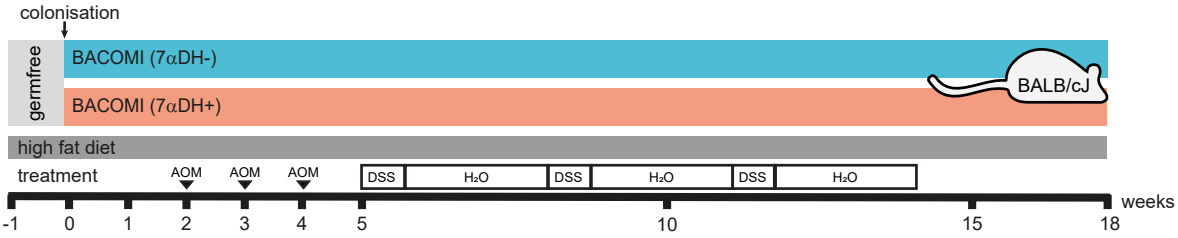

Figure 2.6: Experimental design of the targeted colonisation experiment combined with AOM/DSS treatment. Germfree mice on high fat diet were colonised with a live culture mix of the BACOMI(7αDH-) strains alone or with the addition of *E. muris* (7αDH+). Two weeks after the colonisation, mice were injected with AOM 3 times, followed by DSS treatment via the drinking water 3 times in the next 13 weeks.

2.2.2 Sampling procedure

Mice were exported from the isolators and kept in normal filter-top cages until they were culled by isofluran. The peritoneum was opened and the intestine removed in one piece, including the mesentery. Colon tumours were assessed under a binocular microscope. Gut contents were collected and snap frozen in liquid nitrogen. Mesenteric lymph nodes (MLN) and colon tissue were collected and processed as described in sections 2.2.3 and 2.2.4.

2.2.3 Isolation of immune cells from the mesenteric lymph nodes

Lymph nodes were collected in RPMI + 2 % FCS (P004-16500, PAN Biotech, Germany) stored on ice. Cells were pressed through a 70 µm cell filter (Corning, cat. nr. 431751) into a 50 mL Falcon tube using the top of a syringe plunger of a 5 mL syringe (sterile) and were washed with ca. 2 mL sterile PBS 2-3 times. Once only a white tenacious residue was left on the filter, the filter was washed with 5 mL sterile PBS or until a final volume in the tube of 12.5 mL was reached. The tubes were centrifuged (900 rpm, 10 min, 4 °C), supernatant was discarded, and the cell pellet resuspended in 1 mL of RPMI + 2 % FCS. Cells were counted in a Neubauer improved counting chamber (0.1 mm, 0.0025 mm^2), using 90 µL trypan blue in 10 µL cell suspension. For staining, 2,500 cells/µl medium were used.

2.2.4 Isolation of immune cells from the colon

For isolation of cells from the colon, the colon was washed with PBS, transferred in buffer 1 (Table 2.2) and put on ice until further processing. Once all tissues were ready, the colon was transferred to buffer 2 and put on a gentle shaker for 20 min at 37 °C. Filtered (0.2 µm) eluate was captured and the remaining colon tissue was digested again with buffer 2 for 15 min (37 °C), gently rocking. Filtered eluate was collected in a new tube and the remaining colon was transferred again in 5 ml of buffer 2, incubated on a shaker for 15 min (37 °C), and the resulting eluate was collected. Remaining colon tissue was then incubated in 10 mL of buffer 3, using a new Falcon tube for 45-60 min (37 °C, gently rocking), after which 5 mL of buffer 4 were added and the tubes were shaken vigorously for 10 s. Filtered eluate from buffer 4 was added to eluates from buffer 2 and 3 and centrifuged (500 g, 7 min). Supernatant was removed and cells were resuspended 3 mL FACS buffer. For macrophage staining, 1 mL of the combined eluates was filtered through a 70µm filter, centrifuged (500 g, 5 min) and the pellet was resuspended in 150 µL FACS buffer. The remaining 2 mL of the eluates were used for T cell isolation and therefore centrifuged (500 g, 7 min), and the pellet was resuspended in 4 mL 40% Percoll solution. The 40% Percoll solution was carefully added on top of 70% Percoll solution. Tubes were centrifuged (200 rpm, 20 min, 20 °C) without using the centrifuge break. Cells from the interphase between the Percoll solutions was taken using a Pasteur pipette, transferred to new tubes, and 5 mL PBS were added. After centrifugation (500 g 10 min, 20 °C) to destroy the Percoll gradient, supernatant was removed and cells were resuspended in 150 µL FACS buffer (Table 2.2).

Table 2.2: Buffers used for cell isolation from colon and lymph nodes. RPMI 1640 was always supplemented with 10 % FCS.

Buffer	Composition (Volume per sample)
Buffer 1	5 ml HBSS, 25 µl 1 M DTT, 175 µl FCS
Buffer 2	10 ml HBSS, 90 µl 0.5 M EDTA, 350 µl FCS
Buffer 3	10 ml RPMI 1640 medium, 500 µl FCS, 5 mg, Collagenase A (125 U/mg), 5 mg DNAse (5mg/ml)
Buffer 4	5 ml RPMI 1640 medium, 10 % FCS, 45 µl 0.5 M EDTA
FACS buffer	PBS + 2 % FCS
40 % Percoll	1.6 ml Percoll, 160 µl 10x PBS, 2.24 ml RPMI 1640 medium
70 % Percoll	2.8 ml Percoll, 280 µl 10x PBS, 920 µl RPMI 1640 medium

2.2.5 Immune cell staining and FACS analysis

Immune cells isolated from MLN and colon were transferred to new 1.5 mL tubes, centrifuged, and resuspended in 150 µL FACS buffer. The surface antibodies, Fc block and dead/life staining were added to the sample, resuspended, and incubated for 45 min at 4 °C in the dark. After incubation, 100 µL FACS buffer were added, cells resuspended and centrifuged (500 g, 5 min, RT). Supernatant was discarded and the cell pellets were resuspended in 200 µL fixation buffer (Invitrogen™ cat. nr. 00-5123-43 diluted with Invitrogen™ cat. nr. 00-5223-56 for the panel including Foxp3, Invitrogen™ cat. nr. 00-8222-49 for all other antibody panels) per tube. After incubating (45 min, 4 °C in the dark), cells were centrifuged (500 g, 5 min, RT), pellets were resuspended in 200 µL permeabilisation buffer (Invitrogen™ 00512343) and centrifuged again immediately (500 g, 5 min, RT) before supernatant was discarded. The cell pellet was resuspended in 100 µL permeabilisation buffer containing the intracellular antibodies according to Table 2.3 and incubated (45 min, 4 °C, in the dark). After this last incubation step, 100 µL FACS buffer were added, cells were resuspended and again centrifuged (500 g, 5 min, RT) before supernatant was discarded and cells resuspended in 100 µL FACS buffer, transferred to FACS tubes, and stored at 4 °C in the dark until FACS analysis. For flow cytometry, a FACS Aria III cell sorter (BD Biosciences, United States) was used and data was analysed using the software FlowJo. Gating strategies are specified in Figure 3.8 in section 3.2.

Table 2.3: Antibodies used for immuno-staining. Staining with IFNγ and IL-17A was done, but not successful.

Antibody	Ratio	Manufacturer	ID	Marker
CD3e-FITC	1:400	ThermoFisher	11-0031-82	Surface marker
CD4-FITC	1:1000	ThermoFisher	11-0041-82	Surface marker
CD103-PE	1:40	ThermoFisher	12-1031-82	Surface marker
CD304- PerCP-eFluor 710	1:1000	ThermoFisher	46-3041-82	Surface marker
FOXP3-APC	1:100	ThermoFisher	17-5773-82	Intracellular marker
IFNγ- PerCP-Cy5.5	1:400	ThermoFisher	45-7311-82	Intracellular marker
IL-17A-PE-Cy7	1:200	Biolegend	506921	Intracellular marker
CD8α-eFluor-450	1:400	ThermoFisher	48-0081-82	Surface marker
CD45-PerCPCy5.5	1:200	Biolegend	103131	Surface marker
F4/80-FITC	1:100	eBioscience	11-4801-82	Surface marker
CD11b-PE	1:200	eBioscience	12-0112-81	Surface marker
Ly-6C- PE-Cy7	1:200	Biolegend	128017	Surface marker
CD206 (MMR)-APC	1:200	Biolegend	141707	Surface marker
FC (CD16/CD32 Antibody)	0,5 µg/100 µl	eBioscience	14-0161-82	
FCR block (aC16/32)	1:50	eBioscience	11-0112-82 bzw. 11-0112-85.	
LIVE/DEAD^{TM} Fixable Violet Dead Cell Stain Kit	0,5 µl per sample	ThermoFisher	L34963	
LIVE/DEAD^{TM} Fixable Red Dead Cell Stain Kit		ThermoFisher	L34971	

2.2.6 BA analysis

Caecal content samples, previously stored at -80°C, were lyophilised overnight at –60 °C. The dry weight was determined, and 6 ceramic beads (2.5 mm) were added to each tube. Proportionally to the weight of each sample, 500-1500 µL extraction solvent (methanol/H_2O (2/1) + 0.1% formic acid) were added. A Precellys 24 Tissue Homogenizer (Bertin Instruments, France) was used to homogenise the samples at 6,500 rpm 2 x 20 s beat with 20 s rest in between, followed by centrifugation (21,000 rcf, 15 min, 4 °C). An aliquot of 100 µL from each supernatant or calibration standard was transferred to a 2 mL 96-well plate. Internal standard (ISTD) solution was added (50 µL of each 2 µM CA-d4, CDCA-d_4, TCA-d_4, TUDCA-d_4, DCA-d_4 and LCA-d_4 in methanol) to each well, immediately followed by addition of 600 µL of 0.2% formic acid in H_2O. Sample extracts and ISTDs were mixed using an orbital shaker (300 rpm), followed by centrifugation (3,500 rpm, 5 min, 4 °C). The samples were then extracted by solid phase extraction using a Oasis HLB 96-well uElution plate (Waters, USA), dried in a Biotage®SPE Dry 96 (Biotage, Sweden) at 20 °C, and reconstituted in 100 µL of methanol/H_2O (50/50). Samples were again mixed on an orbital shaker (300 rpm, 5 min), centrifuged (3,500 rpm, 5 min, 4 °C), and injected into the LC-HRMS system.

Quantitative analysis was done using an Agilent ultrahigh-performance liquid chromatography 1290 series coupled in tandem to an Agilent 6530 Accurate-Mass Q-TOF mass spectrometer 66 equipped with a Zorbax Eclipse Plus C18 column (2.1 × 100 mm, 1.8 µm) and a guard column Zorbax Eclipse Plus C18 (2.1 × 5 mm, 1.8 µm)(Agilent technologies, USA). The autosampler was kept at 10 °C and the injection volume was 5 µL. The column compartment temperature was set to 50 °C. Ammonium acetate [5 mM] in water was used as mobile phase A and pure acetonitrile as mobile phase B. The flow rate was 0.4 mL/min with a run time of 26 min and the following gradient: 0-5.5 min, constant

21.5% B; 5.5-6 min, 21.5-24.5% B; 6-10 min, 24.5-25% B; 10-10.5 min, 25-29% B; 10.5-14.5 min, isocratic 29% B; 14.5-15 min, 29-40% B; 15-18 min, 40-45% B; 18-20.5 min, 45-95% B; 20.5-23 min, constant 95% B; 23-23.1 min, 95-21.5% B; 23.10-26 min, isocratic 21.50% B. The system was equilibrated in initial conditions for 3 min at the end of the gradient. Detection was done in negative ionisation mode using the Dual AJS Jet stream ESI Assembly.

Acquisition settings for the QTOF were configured in 4 GHz high-resolution mode (resolution 17,000 FWHM at m/z 1,000) with data storage in profile mode. High-resolution full MS chromatograms were acquired between m/z 100-1700 with 3 spectra/s. The mass spectrometer was calibrated in negative mode every 6 h using ESI-L solution (Agilent technologies, USA). Source parameters were: drying gas flow, 8 L/min; gas temperature, 300 °C; nebuliser pressure, 35 psi; capillary voltage, 3,500 V; nozzle voltage, 1,000 V. Data processing was done using the MassHunter Quantitative software and MassHunter Qualitative software (Agilent technologies, USA) to control the mass accuracy for each run. Quantification of 43 BAs was done using calibration curves and corrected by addition of internal standards to all samples and calibration levels. For generation of extracted ion chromatograms, a retention time window of ±1.5 min and a mass extraction window of ±60 ppm around the theoretical mass of the targeted BA were used.

For all experiments, BAs that were not detected were assumed to be absent, set to 0 nmol/g. Only those BAs detected in at least 50 % of the animals in at least one group were considered for downstream statistical analyses.

2.2.7 16S rRNA gene amplicon sequencing

Bacterial DNA was isolated from caecal and 16S rRNA gene amplicon sequencing was performed as described in section 2.1.5. The number of sequences per sample after filtering was 12,564 ± 3,954. SOTU sequences were identified using EzBioCloud (Yoon et al., 2017).

2.2.8 Contributions

The mouse work of this trial and the FACS sorting and analysis were done by Annika Osswald and Dr. Soeren Ocvirk at the German Institute of Human Nutrition (DIfE) in Potsdam-Rehbrücke (Nuthetal, Germany). DNA extraction, 16S rRNA gene amplicon sequencing, and raw reads file pre-processing (remultiplexing) were done by Ntana Kousetzi and Dr. Nicole Treichel (AG Clavel, University Hospital of RWTH Aachen, Germany). Sample extraction and BA analysis were performed by Colin Volet at the École Polytéchnique Fédérale Lausanne, Switzerland. I contributed to experimental design, participated in the mouse sampling and immune cell isolation, coordinated BA analysis and 16S rRNA gene amplicon sequencing, and analysed the data from all experiments.

2.3 Effect of DCA-producing *E. muris* on the colonic epithelium in gnotobiotic mice

---

This animal experiment was performed under LANUV ethical approval nr. 81-02.04.2018.A425 in accordance with EU regulation 2010/62/EU. Germfree *Apc*$^{1638N/+}$mice (B6/J.129-(Apc1638N)tm) were colonised with the synthetic microbial community OMM12, consisting of 12 murine bacterial species representing 5 major bacterial phyla of the murine gut (Brugiroux et al., 2016), or OMM12+E (OMM12+ *E. muris* DSM 28560^{T}).

2.3.1 Bacterial stock generation

Small serum bottles (1.5 mL, Wheaton, cat. nr. QZY-z113948100ea-100units) were washed with dH_2O, dried, autoclaved, and imported into an MBraun anaerobic chamber (89.3% N_2, 6% CO_2, 4.7% H_2). Previously anaerobically prepared and autoclaved 20 % glycerol in anoxic PBS (Dulbecco´s Phosphate Buffered Saline, Sigma-Aldrich cat. nr. D8537; supplemented with 500 mg/L L-cysteine, 200 mg/L DTT, 1 mg/L resazurin as anaerobic indicator, and gassed in Hungate tubes) was filled into the serum bottles (500 µL), which were then closed with a crimp seal and autoclaved (121 °C, 20 min). After autoclaving, the serum bottles were stored in the anaerobic chamber to reduce diffusion of oxygen through the rubber lid. All bacterial strains were reactivated from glycerol stocks in Anaerobic Akkermansia Medium (AAM, Table 2.4). After two passages into fresh medium, optical density was measured. Cultures were mixed in OD-adjusted ratios in a 100 mL anaerobic bottle with a rubber stopper (mixing volumes are indicated in Table 2.5). An additional mix was generated with the addition of *E. muris* (OMM12+E). The culture mix was then anaerobically transferred into glass vials filled with anaerobic 20% glycerol in a 1:1 ratio using a syringe flushed with anaerobic gas mix. All single bacterial cultures were checked by microscopy and Sanger sequencing and the culture mixes were checked by 16S rRNA gene amplicon sequencing.

Table 2.4: Protocol for preparing the Anaerobic Akkermansia Medium (AAM), adapted for Hungate tubes. Hemin (1 mg/mL) 0.1 % (x1000): 10 mg in 10 mL EtOH p.a., adding 10 M NaOH solution until dissolving of hemin, filter sterilised and stored at -20 °C. Resazurin stock solution: 50 mg/50 mL dH_2O. Menadione (x1000): 5 mg in 10 mL EtOH p.a., sterile filtered and stored at room temperature (protect from light, store in fridge).

Compound	**Company / Cat. nr.**	**Amount for 1 L**
Brain Heart Infusion (BHI)	Oxoid/CM1135	18.5 g
Tryptone	Oxoid/CM0129	15 g
Yeast Extract	Roth/2363.1	5 g
Di-Potassium hydrogen phosphate (K2HPO4)	Supelco/105104	2.5 g
Hemin stock solution	Sigma-Aldrich/H9039	1 mL
Glucose	Sigma-Aldrich/G8270	0.5 g
Sodium carbonate (Na2CO3)	Merck/106392	0.4 g
Resazurin stock solution (1mg/mL)	Fisher Scientific/10371053	1 mL
Mucin	Sigma-Aldrich/M2378-100G	250 mg
dH2O		1 L
Mix thoroughly, adjust pH to 7.2, heat approximately 10 min in microwave (until colour change).		
Flush with anaerobic gas for at least 20 min until it reaches appr. 50 °C, add the cysteine.		
Cysteine hydrochloride	Sigma-Aldrich/C7352	0.5 g
Transfer to anaerobic chamber and fill into Hungates.		
Autoclave (121 °C, 20 min).		
Mix menadione and FCS, sterile filter into an anaerobic, sterile Hungate tube.		
Add 300 µL of this mix per 10 mL medium.		
Menadione (Vit K3)	Sigma-Aldrich/ M5625-25G	0.5 mg
FCS (complement inactivated)	Sigma-Aldrich/F7524-100ML	30 mL (3%)

Table 2.5: Mixing table for OMM12and OMM12+E cryostocks. Culture was collected from a single Hungate tube per strain, except for *Akkermansia muciniphila* YL44, *Turicimonas muris* YL45, *Acutalibacter muris* KB18, since they grew only to a very low OD. *T. muris* YL45 growth is not measurable by OD, therefore the added amount was arbitrarily defined.

OMM12

Strain	**OD**	**1.8 mL /OD**		**comment**
Bifidobacterium animalis YL2 (DSM 26074)	0.9	2.0	mL	
Muribaculum intestinale YL27 (DSM 28989)	1.2	1.5	mL	
Flavonifractor plautii YL31 (DSM 26117)	0.8	2.1	mL	
Enterocloster clostridioformis YL32 (DSM 26114)	1.2	1.5	mL	
Akkermansia muciniphila YL44 (DSM 26127)	0.3	5.9	mL	Hungate 1
Turicimonas muris YL45 (DSM 26109)	-	5.0	mL	Hungate 1
Blautia coccoides YL58 (DSM 26115)	1.0	1.7	mL	
Clostridium innocuum I46 (DSM 26113)	1.7	1.1	mL	
Bacteroides caecimuris I48 (DSM 26085)	2.0	0.9	mL	
Limosilactobacillus reuteri I49 (DSM 32035)	0.8	2.3	mL	
Enterococcus faecalis KB1 (DSM 32036)	1.8	1.0	mL	
Acutalibacter muris KB18 (DSM 26090)	0.2	9.0	mL	2 day old culture
Extibacter muris (DSM 28560^{T})	-	-	mL	
Total volume	-	34.0	mL	

OMM12+E

Strain	**OD**	**1.8 mL /OD**		**comment**
Bifidobacterium animalis YL2 (DSM 26074)	0.9	2.0	mL	
Muribaculum intestinale YL27 (DSM 28989)	1.2	1.5	mL	
Flavonifractor plautii YL31 (DSM 26117)	0.8	2.1	mL	
Enterocloster clostridioformis YL32 (DSM 26114)	1.2	1.5	mL	
Akkermansia muciniphila YL44 (DSM 26127)	0.4	5.1	mL	Hungate 2
Turicimonas muris YL45 (DSM 26109)	-	5.0	mL	Hungate 2
Blautia coccoides YL58 (DSM 26115)	1.0	1.7	mL	
Clostridium innocuum I46 (DSM 26113)	1.7	1.1	mL	
Bacteroides caecimuris I48 (DSM 26085)	2.0	0.9	mL	
Limosilactobacillus reuteri I49 (DSM 32035)	0.8	2.3	mL	
Enterococcus faecalis KB1 (DSM 32036)	1.8	1.0	mL	
Acutalibacter muris KB18 (DSM 26090)	0.2	9.0	mL	1 day old culture
Extibacter muris (DSM 28560^{T})	0.8	2.2	mL	
Total Volume	-	35.4	mL	

2.3.2 Animal experiment

Five-week old germfree *Apc*$^{1638N/+}$ mice were inoculated orally (50 µL) and rectally (100 µL) at day 0 and day 3 with either the OMM12 or the OMM12+E cryostock (Figure 2.7). Mice weighing <15 g were inoculated with equivalent amounts accounting for a maximum of 10% (v/w) body weight. After 2 weeks to reach stabilised colonisation, chow feed was changed to an experimental control diet (ssniff Spezialdiäten GmbH, cat. nr. S5745-E902), which was sterilised by irradiation with 2x25 kGy. Over the course of the experiment, mice were kept in isocages (IsoCage P system, Tecniplast, Italy).

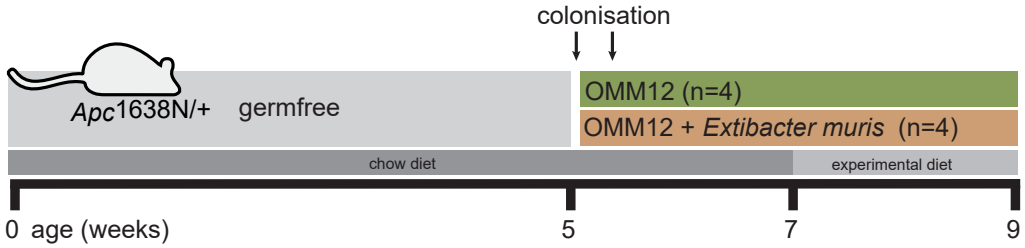

Figure 2.7: Experimental design of the gnotobiotic mouse trial to test epithelial response to an SBA-producing strain in the colon. Mice were colonised twice at 5 weeks of age, either with the synthetic community OMM12 or OMM12+E. The colonisation was repeated 3 days after the first gavage. Each group consisted of two male and two female mice, which were housed in cages of two. Two weeks after the colonisation, the chow diet was switched to a controlled experimental diet.

2.3.3 Sampling procedure

At 9 weeks, mice were culled by isofluran overdose. The colon was carefully removed and immediately put in ice cold sterile PBS (Sigma-Aldrich, cat. nr. D8537-500mL). Fat and mesentery residues were removed from the colon tissue. After cutting the colon open longitudinally with sterile scissors, the gut content was carefully removed with sterile tweezers. Intestinal content was collected, aliquoted and frozen on dry ice.

2.3.4 Epithelial cell isolation

Cell isolation was adapted from a previously established protocol by Dr. Aline Dupont and Dr. Stefan Schlößer, Institute of Medical Microbiology, RWTH Aachen. For this experiment, the protocol was adapted with a special focus on crypt bottom cells. Therefore, cell isolation was tested with *Lgr5* gfp mice analysing different extraction fractions for *Lgr5*-positive cells by FACS. These preliminary experiments also served to establish a FACS protocol, which is specified below. Colon tissue of two mice (one female and one male of the same microbiota/diet group) was pooled in one 50 mL Falcon tube filled with 20 mL ice cold PBS and washed 3 times by vortexing and liquid replacement to remove residual content. The tissue was cut into small pieces (2-5 mm) and transferred into a 50 mL Falcon tube with 30 mL ice cold RPMI + 5% FCS (gibco, cat. nr. 31870-025 and Sigma-Aldrich,

cat. nr. F7524). EDTA was added to a final concentration of 2 mM. The tubes were gently inverted by hand and incubated on a horizontal shaker (Universal Shaker SM 30 Edmund Bühler GmBH) at 110 rpm and room temperature for 15 min. After gently inverting the tubes again, the suspension was passed through a 100 µm cell strainer (Corning, cat. nr. CLS431752). The filtrate was centrifuged (300 g, 5 min, 4 °C) and resuspended in 500 µL PBS-FCS (5 %)-EDTA (0.01 mM) using wide bore pipette tips (VWR Europe, cat. nr. 613-0752), which was called fraction 1. The same procedure was repeated for fractions 2-8. Fractions 6-8 were pooled, centrifuged (300 g, 5 min, 4 °C).

The cell pellets of fractions 6-8 were resuspended in 250 µL PBS-FCS (5 %)-EDTA (0.01 mM) and transferred to a 96-well plate (Greiner BioOne, cat. nr. 651201), blocked with 10 % Normal Rat Serum (Dianova, cat. nr. 012-000-001) and then stained with Epcam-APC (1:200, eBioscience™ cat. nr. 17-5791-82) and CD45-BV510 (1:200, BioLegend, cat. nr. 103138) for 20 min. DAPI (1:200, Roth, cat. nr. 6335.1) was added just before the last centrifugation (300 g, 5 min, 4 °C).

After staining, cells were sorted for single, live, CD45-negative, Epcam-positive cells with a BD FACSAria™ Ilu, equipped with a 100 µm nozzle and kept at 4 °C. Cells were collected in 5 mL PBS-BSA (1 %) (Merck, art. nr. SRE0036), counted, and evaluated for quality and shape with trypan blue (1:1 mix). Cells were resuspended in a smaller volume to have approximately 1,000 cells/µL with the aim of recovering 10,000 cells for RNA sequencing. The following steps were carried out according to the Chromium Next GEM Single Cell 3' Reagent Kits v3.1 protocol, CG000204 Rev D (10x Genomics, Inc., United States). Storage of intermediate steps was done according to the protocol.

2.3.5 Sequencing

After library preparation and quality control, RNA sequencing was performed on a NextSeq 550 with paired-ends (2×75 bp). The target sequencing depth was 20,000 read pairs per cell. For the OMM12+E sample, an estimated number of 5,950 cells with 51,998 mean reads per cell, 7,144 median UMI counts per cell, and 1,544 median genes per cell was recovered. The sequencing saturation was 41.8 %. For the OMM12 sample, an estimated number of 8,161 cells were sequenced, with 32,940 mean reads per cell, 4,537 median UMI counts per cell, and 1,121 median genes per cell. The sequencing saturation was 36.9%.

2.3.6 Analysis

In the basic analysis using the Cell Ranger pipeline (version 6.1.1), reads were aligned to the mouse genome (refdata-cellranger-mm10-3.0.0). Sample integration, creation of a Seurat object, and filtering was done by Johannes Schöneich (AG Costa and AG Hornef, RWTH Aachen) using the scRNA pipeline (`https://github.com/CostaLab/scrna_seurat_pipeline`), which performs quality check, normalisation, feature selection, dimension reduction, clustering, and pathway analysis. Data was log-normalised with a scale factor of 10,000 and centered with a scale maximum of 10. Cells with a number of genes (nFeature_RNA) lower than 400 and number of molecules per cell (nCount_RNA) higher than 40,000 were filtered out. Effects of cell cycling (combined ef-

fects of the calculated G2M.Score and S.Score), mitochondrial (percent.mt) and ribosomal genes (percent.ribo) were regressed out for cell clustering. Genes from the X-inactivation center (*Xist*, *Tsix*, *Jpx*, *Ftx*) were filtered out before clustering to reduce sex-specific effects. Scaling (ScaleData command in Seurat package) shifted the mean gene expression for each gene to 0 and scales expression of genes so that the variance across cells is 1. Unsupervised clustering was performed using a shared nearest neighbors graph with a resolution of 0.3. The downstream analysis using the created seurat object was done by me using the Seurat R package version 4.1.1 (Satija et al., 2015; Butler et al., 2018; Stuart et al., 2019; Hao et al., 2021) using "RNA" as the default assay. UMAP clustering was done with the function "DimPlot" using reduction = "INTE_UMAP". Cell cluster were identified using cell type markers published by Schaum et al. (2018). A permutation test was done to calculate relative proportional cluster differences using the R library 'scProportionTest' available at `https://github.com/rpolicastro/scProportionTest` (scProportionTest version v1.0.0, accessed on 9 September 2023; Miller et al. 2021b). Differential gene expression analysis was performed for each cluster separately with the Seurat function Findmarkers using the Wilcoxon test and default settings.

2.3.7 16S rRNA gene amplicon analysis

Genomic DNA from colon content was isolated and sequenced as described in section 2.1.5. All samples had a minimum of 6,396 reads, with an average of 11,718±3,639 reads per sample. Sequences of the OMM12 strains were identified by blasting against published 16S rRNA gene sequences (NCBI) or else identified using EzBioCloud (Yoon et al., 2017).

2.3.8 BA analysis and SCFA analysis

BA analysis from caecal content was analysed as described in section 2.2.6. For SCFA analysis, approximately 20 mg of mouse caecal content were added to a 2 mL bead beater tube (FastPrep-Tubes, Matrix D, MP Biomedicals Germany GmbH, Eschwege, Germany) and extracted with 1 mL methanol using a bead beater FastPep-24TM 5G, MP Biomedicals Germany GmbH, Eschwege, Germany) equipped with a CoolPrepTM (MP Biomedicals Germany, cooled with dry ice) 3 times (20 s, 6 m/s, 30 s break in between).

Targeted analysis of SCFA was done using the 3-NHP method of Han et al. (2015). Shortly, 40 µL extract were mixed with 15 µL of isotopically labelled standards (ca. 50 µM), 20 µL of 120 mM EDC HCl-6% pyridine-solution and 20 µL of 200 mM 3-NPH HCL solution. Samples were incubated (30 min, 40 °C, 1000 rpm) on an Eppendorf Thermomix (Eppendorf, Hamburg, Germany) and 900 µL acetonitrile/H_2O (50/50, v/v) were added. After centrifugation (13,000 U/min, 2 min), the clear supernatant was used for analysis.

Quantitative measurement was done using a QTRAP 5500 mass spectrometer (Sciex, Darmstadt, Germany) coupled to an ExionLC AD (Sciex, Darmstadt, Germany) ultrahigh performance liquid chromatography system. Electrospray voltage was -4500 V, curtain gas 35 psi, ion source gas 1 was set to 55, ion source gas 2 to 65 and the temperature was set to 500 °C. Multiple reaction monitoring-

parameters were optimised using commercially available standards. The chromatographic separation was done on a 100 × 2.1 mm, 100 1.7 µm, Kinetex C18 column (Phenomenex, Aschaffenburg, Germany) with 0.1% formic acid (eluent A) and 0.1% formic acid in acetonitrile (eluent B) as elution solvents. An injection volume was 1 µL and the flow rate was set to 0.4 mL/min. A gradient elution was used, starting at 23% B for 3 min, then increased to 30% B at 4 min, further increased to 40% B at 6.5 min, and 100% B at 7 min, which was held for 1 min. At 8.5 min, the column was equilibrated at starting conditions (23% B). The column oven temperature was 40 °C and the autosampler 15 °C. Data acquisition and instrumental control were done with the Analyst 1.7 software (Sciex, Darmstadt, Germany).

2.3.9 Contributions

This work was supported by the Flow Cytometry and Genomics Core Facilities of the Interdisciplinary Center for Clinical Research (IZKF) Aachen within the Faculty of Medicine at RWTH Aachen University. Basic analysis of the sequencing data (section 2.3.6) was done by the Genomics Facility. Sample integration, creation of a Seurat object, and filtering was done by Johannes Schöneich (AG Costa and AG Hornef, RWTH Aachen) using the scRNA pipeline (`https://github.com/CostaLab/scrna_seurat_pipeline`). DNA extraction, 16S rRNA gene amplicon sequencing, and raw reads file pre-processing (remultiplexing) were done by Ntana Kousetzi and Dr. Nicole Treichel (AG Clavel, University Hospital of RWTH Aachen, Germany). Sample extraction and BA analysis was performed by Colin Volet at the École Polytéchnique Fédérale Lausanne, Switzerland. SCFAs were analysed at the Bavarian Center for Biomolecular Mass Spectrometry (BayBioMS) by Karin Kleigrewe. Aline Dupont (AG Hornef, University Hospital of RWTH Aachen, Germany) and Atscharah Panyot (AG Clavel,University Hospital of RWTH Aachen, Germany) helped during cell isolation and library preparation. I conducted the animal experiment, did the cell isolation and did analysis of data provided as a seurat object by Johannes Schöneich. Further, I analysed the BA and SCFA data and conducted the downstream analyses of remultiplexed sequences from 16S rRNA gene amplicon sequencing.

2.4 Effect of the bile acid scavenger colestyramine in $APC^{1311/+}$ pigs

This experiment was approved by the Federal Government of Bavaria (permit no. ROB55.2-2-2532.Vet_02-18-33). The pigs were provided by at the Chair of Livestock Biotechnology of the Technical University of Munich (Faculty of Life Science Weihenstephan, Germany). The pig trial was conducted at the animal facility Thalhausen, Life Science Campus Weihenstephan, TU Munich.

2.4.1 Animal experiment

$APC^{1311/+}$ pigs, generated by cross-breeding German land race and minipigs, were used for this trial. At 3 months of age, all pigs underwent colonoscopy to assess initial disease state. Briefly, pigs were narcotised, the distal colon was flushed with tap water to remove content, and colonoscopy was done

using a human sized endoscope (STORZ). Systemic blood was taken from the vena jugularis and plasma was obtained by centrifugation (1,800 g, 10 min). The pigs were then divided into three groups to reach an equal distribution of males and females, polyp state, and litters. At 4 and 7 months of age, all animals were weighed and faecal samples were collected for metabolite measurements and 16S rRNA gene amplicon analysis (snap frozen).

Each pig was fed with 1 kg feed per day. The CTRL and RL diet were adapted from the previous feeding trial (ssniff Spezialdiäten GmbH, cat. nr. S5745-S084 and S5745-S086) (Wortmann et al., 2023). The third group of pigs received the RL diet supplemented with 12g/kg of the BA sequestrant colestyramine (ssniff Spezialdiäten GmbH, cat. nr. S5745-S088; Colestyramin-ratiopharm®, approval nr. 16834.00.00), which is in the range of 4-16 g/day for adult individuals as recommended by the manufacturer. The exact composition of the diets is listed in Appendix Table A.3. To account for the added colestyramine in the total dry volume, cellulose was added to the CTRL and RL diet as a placebo (see Appendix Table A.3).

2.4.2 Sampling procedure

After the colonoscopy at 7 months, the pigs were culled with a cattle gun while they were still in narcosis. Small intestine and large intestine were separated. For the small intestine, a small hole was cut into the mucosa at a proximal (1 m below the sphincter of Oddi) and distal site (1 m before the caecum) to obtain intestinal content. Caecal content was also collected through a small cut in the tissue. The colon was opened longitudinally to assess the polyp state and content was collected from the middle colon. Tissue samples were collected from the proximal colon (1 m below the caecum), middle colon and rectum (30 cm before the anus). Faecal and gut content samples as well as plasma samples were snap frozen and stored at -80 °C. Formalin-fixed, paraffin embedded tissue was stored at room temperature.

2.4.3 Histology

Tissue samples of the proximal colon, middle colon and rectum were fixed using 4 % paraformaldehyde for 24 h and embedded in paraffin wax. For CD3 and Ki67 staining, sections of 3 µm were deparaffinised and dehydrated before unmasking with 10 mM sodium citrate buffer (pH 6.0) and endogenous peroxidases inactivation in 3% H_2O_2 for 10 min. Sections were blocked with 2% goat serum in PBS for 1 h, followed by staining with primary antibodies Ki67 (Rabbit, DSC Innovative Diagnostik-Systeme, cat. nr. KI681C002, dilution 1:400) and CD3ε (mouse, Southern Biotech, dilution 1:100) was done at 4 °C over night. Incubation with secondary antibodies for Ki67 (Goat Anti-Rabbit IgG, Santa Cruz, cat. nr. sc-2780, dilution 1:400) and CD3 (m-IgGκ BP-Biotin, Santa Cruz Biotechnology, cat. nr. sc-516142, dilution 1:200) was done at 4 °C for another night. Peroxidase activity was detected using diaminobenzidine (DAB) substrate for Ki67 stained samples or the VECTASTAIN® Elite© ABC Kit (Vectorlab, cat. nr. PK-6100), respectively. For Alcian Blue - Periodic acid-Schiff (AB-PAS) staining, deparaffinised sections were stained with Alcianblue solution (Sigma, cat. nr. A-4157, 1% in 3% acetic acid, pH 2.5), washed with running dH_2O for 2 min, fol-

lowed by 10 min incubation with 1% periodic acid (Sigma, cat. nr. SLCH5688). Sections were again washed with running dH_2O for 10 min and incubated with pre-warmed (room temperature) Schiffs reagent for 10 min (Sigma, cat. nr. HX04811633) at room temperature. Slides were washed for 5 min in running hot water at evaporation temperature, two times for 30 s with dH_2O, and stained with haematoxylin (Roth, cat. nr. T685.3) for 30 s. This was followed by washing for 5 min in running hot water and dehydration steps (2 min 70% ethanol, 2 min 96% ethanol, 2 min 100% ethanol, 2 min xylene). Ten randomly selected fields (magnification x40) from each tissue section were analysed. Values are presented as the percentage of the stained cells per area. For statistical analysis, the mean value of all 10 measurements per sample was used. Staining of Ki67 was considered positive and quantified only when detected in cell nuclei.

2.4.4 16S rRNA gene amplicon analysis

Genomic DNA from gut content and faeces was isolated and sequenced as described in section 2.1.5, however, an updated version of SILVA (release 138.1) was used as a reference Pruesse et al. (2012). Samples with <5,000 filtered reads were removed, resulting in the exclusion of 3 small intestinal samples (2 from the proximal small intestine and 1 from the distal small intestine) before IMNGS analysis and 33,348 ±20,607 filtered reads per sample. IMNGS was run for all samples together, but for downstream analysis with Rhea and for statistical analysis, samples were separated by gut region.

2.4.5 BA and SCFA analysis

Samples for BA and SCFA analysis were collected in 15 mL Precellys tubes (Tissue grinding CK-mix50_15mL, cat. nr. P000949-LYSK0-A, Bertin Technologies, France), snap frozen, and stored at -80 °C until extraction and analysis. SCFA were measured as described in section 2.3.8, but using 100 mg gut content and 5 mL methanol as extraction solvent instead of 100 mg in 1 mL methanol. BA analysis was done as described by Reiter et al. (2021). Classification of SBAs and PBAs was done based on current literature (Vico-Oton et al., 2023; Studer et al., 2016; Zhang et al., 2012). Only BAs that were present in 50% of the samples of a group (same diet/region/time) were included in the analysis. For statistics, only BAs with a total prevalence of 30% per region were considered. UDCA is a PBA in rodents, but an SBA in humans (Honda et al., 2020; Li and Dawson, 2019). Due to their similarity to humans, UDCA was classified as a SBA in pigs in this thesis.

2.4.6 Lipidomics

Sample preparation for gut content was done as described by Schött et al. (2018). Resulting homogenates were used for both fatty acid (FA) and sterol/stanol analysis. Sterol analysis was done as described by Kunz and Matysik (2019). FA concentrations were measured by gas chromatography coupled to mass spectrometry (GC-MS) as described before (Ecker et al., 2012), with slight modifications. First, samples were derivatised to FA methyl esters (FAME). GC was done using the following settings: Initial column temperature 50 °C for 0.75 min, followed by increases of 40 °C/min to 110 °C,

6 °C/min to 210 °C, 15 °C/min to 250 °C, which was held for 2 min. Iso- and anteiso-FAMEs standards were used to analyse branched chain FAs and to calibrate the instrument response.

2.4.7 Contributions

The following persons contributed to the pig trial: Prof. Angelika Schnieke (design), Dr. habil. Krzysztof Flisikowski (design and supervision), Steffen and Viola Löbnitz (animal care) (all from the Institute of Livestock Biotechnology, TU Munich, Freising).Additional support for the sampling and some of the follow-up analyses was provided by other members of the Institute of Livestock Biotechnology: Liang Wei, Dr. habil. Tatiana Flisikowska, Thomas Winogrodzki, Alexander Rinke Carrapeiro. Liang Wei contributed additionally to immunostaining and analysis of histological samples. Scoring of normal tissue was provided by Dr. Soeren Ocvirk, German Institute of Human Nutrition (DIfE) in Potsdam-Rehbrücke (Nuthetal, Germany). DNA extraction, 16S rRNA gene amplicon sequencing, and raw reads file pre-processing (remultiplexing) were done by Ntana Kousetzi and Dr. Nicole Treichel (AG Clavel, University Hospital of RWTH Aachen, Germany). FA and sterol/stanol analysis of gut content as well as lipidomic analysis of plasma samples was performed in the group of PD Dr. Gerhard Liebisch and Silke Matysik at Uniklinik Regensburg. BA and SCFA were measured at the Bavarian Center for Biomolecular Mass Spectrometry (BayBioMS). David Wylensek (AG Clavel, University Hospital of RWTH Aachen, Germany) and me coordinated the experiment, and planned and executed sampling together with the persons aforementioned. Downstream analyses of remultiplexed sequences from 16S rRNA gene amplicon sequencing were done by me, as well as downstream analysis of all measurements and statistics.

2.5 Statistics and data visualisation

Graphs were created with R in RStudio (R Core Team, 2022; Posit team, 2023) using the tidyverse (Wickham et al., 2019). Statistics were done with the package rstatix (Kassambara, 2023). Comparison of samples over time was done by paired Wilcoxon signed rank test. Comparisons between 3 or more group were done by Kruskal-Wallis test followed by Dunn´s multiple comparisons with Benjamini-Hochberg correction for multiple testing. Experiment-specific criteria used for testing are stated separately in the corresponding result sections. Microbiota β-diversity plots were created in Rhea (Lagkouvardos et al., 2017). Fisher exact tests were also done in Rhea (Lagkouvardos et al., 2017). Heatmaps were created with the ComplexHeatmap package (Gu et al., 2016). Mean values for heatmap visualisation of bacterial families were calculated by considering NAs (non-detected) as zero values. The survival analysis in the FMT trial was done using the R package survival (Therneau, 2022).

CHAPTER 3

Results

The results of this thesis are divided into four sections. First, the effects of pig-derived CRC-associated microbiota on tumour development were tested by performing FMT in germfree *Apc*$^{1638N/+}$ mice. Second, a gnotobiotic mouse model for experimental CRC (AOM/DSS) was used to test the causal effects of the SBA-producing bacterium *E. muris* DSM 28560^{T} (Streidl et al., 2019). Third, the same species (*E. muris*) was used in *Apc*$^{1638N/+}$ mice colonised with the synthetic community OMM12 to study colonic epithelial cell responses at the single-cell level. Finally, an intervention experiment was conducted in *APC*$^{1311/+}$ pigs to test the potentially protective role of the BA colestyramine, which was added to a tumour-promoting Western diet. Together, these experiments represent a framework to study the causal role of SBA and the bacteria that produce them on CRC development.

3.1 Faecal microbiota transplant in a mouse model of CRC

In a previous feeding trial in *APC*$^{1311/+}$ pigs (Wortmann et al., 2023), the effect of a Western diet (RL diet) on tumour development was tested. The RL diet led to significant shifts in microbiota profiles and increased polyp size and number. Furthermore, significantly higher levels of DCA were found in faeces of the RL-fed pigs compared to CTRL-fed pigs (Wortmann et al., 2023). To test the causal role of the shifted microbiota and corresponding metabolic changes, such as increased DCA production, in disease progression, an FMT was conducted. Faecal microbiota of representative pigs fed the CTRL or RL diet (CTRL vs. RL donor-group; n = 3 each) were transplanted into germfree *Apc*$^{1638N/+}$ mice by oral gavage. After three weeks in isocages to reach a stabilised colonisation, the mice were transferred to filter-top cages and were fed a synthetic control diet (CD diet) or CD supplemented with 0.2% cholic acid (BA diet) for additional 23 weeks.

3.1.1 FMT efficacy was low

To assess FMT efficacy, the total number of SOTUs (richness) and the number of equally-common SOTUs above 0.25% rel. abundance (Shannon effective number of species) were compared between the donors (2 cryostocks from each of the 3 donor pigs per diet) and recipients (mouse caecal content; n = 37 for CTRL and 50 for RL). Compared to the inocula used for gavage, both richness and Shannon effective counts were reduced approximately 3-fold in the colonised mice, independently of the donor-group (Figure 3.1 **a**). In line with the reduced number of SOTUs, the overall microbiota profiles based on phylogenetic distances showed a clear separation between microbiota from the donors and recipients (Figure 3.1 **b**). Nonetheless, profiles between the RL and CTRL recipient mice still formed two distinct clusters.

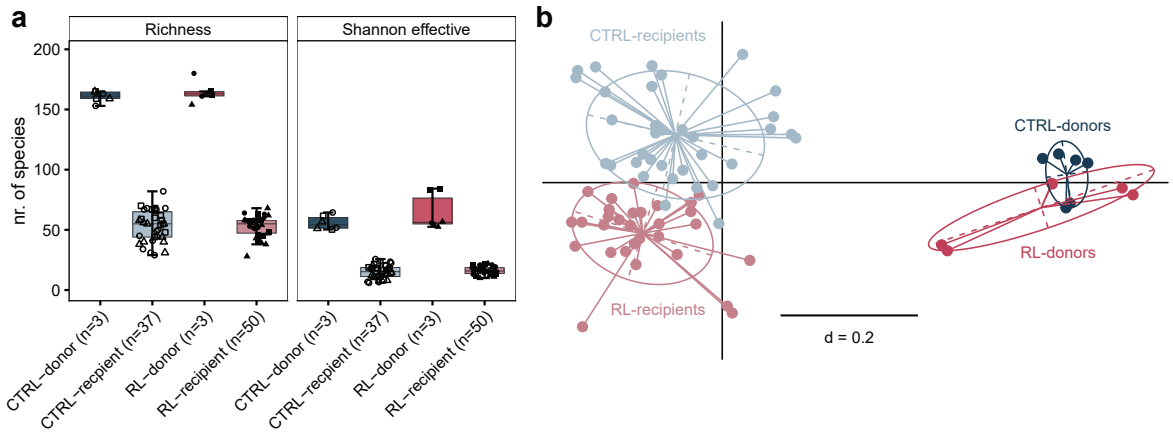

Figure 3.1: FMT efficacy at the level of α- and β-diversity, as analysed by 16S rRNA gene amplicon sequencing in caecal content. **a** Richness, number of observed SOTUs; Shannon effective counts, estimate for the number of equally dominant species. Different donor microbiota are represented with different shapes. **b** Non-metric multidimensional scaling (NMDS) plot of microbial profiles based on generalised UniFrac distances. The microbiota of recipients (mice, light colours) and donors (pigs, dark colours) are coloured according the donor-group (RL, red; CTRL, blue). Statistics for **b**: PERMDISP: p=0.004, PERMANOVA p=0.001. Donor microbiota: n=3 per diet (n=2 stocks sequenced per donor); recipient microbiota: n=37 for CTRL and n=50 for RL (10-19 recipients per donor).

When looking at the presence of all 269 detected SOTUs in the different donor/recipient groups, 145 SOTUs were only present (at least once) in donor pigs, 64 SOTUs were only detected in at least one recipient mouse, and 23 SOTUs were shared between donors and recipients (Figure 3.2 **a**). When comparing only recipient mice, 20 SOTUs were exclusively found in the RL group (i.e. those mice receiving the microbiota from pigs fed the RL diet) and 40 SOTUs were only present in CTRL mice. For the subset of SOTUs that were characteristic for donor pigs or recipient mice, i.e. present in all donor pig samples or all recipient mice of a donor-group (RL or CTRL), rel. abundances were very different between donors and recipients (Figure 3.2 **b**). However, two SOTUs were shared between all donor pigs and all recipient mice at a similar rel. abundance, independent of diet: SOTU6, 99.75% similarity to *Blautia faecicola* and SOTU25, 99.06% similarity to *Phascolarctobacterium*

succinatutens (Figure 3.2 **c**). Three SOTUs were specific for the CTRL groups: SOTU328 (93.57% similarity to *Xylanibacter rarus*, formerly *Prevotella rara*) was most successfully transferred (Figure 3.2 **c**); SOTU343 (88.31% similarity to *Duncaniella muris*) and SOTU635 (87.97% similarity to *Sphaerochaeta pleomorpha*), were only found (rel. abundance >0.25%) in 1 and 2 recipient mice, respectively.

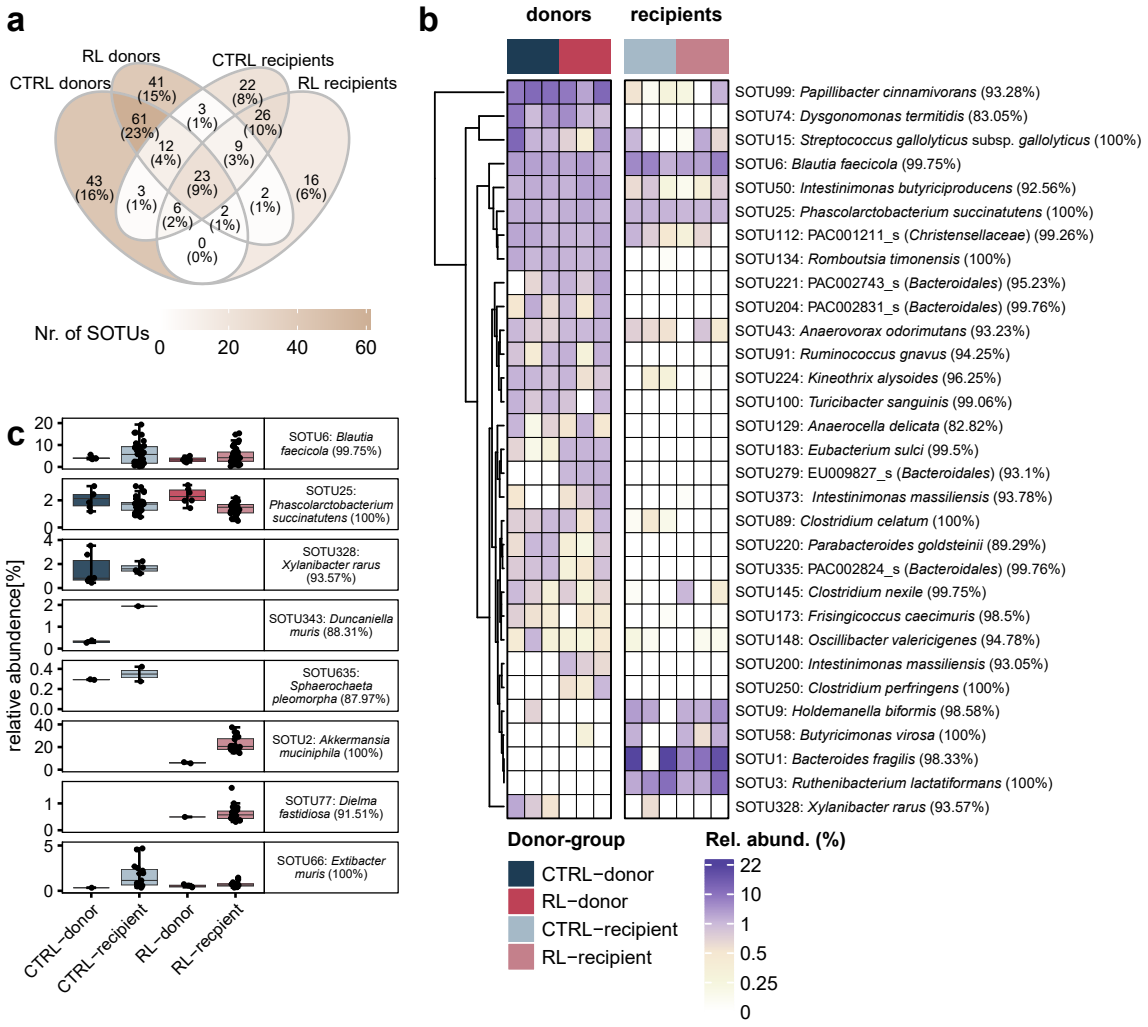

Figure 3.2: FMT efficacy at the level of SOTUs. **a** Venn diagram of SOTUs that were present in either donor or recipient group. All SOTUs that were detected in at least one donor (cryostock of pig faeces) or recipient (mouse caecum content) with a rel. abundance above 0.25% were considered. **b** SOTUs that were present in all donors or recipients of a microbiota group. Their respective mean rel. abundance in the cryostocks used for the inoculation (donors; left) and the recipient mice (right) are shown with a colour gradient. Each column represents stocks or recipients of a given donor pig. For each SOTU, the name of the closest taxonomic hit is indicated, with the percentage sequence similarity in brackets. **c** Rel. abundance of selected SOTUs based on donor/recipient specificity. Donor microbiota: n=3 per diet (2 stocks per donor); recipient microbiota: n=37 for CTRL (14/13/10 mice per donor) and n=50 (19/17/14 mice per donor) for RL. A rel. abundance <0.25% was considered as zero for calculating the average rel. abundance in **b**. In **c**, only values with a rel. abundance >0.25% are shown.

Two SOTUs that were characteristic for the RL donor-group - SOTU2 (*A. muciniphila*, 100% similarity) and SOTU77 (*Dielma fastidiosa*, 91.51% similarity) - were unique for the RL donor-group and successfully transferred to recipient mice (Figure 3.2 **c**). In contrast, three other SOTUs were uniquely found in all donor pigs, but not in RL recipient mice: SOTU200 (93.05% similarity to *Intestinimonas massiliensis*), SOTU250 (100% similarity to *Clostridium perfringens*), and SOTU279 (93.10% similarity to an unnamed *Bacteroidales* species) (Figure 3.2 **b**). To specifically look at the presence of BA-metabolising bacteria, all SOTU sequences from both donors and recipients were blasted against 16S rRNA gene sequences from strains known to produce SBAs by 7αDH (Table 2.1). Only one SOTU (SOTU66) shared >97% similarity with the sequence from DCA-producing species: 100% sequence similarity to *E. muris* and 98.75% similarity to *C. hylemonae*. However, it was found in donors and recipients of all groups (Figure 3.2 **c**).

The discrepancy between donor pigs and recipient mice that was observed at the level of SOTUs was further investigated at the level of bacterial families. Whilst 27 families were found in both donors and recipients (at least one donor pig or one recipient mouse, rel. abundance >0.25%), 19 families were found exclusively in the donors and 14 families exclusively in the recipient mice (Figure 3.3 **a**). Similar to the analysis at the SOTU level, families that were characteristic for a donor or recipient group (RL or CTRL) showed different profiles (i.e., different rel. abundances) depending on the donor pig microbiota (Figure 3.3 **b**). Comparing the most abundant families (mean rel. abundance >15% within a donor or recipient group) between donors and recipients, a high transfer efficiency was observed for *Bacteroidaceae*, *Tannerellacae*, and *Akkermansiaceae*, which had higher rel. abundances in recipients than in the donors, indicating that these families colonised well after transplant. Good engraftment was especially pronounced for the family *Akkermansiaceae*, which was only subdominant in CTRL donors (see Appendix Figure A.1). *Oscillospiraceae*, on the contrary, dropped in rel. abundance due to transfer (Figure 3.3 **c**), indicating that this family profited either from pigs as a host or from their diet. This was even more the case for *Lactobacillaceae*, which were not transferred successfully (only subdominant in some of the recipient mice, Appendix Figure A.1), despite their high rel. abundance in the donor pigs. Transfer efficacy at the level of bacterial phyla is provided in the Appendix (Appendix Figure A.2).

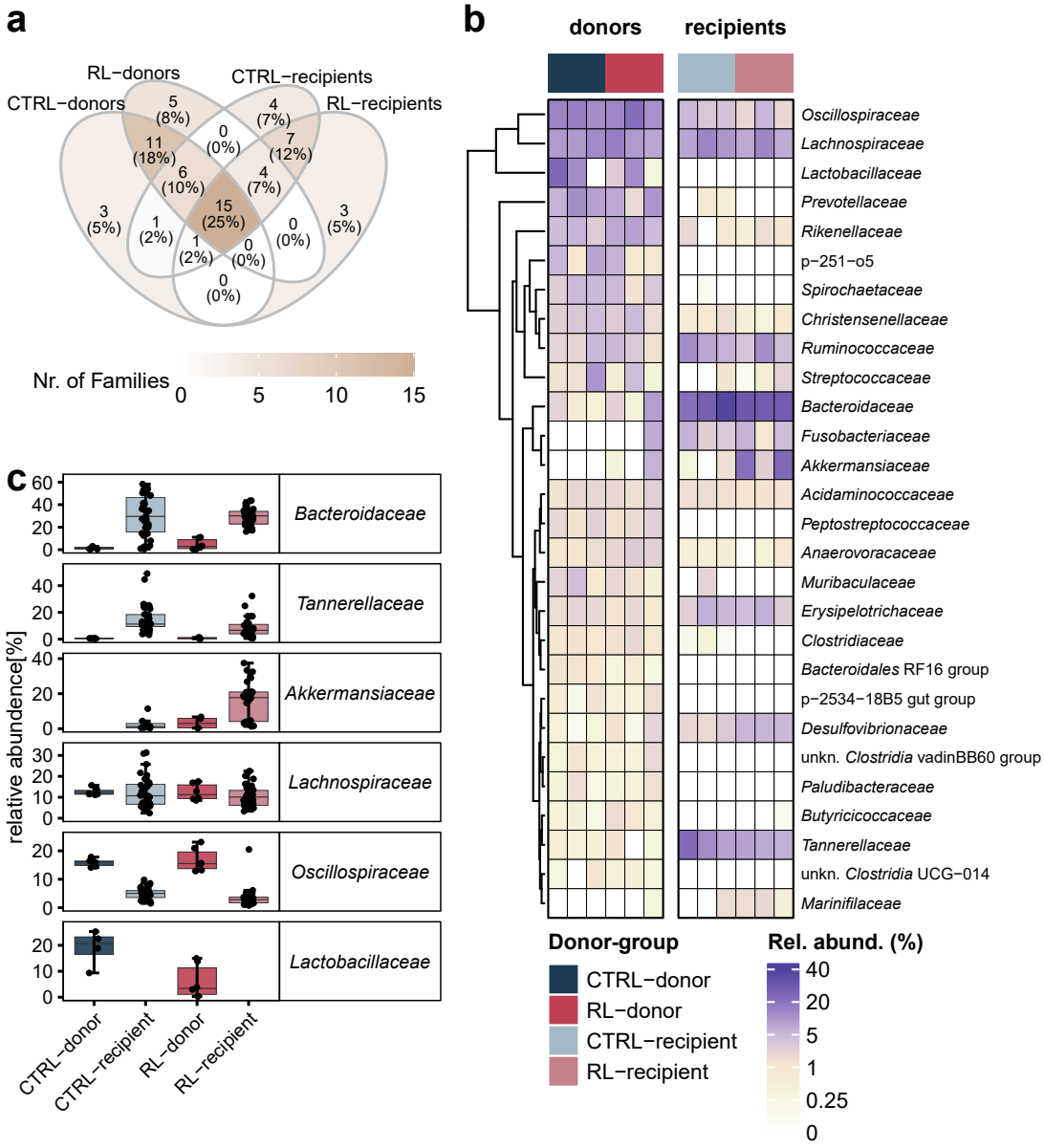

Figure 3.3: FMT efficacy at the level of bacterial families. **a** Venn diagram of bacterial families that were present in either donor or recipient group. All families that were detected in at least one donor (cryostock) or recipient (mouse) with a rel. abundance >0.25% were considered. **b** SOTUs that were present (rel. abundance >0.25%) in all donors or recipients of a microbiota group. Their respective mean rel. abundance in the cryostocks used for the inoculation (donors; left) and the recipient mice (right) are shown with a colour gradient. Each column represents stocks or recipients of a given donor pig. **c** Rel. abundance of the most abundant families in donors or recipients, respectively. Donor microbiota: n=3 pigs per diet (n=2 stocks sequenced per pig); recipient microbiota: n=37 for CTRL (14/13/10 mice per donor) and n=50 (19/17/14 mice per donor) for RL. A rel. abundance <0.25% was considered as zero for calculating the average rel. abundance in **b**. In **c**, only values with a rel. abundance >0.25% are shown. Plot without rel. abundance cut-off of 0.25% can be found in the Appendix (Appendix Figure A.1)

3.1.2 FMT donor and recipient diet affected microbiota profiles in mice

After colonisation with either RL or CTRL microbiota (two donor-groups, each comprising microbiota from three different donors), the recipient mice and control germfree mice were divided into two diet groups for 23 weeks: CD diet or BA diet to enhance the formation of SBAs in the colon. The effect of the different microbiota used for colonisation (donor-groups) and diets were investigated at the end of the feeding period.

At the level of microbiota structure (i.e. comparison of profiles by β-diversity analysis), overall phylogenetic profiles were significantly different between donor-group and diet combinations (PERMANOVA, p =0.001) (Figure 3.4 **a**). Richness and Shannon effective counts (α-diversity parameters) showed a trend towards lower richness with the BA diet, especially in CTRL recipient mice (Figure 3.4 **b**). Pairwise comparisons revealed that the BA diet did not have a significant effect (PERMANOVA p.adj =0.057) in the case of RL recipients (Figure 3.4 **c**). In contrast, diet led to significantly different profiles (PERMANOVA p.adj =0.017) in CTRL recipients (Figure 3.4 **d**). Euclidean clustering of the 50 SOTUs that occurred at >1% rel. abundance in at least one group revealed that recipients of the same donor microbiota were most similar to each other (Figure 3.5 **a**). Recipients of microbiota from donors 916 and 937 (both RL donor microbiota) clustered separately from the rest of the recipient groups. This was likely driven by *A. muciniphila* (SOTU2, 100%) and *Phocaeicola vulgatus* (SOTU4, 99.76%), which were also detected in the RL donors (Figure 3.5 **a**). Separation of the RL recipients of donor microbiota 923 was driven by the very low rel. abundance of *B. fragilis* (SOTU1, 98.33%). Interestingly, *B. wadsworthia* (SOTU33, 100%), which has been associated with CRC in metagenomic datasets (Lee et al., 2023; Yachida et al., 2019), clustered together with *B. thetaiotaomicron* (SOTU141, 100%), which encodes a *bsh* gene (Yao et al., 2018), and *Fusobacterium varium* (SOTU31, 88%) (Figure 3.5 **a**). The genus *Fusobacterium*, mostly represented by *F. nucleatum*, has been associated with colon and caecum tumour tissue (Roelands et al., 2023). Statistical comparison was done for prevalent and abundant SOTUs (prevalence >80% of all mice, rel. abundance >1%). Significantly higher levels of *B. fragilis* and *Mucispirillum schaedleri* (a member of the family *Deferribacteraceae*) were detected in the CTRL_BA group compared to all other groups (Figure 3.5 **b**), indicating that the BA diet had a stronger influence on microbiota composition of CTRL mice. The rel. abundance of Desulfovibrio piger (SOTU26) was more influenced by donor-group than diet and was decreased in RL vs. CTRL recipients. Two SOTUs were only detected in RL recipient mice: SOTU33 (*B. wadsworthia*, 100%) and SOTU 8 (*Bacteroides uniformis*, 100%) (Figure 3.5 **c**). No SOTUs were unique to all CTRL recipient groups.

The only SOTU with high sequence similarity to a known SBA producer (SOTU66, 100% sequence similarity to *E. muris* and 98.75% similarity to *C. hylemonae*) was characterised by higher rel. abundance in the caecum of CTRL recipient mice independent of their diet; however, this result did not reach statistical significance (Figure 3.5 **d**). One SOTU (SOTU110) had 91.25% similarity to *C. scindens*, which is also a known 7αDH+ strain, and was only detected in one RL recipient group (937_BA) (Figure 3.5 **a**). The low sequence similarity however suggests that this SOTU likely belongs to a different genus.

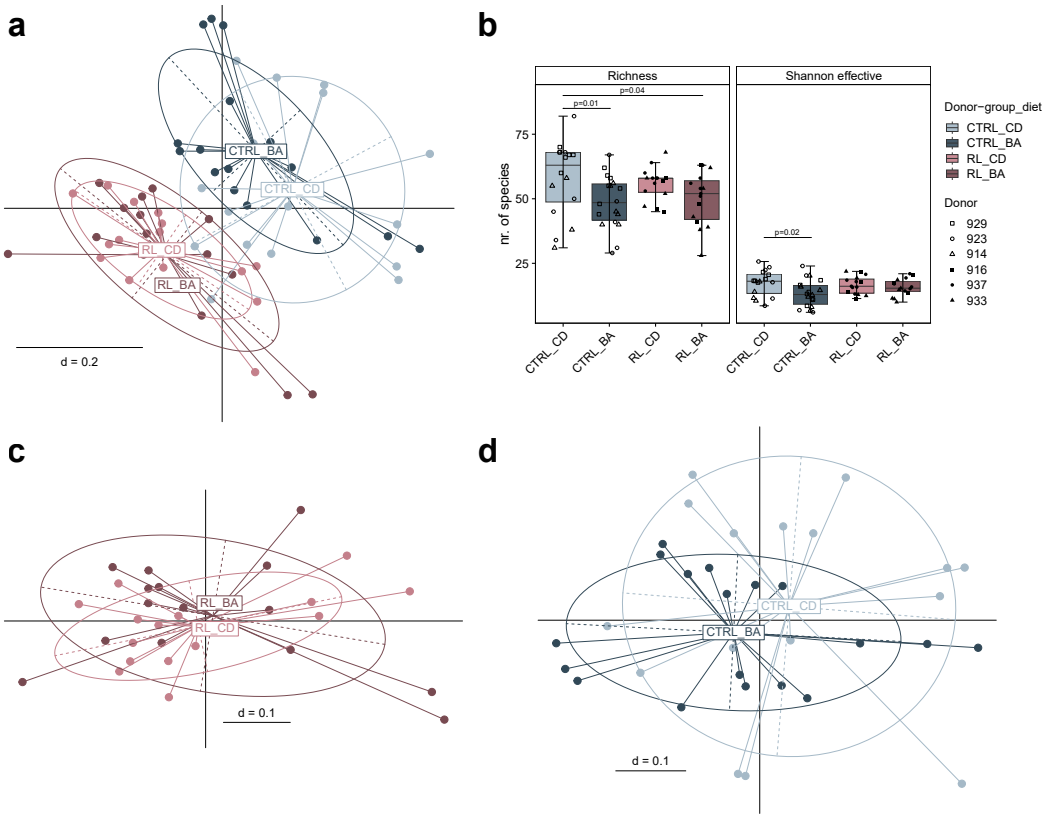

Figure 3.4: Caecal microbiota structure in recipient mice according to donor-group and diet. **a** Generalised UniFrac distances visualised as a NMDS plot (PERMDISP p =0.079, PERMANOVA p =0.001). **b** Richness and Shannon effective counts per donor-group and diet combination. **c** Pairwise comparison of RL recipient mice on CD and BA diet (PERMDISP p.adj =0.44, PERMANOVA p.adj =0.057). **d** Pairwise comparison of CTRL recipient on CD and BA diet (PERMDISP p.adj =0.36, PERMANOVA p.adj =0.017). CTRL = control donors, RL = RL donors, CD = control diet, BA = bile acid diet (0.2% CA). Shapes indicate the different microbiota donors. Statistics: Kruskal-Wallis with Dunn's multiple comparisons. Unadjusted p-values <0.05 are shown (no significance after Benjamini-Hochberg adjustment).

A significant increase in *Desulfovibrionaceae* was observed in RL recipients (Figure 3.5 **e**). This was partly due to the bloom of *B. wadsworthia*, which outweighed the decrease observed for *D. piger*, another member of this family (Figure 3.5 **b**). Differences in other bacterial families were influenced by combinations of donor-group and diet rather than a single parameter. *Oscillospiraceae* for example were significantly lower in RL vs. CTRL recipients only when mice were fed the BA diet. A similar trend was observed for *Ruminococcaceae*, which were significantly lower in RL recipients on BA diet compared to CTRL recipients on CD diet. In the case of *Tannerellaceae*, RL recipients on the CD diet had significantly lower rel. abundances compared to CTRL recipients, which seemed to be recovered in RL recipients fed the BA diet. Other dominant families (*Acidaminococcaceae, Bacteroidaceae, Erysipelotrichaceae, Fusobacteriacae* and *Lachnospiraceae*) showed no significant differences between the different donor-diet groups (Figure 3.5 **e**).

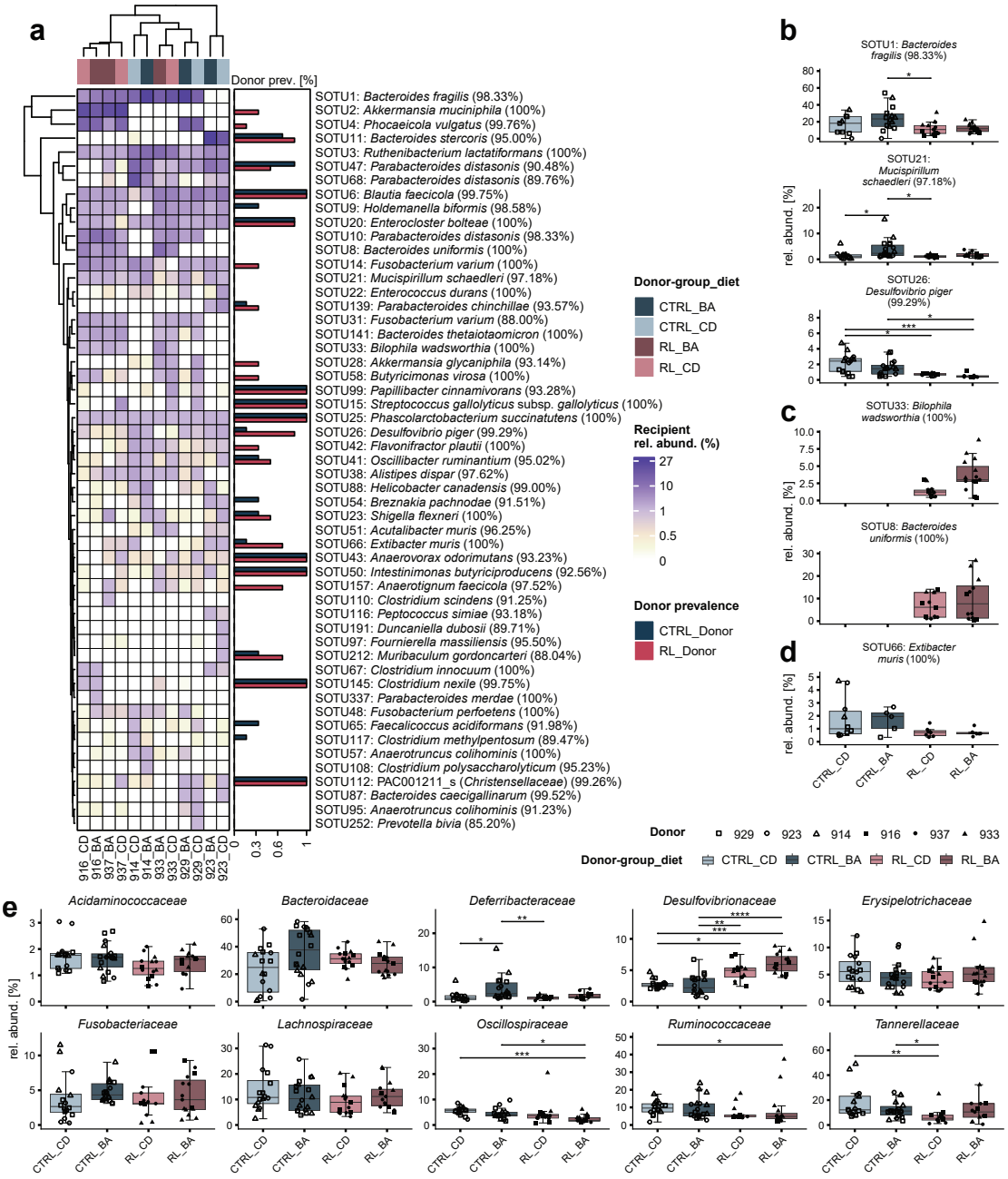

Figure 3.5: Effect of diet and donor-group on microbiota of recipient mice. **a** Dominant SOTUs with a mean rel. abundance of 1% in at least one group of recipient mice. Each column represents the mean rel. abundance of the corresponding SOTU in recipient mice of one donor microbiota fed with either the CD or BA diet. On the right side of the heatmap of rel. abundances, the prevalence of SOTUs in donor pigs is given for each donor-group (CTRL or RL). Columns are clustered by euclidean distance. **b** Significantly different prevalent and abundant SOTUs (present in >80% across all mice and mean rel. abundance >1% within a donor-diet group). **c** Two SOTUs that were only present in RL recipient mice (Fisher exact test p.adj =0 for CTRL-RL comparison). **d** SOTU66, which shared 100% sequence similarity to the SBA-producing species *E. muris* and 98.75% similarity to *C. hylemonae* (rel. abundance in groups not significantly different). **e** Differences in the occurrence of prevalent and abundant bacterial families (same criteria as **b**). CTRL = recipients of microbiota from CTRL donor-group, RL = recipients of microbiota from RL donor-group, CD = control diet (of mice), BA = bile acid diet (of mice). Numbers of mice per group (donor-group-diet combination): CTRL_CD, n=16; CTRL_BA, n=18; RL_CD, n=15; RL_BA, n=15. **b**-**e**: Values with a rel. abundance <0.25% are not shown. Statistics **b** and **e**: Dunn´s multiple comparison after Kruskal-Wallis test, Benjamini-Hochberg adjustment (* p.adj <0.05; *** p.adj <0.001).

3.1.3 FMT had a positive effect on intestinal lesions in *Apc*$^{1638N/+}$ mice

The main goal of the microbiota transfer from pigs to mice was to test the causal effects of the gut microbiota and its ability to produce SBAs on tumour phenotype. The BA diet was hypothesised to further promote intestinal tumours due to increased BA metabolism by the microbiota. Germfree mice were used as a control group due to the absence of microbial BA metabolism. During the course of the experiment, several mice dropped out due to various reasons, e.g. extra-intestinal tumour formation, small intestinal intussusception (a portion of the intestine folds like a telescope, with one segment slipping inside another segment (Azar and Berger, 1997)), or injury caused by fight between male mice. For survival analysis (Figure 3.6 **a** and **b**), the latter case was excluded whilst all other dropouts were considered as real events for plotting the survival curves. A Cox proportional hazards regression model to quantitatively assess the effect of donor-group (microbiota) and diet revealed no significant differences (Figure 3.6 **a**). However, survival curves hinted towards earlier dropouts of mice fed the BA diet, irrespective of the donor-group (Figure 3.6 **b**).

The intestines of all mice (including early dropouts whenever possible), were visually screened for possible lesions using a binocular microscope. A small number of potential tumours or polyps was analysed by histology (e.g. the ones shown in Figure 3.6 **c**). Therefore, the number of lesions refers to the total number of visually counted possible polyps or tumours. The PAR, defined as the region between the pylorus and the duodenum (Prof. Klaus-Peter Janssen, TU Munich; personal communication), and the duodenum were the regions where most mice developed lesions. The number of suspected lesions per mouse along the whole intestine showed significant diet- and microbiota-dependent differences (Figure 3.6 **d**). Germfree mice on control diet (GF_CD) had significantly more lesions compared to recipient mice colonised with CTRL microbiota. This effect was even stronger when mice were fed the BA diet. Germfree mice on BA diet had significantly more lesions than colonised mice independent of the donor microbiota-type (CTRL vs. RL) (Figure 3.6 **d**). The high lesion load in germfree mice on BA diet was especially pronounced in the PAR (not statistically significant) and in the duodenum (p.adj. <0.01) compared to the colonised mice on BA diet (Figure 3.6 **e**). This effect was not observed in germfree mice fed the CD diet. Strikingly, lengthening of the intestine was observed in germfree mice fed the BA diet (Figure 3.6 **f**). These mice were characterised by a 56% longer small intestine compared to the colonised mice on BA diet, and also by a significantly longer colon. No differences were observed between the different groups of colonised mice. Therefore, diet-microbiota interactions seem to influence gut morphology in this mouse model. RBC counting showed a trend towards a higher number of red blood cells in the RL group compared to germfree mice (Appendix Figure A.5 **a**). A similar trend was found for mice with desmoids (Appendix Figure A.5 **b**), while no clear trend was observed in body weight, spleen weight, or faecal occult blood (Appendix Figure A.5 **c**-**e**).

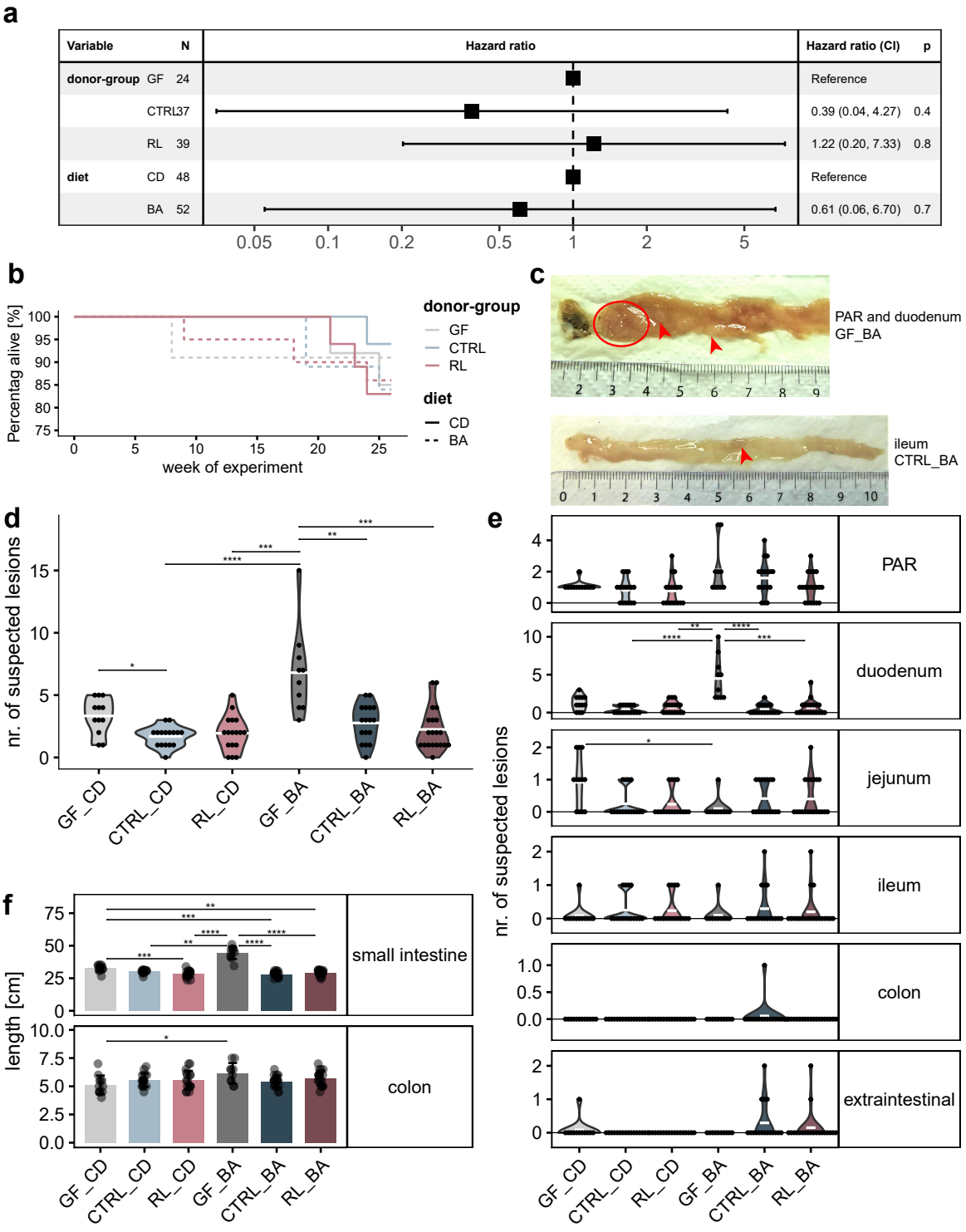

Figure 3.6: (Caption on next page.)

Figure 3.6: (Previous page.) Survival and phenotype in *Apc*$^{1638N/+}$ mice after FMT. **a** Forest plot showing the risk induced by donor-group or diet. The column on the right shows: hazard ratio, 95% confidence intervals, and p-value calculated by the Cox proportional hazards model (diet*donor-group), stratified by sex, with the germfree mice or CD diet as the reference group, respectively. Collateral dropouts (e.g. fight between male mice) were categorised as censored. **b** Percentage of alive animals in the experiment. The y-axis starts at 75% to enhance visualisation. Week 0 corresponds to the week of colonisation (mice aged 4 weeks). Numbers at start (per donor-group and diet combination): GF_CD, n=12; GF_BA, n=12; CTRL_CD, n=17; CTRL_BA, n=20; RL_CD, n=19; RL_BA, n=21. **c** Exemplary macroscopic pictures of two confirmed tumours. Several tumours (microadenoma) in the PAR of a germfree mouse on BA diet (top picture; red circle), with two unconfirmed intestinal lesions in the duodenum (red arrowheads). One tumour (adenoma) in the ileum of a CTRL mouse on BA diet is also shown (arrowhead in the bottom picture). Corresponding microscopic pictures can be found in Appendix Figure A.4. **d** Number of intestinal lesions for each diet and donor-group combination. **e** Number of suspected lesions per gut region and donor-diet combination. **f** Length of the small intestine and colon per diet and donor-group. GF = germfree, CTRL = control donor-group, RL = RL donor-group, CD = control diet, BA = bile acid diet, PAR = periampullary region. Mean number of lesions are indicated with white squares. Statistics: Pairwise comparisons by Dunn´s multiple comparisons with Benjamini-Hochberg adjustment after the Kruskal-Wallis test (* p.adj <0.05; ** p.adj <0.01; *** p.adj <0.001; **** p.adj <0.0001). Colon lesions were excluded from Dunn‘s multiple comparisons due to the high prevalence of zero values.

In summary, faecal microbiota transfer from donor pigs fed with CTRL or RL diet linked to different disease outcome into *Apc*$^{1638+/N}$ mice did not result in the expected causal effect on disease severity. Despite some significant differences in microbiota profiles between the two groups of recipient mice (RL vs. CTRL), the efficacy of microbiota transfer was low, partly explaining the negative results. The diet supplementation with the PBA cholic acid (BA diet) did not affect disease in the recipient mice either. Due to the complex experimental setting with *Apc*$^{1638+/N}$ mice (e.g. length of experiments, many different colonisation groups) and to the small intestine being the primary site of polyp development, this mouse model may not have been optimal to test the specific effect of SBA production on CRC, despite preliminary experiments showing that germfree *Apc*$^{1638+/N}$ mice were characterised by less colonic lesions when compared to their SPF counterparts in multiple animal facilities (Prof. Klaus-Peter Janssen, TU Munich; personal communication). Therefore, a gnotobiotic mouse experiment based on targeted colonisation with synthetic communities was performed in a chemically induced mouse model of CRC.

3.2 DCA-producing *E. muris* worsened disease in a gnotobiotic mouse model of CRC

To reduce the confounding factors associated with transferring complex microbiota (previous section 3.1), germfree BALB/cJ mice were colonised with a minimal synthetic community of cultured human gut bacteria, able to deconjugate conjugated BAs (adapted from Ridlon et al. 2020). Two versions of the synthetic community were used: BACOMI(7αDH-), whose members are able to deconjugate BAs, but cannot perform 7αDH, and BACOMI(7αDH+), which consisted of the same strains, with the addition of *E. muris* DSM 28560^{T}, which has the ability to perform 7αDH (Streidl et al., 2019). Germfree mice were divided into two groups: half of the mice (n=10) were colonised with only BACOMI(7αDH-); the other half (n=10) were colonised with BACOMI(7αDH+). Tumour growth was induced by AOM/DSS treatment as described in the methods (section 2.2). To mimic the negative effects of a Western style diet on CRC development as observed in our previous pig experiment (Wortmann et al., 2023), the mice were fed with a high-fat diet starting one week before colonisation.

These results are partly available as a pre-print on BioRxiv (Wortmann et al., 2023). The mouse work and FACS sorting for this section were done by Dr. Soeren Ocvirk and Annika Oßwald at the German Institute of Human Nutrition (DIfE) in Potsdam-Rehbrücke (Nuthetal, Germany), while I joined in for sampling and did the data analysis and visualisation. Detailed contributions are stated in section 2.2.8.

3.2.1 *E. muris* triggered SBA production *in vivo* and increased tumour numbers

All strains from the synthetic community colonised the mice successfully and *E. muris* was only found in the 7αDH+ mice, as expected (Figure 3.7 **a**). Independent of sex, BACOMI(7αDH+) mice had significantly higher levels of DCA, HCA, LCA, and 12-oxoCDCA (Figure 3.7 **b**). Free and conjugated PBA levels were comparable between the colonisation groups, with the exception of one mouse with very high levels of TαMCA. Even though all mice underwent the same AOM/DSS treatment, BACOMI(7αDH+) mice developed significantly more total tumours in the colon. This effect was mainly driven by significantly higher numbers of small tumours (Figure 3.7 **c**). Despite comparable tumour numbers in female and male BACOMI(7αDH+) mice, the amount of detected DCA was ca. 35x higher in female (1152.2 ±107.9 nmol/g dry weight) than male mice (32.46 ±24.8 nmol/g). Of note, two female mice from the BACOMI(7αDH+) group dropped out early during the experiment, and no sampling was possible for these mice. These results consolidated what was found in a similar experiment, which used *C. scindens* instead of *E. muris* as DCA producer (Wortmann et al., 2023).

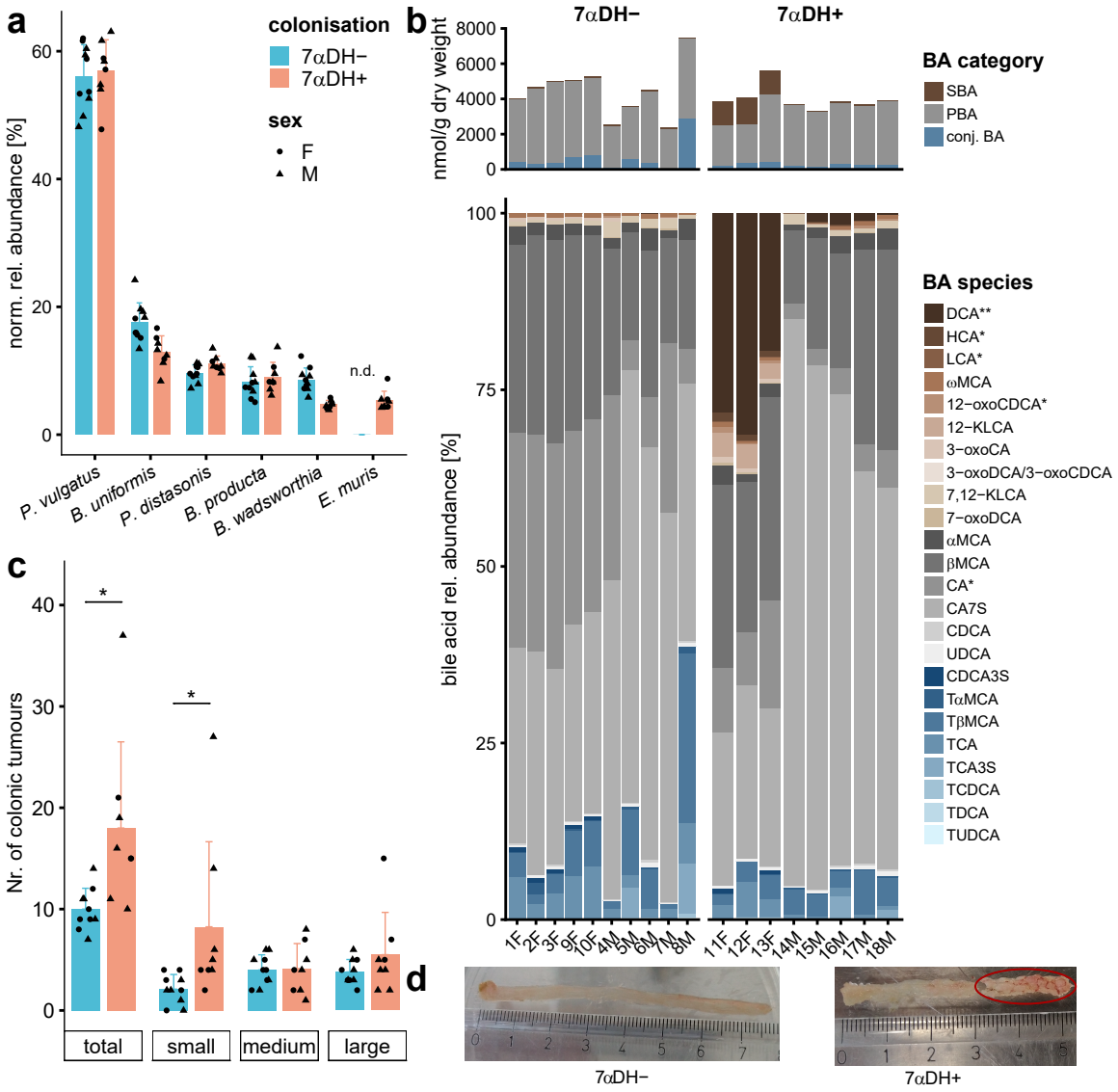

Figure 3.7: BACOMI(7αDH-) and BACOMI(7αDH+) colonisation, phenotype, and BA profiles. **a** Rel. abundance of the BACOMI(7αDH+) strains, as determined by 16S rRNA amplicon sequencing. **b** BA profiles in each mouse. Total amounts of each BA category are plotted on top, relative composition is plotted below. Colour shades of the bottom panel reflect the BA categories depicted in the upper panel. The TαMCA signal partly overlapped with that of TβMCA, leading to reduced accuracy of the signal; TCA3S might be a different unknown sulfated BA than TCA3S. SBA= secondary BA, PBA = primary BA, conj. BA= conjugated BA. Barplots with absolute BA species concentrations can be found in Appendix Figure A.7 **c** Number of colonic tumours. **d** Exemplary pictures of a colon from each colonisation group. Tumours are marked with a red circle. Statistics for **b**: Wilcoxon rank-sum test for comparison of BA concentrations, * p.adj <0.05, ** p.adj <0.01.

3.2.2 *E. muris* affected immune cell populations

Besides the aforementioned main results regarding BAs, microbial colonisation, and tumour numbers, immune cells from the colon and MLN were analysed by FACS. Significantly higher percentage of Ly6C^{low} CD206+ CD11+ F4/80+ cells (contain macrophages) were detected in the colon and MLN of BACOMI(7αDH+) mice compared to BACOMI(7αDH-) mice (Figure 3.8). F4/80^{high} CD206+ macrophages have been previously identified as tumour-associated macrophages (TAM) able to present tumour-associated antigen (Modak et al., 2022). Another subset of CD11b+ F4/80+ cells (Ly6C^{high}) was significantly decreased in the colon of BACOMI(7αDH+) mice, indicating that colonisation had a specific effect on different macrophage subtypes. CD304 (Neuropilin-1) is a surface marker for thymus-derived T_{reg} cells (Weiss et al., 2012). It is thought to mediate Foxp3+ T_{reg} cell infiltration into the tumour site, where they block CD8+ T cells, resulting in enhanced tumour progression because of reduced anti-tumour immune response in mice (Hansen et al., 2012). CD103 is a marker for tissue resident, intra-epithelial lymphocytes (McHugh et al., 2002). High expression of *FOXP3* was proposed as a marker of poor prognosis in a subtype of CRC (Saito et al., 2016). A trend (p.adj =0.08) towards higher total Foxp3+ and Foxp3+CD103+ T cells was observed in the colon of BACOMI(7αDH+) mice but not in the MLN. Also, the trend (p.adj =0.1) of lower CD8a+ T cells in BACOMI(7αDH+) mice was specific to the colon even though a reduction of CD4+ Foxp3+ regulatory T cells and Cd4+ CD8+ T cell activation in MLNs during tumorigenesis was previously reported (Olguín et al., 2018). MLN weight and additional data can be found in the appendix (Appendix Figure A.6).

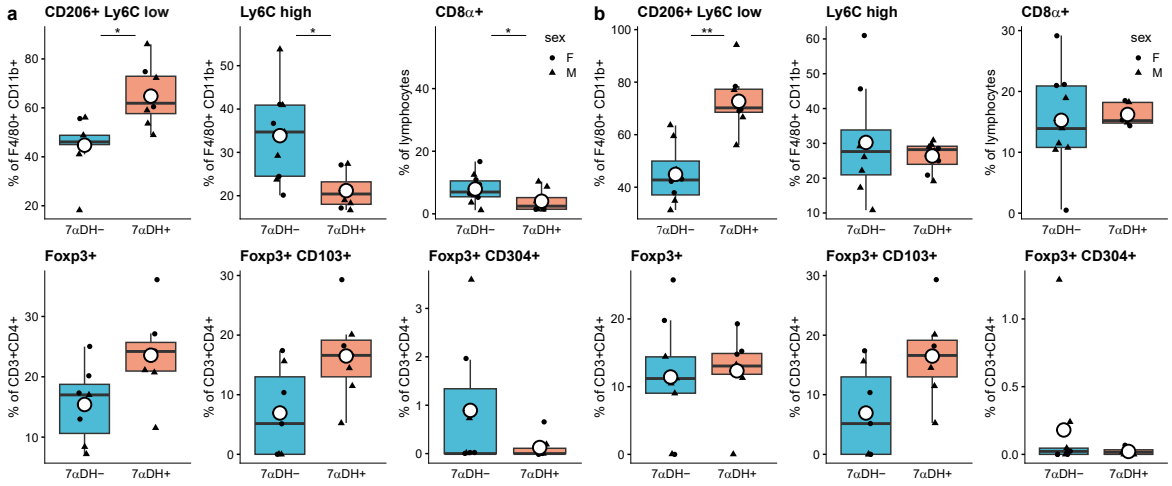

Figure 3.8: Immune cell profiles of mice colonised with BACOMI(7αDH+), including *E. muris*, or BACOMI(7αDH-). F4/80+ CD11b+ cells, cytotoxic T cells (CD8α+), and regulatory T cells (Foxp3+) in the colon (**a**) and MLN (**b**) were measured by FACS. CD45+ CD11b+ F4/80+ cells (containing macrophages) were gated for Ly6C^{low} CD206+ and Ly6C^{high} cells. Regulatory T cells (CD3+ CD4+) were further gated into Foxp3+ cells, Foxp3+ CD103+ and Foxp3+ CD304+ cells. All cells were sorted for sideward-scatter low, forward-scatter high, single cells. Percentages of positive cells of each gate were plotted. Mean values are shown with white circles. Statistics: Wilcoxon rank-sum test, Benjamini-Hochberg adjustment, * p.adj <0.05, ** p <0.01.

In summary, the addition of a single bacterial strain (*E. muris* DSM 28560^{T}) with 7αDH activity led to high levels of DCA in the caecum of gnotobiotic mice, especially in female animals. This was accompanied by higher tumour numbers, with a main effect on small tumours. These findings imply early-stage promotion of tumorigenesis rather than tumour progression. With respect to immune cells, significant differences between the colonisation groups were observed for the two CD206+ CD11+ populations that were analysed. Even though this experiment provided some evidence for tumour-promoting effect of the DCA producer *E. muris*, it did not give insights into the role of DCA in regulating different cells of the colonic epithelium. Therefore, the effect of *E. muris* in the colon was investigated in another gnotobiotic mouse trial using single-cell RNA sequencing (scRNA-Seq).

3.3 DCA-producing *E. muris* affected gene expression in colonic epithelial cells

To further investigate how the SBA producer *E. muris* might influence disease phenotype in mouse models of CRC, as observed in the AOM/DSS mouse experiment (section 3.2), scRNA-Seq analysis of colonic epithelial cells was performed to assess early transcriptional responses to SBA exposure. Gnotobiotic *Apc*$^{1638N/+}$ mice, colonised with either the synthetic community OMM12 (Brugiroux et al., 2016) alone or with the addition of *E. muris* (OMM12+E) were sampled 4 weeks after colonisation for isolation of colonic epithelial cells followed by scRNA-Seq. To take sex and cage effects into account, one female and one male mouse from each colonisation group (OMM12 and OMM12+E) were used for scRNA-Seq. Individual colon tissue was pooled before starting the cell isolation procedure to ensure a sufficient number of cells for sequencing, resulting in one final sample per colonisation for sequencing.

RNA sequencing and Cell Ranger analysis was performed by the the IZKF Core Facility Genomics at the RWTH University Hospital. The sample-specific datasets were then combined, quality filtered, and normalised by Johannes Schöneich (AG Costa and AG Hornef, RWTH Aachen), using a customised version of the Seurat pipeline (`https://github.com/CostaLab/scrna_seurat_pipeline`). Further analysis and visualisation was done by myself in the R programming environment using Seurat version 4.1.1.

3.3.1 *E. muris* colonisation led to significant DCA production

Colonisation profiles in colon (16S rRNA gene amplicon sequencing) and BA concentrations in caecum are depicted in Figure 3.9. Out of the 12 OMM strains, *Muribaculum intestinale, Bifidobacterium animalis*, and *Limosilactobacillus reuteri* were not detected. These strains have been reported colonise only below or at detection limit as determined via targeted qPCR (Eberl et al., 2020). Similarly, *Acutalibacter muris* and *Enterococcus faecalis* were shown to have low colonisation efficiency, with significant inter-facilty differences (Eberl et al., 2020). Indeed, *A. muris* did not colonise OMM12 mice, whilst *E. faecalis* had a substantially higher rel. abundance in the OMM12+E group (0.15% rel. abundance in OMM12 vs. 5.5% rel. abundance in OMM12+E). As expected, *E. muris* was only detected in the OMM12+E group at a mean rel. abundance of 3.7 ±1.2%, including higher levels in male mice (Figure 3.9 **a** and **b**). *Bacteroides caecimuris* was highly abundant in male mice of the OMM12+E group when compared with female animals, which were also housed in separate cages and inoculated with separate cryostocks (data not shown). *A. muris* and *Turicimonas muris* were also more abundant in male mice whilst below detection limit in female mice.

BA concentrations in the caecum were characterised by marked differences between individual mice. Only DCA was significantly different between the two colonisation groups, as it was detected exclusively in OMM12+E mice (Figure 3.9 **c**). Comparing DCA level between the mice, it seemed that higher levels of *E. muris* (Figure 3.9 **b**) were linked to higher DCA levels within a sex group (Figure

3.9 **d**). Although this observation is based on a low number of mice, it is in line with other data showing that female mice produced higher levels of SBAs when colonised with *C. scindens* (Wortmann et al., 2023). Besides the expected differences in bacterial colonisation and BA composition, SCFA production and the body weight of mice over time were analysed. No significant differences were observed for these parameters, consolidating the comparability of the mouse groups in relation to DCA production (Appendix Figure A.8).

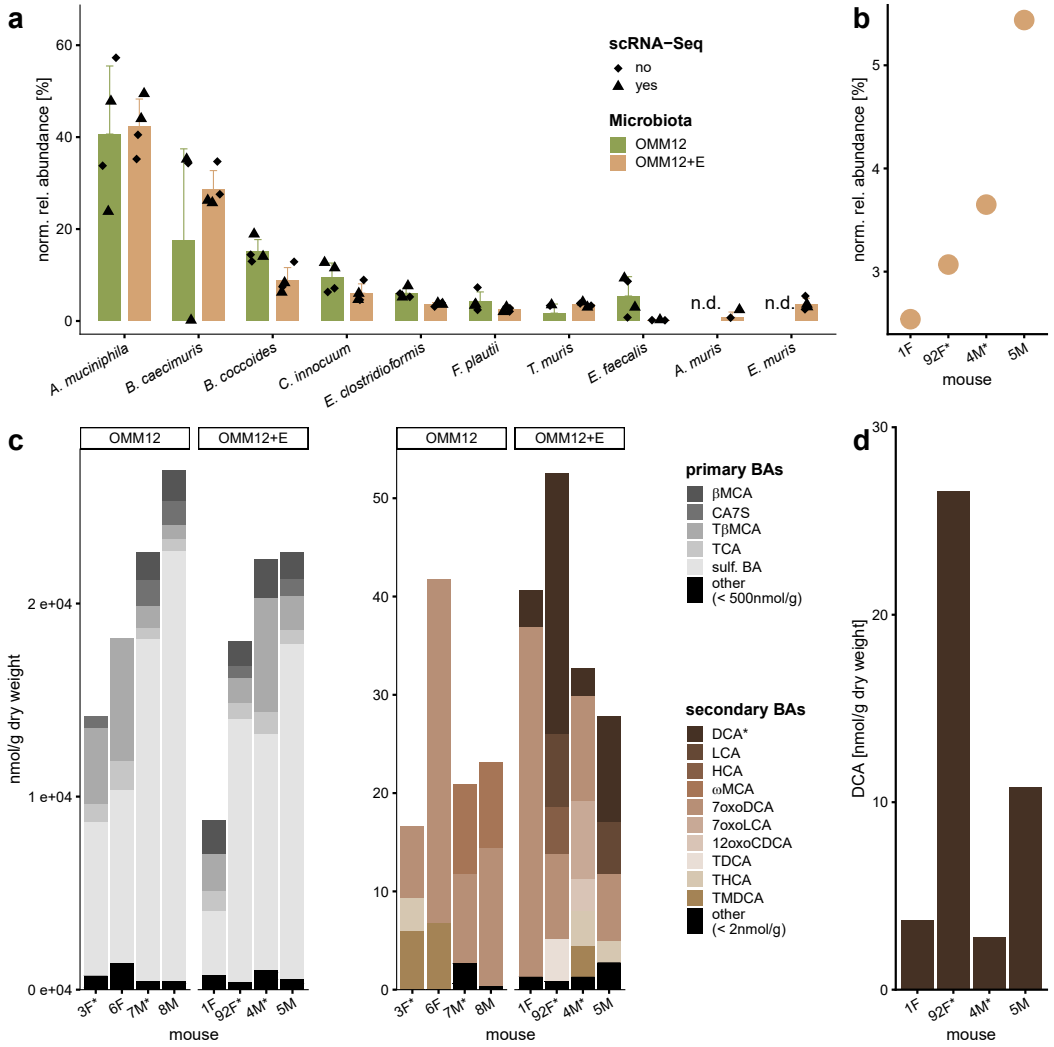

Figure 3.9: Colonisation and BA profiles in the gnotobiotic mice. **a** Rel. abundance of the detected strains in colon content of *Apc*$^{1638N/+}$mice. **b** Rel. abundance of *E. muris* in individual mice of the OMM12+E group. **c** Individual primary (left, greys) and secondary (right, browns) BA profiles in caecal content. **d** Individual DCA levels in OMM12+E mice. Sex of the mice in **b-d** is indicated with corresponding letters (M/F) and mice used for scRNA-seq are indicated with *. Sulf. BA is a sulfated BA, which was not included within our panel of BA standards.

3.3.2 Epithelial cell composition and gene expression differed with *E. muris*

After filtering, 6,941 cells were analysed in the OMM12 group, with an average of 8,914 sequenced molecules and 1,933 unique genes per cell. The OMM12+E sample contained 5,112 cells in total, with 10,313 molecules and 1,993 unique genes per cell. A resolution of 0.3 was applied for clustering, resulting in 13 different cell clusters (Figure 3.10 **a**). The highest number of molecules and genes were detected in clusters 5, 7, and 8 (Appendix Figure A.9 **a** and **b**), making them the most active cell populations in terms of transcription. The percentage of mitochondrial genes, which can be considered as an indicator for dying cells, was relatively high in both groups (25% for OMM12 and 26% for OMM12+E), mostly driven by clusters 3 and 6 (Appendix Figure A.9 **c**). Ribosomal gene expression, which can be viewed as an indicator for cell proliferation (Petibon et al., 2021), was cell type-specific, with on average 3.4% ribosomal genes in the OMM12+E group and 6.3% in the OMM12 group. Comparing the distribution of cells between the two colonisation groups showed differences for clusters 2 (enlarged in OMM12+E mice) and clusters 5, 7 and 8 (smaller in OMM12+E mice) (Figure 3.10 **b** and **c**) . Marker genes from Schaum et al. (2018) were used for cell type assignment (Figure 3.10 **d**). Cluster 2, which had a higher percentage of cells in the OMM12+E group, was identified as enterocytes from the crypt top (*Krt20*$^{+}$). Cluster 5 was identified as proliferating stem cells, expressing *Lgr5* and *Mki67*. Cluster 4 and 7 were both identified as goblet cells, with cluster 4 expressing crypt top marker genes and cluster 7 expressing the crypt bottom marker gene CD44 (Figure 3.10 **d**). Of the two goblet cell clusters, only cluster 7 was underrepresented in OMM12+E mice. It was hypothesised that cluster 8, almost non-existent in OMM12+E mice and characterised by enhanced proliferation (expressing *Mki67*), corresponded to transit amplifying cells that develop into goblet cells of cluster 7. Since the main difference between the two colonisation groups was the presence of the SBA-producing species *E. muris*, a special focus was put on the expression of BA-related genes. Interestingly, ASBT (*Slc10a2*), MRP3 (*Abcc3*), OSTα (*Slc51a*), and OSTβ (*Slc51b*) were highly expressed in cluster 2 (Figure 3.10 **e**), which was characterised by a higher number of cells in OMM12+E mice and was classified as absorptive enterocytes. Cluster 2 also expressed intracellular nuclear BA-binding receptors PXR (*Nr1i2*), VDR (*Vdr)*, and FXR (*Nr4h1*) (Figure 3.10 **f**). The G-protein coupled receptor TGR5 (*Gpbar1*) was mainly expressed in the chromaffin cells (cluster 10), which is consistent with the literature (Perino et al., 2021).

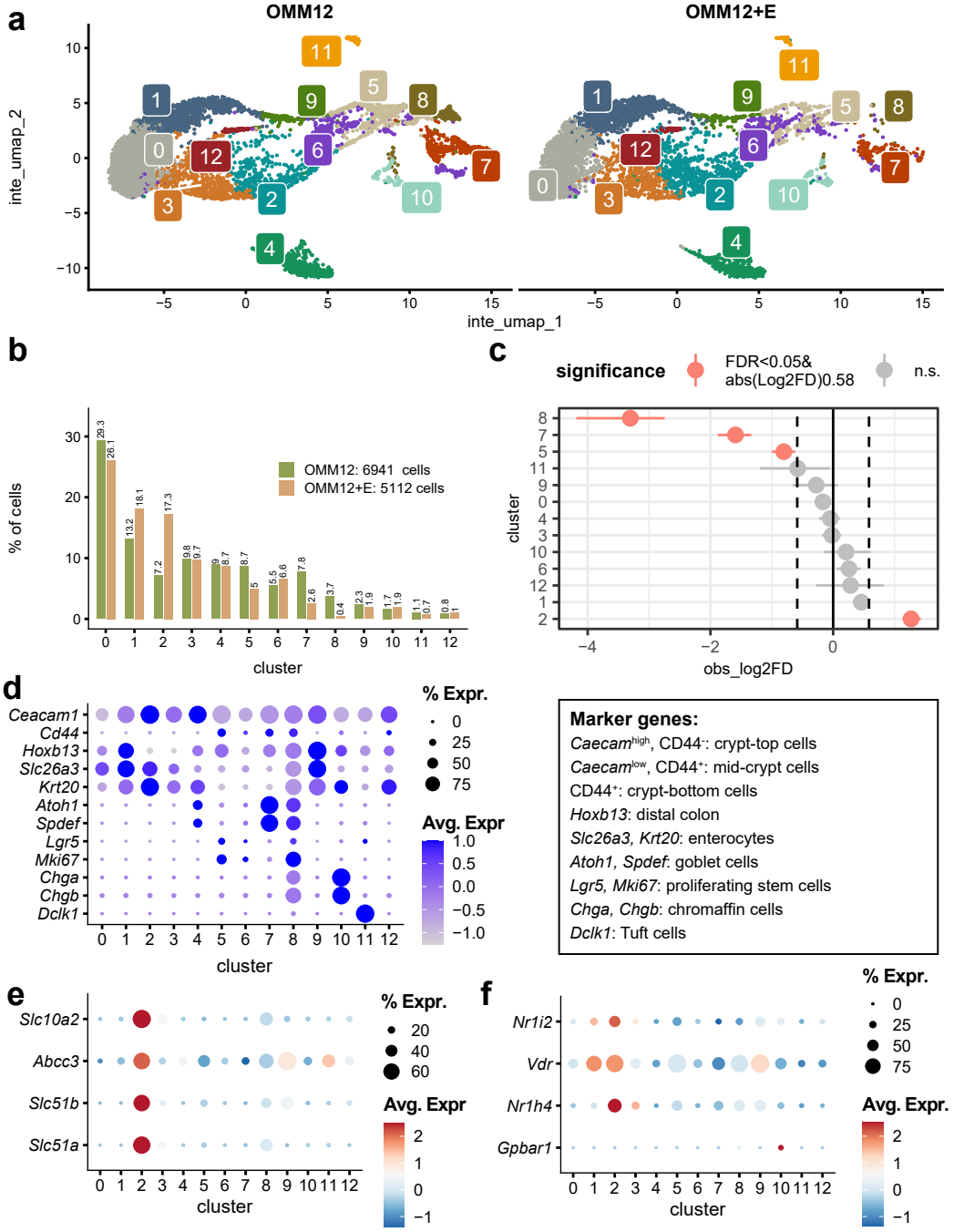

Figure 3.10: Transcriptomic analysis of single cells isolated from the colonic epithelium of gnotobiotic *Apc*$^{1638N/+}$ mice. Each colonisation group represents data from the cells isolated from pooled colons of two mice. **a** Cells were split by colonisation and grouped into 13 clusters. **b** Percentage of cells per cluster for each sample. **c** Statistics (permutation testing and bootstrapping) for the under- or over-representation of cells between the two samples. Positive values indicate a higher percentage of cells in OMM12+E mice, negative values indicate a higher percentage of cells in OMM12 mice. **d** Marker genes for different cell types and their designations (according to Schaum et al. 2018). **e** Genes encoding for BA transporters ASBT (*Slc10a2*) on the apical side of cells, OSTα and OSTβ (*Slc51a* and *Slc51b*), and MRP3 (*Abcc3*) on the basolateral side **f** Genes encoding for BA receptors: PXR (*Nr1i2*), VDR (*Vdr*), FXR (*Nr1h4*), TGR5 (*Gpbar1*). Dot plots were generated with scaled data (mean expression across the dataset is set to 0 with a standard deviation of 1). A negative average expression corresponds to expression below the mean expression of the dataset.

3.3. DCA-producing *E. muris* affected gene expression in colonic epithelial cells

Differential gene expression analysis within each cell cluster between the two mouse colonisation groups revealed significant candidate genes within clusters 2 and 7 that were all upregulated in OMM12+E mice (Figure 3.11). In cluster 2 (absorptive enterocytes), pyruvate dehydrogenase kinase 4 *Pdk4*, galactose-3-O-sulfotransferase 2C (*Gal3st2c*), chloride channel accessory 4A (*Clca4a*), acetyl-Coenzyme A acyltransferase 1B (*Acaa1b*) as well as the intestinal fatty acid-binding protein 2 (*Fabp2*) were significantly and highly (Log2FC >0.9) upregulated. In line with *Fabp2*, also the KEGG (Kyoto Encyclopedia of Genes and Genomes) pathways for FA degradation, elongation, and metabolism were significantly upregulated in cluster 2 of OMM12+E mice (Appendix Figure A.12). *Fabp2* was also significantly uregulated in cluster 10 (chromaffin cells). Aquaporin 4 (*Aqp4*) was upregulated in OMM12+E mice in cluster 5 (stem cells). In cluster 7 (goblet cells from the crypt bottom), genes for the Fc fragment of IgG binding protein (*Fcgbp*), small proline-rich protein 2A3 (*Sprr2a3*), regenerating islet-derived family, member 4 (*Reg4*), and intestinal trefoil factor 3 (*Tff3*) were significantly upregulated. All other cell clusters (0, 1, 3, 4, 6, 8, 9, 11, 12) had no significantly and highly (p.adj <0.05; Log2FC >0.9) upregulated genes in the OMM12+E group (Appendix Figure A.10).

We also looked specifically at the expression of cancer-related genes, i.e., those reported to be expressed in cancer stem cells (Wang et al., 2021). Most of these genes were expressed by cells in clusters 5 (stem cells), 7 (crypt bottom-derived goblet cells) and 8 (transit amplifying cells). Furthermore, cluster 10 (chromaffin cells) expressed *Hopx* and *Sox4*, while *Sox9* was also expressed by cluster 11 (Tuft cells) and 12 (crypt top enterocytes). Prominin 1 (PROM1), also called CD133, is a cell surface marker used to identify human tumours (Todaro et al., 2007). In our mice, *Prom1* was expressed in several clusters: cluster 11 (Tuft cells), 12 (crypt top enterocytes), cluster 2 (absorptive enterocytes) (Appendix Figure A.11). When comparing the expression of these genes between the two groups of mice (OMM12+E vs. OMM12), no significant differences were found.

In addition to the comparative expression of individual genes, pathway analysis provides a more complete overview of cellular processes. The Pathway RespOnsive GENes (PROGENy) method (Schubert et al., 2018) was used to assess perturbations of cancer-related pathways. Wnt signalling, which is promoted by TNFα signalling (Zhao et al., 2020), as well as MAPK and phosphoinositide 3-kinases (Pi3K) signalling are usually upregulated during CRC progression, while tumour-suppressing activity of Transforming growth factor beta (TGFβ) and p53 are downregulated (Baker et al., 1990; Keum and Giovannucci, 2019; Mundade et al., 2014; Shah and Itzkowitz, 2022). Janus kinase - signal transducer and activator of transcription (JAK-STAT) signalling is an immune evasion signature, enriched in several cancer molecular subtypes (Guinney et al., 2015; Khaliq et al., 2022). TNF-related apoptosis-inducing ligand (TRAIL) induces apoptosis of cancer cells and can activate other pathways like NFκB, PI3K, or MAPK (Johnstone et al., 2008). These 3 pathways are also stimulated by hypoxia (Muz et al., 2015). It has previously been shown that DCA can lead to epidermal growth factor receptor-MAPK (EGFR-MAPK) activation in HT-29 human colorectal adenocarcinoma cells (Centuori et al., 2016). OMM12+E mice showed significant upregulation of hypoxia and NFκB, but downregulation of MAPK, PI3K, EGFR (Figure 3.12). Additionally, the tumour-suppressing p53 pathway was upregulated in most clusters of OMM12+E. Cluster 2 (absorptive enterocytes) seemed

to be highly affected by the presence of *E. muris* in the microbiota and showed a significant upregulation of eight different pathways. It was also the only cluster with a very high upregulation of TRAIL and TGFβ, both of which have tumour-suppressing properties (Johnstone et al., 2008). In this context, it appears that the addition of *E. muris* to a minimal microbiota at an early stage of CRC development (as mimicked by the *Apc*$^{1638N/+}$ mouse model) has more tumour-suppressing than tumour-promoting effects. In agreement with this, a significant downregulation of the Wnt pathway was observed (Figure 3.12).

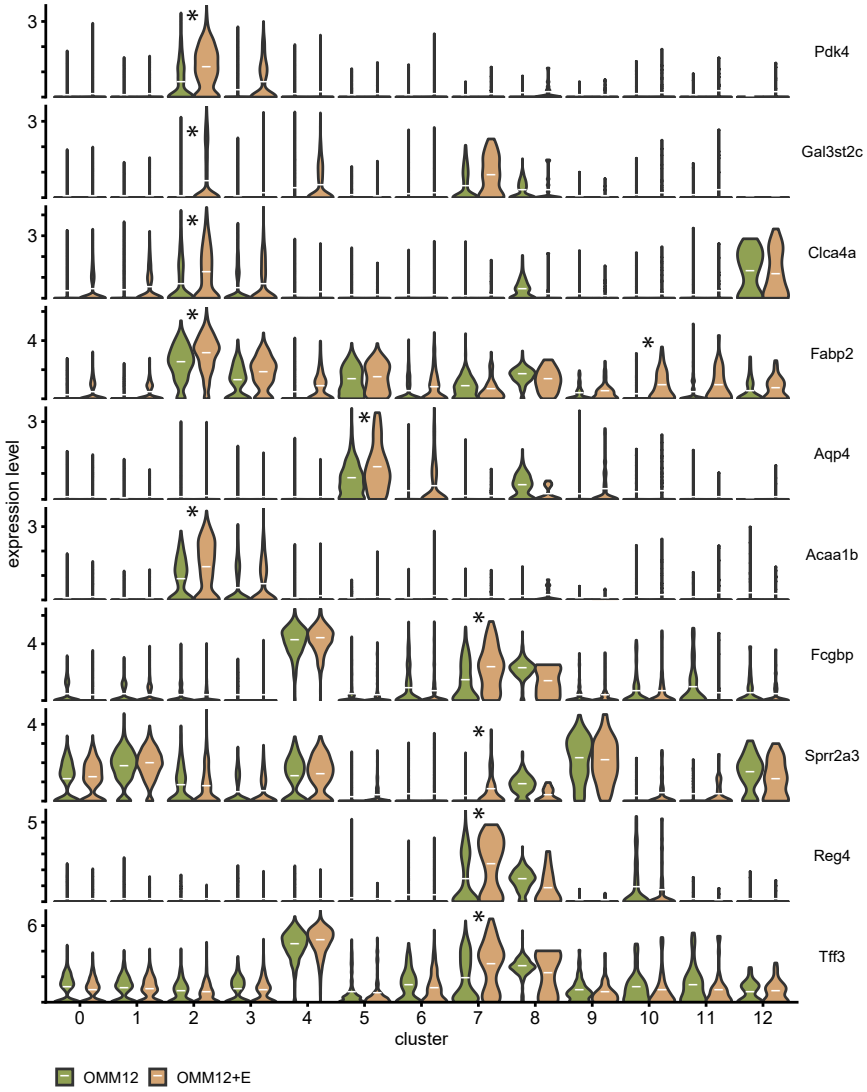

Figure 3.11: Violin plots of differentially expressed (DE) genes (Log2FC >0.9, p.adj <0.05) as determined by the FindMarkers function of Seurat, which uses Wilcoxon tests. Abbreviations: Pyruvate dehydrogenase kinase 4 (*Pdk4*), galactose-3-O-sulfotransferase 2C (*Gal3st2c*), chloride channel accessory 4A (*Clca4a*), acetyl-Coenzyme A acyltransferase 1B (*Acaa1b*), intestinal fatty acid binding protein 2 (*Fabp2*), aquaporin 4 (*Aqp4*), Fc fragment of IgG binding protein (*Fcgbp*), small proline-rich protein 2A3 (*Sprr2a3*), regenerating islet-derived family, member 4 (*Reg4*), intestinal trefoil factor 3 (*Tff3*). Mean gene expression per cluster/colonisation is indicated with white horizontal lines. Log-fold change >0.9 and p <0.05 are indicated with stars.

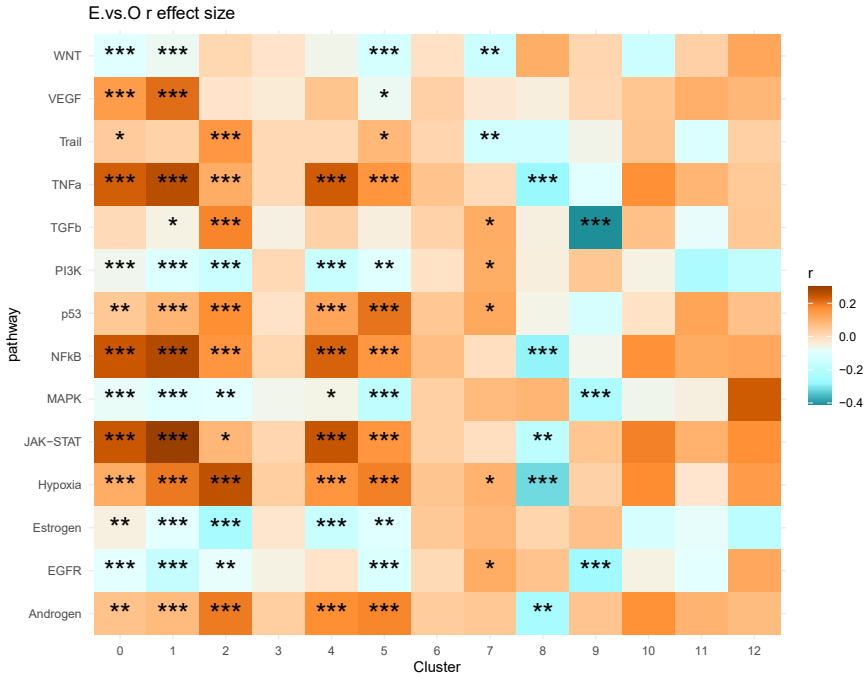

Figure 3.12: PROGENy analysis comparing OMM12+E vs. OMM12. Positive effect size (r) values (orange) indicate upregulation in the OMM12+E mice compared to their OMM12 counterparts, whereas negative effect size (r) values (blue) indicate downregulation compared to the OMM12 group. Statistics: Wilcoxon test, * p <0.05, ** p <0.01, *** p <0.001.

In summary, the addition of the 7αDH+ *E. muris* to a synthetic community of mouse gut bacteria and the associated production of DCA in the intestine was linked to different cell type composition in the colonic epithelium and the identification of a few highly upregulated genes and pathways. Based on the findings from the two gnotobiotic mouse experiments (chapter 3.2 and 3.3), we conclude that SBA production by gut bacteria via 7αDH contributes to early-stage promotion of colorectal tumorigenesis, possibly linked to direct alterations of epithelial responses. To consolidate the role of SBA in CRC development, in line with our previous feeding trial showing that a Western diet worsened disease in *APC*$^{1311/+}$ pigs (Wortmann et al., 2023), we next hypothesised that supplementation of the BA scavenger colestyramine to Western diet would protect from SBA-promoted CRC. If SBAs were a driver of epithelial cell proliferation and CRC development, detrimental effects of the Western diet would be counteracted by the addition of colestyramine.

3.4 The BA scavenger colestyramine reduced intestinal cell proliferation in $APC^{1311/+}$ pigs

Colestyramine is a commonly used drug in cases of hypercholesteremia or in BA malabsorption-associated diarrhea (Scaldaferri et al., 2013). It is an anion exchange resin that works by sequestering BAs in the intestine, which are then not absorbed in the intestine, but excreted in faeces (Scaldaferri et al., 2013). We hypothesised that this drug makes BAs also less available for bacterial transformation into SBAs in the large intestine and therefore would reduce the previously observed high-polyp phenotype of pigs fed a Western style diet enriched in red meat and lard (RL diet) (Wortmann et al., 2023). $APC^{1311/+}$ pigs were divided into three diet groups: CTRL diet, RL diet, and the RL diet supplemented with 12g colestyramine per day (COL). A colonoscopy was done 1 month before the feeding intervention (month 3) to assess initial polyp state. Faecal material was sampled right before the start of the feeding intervention (month 4) and at the end (month 7). Pigs were examined again by colonoscopy and samples were taken from multiple parts along the intestinal tract after culling. These results are partly available as a pre-print on BioRxiv (Wortmann et al., 2023). Detailed contributions are given in section 2.4.7.

3.4.1 Diet intervention influenced colonic cell proliferation, T cell and goblet cell populations, but not polyp phenotype

The number of polyp counted during colonoscopy in the last 40 cm of the colon decreased over time in all COL pigs. However, 3 out of 4 RL pigs were also characterised by decreased polyp numbers, while two pigs on the CTRL diet showed a substantial increase in polyp numbers (Figure 3.13 **a**). When comparing polyp numbers in the whole intestine as counted after dissection, a similar trend was observed, with the exception of one outlier in the COL group (Figure 3.13 **b**). Changes in mean polyp sizes over time did not show a clear trend in any feeding group (Figure 3.13 **c**). Scoring of normal tissue sections showed similar hyperplasia patterns for the three groups, with slightly more hyperplasia in the proximal and middle colon of CTRL pigs (Figure 3.13 **d**).

Despite this absence of differences in polyp phenotype, RL pigs were characterised by significantly higher percentages of proliferating (Ki67+) cells in the rectum. This was reduced by colestyramine intake, which lead to proliferation levels comparable to the control animals (Figure 3.13 **e**). Furthermore, T cell infiltration (CD3+ cells) in the lamina propria was significantly elevated in the proximal colon of RL pigs, which was again prevented in the COL group. In contrast, goblet cells, determined by the percentage of AB-PAS positive area, were significantly increased following colestyramine treatment when compared to RL pigs. The dietary intervention therefore had no effect on colonic polyps or dysplasia, but still affected proliferation of epithelial cells, T cell infiltration, and goblet cells.

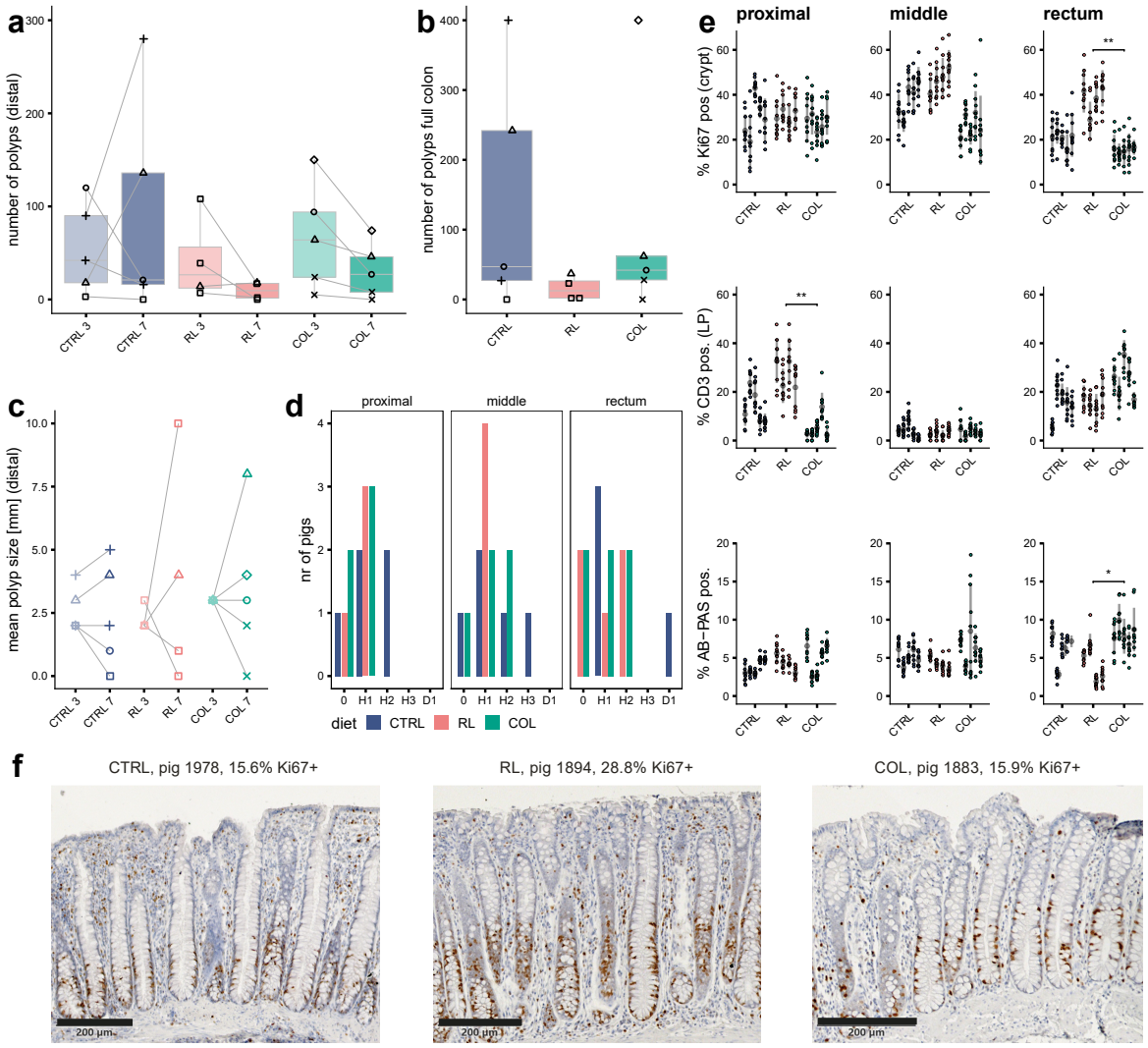

Figure 3.13: Polyp phenotype and histological analysis of colon tissue. **a** Number of polyps in the distal colon (40 cm) as assessed visually by endoscopy before (month 3) and after (month 7) the feeding intervention. **b** Number of polyps throughout the entire colon after the feeding intervention. **c** Mean polyp size before and after the feeding intervention. **d** Normal tissue (off-polyps) scoring in different colon regions: 0 = no change, D = dysplasia, H = hyperplasia, 1 = minimal, 2 = medium, 3 = high-grade. **e** Immunohistochemistry for Ki67 (% of Ki67+ cells in crypt), CD3 (% of CD3+ cells in lamina propria), and neutral and acidic mucins (% AB-PAS+ signal per area measured) in normal tissue of the proximal and middle colon as well as rectum. Mean and standard deviation are indicated in grey. **f** Exemplary tissue sections stained for Ki67. The black bar on each picture represents 200 µm. Statistics in **e**: Kruskal Wallis and Dunn's multiple comparisons of the mean values per pig (grey dots), Benjamini-Hochberg adjustment: * p.adj <0.05, ** p.adj <0.01.

3.4.2 Colestyramine altered microbiota profiles in the distal gut

Gut content from different regions was analysed by 16S rRNA gene amplicon sequencing. For all gut regions, microbiota structure (β-diversity) was significantly different (PERMANOVA p <0.05) between the three diet groups (Figure 3.14 **a**). Separation was especially pronounced in the caecum. In the colon, the COL group clustered separately from the other two groups (Figure 3.14 **a**). Comparison of faecal microbiota structure at the start and end of feeding revealed both time- and diet-dependent clustering (Figure 3.14 **a**). At the level of α-diversity, no significant differences were observed in terms of richness (total number of detected SOTUS). However, Shannon effective counts (approximation for the number of dominant SOTUs) were consistently lowest in RL pigs throughout the intestine compared to the animals fed the COL and CTRL diet (Figure 3.14 **b**). This difference reached statistical significance in the distal gut (caecum and colon). No significant changes were observed by Wilcoxon signed-rank test between the start and the end in either of the diet groups (Figure 3.14 **c**).

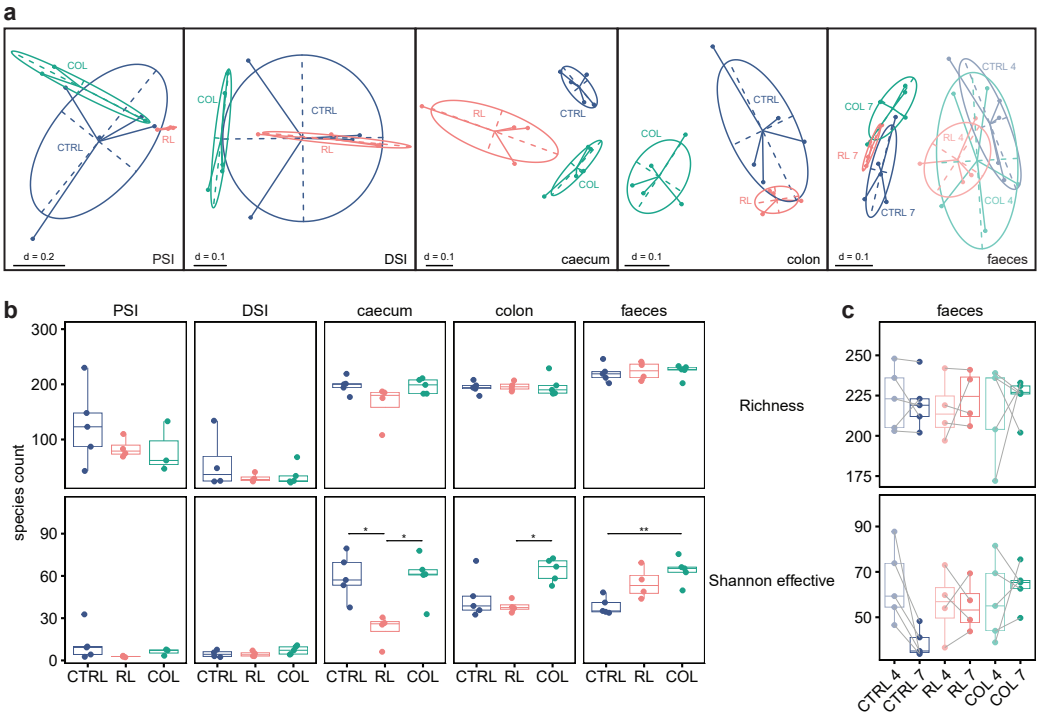

Figure 3.14: Microbiota structure in different gut regions. **a** Multidimensional scaling (MDS) plot of microbial profiles based on generalised UniFrac distances. **b** Richness and Shannon effective counts of species in each gut region and **c** in faeces over time. PSI = proximal small intestine, DSI = distal small intestine. Statistics: **b**, Kruskal-Wallis with Dunn´s multiple comparisons, Benjamini-Hochberg adjustment for comparison of diets: * p.adj <0.05, ** p.adj <0.01; **c**, Paired Wilcoxon signed-rank test (no significant differences).

The rel. abundances of most prevalent phyla (present in >75% of individuals in at least one gut region) showed significant differences between the diet groups in the caecum: RL pigs had significantly higher levels of *Bacillota* (formerly Firmicutes) and lower levels of *Bacteroidota* (formerly Bacteroidetes) (p.adj =0.012), whilst levels in the COL pigs resembled that in the control animals

(Figure 3.15 **a**). The lower richness and Shannon effective species count (Figure 3.14 **b**) were also reflected at the family level, with *Lactobacillaceae* largely dominating the communities in the proximal small intestine of RL pigs (Figure 3.15 **b**). When comparing overall profiles of prevalent bacterial families, the RL group clustered separately from COL and CTRL pigs in the proximal small intestine (Figure 3.16 **a**). Family profiles in the distal small intestine were not as clearly separated (Figure 3.16 **b**) and showed no significant differences between the groups. In contrast, family profiles in the caecum (Figure 3.16 **c**) reflected the separation seen in β-diversity analysis (Figure 3.14 **c**). Like in the proximal small intestine, RL pigs also had elevated levels of *Lactobacillaceae* in the caecum, whilst CTRL pigs had higher levels of *Prevotellaceae* (Figure 3.15 **c**). In the colon, COL pigs had higher levels of *Anaerovoraceae* and *Christensellaceae*, but lower levels of *Lactobacillaceae* (Figure 3.15 **d**). The similarity between CTRL and RL pigs for these families also reflect microbiota profiles (Figure 3.14 **a**) and also the clustering shown in Figure 3.16 **d**. Faecal bacterial family profiles were separated by time point (3.16 **e**), with elevated levels of *Ruminococcaceae* and *Clostridia* UCG.014 in RL pigs, and higher levels of *Anaerovoraceae* in COL pigs (Figure 3.15 **e**).

When comparing all prevalent SOTUs (>75% prevalence in at least one region), the proximal small intestine of COL pigs was characterised by a low rel. abundance of SOTU1 (*Lactobacillus johnsonii*, 100% sequence similarity), whilst RL pigs had a higher rel. abundance of SOTU3 (*L. reuteri*) (Figure 3.15 **f**). These two SOTUs were also elevated in the caecum of RL pigs compared to COL pigs. Furthermore, CTRL pigs had higher levels of SOTU18 (*P. succinatutens*, 99.06% similarity), SOTU112 (*Blautia stercoris*, 98.50%), and SOTU21 (*R. lactaris*, 97.00%) (Figure 3.15 **g**), which, together with *Segatella copri* (previously *Prevotella copri*, Hitch et al. 2022a), were likely responsible for the separation of CTRL microbiota profiles in the caecum (Figure 3.14 and Figure 3.17). COL pigs were characterised by higher levels of SOTU 8 (*Clostridium lentum*, 100%), SOTU221 (*Eubacterium xylanophilum*, 98.48%), SOTU232 (*Aristaeella hokkaidonensis*, 93.03%),SOTU27 (*Intestinimonas butyriciproducens*, 92.56%), and SOTU48 (*Lacrimaspora celerecrescens*, 98.25%). The only SOTU with p.adj <0.1 in the colon was SOTU232 (*A. hokkaidonensis*, 93.03%), which was elevated in COL pigs (Figure 3.15 **h**). The occurrence of five SOTUs was significantly different between the feeding groups, as determined by Fisher exact test (Figure 3.17). SOTU5 (*Romboutsia sedimentorum*, 99.25%), was only present in the proximal small intestine of CTRL and RL pigs. *S. copri* (SOTU28) was predominantly present in caecum and colon of CTRL pigs, whereas *Harryflintia acetispora* (SOTU63) was only found in distal gut regions of RL and COL pigs. SOTU70 (92.88% similarity to *Acetitomaculum ruminis*) and SOTU 83 (*Leyella stercorea*, 98.33%; previously *Prevotella stercorea*, Hitch et al. 2022a) were only found in the CTRL and RL groups (Figure 3.17), further shaping the separate microbiota profile of COL pigs in the distal intestine. All regions were specifically screened for the presence of published SBA producers (see Table 2.1) using BLAST. However, none of the SOTUs detected at >0.25% rel. abundance reached 97% sequence similarity (species-level threshold).

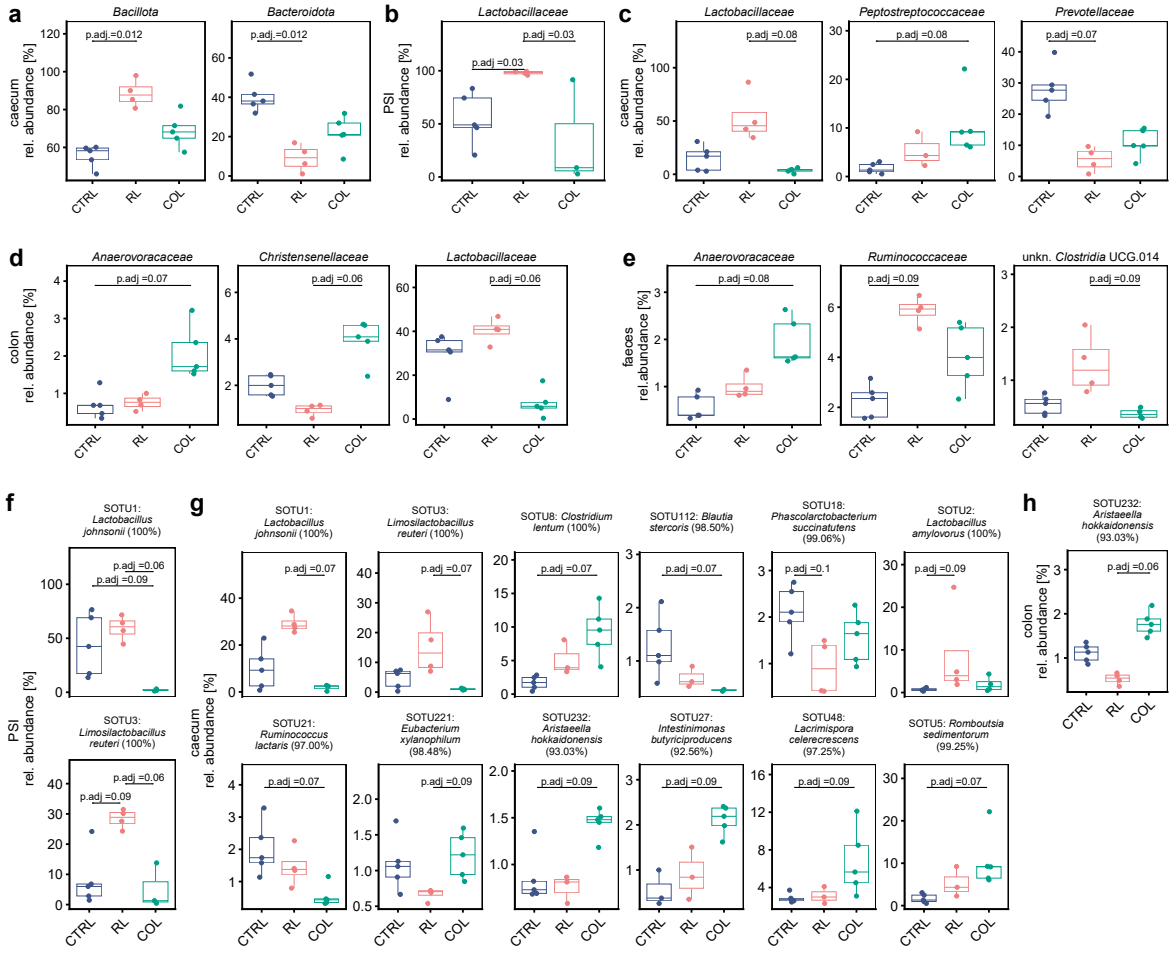

Figure 3.15: Rel. abundance of bacterial taxa between feeding groups in different gut regions (only taxa with p.adj <0.1). **a** Significantly different phyla in the caecum. **b**-**e** Bacterial families in different gut regions: **b** proximal small intestine (PSI), **c** caecum, **d** colon, **e** faeces. **f**-**h** SOTUs in different gut regions: : **f** PSI, **g** caecum, **h** colon. Statistics: Kruskal-Wallis with Dunn´s multiple comparisons, Benjamini-Hochberg adjustment (p.adj <0.1 are shown). Regions are also indicated on the y-axes.

In summary, the dietary intervention had significant effects on α-diversity and composition at the phylum level, especially in the caecum, where all 3 diet groups clustered separately. RL pigs were characterised by high levels of *Lactobacillaceae* in proximal small intestine and caecum, whilst CTRL pigs had high levels of *Prevotellaceae*. Interestingly, RL and CTRL pigs were more similar to each other in the colon, whereas COL pigs clustered separately, with higher levels of *Anaerovoraceae* and *Christensellaceae*. This indicates that a high red-meat and fat content in the diet plays a major role in shaping the microbiota in the caecum and less in the colon, whilst colestyramine had a strong effect both in caecum and colon.

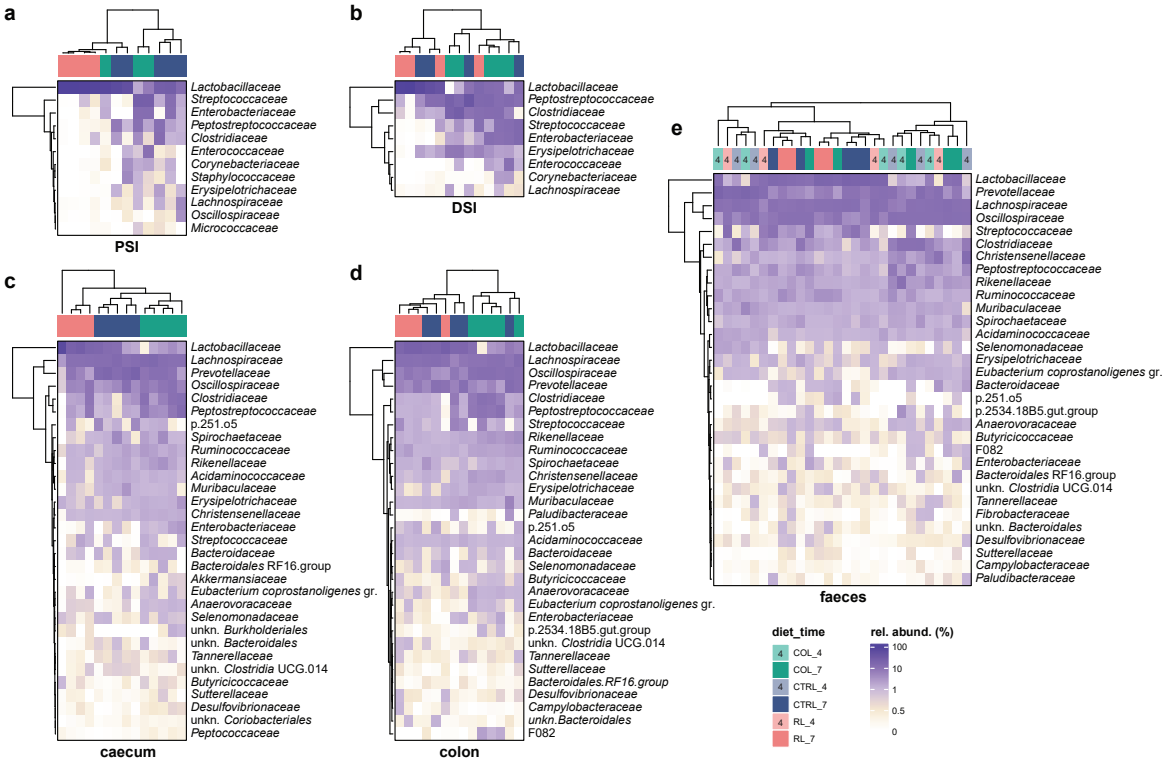

Figure 3.16: Heatmaps with euclidean clustering of pigs based on microbial family composition (rel. abundances) in each gut region: **a** proximal small intestine (PSI), **b** distal small intestine (DSI), **c** caecum, **d** colon, **e** faeces (start and end of feeding period). Diet groups (indicated below each heatmap) and mean rel. abundance of each family are colour coded (see colour legend; 4 = before the start of the experimental feeding intervention at month 4).

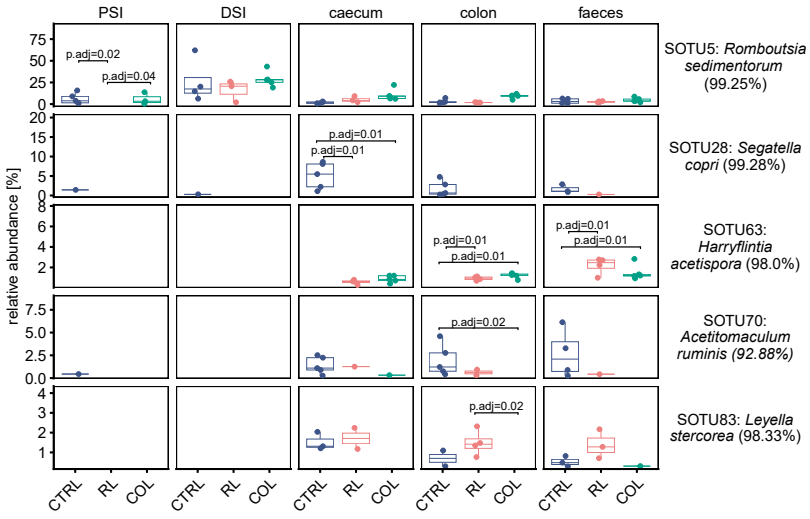

Figure 3.17: SOTUs comparison for presence/absence. SOTUs that tested significant in at least one gut region are shown. Statistics: pairwise Fisher exact test, Benjamini-Hochberg adjustment, prevalence in at least one region >30%, minimum median abundance value 1, all rel. abundance values below 0.25% were set to 0.

3.4.3 Diet and colestyramine affected BA composition

Besides the aforementioned effect on microbiota structure, we hypothesised that colestyramine prevents bacterial conversion of BAs. Therefore, their composition was analysed in proximal small intestine, caecum, colon content, and in faeces of the pigs. Colestyramine is a drug that acts by scavenging BAs (Scaldaferri et al., 2013), making them unavailable for absorption by enterocytes and possibly bacterial conversion in the distal gut. Therefore, higher amounts of conjugated BAs were expected in faeces. Notably, it was assumed that the sample preparation method before BA quantification would separate the colestyramine resin from the BAs, therefore making it not possible to distinguish BAs bound to colestyramine from unbound BAs.

At the end of the feeding period (month 7), BAs were compared between the three feeding groups for different intestinal regions: proximal small intestine, caecum, colon, and faeces. Analysis of variance stratified by gut region (using adonis2, Oksanen et al. 2022) revealed no significant diet effects for overall BA profiles. In line, NMDS plotting of BA profiles showed no clear separation between the three diet groups (Figure 3.18 **a**). Inter-individual differences within a diet group seemed to be larger in the proximal intestine. As expected, the addition of colestyramine led to an accumulation of conjugated BAs in the caecum, colon, and faeces of the pigs (Figure 3.18 **b**). Furthermore, COL pigs had significantly more SBAs in the colon compared to the CTRL and RL pigs, while faecal SBA levels were similar between RL and COL pigs (Figure 3.18 **b**). This could indicate that most (conjugated) SBA absorption happened in the proximal colon. Over time comparison of the BA categories showed a trend towards higher conjugated PBA and SBA in the COL group, but no significant differences, likely due to low numbers of animals and marked inter-individual differences (Figure 3.18 **c**). Analysis of individual BAs also revealed no significant changes when comparing values before and after the intervention, although there was a trend ($p = 0.062$) towards higher DCA and isoLCA in both RL and COL pigs (Appendix Figure A.14 **a**). Rel. abundance of dominant BAs (>1% rel. abundance) in each gut region also revealed inter-individual differences (Figure 3.19 **a**). CTRL and COL pigs had higher levels of conjugated SBAs in the proximal small intestine, while RL pigs had predominantly conjugated PBAs. However, no significant differences were found due to large difference between pigs of each diet group. SBA levels increased in distal intestinal regions, with most significant differences between individual BAs in the caecum (Figure 3.19 **a** and **b**). As observed for total conjugated PBAs and SBAs (Figure 3.18 **b**), there were also differences in individual BA species (Figure 3.19 **a**). The COL diet lead to increased levels of the conjugated PBAs GCDCA, GHCA and TCDCA as well as the conjugated SBAs GHDCA and GUDCA. The increased amounts were most likely due to BA sequestration by colestyramine. These differences were however not significant after pairwise Dunn's multiple comparisons (Appendix Figure A.15 **a**). In colon and faeces, colestyramine did not lead to increased individual conjugated BAs , even though total amounts were significantly higher in the colon (Figures 3.19 **a** and 3.18 **b**). The only differences in these regions were found for SBAs, with significantly higher levels of DCA in COL pigs in the colon (Figure 3.19 **c**). In faeces, elevated levels of DCA were found in both RL and COL pigs, however, this was not significant after adjustment for multiple comparisons (Appendix Figure A.15 **c**).

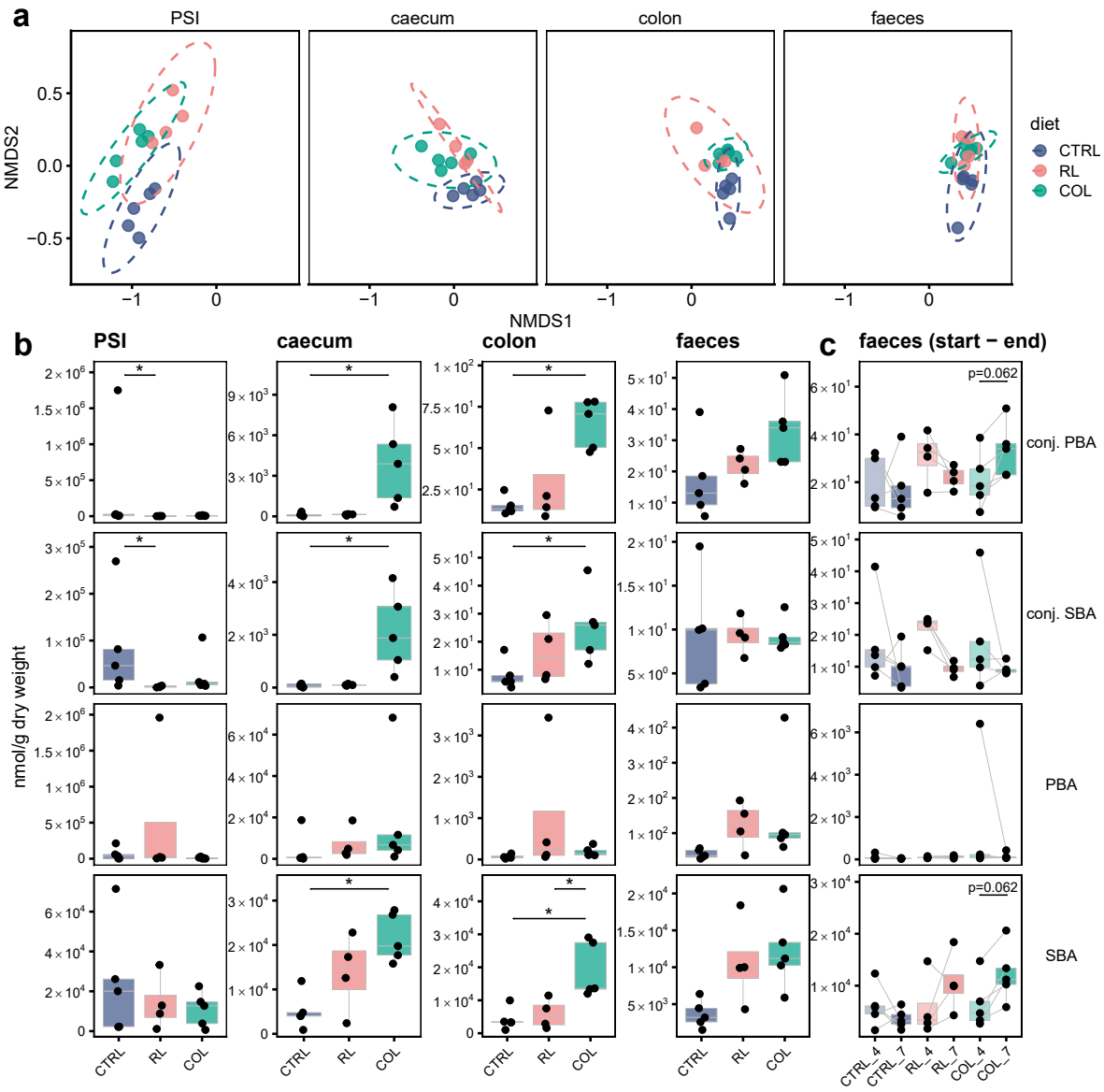

Figure 3.18: Main categories of BAs in different gut regions. **a** BA profiles along the intestinal tract at the end of the feeding period (month 7), visualised as NMDS plots using Bray-Curtis distances, faceted by gut-region. Stress for all plots was <0.2. **b** Conjugated (conj.) PBA, conj. SBA, free PBA, and free SBA concentrations along the intestinal tract at the end of the feeding period (month 7) and **c** over time in faeces. Statistics for **b**: Kruskal-Wallis with Dunn´s multiple comparisons and Benjamini-Hochberg adjustment per region. * p.adj <0.05. Statistics for **c**: paired Wilcoxon signed-rank test test, shown are p <0.1.

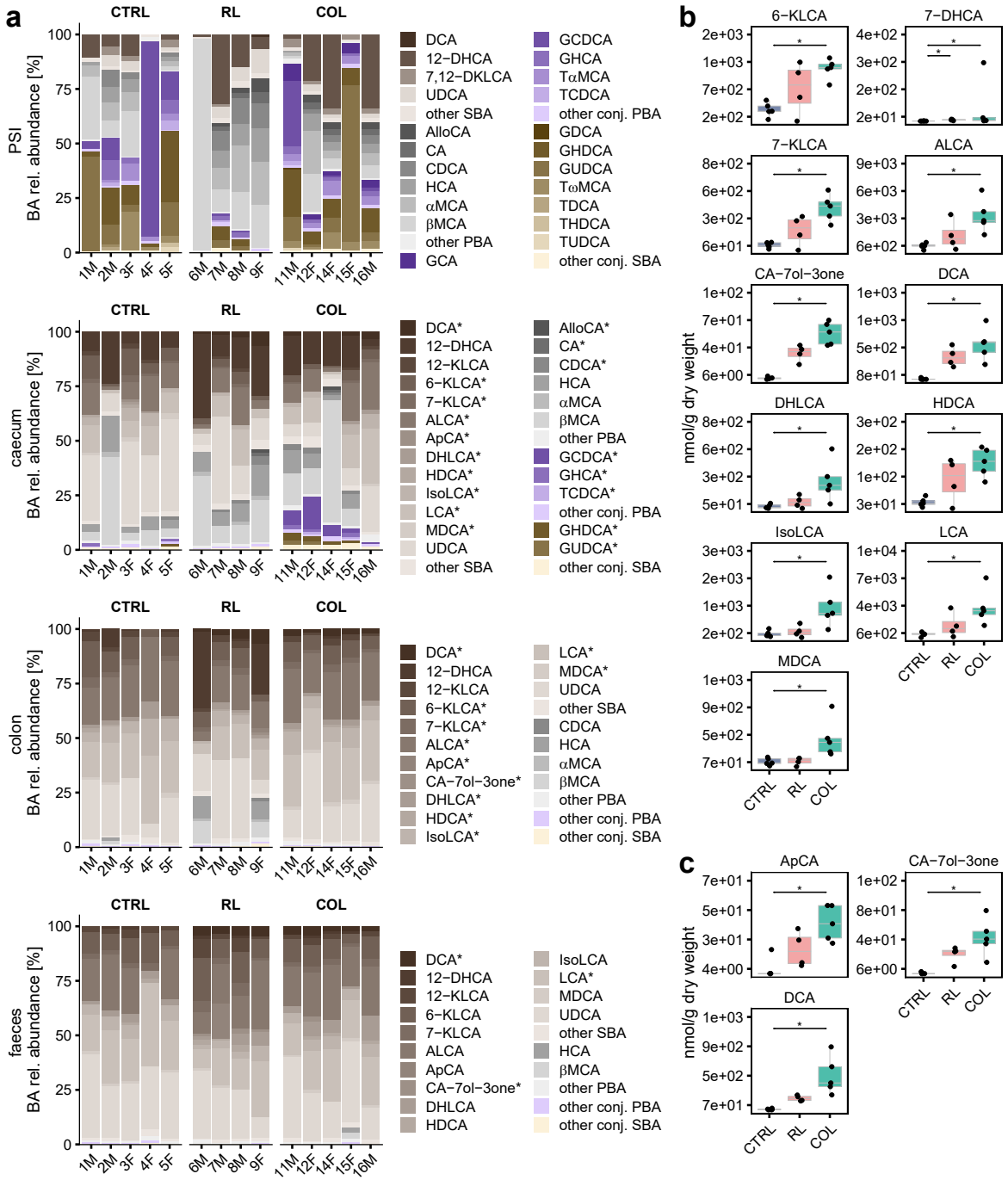

Figure 3.19: Composition of individual BA species in different gut regions after the feeding intervention. **a** Rel. abundance of dominant BAs per gut region. BA categories (SBA, PBA, conj. PBA, conj. SBA) are indicated by different colour shades (brown, grey, purple, beige). All BAs with <1% rel. abundance are combined as other SBA/PBA/conj. PBA/conj. SBA. BAs with significant difference between the three groups are marked with *. Dunn's multiple comparisons of all *BAs are in Appendix Figure A.15. **b** Significantly different SBAs in the caecum (p.adj <0.05). **c** Significantly different SBAs in the colon (p.adj <0.05). Statistics: calculated on BA concentrations; cut-off prevalence per region >30%; Kruskal-Wallis with Dunn´s multiple comparisons and Benjamini-Hochberg adjustment.

Besides BA conversion to SBAs, gut bacteria can metabolise complex carbohydrates from the diet to produce SCFAs. Butyrate-producing species and the expression of genes encoding carbohydrate-degrading enzymes were observed to be decreased in the microbiome of CRC patients compared to controls (Liu et al., 2022; Wirbel et al., 2019). SCFA, in particular butyrate, may thus be a potential confounding factors in our studies. However, the SCFA that were measured in the different intestinal regions were not significantly different between the 3 diet groups in any gut region (Appendix Figure A.17). Additionally, due to colestyramine influencing the levels of cholesterol and other lipids, lipidomic profiles were measured in the different gut locations and in plasma.

3.4.4 Diet composition shaped lipidomic profiles in different gut regions

At the end of the feeding period (month 7), multivariate analysis of all FA in the different gut regions showed that FA profiles in the CTRL group clearly separated from those in RL and COL pigs (Figure 3.20 **a**). Comparing different FA categories revealed significantly higher saturated FA (SA FA), branched chain FA (BC FA) and total FA in different gut locations in the COl and RL group (Figure 3.20 **c**). In the caecum, RL pigs had significantly higher levels of mono-unsaturated FA (MU FA) compared to the CTRL group. No significant differences were observed in poly-unsaturated FA (PU FA) (Figure 3.20 **b**). Comparing different categories of faecal FA revealed no significant changes over time after adjustment for multiple comparisons (Figure 3.20 **c**). However, a trend towards higher SA FA at the end of the feeding period was observed in the RL and especially in the COL group ($p = 0.125$ and $p = 0.062$, respectively), as opposed to the CTRL group ($p = 1$). A similar effect was observed for total FA (highest in COL pigs at the end of the intervention; $p = 0.062$). BC FA did not change in the RL and COL group over time and but they decreased in the CTRL group ($p = 0.062$). MU FA showed a similar increasing trend in all three groups (Figure 3.20 **c**). Comparison of individual FA species revealed that proximal regions had more significant differences in shorter FA between the three diets, whereas in the distal regions more differences occurred in longer FA (Appendix Figure A.18 **a**). One PU FA (FA 20:5-c5,c8,c11,c14,c17) was only present in the colon and faeces (Appendix Figure A.18 **a**), suggesting that it is produced by gut microbes in the distal gut. Interestingly, this FA was also significantly different between the three groups (Kruskal Wallis p.adj <0.05), with lower levels in the CTRL group (negative z-score).

Besides FA levels, sterols and stanols were also measured, because colestyramine in the diet could also influence their metabolism by gut bacteria. Sterols and stanols can originate from the host (e.g. cholesterol), the diet (e.g. brassicasterol or sitostanols), or the microbiota. The term "sterolbiome" has been proposed (Ridlon and Bajaj, 2015) for microbial genes involved in the metabolism of diet derived sterols. Cholesterol can be converted to e.g. coprostanol and it was found that individuals harbouring bacteria with the respective genes for this reaction have lower cholesterol levels in faeces and serum (Kenny et al., 2020). Even though a separation of the diet groups was already observed in the proximal small intestine, significant differences only occurred in the distal gut regions (Figure 3.21 **a**). CTRL pigs had significantly higher levels of plant-derived campesterol, sitosterol, campestanol-5a-3b, and stigmasterol (Figure 3.21 **b**). While no significant difference was found for cholesterol, copronstan-3-ol, likely derived from microbial conversion of cholesterol, was almost exclusively detected in the

colon and faeces of RL and COL pigs. Plasma lipids, including free cholesterol, were not significantly affected by the diet (Appendix Figure A.20). Also the phosphatidylcholine/lysophosphatidylcholine (PC/LPC) ratio, which is sometimes used as a marker for inflammation (Angelini et al., 2014), was not significantly different between the three groups (Appendix Figure A.20 **c**).

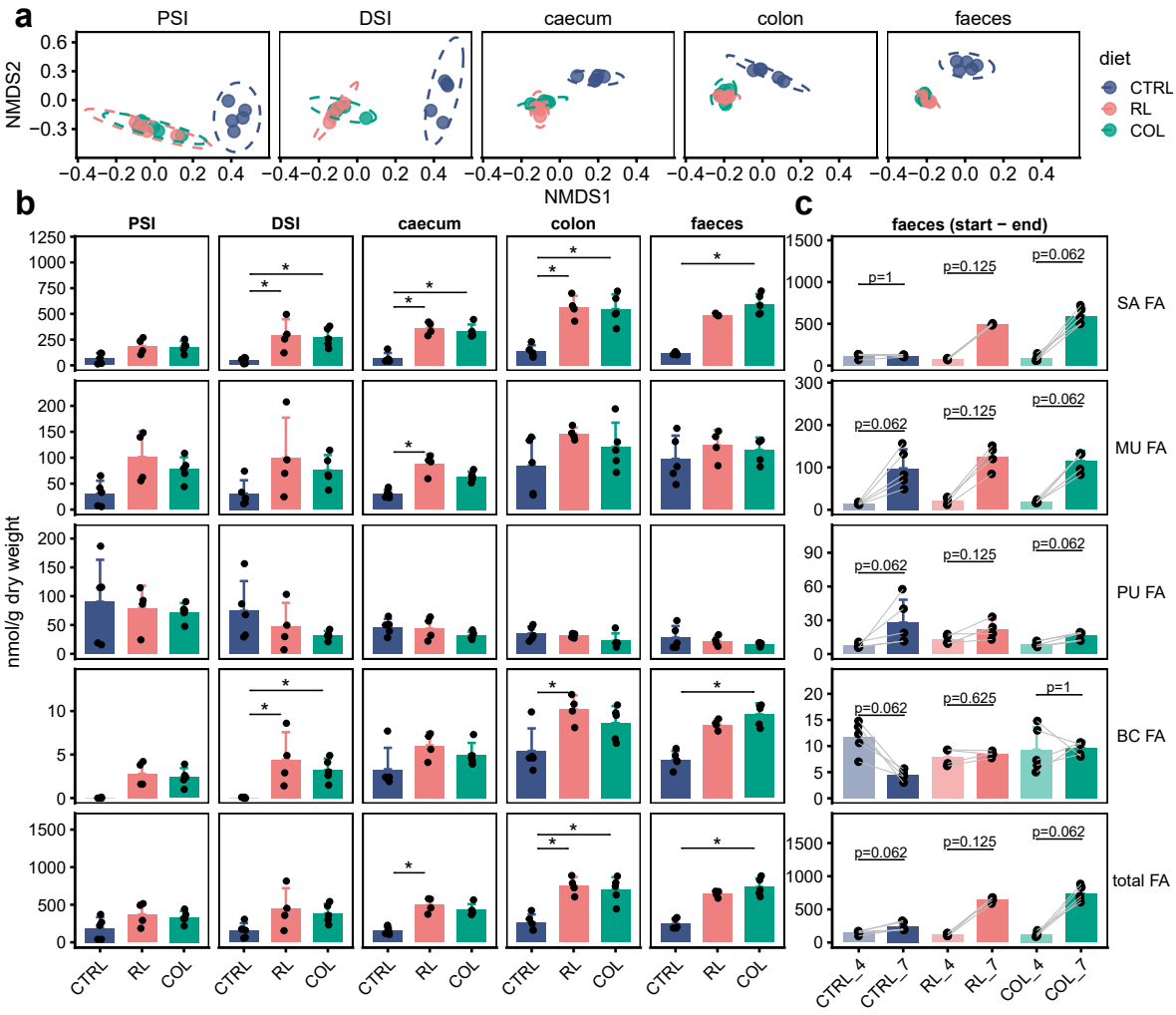

Figure 3.20: FA profiles in different intestinal regions and over time. **a** FA profiles visualised by NMDS plots using Bray-Curtis distances, faceted by gut region. Stress: 0.07. **b** Comparison of FA categories (see labels on the far right of the figure) at the end of the feeding period. **c** FA categories over time: branched chain FA (BC FA), saturated FA (SA FA), mono-unsaturated FA (MU FA), poly-unsaturated FA (PU FA), and total FA. Statistics: **b** Wilcoxon rank-sum test, Benjamini-Hochberg adjustment: * p.adj <0.05, ** p.adj <0.01. ; **c** paired Wilcoxon signed-rank test. Concentrations of 0 nmol/g are not plotted but were included for the statistics.

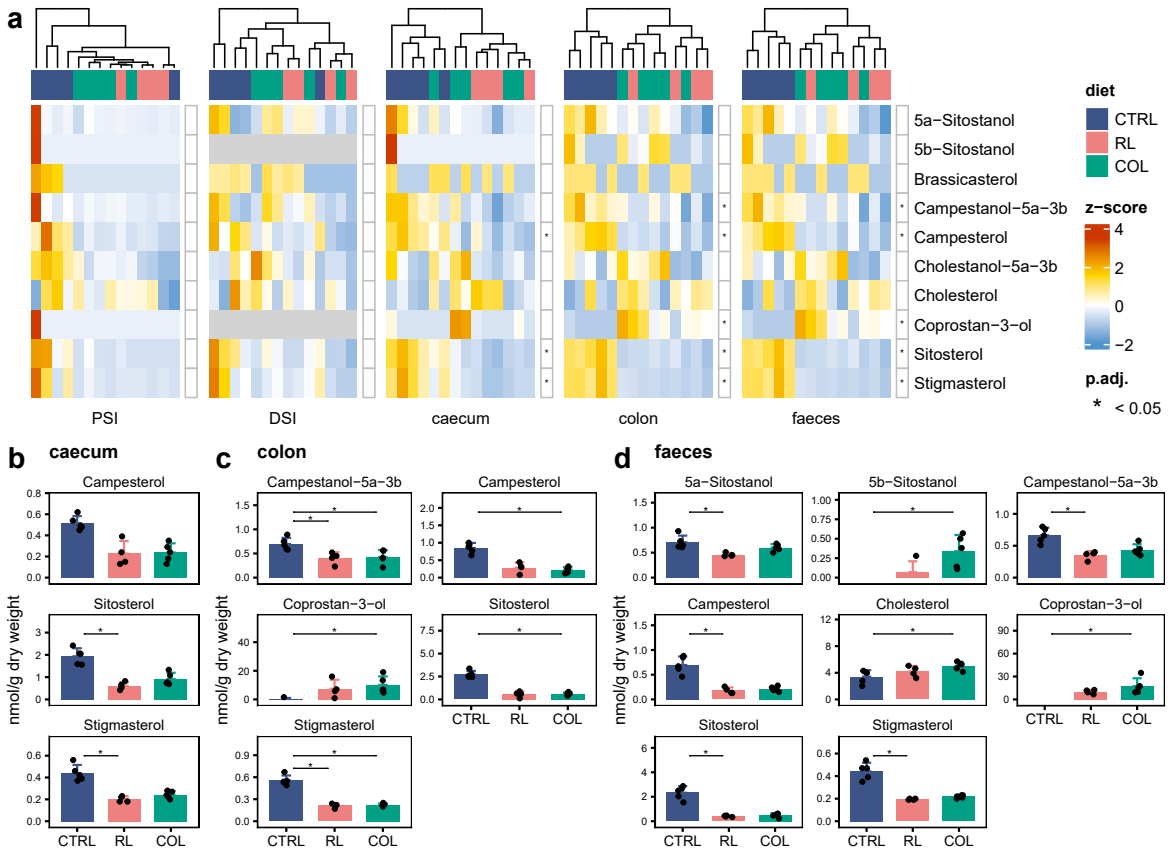

Figure 3.21: Sterol and stanol profiles at the end of the feeding period in different intestinal locations. **a** Heatmap of normalised sterol/stanol concentrations. Non-detected compounds are coloured in grey; stars indicate statistical significance (Kruskal-Wallis test). **b**-**d** Concentrations of sterol/stanols with significant differences between diet groups (Dunn's multiple comparisons). Statistics: **a** Kruskal-Wallis; **b**-**d** Dunn's multiple comparisons; **a**-**d** Benjamini-Hochberg adjustment; * p.adj <0.05. Zeroes are not plotted, but were included for statistical analysis. Comparisons of all sterols/stanols per gut region can be found in Appendix Figure A.19.

In summary, the effect of colestyramine on decreasing polyp numbers in the distal colon was biased by inconsistent phenotypes in the reference groups (CTRL and RL pigs). However, a significant decrease in epithelial cell proliferation and CD3+ cell density was observed in the colon due to treatment. The dietary intervention had a substantial influence on microbiota diversity and composition, especially in the distal intestine (caecum and colon). Significantly higher conjugated BA levels, including SBAs, were observed in the caecum/colon/faeces of the pigs fed the BA scavenger colestyramine (COL). The dietary intervention also had an impact on FA profiles and the amount of certain sterols/stanols in distal gut regions, but not on plasma lipids.

CHAPTER 4

Discussion

Microbially produced SBAs have been associated with CRC. However, proof of causality and mechanistic effects *in vivo* are still scarce. Addressing this issue is complicated by the diversity of BA species and their functions , host-microbe and microbe-microbe interactions. Additionally, CRC is a heterogeneous disease that takes years to develop, involving a sequence of different genetic events, and also changes in microbiota and immune responses. Therefore, we used several CRC animal models, dietary interventions, gnotobiotic and complex microbiota colonisation approaches, and multi-omics techniques to gain novel insights into the causal relationship between microbial SBAs and CRC.

4.1 Effect of BAs on tumours in animal models of experimental CRC

In gnotobiotic AOM/DSS-treated mice fed a high-fat diet, *E. muris* colonisation (BACOMI(7αDH+) mice) caused significantly higher number of tumours compared to BACOMI(7αDH-) colonisation. This confirms findings from our collaborators on the causal effects of *C. scindens* instead of *E. muris* as a DCA producer (Wortmann et al., 2023). DCA was only detected in BACOMI(7αDH+) mice, as expected. Female mice colonised with BACOMI(7αDH+) had a higher percentage of CA and DCA as well as total SBA levels compared to male mice. Interestingly, male and female mice had similar tumour numbers in this experiment, despite different BA profiles. This can be partly explained by sex-specific differences in CRC risk. Testosterone was shown to enhance CRC risk in male mice and rats (Song et al., 2021; Amos-Landgraf et al., 2014). Next to CRC risk, there are also sex-specific differences in BA metabolism. Also in the gnotobiotic trial with OMM12+E colonised *Apc*$^{1638N/+}$ mice, there was a sex-specific trend for DCA and the rel. abundance of *E. muris*: for the two female mice, lower *E. muris* rel. abundance lead to higher DCA levels compared to male mice. Fu et al. (2012) showed that female mice with complex microbiota had higher serum and liver DCA concentrations compared to male mice, which could indicate that female mice produce more SBAs and/or are more efficient in recycling SBAs by enterohepatic circulation. Additionally, CA was found to induce 7αDH (Vico-Oton et al., 2023).

Male and female *APC*$^{1311/+}$ pigs did not show the same drastic sex-specific differences in SBA levels as the two gnotobiotic mouse models. Instead, marked inter-individual differences were observed. Nevertheless, all RL pigs, which were characterised by DCA concentrations of 166 ±40 nmol/g dry weight in the colon, showed increased proliferation in the distal colon compared to CTRL and COL

pigs. This is in line with findings from Bartram et al. (1995), who showed that a DCA concentration of 5 µM induced proliferation in healthy human colon biopsies. In the feeding intervention, *APC*$^{1311/+}$ pigs on COL diet showed less proliferation, even though their colonic DCA levels were higher (488 ±271 nmol/g dry weight). This points towards an intracellular effect of SBAs on proliferation, which may be reduced by the BA scavenger colestyramine, preventing cellular uptake of BAs. In contrast, scRNA-Seq of *Apc*$^{1638N/+}$ mice showed that cells expressing the proliferation marker *Lgr5* (cluster 5 and cluster 8) were more abundant in OMM12 mice compared to OMM12+E. Especially the transit amplifying cells of cluster 8 were very low abundant in OMM12+E mice. A possible explanation could be that OMM12+E mice had longer crypts and therefore less cells were isolated from the crypt bottom. This would also explain the higher amount of absorptive enterocytes (cluster 2) in the OMM12+E group.

In the short-term gnotobiotic experiment in *Apc*$^{1638N/+}$ mice colonised with OMM12 or OMM12+E, the only significantly different BA was DCA. While TβMCA and DCA are FXR antagonists, CDCA and TCA are FXR agonist (Fu et al., 2019; Thomas et al., 2008; Sayin et al., 2013). Despite the presence of the FXR antagonist DCA, we observed no significant difference in the expression of the FXR target gene *Ibabp* (*Fapb6*), neither in cluster 2 (absorptive enterocytes) nor in cluster 5 (stem cells). This could be due to the FXR antagonist TβMCA, which was equally abundant in both OMM12 and OMM12+E mice. FXR itself was also not differentially expressed in OMM12 vs. OMM12+E mice and therefore did not contribute to differential expression of its target genes. Also in AOM/DSS-treated mice, TβMCA levels were similar for both BACOMI(7αDH-) and BACOMI(7αDH+) colonised mice, while DCA levels up to 1,277 nmol/g dry weight were detected in the caecum of BACOMI(7αDH+) mice. In line with the presence of DCA, the number of small tumours was significantly higher in BACOMI(7αDH+) mice compared to mice without *E. muris*. Fu et al. (2019) found that the FXR antagonist TβMCA-induced proliferation of two different CRC cell lines and intestinal organoids from *Apc*$^{Min/+}$ mice, while the FXR agonist FexD prevented the TβMCA caused organoid growth and suppressed expression of stem cell genes *Lgr5* and *Olfm4*. They also detected high levels of both TβMCA and DCA with increased tumour load in *Apc*$^{Min/+}$ mice (Fu et al., 2019). In line, Modica et al. (2008) suggested that DCA and TβMCA might act as a tumour promoter in both inflammatory conditions and in the context of certain genetic mutations like in *Apc*$^{Min/+}$ mice via FXR antagonism. In *APC*$^{1311/+}$ pigs, the COL diet lead to elevated HDCA in the colon. In piglets, HDCA supplementation enhanced FXR, but not TGR5 expression (Song et al., 2020), indicating that HDCA is an FXR agonist. Furthermore, Song et al. (2020) found that dietary HDCA suppressed intestinal epithelial cell proliferation in weaned piglets through FXR dependent downregulation of the PI3K/AKT (protein kinase B) pathway. In *APC*$^{1311/+}$ pigs , the FXR agonist HDCA might have had a reducing effect on colonic IEC proliferation in the COL group, while the FXR antagonists DCA and TβMCA possibly had a tumour promoting effect in AOM/DSS treated BACOMI(7αDH+) mice.

In the FMT trial, we mainly observed tumours in the small intestine of *Apc*$^{1638N/+}$ mice, which is in line with the literature (Smits et al., 1997; Fodde and Smits, 2001; Fodde et al., 1994). Surprisingly, there was no difference in lesions between the different diet groups of colonised *Apc*$^{1638N/+}$

mice. Therefore, it can be assumed that neither the diet (CD or BA diet) nor the specific microbiota composition affected the phenotype of the *Apc*$^{1638N/+}$ mice. However, the presence of a microbiota in general did have an effect on both intestinal lesions and intestinal length, which was also influenced by diet. Germfree *Apc*$^{1638N/+}$ mice on BA diet had both a significantly higher total number of suspected lesions and a longer small intestine compared to germfree mice on CD diet as well as all colonised mice. Since germfree mice lack any bacterial BA metabolism, this effect likely originated directly from unusually high levels of CA in their intestine. Enterohepatic circulation of CA can lead to formation of TCA and TβMCA in the liver, which are released into the proximal small intestine. On the one hand, the presence of TβMCA for example might have antagonised FXR and thereby induced proliferation of stem cells, as reported by Fu et al. (2019). On the other hand, *in vitro* experiments showed that 25 µM TCA, which is an FXR agonist, enhanced proliferation of cells from mouse colon and small intestine in an EGFR-dependent fashion, whilst 50 µM DCA reduced proliferation via FXR (Dossa et al., 2016). Increased levels of GCA and TCA were also found in an early CRC stage (S0) (Yachida et al., 2019). Therefore, both TCA and TβMCA might have affected the phenotype we observed in the germfree *Apc*$^{1638N/+}$ mice, but by different mechanisms. These findings emphasise that it is important to consider the composition of the whole BA pool, which also depends on the host species.

The BA receptor TGR5 is activated by different conjugated and deconjugated BAs in the order LCA > DCA > CDCA > CA, with taurine-conjugated BAs having higher activation potency (Perino et al., 2021). In our OMM12(+E) mice, TGR5 was mainly expressed in chromaffin cells (cluster 10), with no significant difference between the two groups. This might me due to the varying levels of BAs of the mice that were pooled for each group. LCA was only detected in 1 of the 2 OMM12+E mice subjected to scRNA-Seq and none of the OMM12 mice. Also DCA levels differed between the two mice that were analysed by scRNA-Seq. *APC*$^{1311/+}$ pigs on COL diet and BACOMI(7αDH+) mice had increased levels of LCA and DCA in the colon and caecum, respectively. In an animal model of UC (DSS in drinking water), Sinha et al. (2020) found that DCA and LCA (5 mg/150 µL, applied by enema) ameliorated colon histopathology, which was dependent on TGR5. In line, reduced levels of SBAs were detected in stool samples of patients with ulcerative colitis pouches (Sinha et al., 2020). Furthermore, Sorrentino et al. (2020) found that TGR5 activation by BAs promoted regeneration of the intestinal epithelium by promoting intestinal stem cell renewal. In contrast, Liu et al. (2021) reported that colonic tumours of AOM/DSS treated mice had significantly higher mRNA levels of TGR5. The dual nature of TGR5 - necessary for anti-inflammatory effect of LCA (Sinha et al., 2020) but enhanced TGR5 levels in tumours (Li et al., 2019) - seems to be dependent on concentration of different BAs. In our AOM/DSS treated mice BACOMI(7αDH+), the amount of SBAs produced by *E. muris*, especially DCA and LCA, seemed to be enough to promote tumour formation under inflammatory conditions. In *APC*$^{1311/+}$ pigs, TGR5 activation might have protected COL and RL pigs from detrimental effects of their Western-type diet. In our short-term experiment with *Apc*$^{1638N/+}$ mice, the detected DCA levels (2.8- 26.6 nmol/g dry weight) in OMM12+E might have not been sufficient to induce TGR5 dependent tumour promotion. In line, the EGFR pathway was downregulated OMM12+E mice, as well as MAPK. TGR5 was shown to be involved in BA induced activation of

EGFR (Yasuda et al., 2007). In HT-29 human colorectal adenocarcinoma cells, EGFR-MAPK could be activated by DCA through calcium signalling (Centuori et al., 2016). Additionally, Liang et al. (2018) found that DCA (<1 μM) promoted EGFR-MAPK signalling in Caco-2 cells and *ex vivo* human intestinal enteroids. However, Liang et al. (2018) also reported that this activating effect peaked at 2-5 min and returned to baseline after 15 min. For our scRNA-Seq experiment, the time from sampling the $Apc^{1638N/+}$ mice was longer than 15 minutes, which would explain the lack of EGFR-MAPK upregulation.

PROGENy analysis revealed significant upregulation of the hypoxia pathway in OMM12+E compared to OMM12 colonised $Apc^{1638N/+}$ mice. Hypoxia can cause mitochondrial production of ROS and lead to oxidative stress in the cell (D'Aiuto et al., 2022). Lechner et al. (2002) found that both 50 and 500 mM DCA treatment of gastrointestinal cancer cells (St 23132 cells, originating from gastric adenocarcinoma) for 6 h induced thioredoxin reductase mRNA expression, implying that DCA causes oxidative stress and even oxidative burst. Thioredoxin reductase upregulation would therefore be a defense mechanism of the cells (Lechner et al., 2002). In HCT 116 cells, DCA at a concentration of 0.3 mM was associated with increased ROS and genomic DNA fragmentation (Zeng et al., 2015). These findings indicate that DCA might have promoted mitochondrial ROS generation in OMM12+E mice. ROS can activate NFκB signalling (Morgan and Liu, 2011), and this pathway was indeed significantly upregulated in OMM12+E mice. This is also in line with findings from Payne et al. (1998), who found that DCA treatment activated NFκB in HTC 116 cells (0.5 mM NaDCA for 4h) as well as cells at the base of human colon crypt specimens with apoptosis resistance (1.0 mM NaDCA for 3 h).

Two of the animal models used in this thesis were based on mutations in the *APC* gene. Mutations in the *APC* gene also cause Wnt pathway activation in human cancer (Karim et al., 2004). We hypothesised that SBAs would promote tumour formation initiated by Wnt signalling. In OMM12+E colonised $Apc^{1638N/+}$ mice, no upregulation of the Wnt pathway (β-catenin pathway) was detected. In fact, 2 epithelial cell clusters (0 and 1) as well as stem cells (cluster 5) and goblet cells (cluster 7) showed significant down-regulation of this pathway, indicating that the Wnt pathway is not affected by DCA. In contrast, the PROGENy pathway of tumour-suppressor p53 was significantly upregulated in OMM12+E colonised $Apc^{1638N/+}$ mice. This is in line with findings from Qiao et al. (2001), who found that transcript levels of p53 were upregulated by DCA in a dose-dependent fashion in HCT 116 cells, which was not the case with CA or UDCA.

The significant upregulation of the PROGENy p53 pathway in OMM12+E mice may have caused apoptosis of goblet cells in cluster 7, as we observed lower cell numbers of this cluster in $Apc^{1638N/+}$ mice colonised with OMM12+E by scRNA-Seq. Also $APC^{1311/+}$ pigs on RL diet had lower goblet cells in the distal colon compared to the other two diet groups. Goblet cells produce and secrete mucus, and aberrant mucus production hampers the separation between bacteria and epithelial cells (Coleman and Haller, 2021). A dysfunctional mucus layer is also associated with CRC (Coleman et al., 2018; Bossuyt et al., 2009). While the lower number of goblet cells we observed in OMM12+E mice might have been due to different cell isolation efficiency, it could also be the effect of DCA. Treatment of mucosa samples with 1 mM NaDCA for 3h lead to reduced apoptosis in goblet cells

of normal tissue when patients had polyps or a history of cancer as opposed to induced apoptosis in samples from patients with no history of neoplasia (Bernstein et al., 1999). This could indicate that in our short term trial with *Apc*$^{1638N/+}$ mice, the *Apc* mutation was not sufficient to render these mutant cells resistant to apoptosis of goblet cells. Additionally, Bossuyt et al. (2009) found that *Atoh1*, which was primarily expressed in goblet cells within cluster 7 (lower in OMM12+E mice), has a tumour-suppressor function in mice. Therefore, the lower number of goblet cells in Cluster 7 of OMM12+E mice could indicate impaired tumour-suppression in these mice.

Even though less cells were detected in cluster 7 (goblet cells) in OMM12+E mice, *Reg4* was significantly upregulated in cluster 7 of this group. REG4 has been associated with an aggressive CRC phenotype and unfavourable clinical parameters like chemoradiotherapy resistance (Zhang et al., 2021a). Furthermore, overexpression of REG4 was proposed as an early event in colorectal carcinogenesis and it has been proposed as a diagnostic and prognostic biomarker as well as a possible therapeutic target, even though there are conflicting results depending on different cancer phenotypes (Zhang et al., 2021a). Cluster 2 of OMM12+E mice showed significant upregulation of *Pdk4* as well as *Fabp2*. Leclerc et al. (2013) found increased expression of *PDK4* in the normal mucosa of CRC patients compared to control subjects. Epithelial signatures as well as several metabolic pathways, e.g. fatty acid metabolism are characteristic for CMS3 tumours (Guinney et al., 2015). Narahara et al. (2000) found that diet supplementation with 0.3% DCA for 45 weeks resulted in increased incidence of colon tumours as well as *Kras* point mutations in these tumours in AOM treated rats. These findings suggest that goblet cells of cluster 7 and enterocytes of cluster 2 might be responding to DCA production by *E. muris* and push the *Apc* mutation induced phenotype in a direction of CMS3 tumours, which is also characterised by *KRAS* mutations (Miller et al., 2021a; Guinney et al., 2015).

In our gnotobiotic OMM12+E *Apc*$^{1638N/+}$ mice, caecal DCA levels were between 2.8 and 26.6 nmol/g dry weight. Assuming that 1 g of gut content contains a similar amount of bacteria and metabolites as 1 mL, resulting in 2.8-26.6 µM DCA, this is much lower than the concentrations used for most *in vitro* experiments, e.g. 0.3 mM used by Zeng et al. (2015) or 0.5 and 1 mM used by Payne et al. (1998). In summary, multiple factors, such the host species, sex, inflammation, genetic background and BA composition can influence the effects of SBAs in CRC development. Stem cells, absorptive enterocytes, and goblet cells might be the cell types that are most affected by SBAs. In gnotobiotic AOM/DSS treated mice on a high-fat diet, DCA production by *E. muris* promoted tumorigenesis, while the RL diet in pigs did not. Therefore, composition of the BA pool needs to be considered, since BA receptors like FXR and TGR5 can be differentially activated and induce different downstream reactions. In germfree *Apc*$^{1638N/+}$ mice, proliferation was promoted by CA supplementation. From the gnotobiotic experiment comparing cell-level changes between *Apc*$^{1638N/+}$ mice colonised with OMM12 or OMM12+E, the addition of DCA-producing *E. muris* might promote expression of PROGENy pathways for hypoxia, p53, and NFκB. The inducible transcription factor κB can activate the transcription of various genes and thus can regulate e.g. cell proliferation, apoptosis, or inflammation (Liu et al., 2017). It also influences the production of inflammatory cytokines, which in turn can lead to activation and differentiation of inflammatory T cells (Liu et al., 2017).

4.2 Influence of BAs on the immune system

Total CD3+ CD4+ Foxp3+ T cells (T_{reg} cells) were slightly higher in the colon of BACOMI(7αDH+) mice, which also had a higher number of small tumors. Several SBAs were found to interact with Foxp3+ T cells. Hang et al. (2019) reported that the BA metabolites 3-oxoLCA and iso-alloLCA reduced T_H17 cell differentiation while they induced differentiation of T_{reg} cells. Iso-alloLCA was shown to induce T_{reg} cell differentiation via the nuclear receptor NR4A1 (Li et al., 2021). Campbell et al. (2020) discovered that isoDCA increased Foxp3 induction by diminishing immunostimmulatory properties of DCs. This effect was found to be FXR-dependent (Campbell et al., 2020). Interestingly, no iso-BAs were detected in OMM12 mice with or without *E. muris*, which would be the product of 3β-hydroxysteroid dehydrogenase (3β-HSDH) (Marion et al., 2019). This can be explained by the difference in colonisation. Out of the 3 OMM12 strains that express 3β-HSDH - *A. muris*, *A. muciniphila*, and *B. caecimuris* (Marion et al., 2020) - only *B. caecimuris* colonised OMM12+E mice consistently and its occurrence was characterised by marked inter-individual variations between OMM12 mice. *A. muris* was only detected in OMM12+E mice. Marion et al. (2020) showed that the addition of DCA-producing *C. scindens* to OMM12 affected BA metabolism and the expression of BA-metabolising enzymes like 3β-HSDH. In the feeding intervention with $APC^{1311/+}$ pigs, isoDCA was only detected in the proximal small intestine, with no significant differences between the feeding groups. In line with the lack of the known Foxp3 inducing BAs, the differences of Foxp3+ T cells in colon and MLN of BACOMI(7αDH+) colonised mice were not significantly different compared to BACOMI(7αDH-).

In contrast to slightly upregulated Foxp3+ T cells, CD8α+ T cells were significantly downregulated in BACOMI(7αDH+) mice. Cytotoxic CD8+ T cells have been associated with better clinical outcome for hepatocellular carcinoma (Gabrielson et al., 2016). Dysfunction of CD8+ T cells can happen late during cancer development and is induced by the tumour microenvironment, including TAM, Foxp3+ CD4+ T cells, inhibitory checkpoint signalling pathways, IL-10, TFG-β, or physiological changes like hypoxia (Philip and Schietinger, 2022). This indicates that the tumour microenvironment in the colon of BACOMI(7αDH+) mice might have prevented CD8+ T cell functionality. Further characterisation of these T cells, e.g. with markers for dysfunction like PD1, LAG3, CD38, CD39, IFNγ, or TIM3 (Philip and Schietinger, 2022) would be needed to confirm this hypothesis.

BACOMI(7αDH+) mice had significantly higher levels of F4/80+ CD11b+ CD206+ $Ly6C^{low}$ cells in the colon and MLN, while CD8+ T cells were slightly higher in BACOMI(7αDH-) mice. F4/80 and CD11b can be markers for marcophages, but are also found on eosinophils in mice (McGarry and Stewart, 1991; Thorne et al., 1990). Modak et al. (2022) found that in mouse tumour models, CD206+ macrophages (TAM) can cross-present antigens to CD8+ T cells, which in turn gain antigen-specific cytotoxic function. Wang et al. (2020) reported that DCA did not affect CD206+ cells in vancomycin-treated, high-fat diet fed mice. The increased F4/80+ CD11b+ CD206+ cell fraction could therefore be attributed to higher tumours in BACOMI(7αDH+) mice. F4/80+ CD11b+ $Ly6C^{high}$ cells were significantly elevated in the colon of BACOMI(7αDH-) compared to BACOMI(7αDH+) colonised

mice. Li et al. (2022b) reported that Ly6C^{high} macrophages develop from monocytes during inflammation and are enriched as a response to acute inflammation and have pro-inflammatory functions. Activation of TGR5 on macrophages and monocytes was found to mediate anti-inflammatory effects (Perino and Schoonjans, 2015). Even though Wang et al. (2020) did not find an effect of DCA on CD206+ macrophages, DCA produced by *E. muris* might have activated TGR5 and therefore elicited an anti-inflammatory effect with reduced chemokine and inflammatory cytokine expression (Perino and Schoonjans, 2015). This could indicate that DCA, which is a potent activator of TGR5, protected BACOMI(7αDH+) mice from DSS-induced colitis, as suggested by Sorrentino et al. (2020), by preventing Ly6C^{high} macrophage accumulation and promoting CD206+ cell accumulation. No significant differences were found in macrophage levels (Iba+ cells) in *APC*$^{1311/+}$ pigs (data not shown). However, further characterisation might have revealed differences between specific macrophage types.

The combination of lower numbers of cytotoxic CD8+ T cells and the trend of higher total Foxp3+ T_{reg} cells and F4/80+ CD11b+ CD206+ we observed in BACOMI(7αDH+) colonised mice indicates that the immune system is involved in the CRC promoting role of DCA in the context of inflammation. Additional BAs, e.g. iso-alloLCA or isoDCA might affect immune cells, which in turn affect tumour progression. Therefore, it remains to be resolved if the changes in the T cells and F4/80+ CD11b+ cells were due to BAs influencing the immune system directly, or if immune cells were rather attracted by the tumours themselves. These mechanisms might also be different between sporadic and colitis-associated CRC. To conclude, more detailed immune cell analyses are needed, along with consistent BA analysis, to elucidate the T cell phenotype in SBA-induced CRC development in the context of a Western diet.

4.3 Interplay between BAs and microbiota

In the feeding intervention, RL pigs had reduced α-diversity (Shannon effective counts) compared to CTRL and COL pigs, especially in the caecum. Whilst RL and COL pigs had similar levels of DCA in the colon, COL pigs were also characterised by significantly higher levels of conjugated PBAs in caecum and colon. In contrast to conjugated BAs, unconjugated/free BAs are weak acids, which have bactericidal properties at neutral pH (Islam et al., 2011). Gram-positive bacteria were found to be more sensitive than Gram-negative bacteria (Tian et al., 2020). In mice, the addition of CA and CDCA lead to a significant drop in Shannon effective counts compared to a control diet (Just et al., 2018), whereas a high-fat diet did not have an effect on Shannon effective. In COL pigs, colestyramine might therefore have prevented DCA from affecting other microbiota members.

In the FMT trial, a trend towards lower richness and Shannon effective counts was observed with the BA diet. This effect seemed to be more pronounced in mice that received the CTRL microbiota from donor pigs. Comparison of β-diversity also revealed a stronger effect of the BA diet in the CTRL group compared to the RL group, suggesting that the RL microbiota contained more BA tolerant species. Indeed, we detected the *bsh* positive *B. uniformis* and the taurine-respiring *B. wadsworthia*

only in the caecum of RL recipient mice, not in CTRL recipients. We also observed higher *Desulfovibrionaceae* levels in RL recipient mice compared to CTRL recipient mice, partly driven by *B. wadsworthia*. This effect was even stronger with the addition of CA to the diet of the *Apc*$^{1638N/+}$ mice. In line with this finding, *Desulfovibrionaceae* levels increased in pigs fed with the RL diet (Wortmann et al., 2023), whose faecal microbiota was used for the FMT trial with the *Apc*$^{1638N/+}$ mice. In the literature, feeding SPF mice with a CDCA- and CA-supplemented diet as well as a high-fat diet lead to significantly increased levels of *Desulfovibrionaceae* (Just et al., 2018), emphasising the importance of both BAs and diet for microbiota composition. Also in humans, an animal-based diet lead to increased levels of total BAs, including DCA and also promoted bacterial taxa with bile resistance (David et al., 2014). *B. wadsworthia* growth is promoted by TCA (Devkota et al., 2012), but this species does not have a *bai* operon. Therefore, its association with elevated DCA might be due to generally higher levels of TCA, which, after conjugation, can be transformed to DCA. A combined metagenomic and metabolomic analysis found that *B. wadsworthia* was significantly associated with DCA, which was elevated in multiple polypoid adenomas with low-grade dysplasia (Yachida et al., 2019). Since in our FMT trial, the RL recipient mice did not have higher levels of intestinal lesions, it can be assumed that *B. wadsworthia* did not have a detrimental effect, at least in this mouse model. Cao et al. (2017) found promoted intestinal tumorigenesis in mice that were only colonised with faecal microbiota from mice that were previously on a high DCA diet, showing that the DCA shaped microbiota also plays an important role for CRC promotion.

The dietary intervention with RL diet in *APC*$^{1311/+}$ pigs lead to higher levels of *Bacillota* and lower levels of *Bacteroidota*. Furthermore, increased levels of *Lactobacillaceae*, especially *L. johnsonii* (SOTU1, 100%) were detected in several intestinal regions of RL fed pigs. Members of the family *Lactobacillaceae*, including *L. johnsonii* have a highly active BSH (Song et al., 2019; Elkins and Savage, 1998). Interestingly, SOTU1 (*L. johnsonii*) was significantly lower in the proximal small intestine of COL pigs. With the lack of this *bsh*-positive species, together with the BA scavenger colestyramine in the diet, we expected lower levels of free BAs and higher levels of conjugated BAs. Indeed, COL pigs had significantly higher conjugated PBAs and SBAs compared to the CTRL group. However, no significant differences were detected for free PBAs. In the FMT trial, *Lactobacillaceae* were not transferred from donor pigs into *Apc*$^{1638N/+}$ mice. This difference could be due to different BA conjugation patterns in pigs and mice and the microbiota that is adapted to these conjugated BAs. In pigs, BAs are predominantly conjugated with glycine, whereas in mice, BAs are conjugated to taurine (Spinelli et al., 2016; Li and Dawson, 2019). Therefore, it can be concluded that *Lactobacillaceae* and potentially their BSH activity are dependent on host species and diet.

Besides high PBA levels, COL pigs had higher total SBAs in the colon compared to both RL and CTRL pigs. The high amount of conjugated SBA in the caecum indicates that enterohepatic circulation of BAs was not disrupted by colestyramine. Therefore, the applied dose (12g/kg feed) was probably not sufficient to scavenge all BAs. Although none of the published bacterial strains with a *bai* operon were detected in the pigs by 16S rRNA gene amplicon sequencing, they might have failed DNA extraction during the sample preparation. For example, our lab found that DNA of HSDH positive *Coriobacteriia* was extracted more efficiently with an enzymatic lysis step using lysozyme (not

published), which is not standard for the 16S rRNA gene amplicon sequencing sample preparation. Furthermore, even though increased *bai* genes were detected in metagenomes of CRC patients, no significant upregulation of known DCA producers like *C. scindens* or *C. hylaemonae* was observed (Wirbel et al., 2019). This indicates that the majority of DCA producing bacteria is unknown, or that they are subdominant and therefore escape sequencing, while still being extremely efficient in generating SBAs. Also in a previous feeding trial (Wortmann et al., 2023), no SBA producing strain was detected in the 16S rRNA gene amplicon data, nor by qPCR by using a primer for *baiCD* (data not published). In line, none of the known SBA producing strains was detected in *Apc*$^{1638N/+}$ mice that got the microbiota of the pigs in which increased levels of DCA were measured (Wortmann et al., 2023). However, we found higher levels of *Oscillospiraceae* in the colon of COL pigs, which was accompanied by significantly higher SBA levels. Kim et al. (2022) found an uncultured 7αDH+ bacterial clade affiliated with *Oscillospiraceae* and suggested that his family may be efficient at BA dehydroxylation by having a complete *bai* operon and a *bsh* gene. In *Apc*$^{1638N/+}$ mice colonised with pig microbiota in the FMT trial, this family was lower abundant in RL recipients, which might have also contributed to the lack of SBA induced lesions. Even though *bai* genes can be identified by genome sequencing and qPCR, there is still a need for cultured and characterised bacteria harboring the *bai* operon. This would enable the identification of *bai* operon harboring bacteria by high-throughput 16S rRNA gene amplicon analysis.

To summarise, microbiota was affected by both diet, CA supplementation, as well as the presence of the DCA producing *E. muris*. In the FMT trial with *Apc*$^{1638N/+}$ mice, the BA diet reduced richness and Shannon effective counts, similar to the RL diet in *APC*$^{1311/+}$ pigs. BA deconjugating bacteria (expressing *bsh*) were promoted by the RL diet in *APC*$^{1311/+}$ pigs. Furthermore, BA resistant taxa like *Desulfovibrionaceae* might profit from elevated BA levels and also influence CRC development, e.g. *B. wadsworthia*. However, host species specific differences in BA composition also need to be considered with regard to relevance of the findings for humans.

4.4 Translation and human relevance

Microbiota transplant is currently used as a therapeutic treatment for *Clostridium difficile* infection in humans (Cammarota et al., 2017). However, it can also be used as a tool to investigate the role of microbiota in disease development. To study the effects of microbiota-mediated SBA metabolism on tumour phenotype, faecal microbiota from pigs was transplanted into germfree *Apc*$^{1638N/+}$ mice. Microbiota transfer efficacy in this experiment was low, with a 3-fold reduction in richness and Shannon effective counts. This could have been caused by a high number of non-viable bacteria in the gavage stocks, which were still detected by 16S rRNA gene amplicon sequencing. Some SOTUs were only detected in mice, not in the donor samples. Different host environments, including diet, BA pool composition, or intestinal physiology, might favour the growth of different strains. The transfer into mice might have promoted the growth of subdominant bacteria that were not detected by 16S rRNA gene amplicon sequencing in the donor stocks. Wong et al. (2017) found that transfer of a

mix of stool samples from CRC patient and healthy controls into germfree C57BL/6 mice lead to significantly higher proliferation, but similar to our findings, no visible histological differences were detected between the recipients of CRC or healthy patient microbiota. In line with a drop in Richness and Shannon effective counts we observed in the FMT recipient mice, Wong et al. (2017) observed a significant drop in Shannon-Weaver's diversity over time for both recipient groups between 8 and 32 weeks after colonisation.

The transfer of microbiota from humans or pigs into mice poses several problems. Lifestyle, diet, or other factors that have a strong effect on gut microbiota composition in humans, are normally absent in mice, which makes it unlikely that diseases are replicated by microbiota transfer into mice (Walter et al., 2020; David et al., 2014). While host and microbiota normally evolve together with age, the transfer of foreign microbiota into germfree mice might lead to different host-microbe interactions in the recipient mice and therefore different pathological outcomes (Arrieta et al., 2016). Li et al. (2019) colonised antibiotic-treated, previously SPF *Apc*$^{\text{Min/+}}$ mice with faeces from CRC patients or healthy controls. They found that recipients of CRC patient microbiota had increased tumour numbers and proliferation and a lower number of goblet cells in the colon. Even though they did not analyse transfer efficacy in detail, microbiota composition at the genus level was quite different between donors and recipients (Li et al., 2019). However, similar to our FMT experiment, also the recipient mice had different bacterial abundance between the two groups at the genus level (Li et al., 2019). Even though confounding factors like lifestyle or diet were excluded in the donor pigs for the FMT trial, host specific differences might have dampened the phenotype. Furthermore, the lack of tumours detected in the colon of *Apc*$^{\text{1638N/+}}$ mice was most likely mouse model-dependent, since it has been shown before that *Apc*$^{\text{1638N/+}}$ mice develop adenomas and adeno-carcinomas mainly in the small intestine (Fodde et al., 1994).

Besides complex microbiota, we used two different synthetic microbial consortia to study the effect of the DCA producer *E. muris* on tumour development and intestinal epithelial cells. With the background of a high-fat diet, *E. muris* caused significantly higher tumour numbers in AOM/DSS-treated mice. The use of *Apc* animal models simulates a genetic predisposition for CRC like FAP, or the classic CRC pathway. In colitis-associated CRC, the *Apc* deletion only happens later in the cancer development process. Therefore, inflammation and carcinogens like AOM seem to boost the the tumorigenic effect of DCA in the context of a high-fat diet or the other way around.

In *APC*$^{\text{1311/+}}$ pigs, dietary colestyramine supplementation (12g/d) reduced proliferation of epithelial cells in the distal colon. This is in line with Li et al. (2022a), who found that colestyramine prevented high-fat diet induced upregulation of β-catenin gene expression in mice. Additionally, Xie et al. (2016) reported that 2% colestyramine in a high-fat diet significantly reduced the number of malignant lesions in the liver in a mouse model for steatohepatitis-hepatocellular carcinoma. Whilst colestyramine is currently used to treat patients with hypercholesteremia or BA malabsorption induced diarrhea (Scaldaferri et al., 2013), this BA scavenger might be a supplementary treatment option for patients with polyps or early stage CRC, especially if they consume a high-fat diet.

Both complex microbiota and gnotobiotic colonisation as well as the use of different animal models offer valuable insights in the effects of diet and the effects of BAs. For example, palmitic acid (C16:0), stearic acid (C18:0), and arachidonic acid (C20:4-c5,c8,c11,c14 (n-6)) were significantly upregulated with both the RL and the COL diet in $APC^{1311/+}$ pigs. This reflects findings from Wan et al. (2019), who found that faecal levels of these fatty acids were also were elevated with a high-fat diet intervention in humans. This confirms that the dietary intervention in pigs provides human relevant information. However, limitations of each model have to be considered when translating the findings to humans. Several limitations have to be considered also with the experiments of this thesis, as discussed next.

4.5 Limitations and considerations

Metagenomic studies have found several bacterial species that are associated with different CRC stages (Zeller et al., 2014; Yachida et al., 2019; Wirbel et al., 2019; Thomas et al., 2019). These species could have been potential confounding factors in our studies using complex microbiota. For example, *P. succinatutens* was significantly increased in faecal metagenomes from patients with multiple polypoid adenomas with low-grade dysplasia and stage 0 CRC (intramucosal carcinoma, polypoid adenomas with high-grade dysplasia), indicating that this species may play a role in early stages of CRC (Yachida et al., 2019). Interestingly, *P. succinatutens* was significantly higher in the caecum of CTRL pigs compared to RL pigs in the feeding intervention trial. In fact, higher tumours were observed in the CTRL group compared to the other two groups at the end of the feeding period. Therefore, *P. succinatutens* might have profited from the genetically induced CRC predisposition of the $APC^{1311/+}$ pigs rather than dietary conditions. In the FMT trial, *P. succinatutens* was found in all donor pigs and mouse recipients, with slightly lower levels in mice. No differences were observed between the different groups of recipient mice, indicating that in the FMT trial, *P. succinatutens* was no confounding factor.

Wong et al. (2017) proposed that CRC might be influenced by "keystone pathogens", which remodel the microbiota and affect tumour milieu even if they are lowly abundant. Therefore, they proposed a polymicrobial mix rather than single bacterial strains affect CRC development. Also Zeller et al. (2014) identified a panel of 22 species collectively elevated in CRC. In our experiment with the BACOMI(7αDH+/-) consortium, *B. wadsworthia* was present in all mice. Therefore, we cannot exclude that the increase in tumours observed with *E. muris* was dependent on the presence of hydrogen sulfide produced by *B. wadsworthia*. Furthermore, batch effects cannot be excluded for this trial, since the two groups of mice (with or without *E. muris*) were colonised and sampled several months apart from each other.

Similar to the results we observed in our pig feeding trial, no significant differences were found in terms of richness in a high-fat diet intervention trial in humans (Wan et al., 2019). Diversity estimated by Shannon effective number of species was lower in the high-fat diet group (Wan et al., 2019). We also observed significantly lower Shannon effective counts in the caecum of RL pigs compared

to CTRL and COL pigs. The fact that the COL group also had a higher Shannon effective count implicates that not the high-fat content, but the related intestinal BA levels or composition played a major role in this observation. While the COL diet was supplemented with colestyramine, both the RL diet and the CTRL diet contained cellulose as a sham, which might have affected microbiota in CTRL and RL pigs.

Our animal models with mutations of the *APC* gene (*Apc*$^{1638N/+}$ mice and *APC*$^{1311/+}$ pigs) did not develop the expected phenotypes. Therefore, BAs might act in a *APC*-independent fashion during CRC development. Readouts of each trial besides microbiota analysis varied between the studies. For instance, immune cell readouts were limited for the feeding intervention in *APC*$^{1311/+}$ pigs, while a more detailed analysis was performed for experiments with the gnotobiotic mice. The scRNA-Seq was only done with two pooled mice per group in one replicate. For the feeding intervention in *APC*$^{1311/+}$ pigs, each group comprised only 4 or 5 animals, which reduced statistical power of this experiment. The limited number of animals per group has to be considered when interpreting the results, even though pig studies are difficult to perform with high numbers of animals.

As discussed above, different BA compositions and concentrations can lead to different outcomes. For the FMT trial, no BA measurements were done, so conclusions about the role of SBAs in this trial remain hypothetical. Furthermore, comparability of BA measurements from different host species and performed in different facilities is difficult. For this thesis, BA measurements of mouse and pig samples were conducted at two different facilities with different methods. Therefore, statistical analysis of the results might be affected by different sizes of analysed BA panels, which leads to reduced power with an increased number of post-hoc comparisons. The extraction method can also affect the amount of measurable BAs. Both the extraction and analysis method may affect quantification (Haange et al., 2022), which limits comparability between studies. Therefore, BA measurements in humans might not yet be suitable for diagnostic purposes.

CHAPTER 5

Conclusion and Outlook

Many studies have identified an association between Western diet, SBAs and CRC. However, the causal effects of *in vivo* produced SBAs still need to be elucidated. Composition of the intestinal BA pool, which varies between different host species, as well as the concentration of each BA play a crucial role in determining the fate of BA effects on cellular responses. BAs have a wide range of functions and their balance is regulated by various feedback mechanisms (Perino et al., 2021). This makes studying the effects of certain BA species *in vivo* complicated. Supplementing feed or water of experimental animals with DCA or other BAs will inevitably lead to a disturbance of the physiological BA signalling network. This disruption might cause a variety of downstream effects and unexpected outcomes. Additionally, new BAs are still being discovered, e.g. by Quinn et al. (2020) and Sato et al. (2021), which have not been studied as thoroughly as e.g. DCA.

Additionally, the BA pool is inseparably connected to the gut microbiota and to diet. These three factors influence each other. In the context of experimental inflammation in combination with a carcinogen (AOM/DSS treatment) on the background of a high-fat diet, the DCA-producing *E. muris* caused increased tumour numbers in gnotobiotic mice. Our findings indicate that DCA might have a tumour-promoting role by influencing the intestinal epithelium. In $APC^{1311/+}$ pigs, the RL diet caused increased proliferation in the distal colon, which was prevented by the BA scavenger colestyramine. However, in this experiment, the expected increase in tumour numbers (Wortmann et al., 2023) was not confirmed. This emphasises that CRC development is a multi-factorial disease. The varying results regarding DCA-producing bacteria likely depend on specific experimental conditions, such as the context of other bacterial species present within synthetic communities and native communities, environmental factors such as carcinogen exposure, stress due to housing, inflammatory state, and type of (high-fat) diet.

To study the role of individual SBAs in a targeted fashion, different experimental approaches could be used. To our knowledge, no *bai* operon knock-out bacterial strain has been generated so far. The generation of such a knock-out would offer the possibility to specifically study the effects of DCA produced *in vivo* without potential confounding factors of strain-dependent differences in other metabolites. Another promising approach was reported by Funabashi et al. (2020), who engineered the *bai* operon into non-native producing *Clostridium sporogenes*, even though they reported lower levels of DCA production in mono-colonised mice compared to *C. scindens*. Minimal consortia with different BA conversion capacities could be used to study the effect of different BA pools on CRC development and the involvement of specific immune responses. In this regard, both colitis-associated

CRC models like AOM/DSS-treated mice as well as models for sporadic CRC (e.g. *Apc* mutant mice) should be considered, since BA composition has different effects in these scenarios. The use of $Cyp2a12^{-/-}Cyp2c70^{-/-}$ double knock-out mice, which have a BA pool more similar to humans (Ueda et al., 2022), could be used to avoid confounding effects of UDCA, which is normally a PBA in mice. Furthermore, mice with intestinal knock-out of *Tgr5* or *Fxr*, as well as a non-tumorigenic FGF19 variant (Zhou et al., 2014; Luo et al., 2014) could be used in combination with minimal bacterial consortia to investigate causality and mechanisms *in vivo*.

In this thesis, a variety of animal models and microbiota manipulations was used to investigate the effects of SBAs in CRC. Our findings from both gnotobiotic trials indicated that BAs play a role in early-stage promotion of tumorigenesis. In the future, routine BA quantification could be used in combination with colonoscopy to assess the risk of patients to develop CRC. Furthermore, our findings emphasise the importance of multiple factors such as diet, genetic factors, carcinogen exposure, or inflammation. Long-term consumption of low-fat, high-fibre diets could be a sound strategy to prevent disease in populations at risk, even though compliance to such diets can be a challenge. Bile acid scavengers like colestyramine might be a supplementary intervention option to reduce the SBA stress on the colonic epithelium. Our studies provide a valuable background for future research in this direction.

Bibliography

Afrizal A., Hitch T. C., Viehof A., et al. Anaerobic single-cell dispensing facilitates the cultivation of human gut bacteria. *Environmental Microbiology*, 24(9):3861–3881, 2022.

Ai D., Pan H., Li X., et al. Identifying Gut Microbiota Associated With Colorectal Cancer Using a Zero-Inflated Lognormal Model. *Frontiers in Microbiology*, 10:1–8, 2019.

Alzahrani S. M., Al Doghaither H. A., and Al-Ghafari A. B. General insight into cancer: An overview of colorectal cancer. *Molecular and Clinical Oncology*, 15(6):1–8, 2021.

Amos-Landgraf J. M., Heijmans J., Wielenga M. C., et al. Sex disparity in colonic adenomagenesis involves promotion by male hormones, not protection by female hormones. *Proceedings of the National Academy of Sciences*, 111(46):16514–16519, 2014.

Angelini R., Vortmeier G., Corcelli A., and Fuchs B. A fast method for the determination of the PC/LPC ratio in intact serum by MALDI-TOF MS: An easy-to-follow lipid biomarker of inflammation. *Chemistry and Physics of Lipids*, 183:169–175, 2014.

Arrieta M.-C., Walter J., and Finlay B. B. Human microbiota-associated mice: a model with challenges. *Cell Host & Microbe*, 19(5):575–578, 2016.

Asnicar F., Berry S. E., Valdes A. M., et al. Microbiome connections with host metabolism and habitual diet from 1,098 deeply phenotyped individuals. *Nature Medicine*, 27(2):321–332, 2021.

Attene-Ramos M. S., Wagner E. D., Plewa M. J., and Gaskins H. R. Evidence that hydrogen sulfide is a genotoxic agent. *Molecular Cancer Research*, 4(1):9–14, 2006.

Azar T. and Berger D. L. Adult intussusception. *Annals of surgery*, 226(2):134, 1997.

Baker S. J., Preisinger A. C., Jessup J. M., et al. p53 gene mutations occur in combination with 17p allelic deletions as late events in colorectal tumorigenesis. *Cancer Research*, 50(23):7717–7722, 1990.

Bartram H.-P., Scheppach W., Englert S., et al. Effects of deoxycholic acid and butyrate on mucosal prostaglandin E2 release and cell proliferation in the human sigmoid colon. *Journal of Parenteral and Enteral Nutrition*, 19(3):182–186, 1995.

Bayerdörffer E., Mannes G., Ochsenkühn T., et al. Unconjugated secondary bile acids in the serum of patients with colorectal adenomas. *Gut*, 36(2):268–273, 1995.

Becht E., Reyniès A.d, Giraldo N. A., et al. Immune and stromal classification of colorectal cancer is associated with molecular subtypes and relevant for precision immunotherapy. *Clinical Cancer Research*, 22(16):4057–4066, 2016.

Begley M., Gahan C. G., and Hill C. The interaction between bacteria and bile. *FEMS Microbiology Reviews*, 29(4):625–651, 2005.

Bernstein C., Bernstein H., Garewal H., et al. A bile acid-induced apoptosis assay for colon cancer risk and associated quality control studies. *Cancer Research*, 59(10):2353–2357, 1999.

Bernstein C., Holubec H., Bhattacharyya A. K., et al. Carcinogenicity of deoxycholate, a secondary bile acid. *Archives of Toxicology*, 85:863–871, 2011.

Blighe K., Rana S., and Lewis M. EnhancedVolcano: Publication-ready volcano plots with enhanced colouring and labeling. `https://github.com/kevinblighe/EnhancedVolcano`, 2018. Accessed: 2023-08-22.

Bossuyt W., Kazanjian A., De Geest N., et al. Atonal homolog 1 is a tumor suppressor gene. *PLoS Biology*, 7(2):e1000039, 2009.

Bouvard V., Loomis D., Guyton K. Z., et al. Carcinogenicity of consumption of red and processed meat. *The Lancet Oncology*, 16(16):1599–1600, 2015.

Braumüller H., Mauerer B., Andris J., et al. The cytokine network in colorectal cancer: Implications for new treatment strategies. *Cells*, 12(1):138, 2022.

Brugiroux S., Beutler M., Pfann C., et al. Genome-guided design of a defined mouse microbiota that confers colonization resistance against *Salmonella enterica* serovar Typhimurium. *Nature Microbiology*, 2(2):1–12, 2016.

Buchner A. M. and Lichtenstein G. R. Evaluation and detection of dysplasia in IBD: The role of chromoendoscopy and enhanced imaging techniques. *Current Treatment Options in Gastroenterology*, 14:73–82, 2016.

Bunnett N. W. Neuro-humoral signalling by bile acids and the TGR5 receptor in the gastrointestinal tract. *The Journal of Physiology*, 592(Pt 14):2943, 2014.

Burrin D., Stoll B., and Moore D. Digestive physiology of the pig symposium: intestinal bile acid sensing is linked to key endocrine and metabolic signaling pathways. *Journal of Animal Science*, 91(5):1991–2000, 2013.

Bürtin F., Mullins C. S., and Linnebacher M. Mouse models of colorectal cancer: Past, present and future perspectives. *World Journal of Gastroenterology*, 26(13):1394, 2020.

Butler A., Hoffman P., Smibert P., Papalexi E., and Satija R. Integrating single-cell transcriptomic data across different conditions, technologies, and species. *Nature Biotechnology*, 36(5):411–420, 2018.

Cammarota G., Ianiro G., Tilg H., et al. European consensus conference on faecal microbiota transplantation in clinical practice. *Gut*, 66(4):569–580, 2017.

Campbell C., McKenney P. T., Konstantinovsky D., et al. Bacterial metabolism of bile acids promotes peripheral Treg cell generation. *Nature*, 581(7809):475, 2020.

Cao H., Xu M., Dong W., et al. Secondary bile acid-induced dysbiosis promotes intestinal carcinogenesis. *International Journal of Cancer*, 140(11):2545–2556, 2017.

Carethers J. M. and Jung B. H. Genetics and genetic biomarkers in sporadic colorectal cancer. *Gastroenterology*, 149(5):1177–1190, 2015.

Centuori S. M., Gomes C. J., Trujillo J., et al. Deoxycholic acid mediates non-canonical EGFR-MAPK activation through the induction of calcium signaling in colon cancer cells. *Biochimica Et Biophysica Acta (BBA)-Molecular and Cell Biology of Lipids*, 1861(7):663–670, 2016.

Clinton S. K., Giovannucci E. L., and Hursting S. D. The world cancer research fund/American institute for cancer research third expert report on diet, nutrition, physical activity, and cancer: impact and future directions. *The Journal of Nutrition*, 150(4):663–671, 2020.

Coleman O. I. and Haller D. Microbe–mucus interface in the pathogenesis of colorectal cancer. *Cancers*, 13(4):616, 2021.

Coleman O. I., Lobner E. M., Bierwirth S., et al. Activated ATF6 induces intestinal dysbiosis and innate immune response to promote colorectal tumorigenesis. *Gastroenterology*, 155(5):1539–1552, 2018.

Dai Z., Coker O. O., Nakatsu G., et al. Multi-cohort analysis of colorectal cancer metagenome identified altered bacteria across populations and universal bacterial markers. *Microbiome*, 6(1): 1–12, 2018.

David L. A., Maurice C. F., Carmody R. N., et al. Diet rapidly and reproducibly alters the human gut microbiome. *Nature*, 505(7484):559–563, 2014.

Dawson P. A. Role of the intestinal bile acid transporters in bile acid and drug disposition. *Drug Transporters*, pages 169–203, 2011.

De Robertis M., Massi E., Poeta M. L., et al. The AOM/DSS murine model for the study of colon carcinogenesis: From pathways to diagnosis and therapy studies. *Journal of Carcinogenesis*, 10, 2011.

Devkota S., Wang Y., Musch M. W., et al. Dietary-fat-induced taurocholic acid promotes pathobiont expansion and colitis in Il10-/- mice. *Nature*, 487(7405):104–108, 2012.

Dienstmann R., Vermeulen L., Guinney J., et al. Consensus molecular subtypes and the evolution of precision medicine in colorectal cancer. *Nature Reviews Cancer*, 17(2):79–92, 2017.

Dmitrieva-Posocco O., Wong A. C., Lundgren P., et al. β-Hydroxybutyrate suppresses colorectal cancer. *Nature*, 605(7908):160–165, 2022.

Doerner K. C., Takamine F., LaVoie C. P., Mallonee D. H., and Hylemon P. B. Assessment of fecal bacteria with bile acid 7 alpha-dehydroxylating activity for the presence of bai-like genes. *Applied and Environmental Microbiology*, 63(3):1185–1188, 1997.

Dominguez-Bello M. G., Costello E. K., Contreras M., et al. Delivery mode shapes the acquisition and structure of the initial microbiota across multiple body habitats in newborns. *Proceedings of the National Academy of Sciences*, 107(26):11971–11975, 2010.

Donohoe D. R., Holley D., Collins L. B., et al. A gnotobiotic mouse model demonstrates that dietary fiber protects against colorectal tumorigenesis in a microbiota-and butyrate-dependent manner. *Cancer Discovery*, 4(12):1387–1397, 2014.

Dossa A. Y., Escobar O., Golden J., et al. Bile acids regulate intestinal cell proliferation by modulating EGFR and FXR signaling. *American Journal of Physiology-Gastrointestinal and Liver Physiology*, 310(2):G81–G92, 2016.

Dow L. E., O'Rourke K. P., Simon J., et al. Apc restoration promotes cellular differentiation and reestablishes crypt homeostasis in colorectal cancer. *Cell*, 161(7):1539–1552, 2015.

D'Aiuto N., Hochmann J., Millán M., et al. Hypoxia, acidification and oxidative stress in cells cultured at large distances from an oxygen source. *Scientific Reports*, 12(1):21699, 2022.

Eberl C., Ring D., Münch P. C., et al. Reproducible colonization of germ-free mice with the oligo-mouse-microbiota in different animal facilities. *Frontiers in Microbiology*, 10:2999, 2020.

Ecker J., Scherer M., Schmitz G., and Liebisch G. A rapid GC–MS method for quantification of positional and geometric isomers of fatty acid methyl esters. *Journal of Chromatography B*, 897: 98–104, 2012.

Edgar R. C. Search and clustering orders of magnitude faster than BLAST. *Bioinformatics*, 26(19): 2460–2461, 2010.

Edgar R. C. UPARSE: Highly accurate OTU sequences from microbial amplicon reads. *Nature Methods*, 10(10):996–998, 2013.

El Marjou F., Janssen K.-P., Hung-Junn Chang B., et al. Tissue-specific and inducible Cre-mediated recombination in the gut epithelium. *Genesis*, 39(3):186–193, 2004.

Elkins C. A. and Savage D. C. Identification of genes encoding conjugated bile salt hydrolase and transport in *Lactobacillus johnsonii* 100-100. *Journal of Bacteriology*, 180(17):4344–4349, 1998.

Farhana L., Nangia-Makker P., Arbit E., et al. Bile acid: a potential inducer of colon cancer stem cells. *Stem Cell Research & Therapy*, 7(1):1–10, 2016.

Flisikowska T., Merkl C., Landmann M., et al. A porcine model of familial adenomatous polyposis. *Gastroenterology*, 143(5):1173–1175, 2012.

Fodde R. and Smits R. Disease model: familial adenomatous polyposis. *Trends in Molecular Medicine*, 7(8):369–373, 2001.

Fodde R., Edelmann W., Yang K., et al. A targeted chain-termination mutation in the mouse Apc gene results in multiple intestinal tumors. *Proceedings of the National Academy of Sciences*, 91 (19):8969–8973, 1994.

Freed-Pastor W. A. and Prives C. Mutant p53: one name, many proteins. *Genes & Development*, 26 (12):1268–1286, 2012.

Fu T., Coulter S., Yoshihara E., et al. FXR regulates intestinal cancer stem cell proliferation. *Cell*, 176(5):1098–1112, 2019.

Fu Z. D., Csanaky I. L., and Klaassen C. D. Gender-divergent profile of bile acid homeostasis during aging of mice. *PLOS ONE*, 7(3):e32551, 2012.

Funabashi M., Grove T. L., Wang M., et al. A metabolic pathway for bile acid dehydroxylation by the gut microbiome. *Nature*, 582(7813):566–570, 2020.

Gabrielson A., Wu Y., Wang H., et al. Intratumoral CD3 and CD8 T-cell densities associated with relapse-free survival in HCC. *Cancer Immunology Research*, 4(5):419–430, 2016.

Gonzalez L. M., Moeser A. J., and Blikslager A. T. Porcine models of digestive disease: the future of large animal translational research. *Translational Research*, 166(1):12–27, 2015.

Gordon J., Knowlton N., Relman D. A., Rohwer F., and Youle M. Superorganisms and holobionts. *Microbe*, 8(4):152–153, 2013.

Gu Z., Eils R., and Schlesner M. Complex heatmaps reveal patterns and correlations in multidimensional genomic data. *Bioinformatics*, 32(18):2847–2849, 2016.

Guinney J., Dienstmann R., Wang X., et al. The consensus molecular subtypes of colorectal cancer. *Nature Medicine*, 21(11):1350–1356, 2015.

Haange S.-B., Till A., Bergh P.-O., et al. Ring trial on quantitative assessment of bile acids reveals a method-and analyte-specific accuracy and reproducibility. *Metabolites*, 12(7):583, 2022.

Han J., Lin K., Sequeira C., and Borchers C. H. An isotope-labeled chemical derivatization method for the quantitation of short-chain fatty acids in human feces by liquid chromatography–tandem mass spectrometry. *Analytica Chimica Acta*, 854:86–94, 2015.

Hang S., Paik D., Yao L., et al. Bile acid metabolites control TH17 and Treg cell differentiation. *Nature*, 576(7785):143–148, 2019.

Hansen W., Hutzler M., Abel S., et al. Neuropilin 1 deficiency on CD4+ Foxp3+ regulatory T cells impairs mouse melanoma growth. *Journal of Experimental Medicine*, 209(11):2001–2016, 2012.

Hao Y., Hao S., Andersen-Nissen E., et al. Integrated analysis of multimodal single-cell data. *Cell*, 184(13):3573–3587, 2021.

Heinken A., Ravcheev D. A., Baldini F., et al. Systematic assessment of secondary bile acid metabolism in gut microbes reveals distinct metabolic capabilities in inflammatory bowel disease. *Microbiome*, 7(1):1–18, 2019.

Hitch T. C., Bisdorf K., Afrizal A., et al. A taxonomic note on the genus Prevotella: Description of four novel genera and emended description of the genera Hallella and Xylanibacter. *Systematic and Applied Microbiology*, 45(6):126354, 2022a.

Hitch T. C., Hall L. J., Walsh S. K., et al. Microbiome-based interventions to modulate gut ecology and the immune system. *Mucosal Immunology*, 15(6):1095–1113, 2022b.

Hite N., Klinger A., Hellmers L., et al. An optimal orthotopic mouse model for human colorectal cancer primary tumor growth and spontaneous metastasis. *Diseases of the Colon & Rectum*, 61(6): 698–705, 2018.

Hofmann A. F. and Hagey L. Bile acids: chemistry, pathochemistry, biology, pathobiology, and therapeutics. *Cellular and Molecular Life Sciences*, 65:2461–2483, 2008.

Hofmann A. F. and Hagey L. R. Key discoveries in bile acid chemistry and biology and their clinical applications: history of the last eight decades. *Journal of Lipid Research*, 55(8):1553–1595, 2014.

Hofmann A. F., Hagey L. R., and Krasowski M. D. Bile salts of vertebrates: Structural variation and possible evolutionary significance. *Journal of Lipid Research*, 51(2):226–246, 2010.

Honda A., Miyazaki T., Iwamoto J., et al. Regulation of bile acid metabolism in mouse models with hydrophobic bile acid composition. *Journal of Lipid Research*, 61(1):54–69, 2020.

Huang L., Wei W., Huang X., et al. High-fat diets enhance and delay ursodeoxycholic acid absorption but elevate circulating hydrophobic bile salts. *Frontiers in Pharmacology*, 14:1168144, 2023.

Imray C., Radley S., Davis A., et al. Faecal unconjugated bile acids in patients with colorectal cancer or polyps. *Gut*, 33(9):1239–1245, 1992.

Islam K. S., Fukiya S., Hagio M., et al. Bile acid is a host factor that regulates the composition of the cecal microbiota in rats. *Gastroenterology*, 141(5):1773–1781, 2011.

Itzkowitz S. H. and Yio X. Inflammation and cancer IV. Colorectal cancer in inflammatory bowel disease: the role of inflammation. *American Journal of Physiology-Gastrointestinal and Liver Physiology*, 287(1):G7–G17, 2004.

Janney A., Powrie F., and Mann E. H. Host–microbiota maladaptation in colorectal cancer. *Nature*, 585(7826):509–517, 2020.

Jasperson K. W., Tuohy T. M., Neklason D. W., and Burt R. W. Hereditary and familial colon cancer. *Gastroenterology*, 138(6):2044–2058, 2010.

Joanito I., Wirapati P., Zhao N., et al. Single-cell and bulk transcriptome sequencing identifies two epithelial tumor cell states and refines the consensus molecular classification of colorectal cancer. *Nature Genetics*, 54(7):963–975, 2022.

Johnson A. J., Vangay P., Al-Ghalith G. A., et al. Daily sampling reveals personalized diet-microbiome associations in humans. *Cell Host & Microbe*, 25(6):789–802, 2019.

Johnstone R. W., Frew A. J., and Smyth M. J. The TRAIL apoptotic pathway in cancer onset, progression and therapy. *Nature Reviews Cancer*, 8(10):782–798, 2008.

Just S., Mondot S., Ecker J., et al. The gut microbiota drives the impact of bile acids and fat source in diet on mouse metabolism. *Microbiome*, 6(1):1–18, 2018.

Kadosh E., Snir-Alkalay I., Venkatachalam A., et al. The gut microbiome switches mutant p53 from tumour-suppressive to oncogenic. *Nature*, 586(7827):133–138, 2020.

Karim R. Z., Tse G. M., Putti T. C., Scolyer R. A., and Lee C. S. The significance of the Wnt pathway in the pathology of human cancers. *Pathology*, 36(2):120–128, 2004.

Kassambara A. *rstatix: Pipe-Friendly Framework for Basic Statistical Tests*, 2023. R package version 0.7.2.

Kawano A., Ishikawa H., Kamano T., et al. Significance of fecal deoxycholic acid concentration for colorectal tumor enlargement. *Asian Pacific Journal of Cancer Prevention*, 11(6):1541–1546, 2010.

Kenny D. J., Plichta D. R., Shungin D., et al. Cholesterol Metabolism by Uncultured Human Gut Bacteria Influences Host Cholesterol Level. *Cell Host & Microbe*, 28(2):245–257.e6, 2020.

Keum N. and Giovannucci E. Global burden of colorectal cancer: emerging trends, risk factors and prevention strategies. *Nature Reviews Gastroenterology & Hepatology*, 16(12):713–732, 2019.

Khaliq A. M., Erdogan C., Kurt Z., et al. Refining colorectal cancer classification and clinical stratification through a single-cell atlas. *Genome Biology*, 23(1):1–30, 2022.

Kim I., Ahn S.-H., Inagaki T., et al. Differential regulation of bile acid homeostasis by the farnesoid X receptor in liver and intestine. *Journal of Lipid Research*, 48(12):2664–2672, 2007.

Kim K. H., Park D., Jia B., et al. Identification and characterization of major bile acid 7α-dehydroxylating bacteria in the human gut. *mSystems*, 7(4):e00455–22, 2022.

Kitahara M., Takamine F., Imamura T., and Benno Y. *Clostridium hiranonis* sp. nov., a human intestinal bacterium with bile acid 7alpha-dehydroxylating activity. *Int. J. Syst. Evol. Microbiol.*, 51(1):39–44, 2001.

Kopylova E., Noé L., and Touzet H. SortMeRNA: Fast and accurate filtering of ribosomal RNAs in metatranscriptomic data. *Bioinformatics*, 28(24):3211–3217, 2012.

Kuipers F., Bloks V. W., and Groen A. K. Beyond intestinal soap—bile acids in metabolic control. *Nature Reviews Endocrinology*, 10(8):488–498, 2014.

Kunz S. and Matysik S. A comprehensive method to determine sterol species in human faeces by GC-triple quadrupole MS. *The Journal of Steroid Biochemistry and Molecular Biology*, 190:99–103, 2019.

Lagkouvardos I., Joseph D., Kapfhammer M., et al. IMNGS: A comprehensive open resource of processed 16S rRNA microbial profiles for ecology and diversity studies. *Scientific Reports*, 6 (April):1–9, 2016.

Lagkouvardos I., Fischer S., Kumar N., and Clavel T. Rhea: a transparent and modular R pipeline for microbial profiling based on 16S rRNA gene amplicons. *PeerJ*, 5:e2836, 2017.

Lakso M., Sauer B., Mosinger Jr B., et al. Targeted oncogene activation by site-specific recombination in transgenic mice. *Proceedings of the National Academy of Sciences*, 89(14):6232–6236, 1992.

Lechner S., Müller-Ladner U., Schlottmann K., et al. Bile acids mimic oxidative stress induced upregulation of thioredoxin reductase in colon cancer cell lines. *Carcinogenesis*, 23(8):1281–1288, 2002.

Leclerc D., Lévesque N., Cao Y., et al. Genes with aberrant expression in murine preneoplastic intestine show epigenetic and expression changes in normal mucosa of colon cancer patients. *Cancer Prevention Research*, 6(11):1171–1181, 2013.

Lee J. W. J., Plichta D. R., Asher S., et al. Association of distinct microbial signatures with premalignant colorectal adenomas. *Cell Host & Microbe*, 31(5):827–838, 2023.

Lee K. A., Thomas A. M., Bolte L. A., et al. Cross-cohort gut microbiome associations with immune checkpoint inhibitor response in advanced melanoma. *Nature Medicine*, 28(3):535–544, 2022.

Li J. and Dawson P. A. Animal models to study bile acid metabolism. *Biochimica et Biophysica Acta (BBA)-Molecular Basis of Disease*, 1865(5):895–911, 2019.

Li J. N. and Yuan S. Y. Fecal occult blood test in colorectal cancer screening. *Journal of Digestive Diseases*, 20(2):62–64, 2019.

Li J.-Y., Gillilland III M., Lee A. A., et al. Secondary bile acids mediate high-fat diet–induced upregulation of R-spondin 3 and intestinal epithelial proliferation. *JCI Insight*, 7(19), 2022a.

Li L., Li X., Zhong W., et al. Gut microbiota from colorectal cancer patients enhances the progression of intestinal adenoma in *Apc*$^{min/+}$ mice. *EBioMedicine*, 48:301–315, 2019.

Li W., Hang S., Fang Y., et al. A bacterial bile acid metabolite modulates Treg activity through the nuclear hormone receptor NR4A1. *Cell Host & Microbe*, 29(9):1366–1377, 2021.

Li Y.-h., Zhang Y., Pan G., et al. Occurrences and Functions of Ly6Chi and Ly6Clo Macrophages in Health and Disease. *Frontiers in Immunology*, 13:901672, 2022b.

Liang H., Estes M. K., Zhang H., Du G., and Zhou Y. Bile acids target proteolipid nano-assemblies of EGFR and phosphatidic acid in the plasma membrane for stimulation of MAPK signaling. *PLOS ONE*, 13(8):e0198983, 2018.

Lin S., Stoll B., Robinson J., et al. Differential action of TGR5 agonists on GLP-2 secretion and promotion of intestinal adaptation in a piglet short bowel model. *American Journal of Physiology-Gastrointestinal and Liver Physiology*, 316(5):G641–G652, 2019.

Liu L., Yang M., Dong W., et al. Gut dysbiosis and abnormal bile acid metabolism in colitis-associated cancer. *Gastroenterology Research and Practice*, 2021, 2021.

Liu N.-N., Jiao N., Tan J.-C., et al. Multi-kingdom microbiota analyses identify bacterial–fungal interactions and biomarkers of colorectal cancer across cohorts. *Nature Microbiology*, 7(2):238–250, 2022.

Liu T., Zhang L., Joo D., and Sun S.-C. NF-κB signaling in inflammation. *Signal Transduction and Targeted Therapy*, 2(1):1–9, 2017.

Louis P., Hold G. L., and Flint H. J. The gut microbiota, bacterial metabolites and colorectal cancer. *Nature Reviews Microbiology*, 12(10):661–672, 2014.

Luo J., Ko B., Elliott M., et al. A nontumorigenic variant of FGF19 treats cholestatic liver diseases. *Science translational medicine*, 6(247):247ra100–247ra100, 2014.

Lynch S. V. and Pedersen O. The human intestinal microbiome in health and disease. *New England Journal of Medicine*, 375(24):2369–2379, 2016.

Macpherson A. J. and Uhr T. Induction of Protective IgA by Intestinal Dendritic Cells Carrying Commensal Bacteria. *Science*, 303(5664):1662–1665, 2004.

Mager L. F., Burkhard R., Pett N., et al. Microbiome-derived inosine modulates response to checkpoint inhibitor immunotherapy. *Science*, 369(6510):1481–1489, 2020.

Malard F., Dore J., Gaugler B., and Mohty M. Introduction to host microbiome symbiosis in health and disease. *Mucosal Immunology*, 14(3):547–554, 2021.

Manichanh C., Borruel N., Casellas F., and Guarner F. The gut microbiota in IBD. *Nature Reviews Gastroenterology & Hepatology*, 9(10):599–608, 2012.

Marchesi J. R. Human distal gut microbiome. *Environmental Microbiology*, 13(12):3088–3102, 2011.

Marion S., Studer N., Desharnais L., et al. *In vitro* and in *vivo* characterization of *Clostridium scindens* bile acid transformations. *Gut Microbes*, 10(4):481–503, 2019.

Marion S., Desharnais L., Studer N., et al. Biogeography of microbial bile acid transformations along the murine gut. *Journal of Lipid Research*, 61(11):1450–1463, 2020.

Martino C., Dilmore A. H., Burcham Z. M., et al. Microbiota succession throughout life from the cradle to the grave. *Nature Reviews Microbiology*, 20(12):707–720, 2022.

Matson V., Fessler J., Bao R., et al. The commensal microbiome is associated with anti–PD-1 efficacy in metastatic melanoma patients. *Science*, 359(6371):104–108, 2018.

McGarry M. and Stewart C. Murine eosinophil granulocytes bind the murine macrophage-monocyte specific monoclonal antibody F4/80. *Journal of Leukocyte Biology*, 50(5):471–478, 1991.

McHugh R. S., Whitters M. J., Piccirillo C. A., et al. CD4+ CD25+ immunoregulatory T cells: gene expression analysis reveals a functional role for the glucocorticoid-induced TNF receptor. *Immunity*, 16(2):311–323, 2002.

McKenney P. T., Yan J., Vaubourgeix J., et al. Intestinal bile acids induce a morphotype switch in vancomycin-resistant Enterococcus that facilitates intestinal colonization. *Cell Host & Microbe*, 25(5):695–705, 2019.

Meslier V., Laiola M., Roager H. M., et al. Mediterranean diet intervention in overweight and obese subjects lowers plasma cholesterol and causes changes in the gut microbiome and metabolome independently of energy intake. *Gut*, 69(7):1258–1268, 2020.

Metwaly A., Reitmeier S., and Haller D. Microbiome risk profiles as biomarkers for inflammatory and metabolic disorders. *Nature Reviews Gastroenterology & Hepatology*, 19(6):383–397, 2022.

Miller S. A., Ghobashi A. H., and O'Hagan H. M. Consensus molecular subtyping of colorectal cancers is influenced by goblet cell content. *Cancer Genetics*, 254:34–39, 2021a.

Miller S. A., Policastro R. A., Sriramkumar S., et al. LSD1 and aberrant DNA methylation mediate persistence of enteroendocrine progenitors that support BRAF-mutant colorectal cancer. *Cancer Research*, 81(14):3791–3805, 2021b.

Modak M., Mattes A.-K., Reiss D., et al. CD206+ tumor-associated macrophages cross-present tumor antigen and drive antitumor immunity. *JCI Insight*, 7(11), 2022.

Modica S., Murzilli S., Salvatore L., Schmidt D. R., and Moschetta A. Nuclear bile acid receptor FXR protects against intestinal tumorigenesis. *Cancer Research*, 68(23):9589–9594, 2008.

Morgan M. J. and Liu Z.-g. Crosstalk of reactive oxygen species and NF-κB signaling. *Cell Research*, 21(1):103–115, 2011.

Moser A. R., Pitot H. C., and Dove W. F. A dominant mutation that predisposes to multiple intestinal neoplasia in the mouse. *Science*, 247(4940):322–324, 1990.

Moser A. R., Luongo C., Gould K. A., et al. *Apc*$^{\text{Min}}$: A mouse model for intestinal and mammary tumorigenesis. *Eur. J. Cancer*, 31(7):1061–1064, 1995.

Mundade R., Imperiale T. F., Prabhu L., Loehrer P. J., and Lu T. Genetic pathways, prevention, and treatment of sporadic colorectal cancer. *Oncoscience*, 1(6):400, 2014.

Muz B., Puente P.d. l, Azab F., and Kareem Azab A. The role of hypoxia in cancer progression, angiogenesis, metastasis, and resistance to therapy. *Hypoxia*, pages 83–92, 2015.

Nakagama H., Ochiai M., Ubagai T., et al. A rat colon cancer model induced by 2-amino-1-methyl-6-phenylimidazo [4, 5-b] pyridine, PhIP. *Mutation Research/Fundamental and Molecular Mechanisms of Mutagenesis*, 506:137–144, 2002.

Narahara H., Tatsuta M., Iishi H., et al. K-ras point mutation is associated with enhancement by deoxycholic acid of colon carcinogenesis induced by azoxymethane, but not with its attenuation by all-trans-retinoic acid. *International Journal of Cancer*, 88(2):157–161, 2000.

Oksanen J., Simpson G. L., Blanchet F. G., et al. *vegan: Community Ecology Package*, 2022. R package version 2.6-4.

Olguín J. E., Medina-Andrade I., Molina E., et al. Early and partial reduction in CD4+ Foxp3+ regulatory T cells during colitis-associated colon cancer induces CD4+ and CD8+ T cell activation inhibiting tumorigenesis. *Journal of Cancer*, 9(2):239, 2018.

O'Neill A. M., Burrington C. M., Gillaspie E. A., et al. High-fat Western diet–induced obesity contributes to increased tumor growth in mouse models of human colon cancer. *Nutrition Research*, 36(12):1325–1334, 2016.

O'Shea E. F., Cotter P. D., Stanton C., Ross R. P., and Hill C. Production of bioactive substances by intestinal bacteria as a basis for explaining probiotic mechanisms: bacteriocins and conjugated linoleic acid. *International Journal of Food Microbiology*, 152(3):189–205, 2012.

Ou J., Carbonero F., Zoetendal E. G., et al. Diet, microbiota, and microbial metabolites in colon cancer risk in rural Africans and African Americans. *The American Journal of Clinical Nutrition*, 98(1):111–120, 2013.

O'Keefe S. J., Li J. V., Lahti L., et al. Fat, fibre and cancer risk in African Americans and rural Africans. *Nature Communications*, 6(1):1–14, 2015.

Payne C. M., Crowley C., Washo-Stultz D., et al. The stress-response proteins poly (ADP-ribose) polymerase and NF-κB protect against bile salt-induced apoptosis. *Cell Death & Differentiation*, 5(7):623–636, 1998.

Payne C. M., Weber C., Crowley-Skillicorn C., et al. Deoxycholate induces mitochondrial oxidative stress and activates NF-κB through multiple mechanisms in HCT-116 colon epithelial cells. *Carcinogenesis*, 28(1):215–222, 2007.

Perino A. and Schoonjans K. TGR5 and immunometabolism: insights from physiology and pharmacology. *Trends in Pharmacological Sciences*, 36(12):847–857, 2015.

Perino A., Demagny H., Velazquez-Villegas L., and Schoonjans K. Molecular physiology of bile acid signaling in health, disease, and aging. *Physiological Reviews*, 101(2):683–731, 2021.

Peters U., Bien S., and Zubair N. Genetic architecture of colorectal cancer. *Gut*, 64(10):1623–1636, 2015.

Petibon C., Ghulam M. M., Catala M., and Elela S. A. Regulation of ribosomal protein genes: An ordered anarchy. *Wiley Interdisciplinary Reviews: RNA*, 12(3):e1632., 2021.

Philip M. and Schietinger A. CD8+ T cell differentiation and dysfunction in cancer. *Nature Reviews Immunology*, 22(4):209–223, 2022.

Pleguezuelos-Manzano C., Puschhof J., Rosendahl Huber A., et al. Mutational signature in colorectal cancer caused by genotoxic pks+ *E. coli*. *Nature*, 580(7802):269–273, 2020.

Posit team . *RStudio: Integrated Development Environment for R*. Posit Software, PBC, Boston, MA, 2023.

Pruesse E., Peplies J., and Glöckner F. O. SINA: Accurate high-throughput multiple sequence alignment of ribosomal RNA genes. *Bioinformatics*, 28(14):1823–1829, 2012.

Qiao D., Gaitonde S. V., Qi W., and Martinez J. D. Deoxycholic acid suppresses p53 by stimulating proteasome-mediated p53 protein degradation. *Carcinogenesis*, 22(6):957–964, 2001.

Quinn R. A., Melnik A. V., Vrbanac A., et al. Global chemical effects of the microbiome include new bile-acid conjugations. *Nature*, 579(7797):123–129, 2020.

R Core Team . *R: A Language and Environment for Statistical Computing*. R Foundation for Statistical Computing, Vienna, Austria, 2022.

Reddy B. S. Diet and excretion of bile acids. *Cancer Research*, 41(9_Part_2):3766–3768, 1981.

Reddy B. S. and Wynder E. L. Large-bowel carcinogenesis: fecal constituents of populations with diverse incidence rates of colon cancer. *Journal of the National Cancer Institute*, 50(6):1437–1442, 1973.

Reiter S., Dunkel A., Metwaly A., et al. Development of a Highly Sensitive Ultra-High-Performance Liquid Chromatography Coupled to Electrospray Ionization Tandem Mass Spectrometry Quantitation Method for Fecal Bile Acids and Application on Crohn's Disease Studies. *Journal of Agricultural and Food Chemistry*, 69(17):5238–5251, 2021.

Ridlon J. M. and Bajaj J. S. The human gut sterolbiome: bile acid-microbiome endocrine aspects and therapeutics. *Acta Pharmaceutica Sinica B*, 5(2):99–105, 2015.

Ridlon J. M., Kang D.-J., and Hylemon P. B. Bile salt biotransformations by human intestinal bacteria. *Journal of Lipid Research*, 47(2):241–259, 2006.

Ridlon J. M., Kang D.-J., and Hylemon P. B. Isolation and characterization of a bile acid inducible 7α-dehydroxylating operon in Clostridium hylemonae TN271. *Anaerobe*, 16(2):137–146, 2010.

Ridlon J. M., Kang D. J., Hylemon P. B., and Bajaj J. S. Bile Acids and the Gut Microbiome. *Current Opinion in Gastroenterology*, 30(3):332, 2014.

Ridlon J. M., Devendran S., Alves J. M., et al. The 'in vivo lifestyle'of bile acid 7α-dehydroxylating bacteria: comparative genomics, metatranscriptomic, and bile acid metabolomics analysis of a defined microbial community in gnotobiotic mice. *Gut Microbes*, 11(3):381–404, 2020.

Roelands J., Kuppen P. J., Ahmed E. I., et al. An integrated tumor, immune and microbiome atlas of colon cancer. *Nature Medicine*, pages 1–14, 2023.

Rothschild D., Weissbrod O., Barkan E., et al. Environment dominates over host genetics in shaping human gut microbiota. *Nature*, 555(7695):210–215, 2018.

Rubinstein M. R., Wang X., Liu W., et al. *Fusobacterium nucleatum* promotes colorectal carcinogenesis by modulating E-cadherin/β-catenin signaling via its FadA adhesin. *Cell Host & Microbe*, 14 (2):195–206, 2013.

Saito T., Nishikawa H., Wada H., et al. Two FOXP3+ CD4+ T cell subpopulations distinctly control the prognosis of colorectal cancers. *Nature Medicine*, 22(6):679–684, 2016.

Satija R., Farrell J. A., Gennert D., Schier A. F., and Regev A. Spatial reconstruction of single-cell gene expression data. *Nature Biotechnology*, 33(5):495–502, 2015.

Sato Y., Atarashi K., Plichta D. R., et al. Novel bile acid biosynthetic pathways are enriched in the microbiome of centenarians. *Nature*, 599(7885):458–464, 2021.

Sayin S. I., Wahlström A., Felin J., et al. Gut Microbiota Regulates Bile Acid Metabolism by Reducing the Levels of Tauro-beta-muricholic Acid, a Naturally Occurring FXR Antagonist. *Cell Metabolism*, 17(2):225–235, 2013.

Scaldaferri F., Pizzoferrato M., Ponziani F. R., Gasbarrini G., and Gasbarrini A. Use and indications of cholestyramine and bile acid sequestrants. *Internal and Emergency Medicine*, 8:205–210, 2013.

Schaum N., Karkanias J., Neff N. F., et al. Single-cell transcriptomics of 20 mouse organs creates a Tabula Muris. *Nature*, 562(7727):367–372, 2018.

Schmitt M. and Greten F. R. The inflammatory pathogenesis of colorectal cancer. *Nature Reviews Immunology*, 21(10):653–667, 2021.

Schött H.-F., Krautbauer S., Höring M., Liebisch G., and Matysik S. A validated, fast method for quantification of sterols and gut microbiome derived 5α/β-stanols in human feces by isotope dilution LC–high-resolution MS. *Analytical Chemistry*, 90(14):8487–8494, 2018.

Schubert M., Klinger B., Klünemann M., et al. Perturbation-response genes reveal signaling footprints in cancer gene expression. *Nature Communications*, 9(1):20, 2018.

Sekirov I., Russell S. L., Antunes L. C. M., and Finlay B. B. Gut microbiota in health and disease. *Physiological Reviews*, 2010.

Sender R., Fuchs S., and Milo R. Are We Really Vastly Outnumbered? Revisiting the Ratio of Bacterial to Host Cells in Humans. *Cell*, 164(3):337–340, 2016.

Sepich-Poore G. D., Zitvogel L., Straussman R., et al. The microbiome and human cancer. *Science*, 371(6536):eabc4552, 2021.

Shah S. C. and Itzkowitz S. H. Colorectal cancer in inflammatory bowel disease: mechanisms and management. *Gastroenterology*, 162(3):715–730, 2022.

Shen L., Toyota M., Kondo Y., et al. Integrated genetic and epigenetic analysis identifies three different subclasses of colon cancer. *Proceedings of the National Academy of Sciences*, 104(47): 18654–18659, 2007.

Simrén M., Barbara G., Flint H. J., et al. Intestinal microbiota in functional bowel disorders: a Rome foundation report. *Gut*, 62(1):159–176, 2013.

Singh R. K., Chang H.-W., Yan D., et al. Influence of diet on the gut microbiome and implications for human health. *Journal of Translational Medicine*, 15(1):1–17, 2017.

Sinha S. R., Haileselassie Y., Nguyen L. P., et al. Dysbiosis-induced secondary bile acid deficiency promotes intestinal inflammation. *Cell Host & Microbe*, 27(4):659–670, 2020.

Slattery M. L., Boucher K. M., Caan B. J., Potter J. D., and Ma K.-N. Eating patterns and risk of colon cancer. *American Journal of Epidemiology*, 148(1):4–16, 1998.

Smits R., Kartheuser A., Jagmohan-Changur S., et al. Loss of Apc and the entire chromosome 18 but absence of mutations at the Ras and Tp53 genes in intestinal tumors from Apc1638N, a mouse model for Apc-driven carcinogenesis. *Carcinogenesis*, 18(2):321–327, 1997.

So S. Y., Wu Q., and Savidge T. Role of gut microbiota in food safety. In *Present Knowledge in Food Safety*, pages 812–828. Elsevier, 2023.

Song C.-H., Kim N., Nam R. H., et al. Testosterone strongly enhances azoxymethane/dextran sulfate sodium-induced colorectal cancer development in C57BL/6 mice. *American Journal of Cancer Research*, 11(6):3145, 2021.

Song M., Yang Q., Zhang F., et al. Hyodeoxycholic acid (HDCA) suppresses intestinal epithelial cell proliferation through FXR-PI3K/AKT pathway, accompanied by alteration of bile acids metabolism profiles induced by gut bacteria. *The FASEB Journal*, 34(5):7103–7117, 2020.

Song Z., Cai Y., Lao X., et al. Taxonomic profiling and populational patterns of bacterial bile salt hydrolase (BSH) genes based on worldwide human gut microbiome. *Microbiome*, 7:1–16, 2019.

Sorrentino G., Perino A., Yildiz E., et al. Bile Acids Signal via TGR5 to Activate Intestinal Stem Cells and Epithelial Regeneration. *Gastroenterology*, 159(3):956–968.e8, 2020.

Spinelli V., Lalloyer F., Baud G., et al. Influence of Roux-en-Y gastric bypass on plasma bile acid profiles: a comparative study between rats, pigs and humans. *International Journal of Obesity*, 40 (8):1260–1267, 2016.

Streidl T., Kumar N., Suarez L. N., Rohn S., and Clavel T. Extibacter. *Bergey's Manual of Systematics of Archaea and Bacteria*, pages 1–7, 2019.

Streidl T., Karkossa I., Segura Muñoz R. R., et al. The gut bacterium Extibacter muris produces secondary bile acids and influences liver physiology in gnotobiotic mice. *Gut Microbes*, 13(1): 1–21, 2021.

Stuart T., Butler A., Hoffman P., et al. Comprehensive Integration of Single-Cell Data. *Cell*, 177(7): 1888–1902.e21, 2019.

Studer N., Desharnais L., Beutler M., et al. Functional intestinal bile acid 7α-dehydroxylation by Clostridium scindens associated with protection from Clostridium difficile infection in a gnotobiotic mouse model. *Frontiers in Cellular and Infection Microbiology*, 6:191, 2016.

Sung H., Ferlay J., Siegel R. L., et al. Global cancer statistics 2020: GLOBOCAN estimates of incidence and mortality worldwide for 36 cancers in 185 countries. *CA: A Cancer Journal for Clinicians*, 71(3):209–249, 2021.

Sung J., Shaffer E., and Costerton J. Antibacterial activity of bile salts against common biliary pathogens: effects of hydrophobicity of the molecule and in the presence of phospholipids. *Digestive Diseases and Sciences*, 38:2104–2112, 1993.

Suzuki R., Kohno H., Sugie S., Nakagama H., and Tanaka T. Strain differences in the susceptibility to azoxymethane and dextran sodium sulfate-induced colon carcinogenesis in mice. *Carcinogenesis*, 27(1):162–169, 2005.

Takahashi S., Fukami T., Masuo Y., et al. Cyp2c70 is responsible for the species difference in bile acid metabolism between mice and humans. *Journal of Lipid Research*, 57(12):2130–2137, 2016.

Takamine F. and Imamura T. Isolation and characterization of bile acid 7-dehydroxylating bacteria from human feces. *Microbiology and Immunology*, 39(1):11–18, 1995.

Therneau T. M. *A Package for Survival Analysis in R*, 2022. R package version 3.4-0.

Thomas A. M., Manghi P., Asnicar F., et al. Metagenomic analysis of colorectal cancer datasets identifies cross-cohort microbial diagnostic signatures and a link with choline degradation. *Nature Medicine*, 25(4):667–678, 2019.

Thomas C., Pellicciari R., Pruzanski M., Auwerx J., and Schoonjans K. Targeting bile-acid signalling for metabolic diseases. *Nature Reviews Drug Discovery*, 7(8):678–693, 2008.

Thomas C., Gioiello A., Noriega L., et al. TGR5-mediated bile acid sensing controls glucose homeostasis. *Cell Metabolism*, 10(3):167–177, 2009.

Thorne K. J., Richardson B. A., Mazza G., and Butterworth A. E. A new method for measuring eosinophil activating factors, based on the increased expression of CR3 α chain (CD11b) on the surface of activated eosinophils. *Journal of Immunological Methods*, 133(1):47–54, 1990.

Tian Y., Gui W., Koo I., et al. The microbiome modulating activity of bile acids. *Gut Microbes*, 11 (4):979–996, 2020.

Todaro M., Alea M. P., Di Stefano A. B., et al. Colon cancer stem cells dictate tumor growth and resist cell death by production of interleukin-4. *Cell Stem Cell*, 1(4):389–402, 2007.

Trabelsi M.-S., Daoudi M., Prawitt J., et al. Farnesoid X receptor inhibits glucagon-like peptide-1 production by enteroendocrine L cells. *Nature Communications*, 6(7629):1–13, 2015.

Tremaroli V. and Bäckhed F. Functional interactions between the gut microbiota and host metabolism. *Nature*, 489(7415):242–249, 2012.

Turnbaugh P. J., Ridaura V. K., Faith J. J., et al. The effect of diet on the human gut microbiome: a metagenomic analysis in humanized gnotobiotic mice. *Science Translational Medicine*, 1(6):1–12, 2009.

Ueda H., Honda A., Miyazaki T., et al. Sex-, age-, and organ-dependent improvement of bile acid hydrophobicity by ursodeoxycholic acid treatment: A study using a mouse model with human-like bile acid composition. *PLOS ONE*, 17(7):1–18, 2022.

Valles-Colomer M., Blanco-Míguez A., Manghi P., et al. The person-to-person transmission landscape of the gut and oral microbiomes. *Nature*, pages 1–11, 2023.

Vétizou M., Pitt J. M., Daillère R., et al. Anticancer immunotherapy by CTLA-4 blockade relies on the gut microbiota. *Science*, 350(6264):1079–1084, 2015.

Vico-Oton E., Volet C., Jacquemin N., et al. Strain-dependent induction of primary bile acid 7-dehydroxylation by cholic acid. *BioRxiv*, 2023.

Walter J. and Ley R. The human gut microbiome: ecology and recent evolutionary changes. *Annual Review of Microbiology*, 65:411–429, 2011.

Walter J., Armet A. M., Finlay B. B., and Shanahan F. Establishing or exaggerating causality for the gut microbiome: lessons from human microbiota-associated rodents. *Cell*, 180(2):221–232, 2020.

Wan Y., Wang F., Yuan J., et al. Effects of dietary fat on gut microbiota and faecal metabolites, and their relationship with cardiometabolic risk factors: a 6-month randomised controlled-feeding trial. *Gut*, 68(8):1417–1429, 2019.

Wang H., Gong P., Chen T., et al. Colorectal Cancer Stem Cell States Uncovered by Simultaneous Single-Cell Analysis of Transcriptome and Telomeres. *Advanced Science*, 8(8):2004320, 2021.

Wang L., Gong Z., Zhang X., et al. Gut microbial bile acid metabolite skews macrophage polarization and contributes to high-fat diet-induced colonic inflammation. *Gut Microbes*, 12(1):1819155, 2020.

Wang S., Dong W., Liu L., et al. Interplay between bile acids and the gut microbiota promotes intestinal carcinogenesis. *Molecular Carcinogenesis*, 58(7):1155–1167, 2019.

Weiss J. M., Bilate A. M., Gobert M., et al. Neuropilin 1 is expressed on thymus-derived natural regulatory T cells, but not mucosa-generated induced Foxp3+ T reg cells. *Journal of Experimental Medicine*, 209(10):1723–1742, 2012.

Wells J. E. and Hylemon P. B. Identification and characterization of a bile acid 7α-dehydroxylation operon in Clostridium sp. strain TO-931, a highly active 7α-dehydroxylating strain isolated from human feces. *Applied and Environmental Microbiology*, 66(3):1107–1113, 2000.

Wickham H., Averick M., Bryan J., et al. Welcome to the tidyverse. *Journal of Open Source Software*, 4(43):1686, 2019.

Wirbel J., Pyl P. T., Kartal E., et al. Meta-analysis of fecal metagenomes reveals global microbial signatures that are specific for colorectal cancer. *Nature Medicine*, 25(4):679–689, 2019.

Wong S. H., Zhao L., Zhang X., et al. Gavage of fecal samples from patients with colorectal cancer promotes intestinal carcinogenesis in germ-free and conventional mice. *Gastroenterology*, 153(6): 1621–1633, 2017.

Worthmann A., John C., Rühlemann M. C., et al. Cold-induced conversion of cholesterol to bile acids in mice shapes the gut microbiome and promotes adaptive thermogenesis. *Nature Medicine*, 23(7): 839–849, 2017.

Wortmann E., Osswald A., Wylensek D., et al. Secondary bile acid production by gut bacteria promotes Western diet-associated colorectal cancer. *BioRxiv*, 2023.

Wu S., Lim K.-C., Huang J., Saidi R. F., and Sears C. L. *Bacteroides fragilis* enterotoxin cleaves the zonula adherens protein, E-cadherin. *Proceedings of the National Academy of Sciences*, 95(25): 14979–14984, 1998.

Wu S., Morin P. J., Maouyo D., and Sears C. L. *Bacteroides fragilis* enterotoxin induces c-Myc expression and cellular proliferation. *Gastroenterology*, 124(2):392–400, 2003.

Wu Y., Jiao N., Zhu R., et al. Identification of microbial markers across populations in early detection of colorectal cancer. *Nature Communications*, 12(1):3063, 2021.

Xie G., Wang X., Huang F., et al. Dysregulated hepatic bile acids collaboratively promote liver carcinogenesis. *International Journal of Cancer*, 139(8):1764–1775, 2016.

Yachida S., Mizutani S., Shiroma H., et al. Metagenomic and metabolomic analyses reveal distinct stage-specific phenotypes of the gut microbiota in colorectal cancer. *Nature Medicine*, 25(6):968–976, 2019.

Yao L., Seaton S. C., Ndousse-Fetter S., et al. A selective gut bacterial bile salt hydrolase alters host metabolism. *eLife*, 7:e37182, 2018.

Yasuda H., Hirata S., Inoue K., et al. Involvement of membrane-type bile acid receptor M-BAR/TGR5 in bile acid-induced activation of epidermal growth factor receptor and mitogen-activated protein kinases in gastric carcinoma cells. *Biochemical and Biophysical Research Communications*, 354 (1):154–159, 2007.

Yetti H., Naito H., Yuan Y., et al. Bile acid detoxifying enzymes limit susceptibility to liver fibrosis in female SHRSP5/Dmcr rats fed with a high-fat-cholesterol diet. *PLOS ONE*, 13(2):e0192863, 2018.

Yoon S.-H., Ha S.-M., Kwon S., et al. Introducing EzBioCloud: a taxonomically united database of 16S rRNA gene sequences and whole-genome assemblies. *International Journal of Systematic and Evolutionary Microbiology*, 67(5):1613, 2017.

Yu J., Feng Q., Wong S. H., et al. Metagenomic analysis of faecal microbiome as a tool towards targeted non-invasive biomarkers for colorectal cancer. *Gut*, 66(1):70–78, 2017.

Zeller G., Tap J., Voigt A. Y., et al. Potential of fecal microbiota for early-stage detection of colorectal cancer. *Molecular Systems Biology*, 10(11):766, 2014.

Zeng H., Claycombe K. J., and Reindl K. M. Butyrate and deoxycholic acid play common and distinct roles in HCT116 human colon cell proliferation. *The Journal of Nutritional Biochemistry*, 26(10): 1022–1028, 2015.

Zhang J., Zhu Z., Miao Z., et al. The clinical significance and mechanisms of REG4 in human cancers. *Frontiers in Oncology*, 10:559230, 2021a.

Zhang S., Gang X., Yang S., et al. The Alterations in and the Role of the Th17/Treg Balance in Metabolic Diseases. *Front. Immunol.*, 12:678355, 2021b.

Zhang Y., Limaye P. B., Lehman-McKeeman L. D., and Klaassen C. D. Dysfunction of Organic Anion Transporting Polypeptide 1a1 Alters Intestinal Bacteria and Bile Acid Metabolism in Mice. *PLOS ONE*, 7(4):1–11, 2012.

Zhao L.-Y., Mei J.-X., Yu G., et al. Role of the gut microbiota in anticancer therapy: from molecular mechanisms to clinical applications. *Signal Transduction and Targeted Therapy*, 8(1):201, 2023.

Zhao X., Ma L., Dai L., et al. TNF-α promotes the malignant transformation of intestinal stem cells through the NF-κB and Wnt/β-catenin signaling pathways. *Oncology Reports*, 44(2):577–588, 2020.

Zheng X., Chen T., Jiang R., et al. Hyocholic acid species improve glucose homeostasis through a distinct TGR5 and FXR signaling mechanism. *Cell Metabolism*, 33(4):791–803, 2021.

Zhou M., Wang X., Phung V., et al. Separating tumorigenicity from bile acid regulatory activity for endocrine hormone FGF19. *Cancer Research*, 74(12):3306–3316, 2014.

Zilber-Rosenberg I. and Rosenberg E. Role of microorganisms in the evolution of animals and plants: the hologenome theory of evolution. *FEMS Microbiology Reviews*, 32(5):723–735, 2008.

APPENDIX A

Appendix

A.1 Appendix for Chapter 3.1: Faecal microbiota transplant in a mouse model of CRC

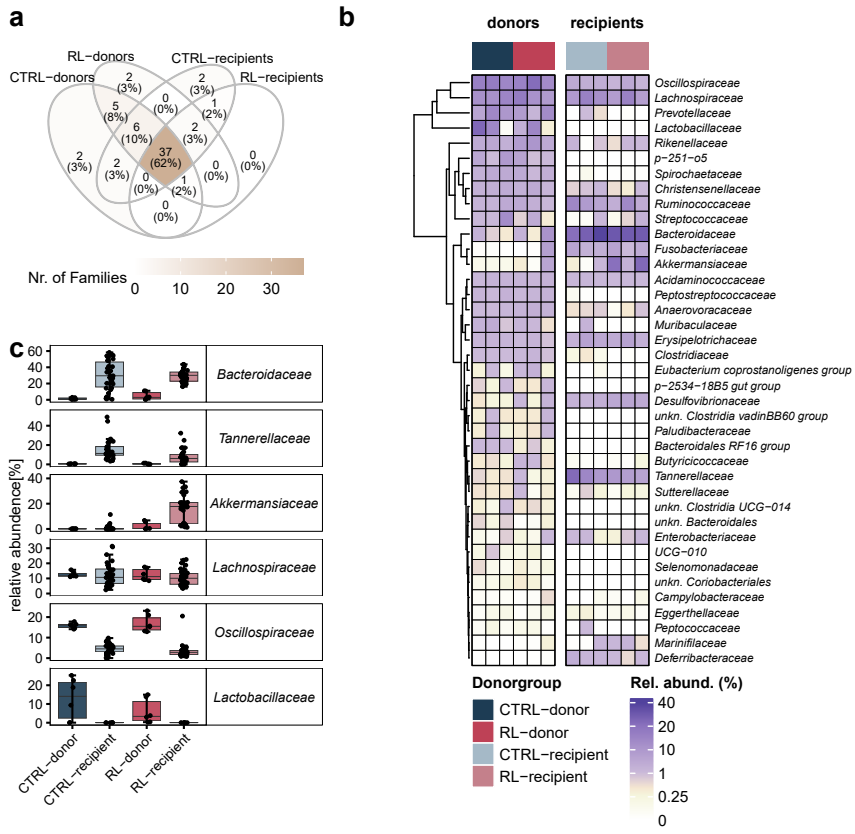

Figure A.1: Transfer efficacy of bacterial families including subdominant families (rel. abundance < 0.25%). **a** Venn diagram of bacterial families that were present in either donor or recipient group. All families that were detected in at least one donor (cryostock) or recipient (mouse) were considered. **b** SOTUs that were present in all donors or recipients of a donor-group. Their respective mean rel. abundance in the cryostocks used for the inoculation (donors; left) and the recipient mice (right) are shown with a colour gradient. Each column represents stocks or recipients of a given donor pig. **c** Rel. abundance of the most abundant families in donors or recipients, respectively. Donor microbiota: n=3 pigs per diet (n=2 stocks sequenced per pig); recipient microbiota: n=37 for CTRL (14/13/10 mice per donor) and n=50 (19/17/14 mice per donor) for RL.

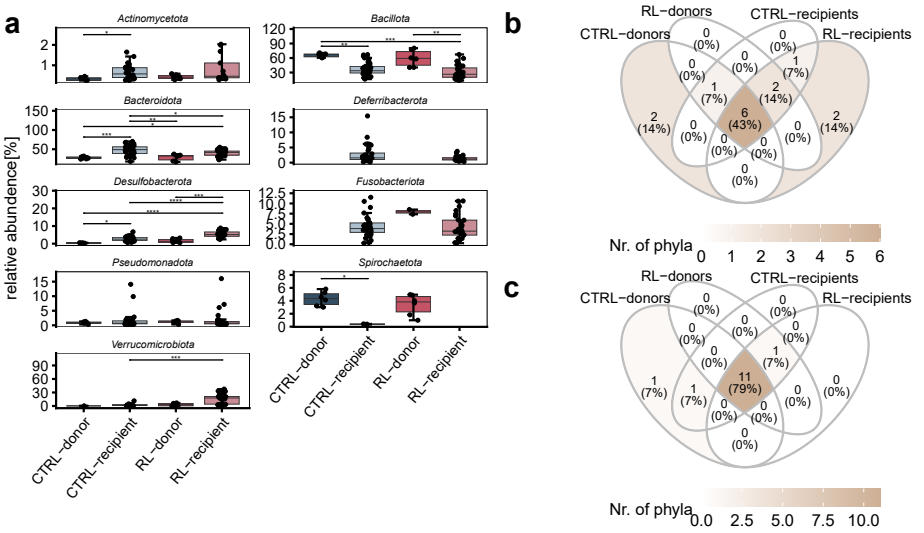

Figure A.2: Rel. abundance of bacterial phyla in *Apc*$^{1638N/+}$ mice, divided by donor-group. **a** Rel. abundance of phyla with a prevalence >0.8 per group. **b** Venn diagram of bacterial phyla that were present in either donor or recipient group. All phyla that were detected in at least one donor (cryostock) or recipient (mouse) with a rel. abundance above 0.25% were considered. **c** Same as **b**, but without the rel. abundance cut-off. Statistics for **a**: Kruskal-Wallis with Dunn´s multiple comparisons (Benjamini-Hochberg adjustment), *: p.adj <0.05, **: p.adj <0.01, ***: p.adj <0.001.

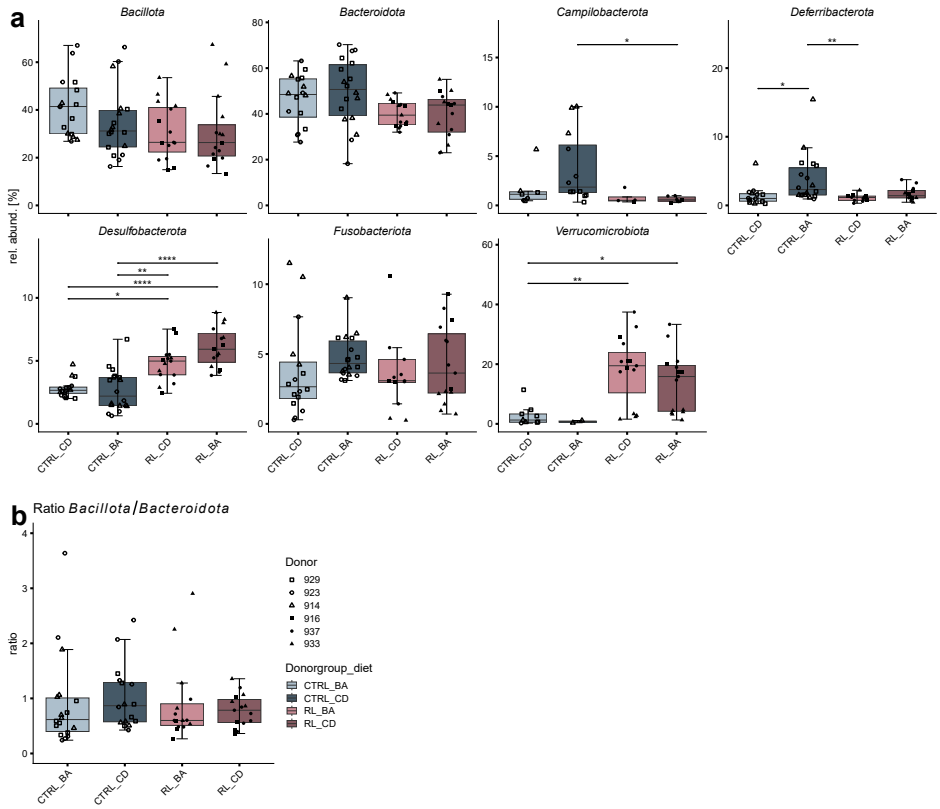

Figure A.3: Rel. abundance of bacterial phyla in *Apc*$^{1638N/+}$ mice, divided by donor-group and diet. **a** Rel. abundance of bacterial phyla with a prevalence > 0.3. **b** Ratio between *Bacillota* and *Bacteroidota*. Statistics: Kruskal-Wallis with Dunn´s multiple comparisons (Benjamini-Hochberg adjustment), *: p.adj <0.05, **: p.adj <0.01, ***: p.adj <0.001, ****: p.adj <0.0001.

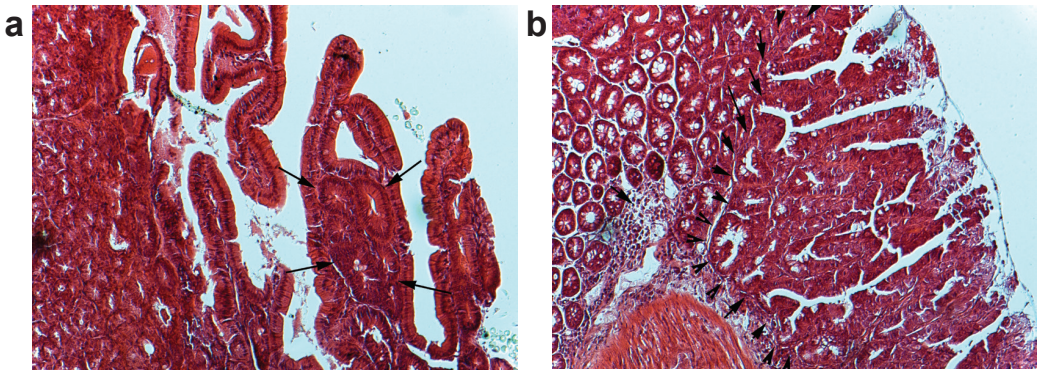

Figure A.4: Exemplary HE staining of tumours shown in Figure 3.6**c**, 100X enlargement. **a** An early adenoma in the PAR (GF_BA mouse). The black arrows show a layer of normal epithelium, under which several irregular dysplastic tumour glands are located. **b** An ileal tumour (CTRL_BA mouse). Black arrows show the outer border of the tumour. The tumour itself is depleted in goblet cells. Stainings and analysis were kindly provided by Prof. Klaus-Peter Janssen (Klinikum rechts der Isar, Technical University of Munich, Germany).

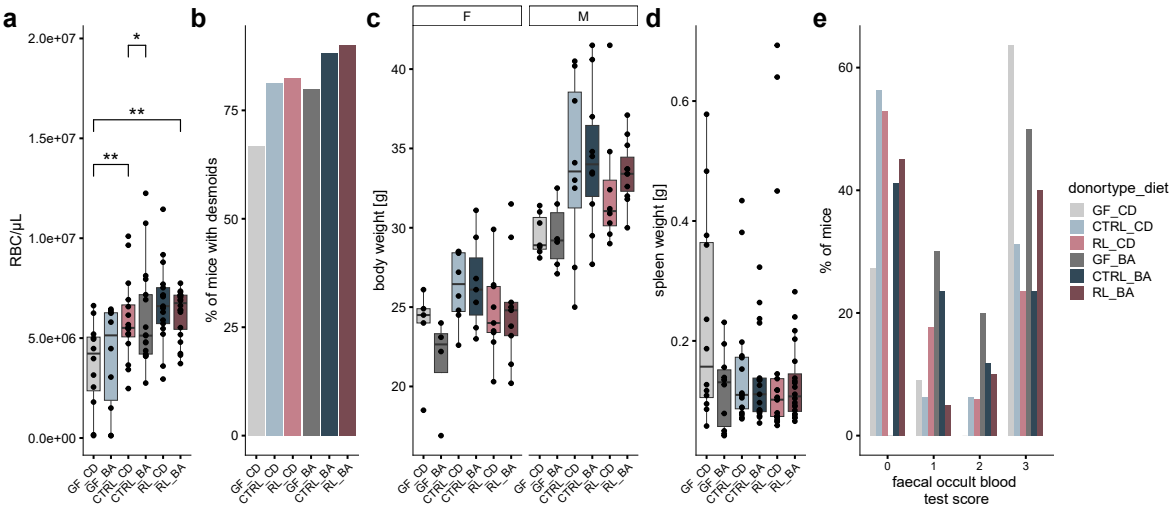

Figure A.5: Additional phenotype data. **a** Number of red blood cells (RBC/µL) **b** Percentage of mice with desmoids per group. **c** Body weight at the time of sampling. **d** Spleen weight. **e** Percentage of mice for each faecal occult blood test score. Arbitrary score assigned according to intensity of blue colouring of sample: 0 = test not positive, 1= test slightly positve, 2= test positive, 3= test very positive. Statistics for **a**: Kruskal-Wallis with Dunn´s multiple comparisons (Benjamini-Hochberg adjustment), *: p.adj <0.05, **: p.adj <0.01.

Table A.1: Composition of mouse diets for the FMT trial. CD : control diet, BA : CD diet + 0.2% CA.

Diet : 12 kJ% fat, 5% SBO, 5% sucrose	**CD**	**BA**
Art. Nr.	**S5745-E902**	**S5745-E903**
Cholic acid [%]	0	0.2
Crude protein [%]	21.0	21.0
Crude fat [%]	5.1	5.1
Crude fibre [%]	5.0	5.0
Crude ash [%]	5.4	5.4
Starch [%]	45.9	45.9
Sugar [%]	6.1	6.1
Vitamine A [IE/UI]	18,000	18,000
Vitamine D3 [IE/UI]	1,800	1,800
Vitamine E [mg]	180	180
Vitamine K3 [mg]	24	24
Vitamine C [mg]	36	36
Copper [mg]	14	14

A.2 Appendix for Chapter 3.2: DCA-producing *E. muris* worsened disease in a gnotobiotic mouse model of CRC

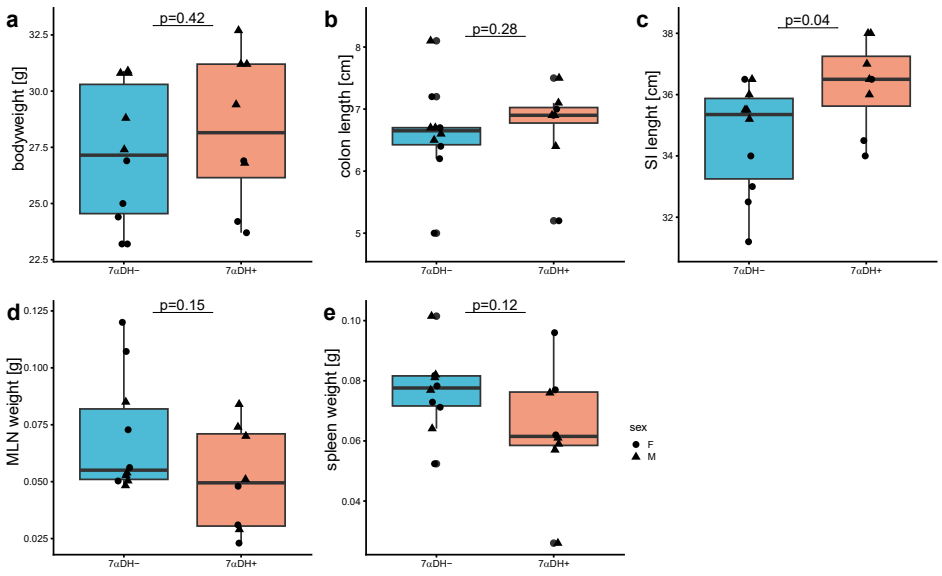

Figure A.6: Metadata of BACOMI trial. **a** Body weight, **b** colon length, **c** small intestinal length, **d** MLN weight, **e** spleen weight. Statistics: Wilcoxon rank-sum test.

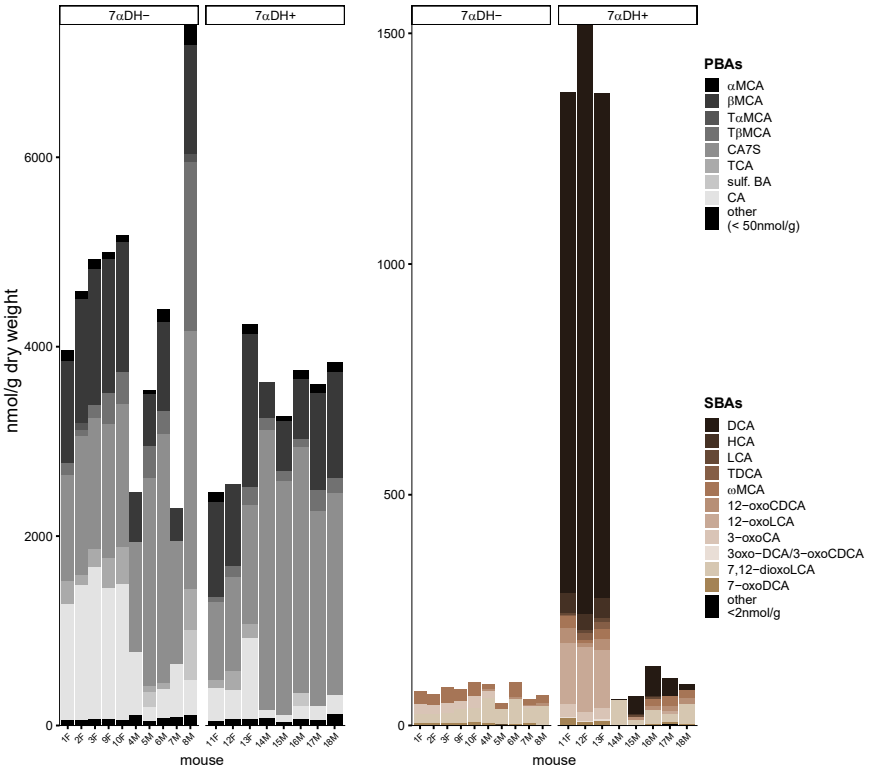

Figure A.7: BA concentrations in BACOMI mice, split by category.

Table A.2: Feed composition for AOM/DSS mouse trial.

Ingredients	**g/kg**
Casein (Bayerische Milchindustrie, Germany)	270
Wheat starch (Kröner, Germany)	150
Maltodextrin (Altromin, Germany)	140
Sucrose (Gut & Günstig, Edeka, Germany)	100
Palm kernel fat (Palmin, Peter Kölln, Germany)	110
Sunflower oil (Gut & Günstig, Edeka, Germany)	110
Cellulose (J.Rettenmeier und Söhne, Germany)	50
Mineral mixture (C1000, Altromin)	50
Vitamin mixture (C1000, Altromin)	20

A.3 Appendix for Chapter 3.3: DCA-producing *E. muris* affected gene expression in colonic epithelial cells

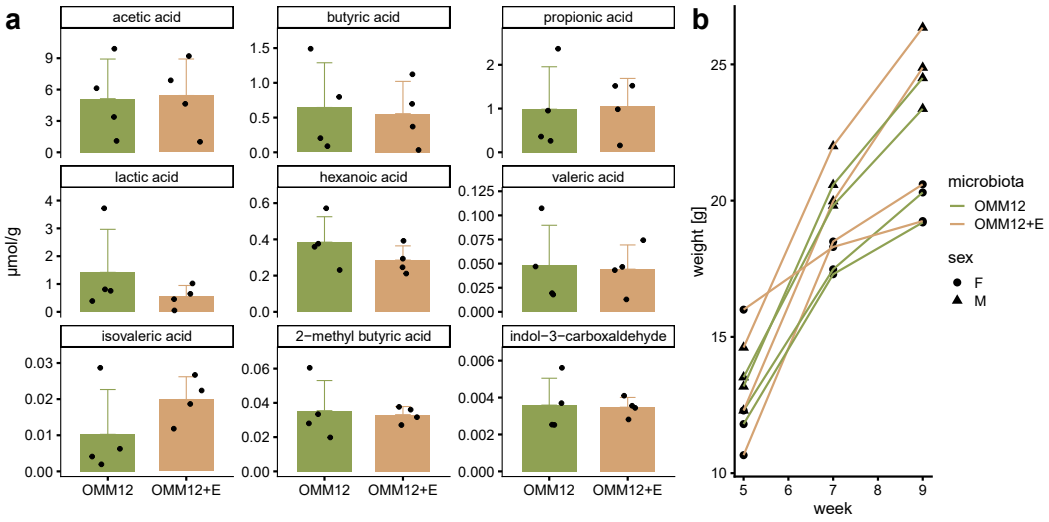

Figure A.8: a SCFA concentrations in colon content for mice in the two colonisation groups. **b** Body Weight over the course of the experiment. Endpoints were compared by Wilcoxon rank-sum test and Benjamini-Hochberg adjustment; no significant difference was found.

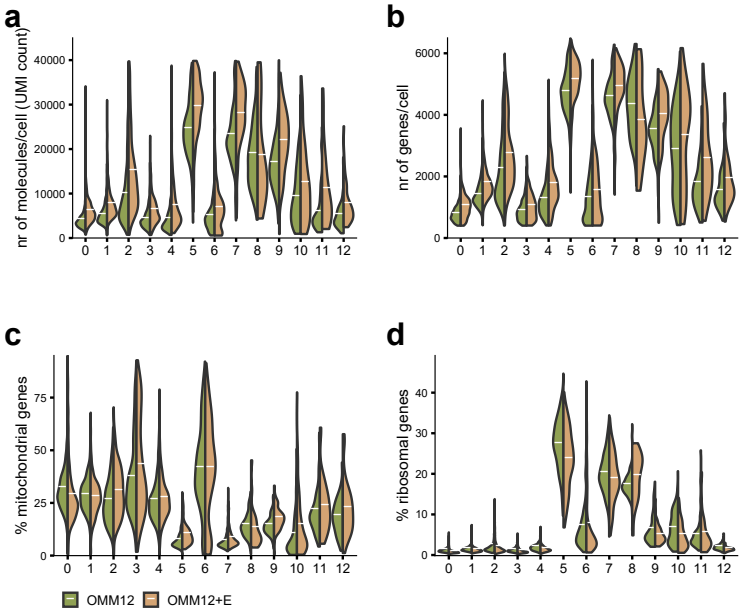

Figure A.9: a Number (nr) of molecules per cell (UMI= unique molecular identifier count), **b** number of unique genes per cell, **c** percentage of mitochondrial genes per cluster, **d** percentage of ribosomal genes per cluster. Mean expression within each group and cell cluster is indicated with white lines.

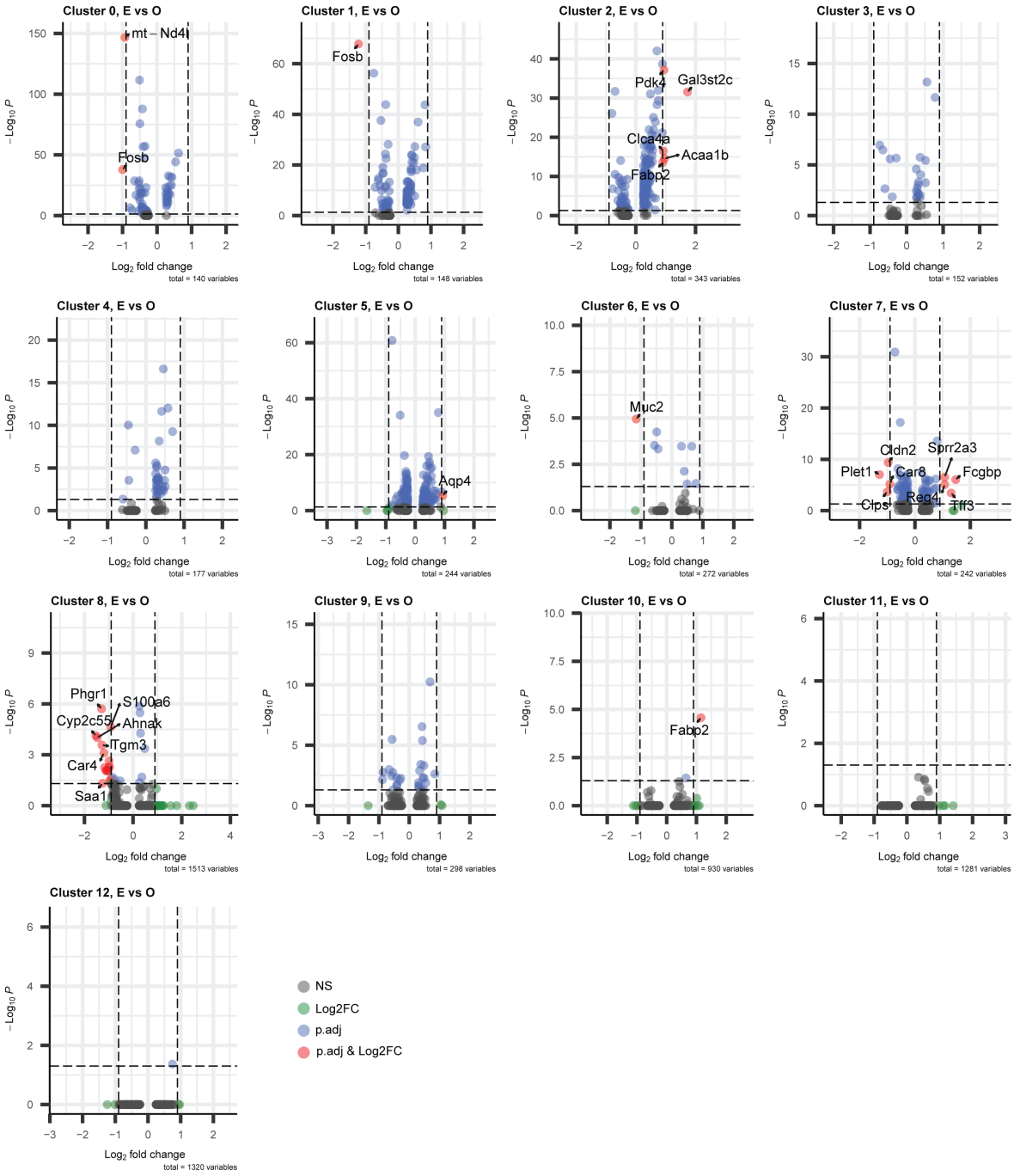

Figure A.10: Volcano plots of differentially expressed genes. Cut-offs were set to p <0.05 and Log2FC >0.9. Plots were created with the R package Enhancedvolcano (Blighe et al., 2018).

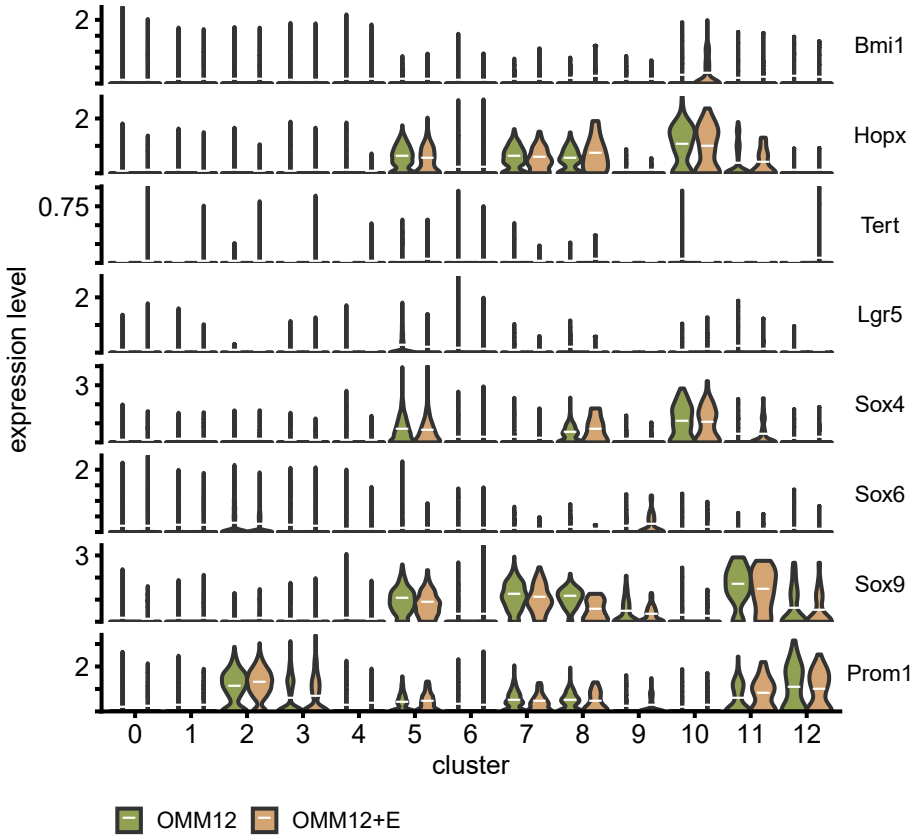

Figure A.11: Expression of proposed cancers stem cell marker genes (Wang et al., 2021). Mean expression within each group and cell cluster is indicated with white lines. No significant differences were found between OMM12 and OMM12+E.

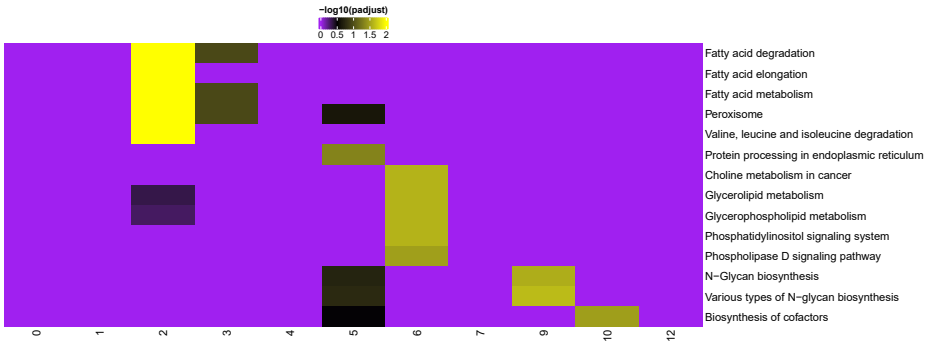

Figure A.12: KEGG pathways that are upregulated in the OMM12+E group compared to the OMM12 group.

A.4 Appendix for Chapter 3.4: The BA scavenger colestyramine reduced intestinal cell proliferation in *APC*$^{1311/+}$ pigs

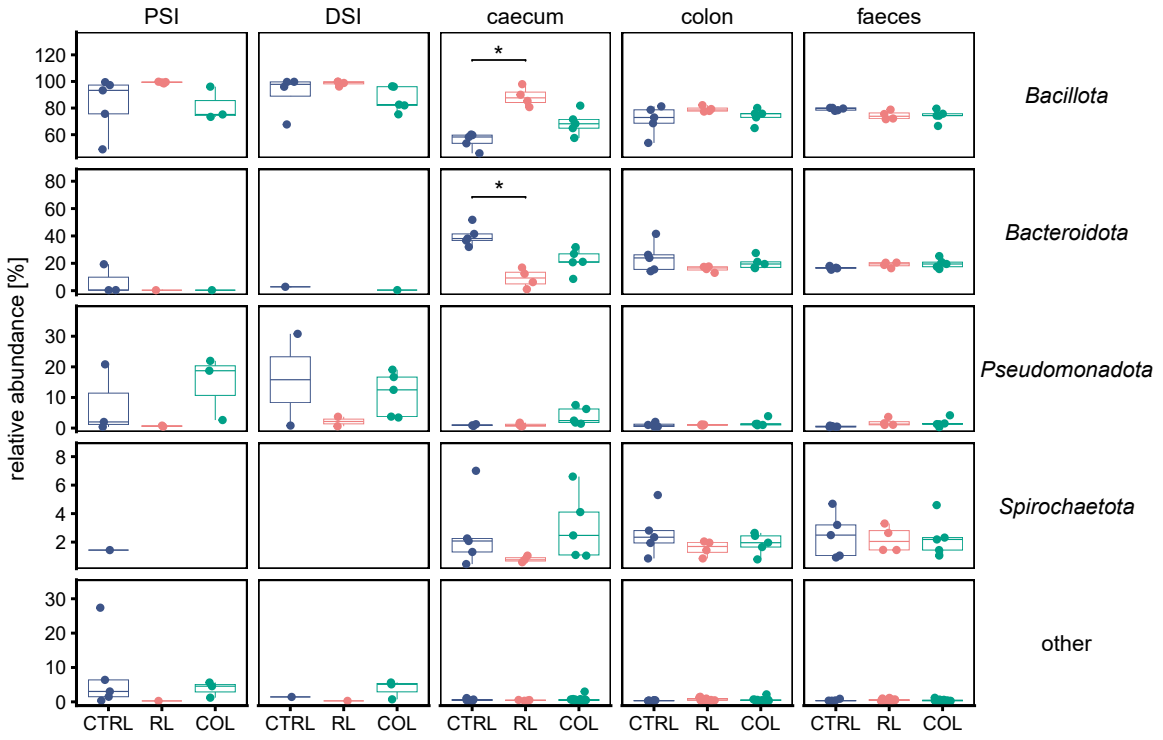

Figure A.13: Rel. abundance of most prevalent phyla (prevalence in at least one region >0.75). Statistics: Kruskal-Wallis with Dunn´s multiple comparisons (Benjamini-Hochberg adjustment for comparison of diets), *: p.adj <0.05.

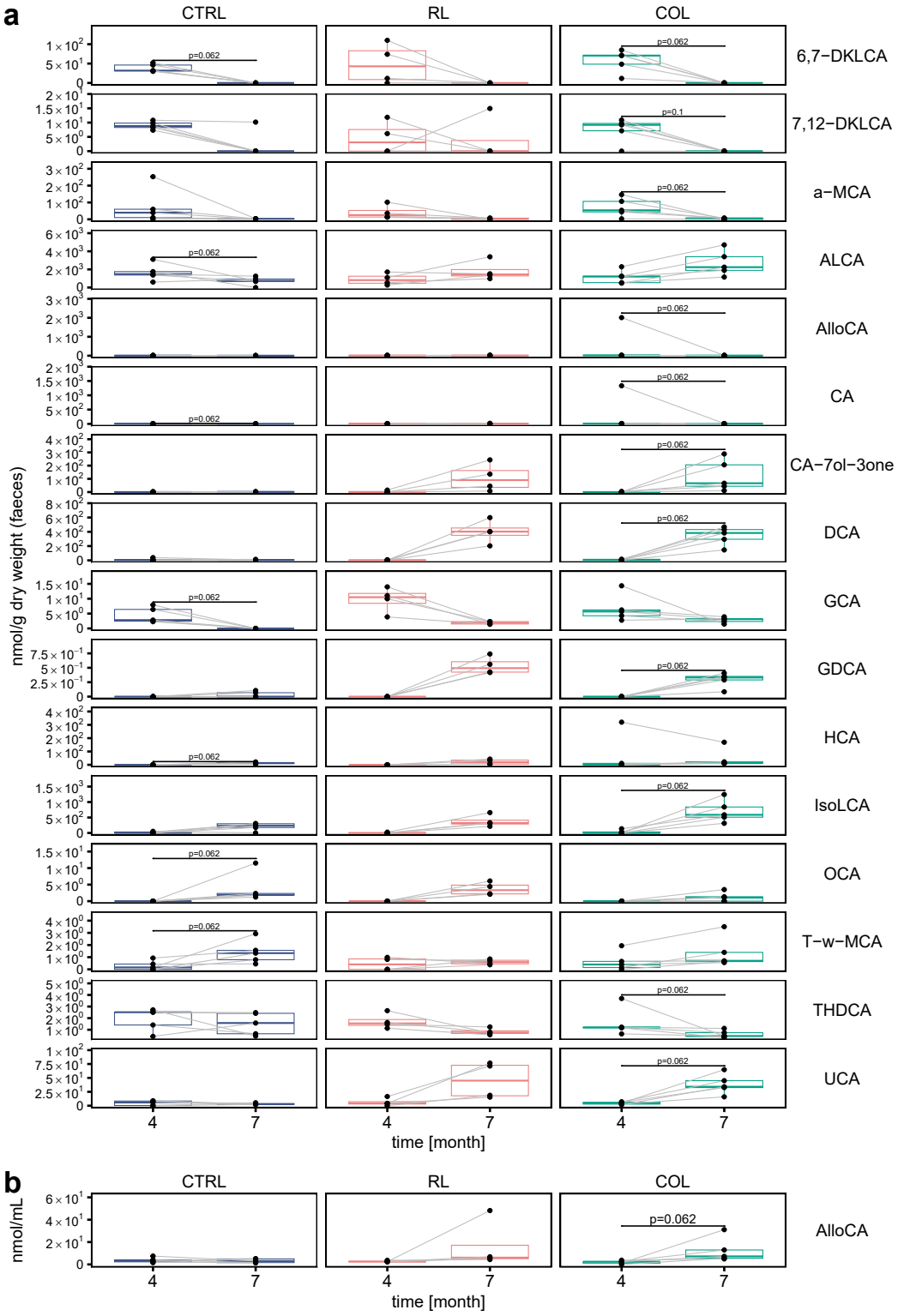

Figure A.14: Changes of BA species over time, before the start of the feeding intervention (month 4) and at the end (month 7) in **a** faeces and **b** plasma. Shown are only BAs with a prevalence <0.75 and p $\leq$0.1 in one of the diet groups. Statistics: Wilcoxon signed-rank test, only p $\leq$0.1 are shown.

Figure A.15: Abundant BAs (>1%) statistically significant different according to Kruskal-Wallis (p.adj <0.05) in different gut regions: **a** caecum, **b** colon, **c** faeces. Statistics: Kruskal-Wallis with Dunn's multiple comparisons and Benjamini-Hochberg correction; p.adj values are shown where p <0.05, * p.adj. <0.05.

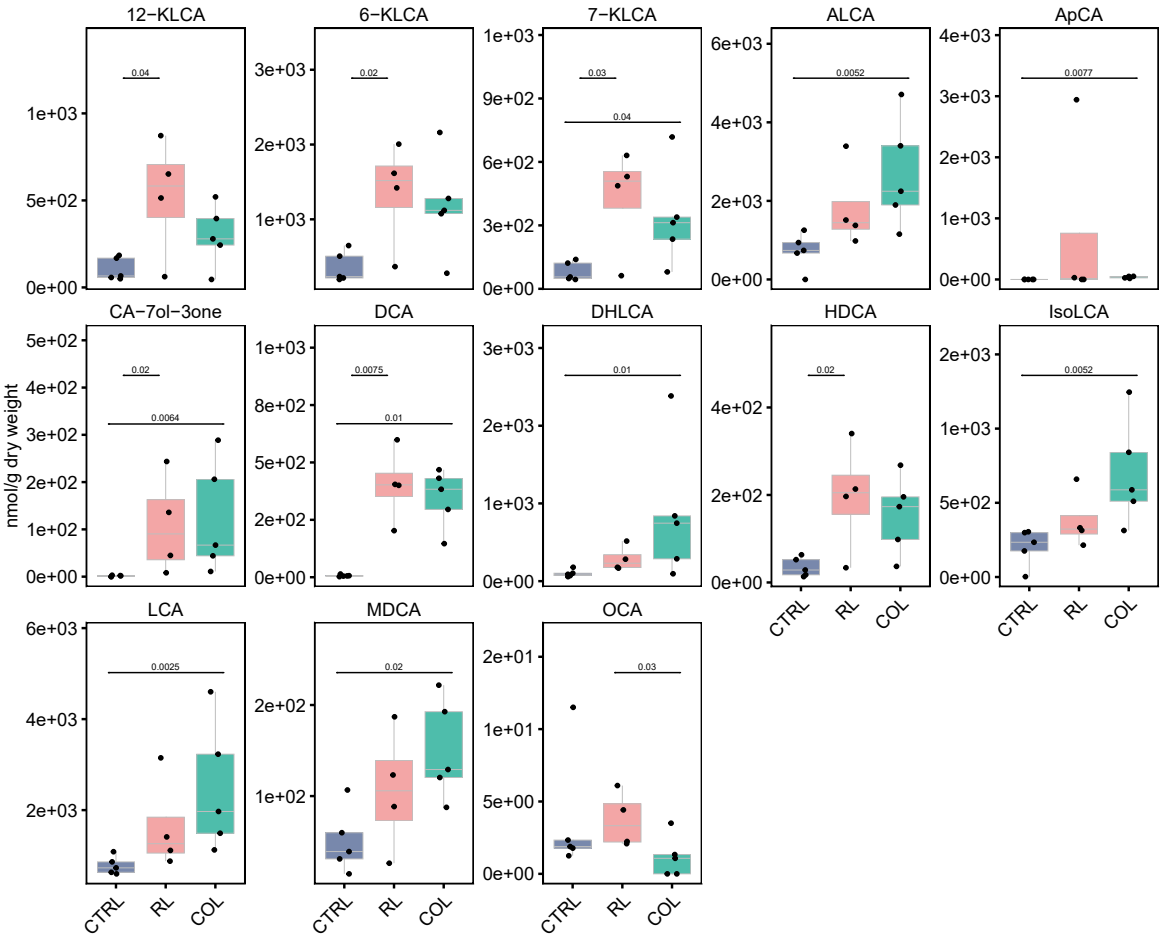

Figure A.16: SBAs in faeces after the feeding intervention (p $\leq$0.05, prevalence >0.3), without abundance cut-off. Statistics: Kruskal-Wallis with Dunn´s multiple comparisons. No significant differences were found after adjustment. Shown are unadjusted p-values.

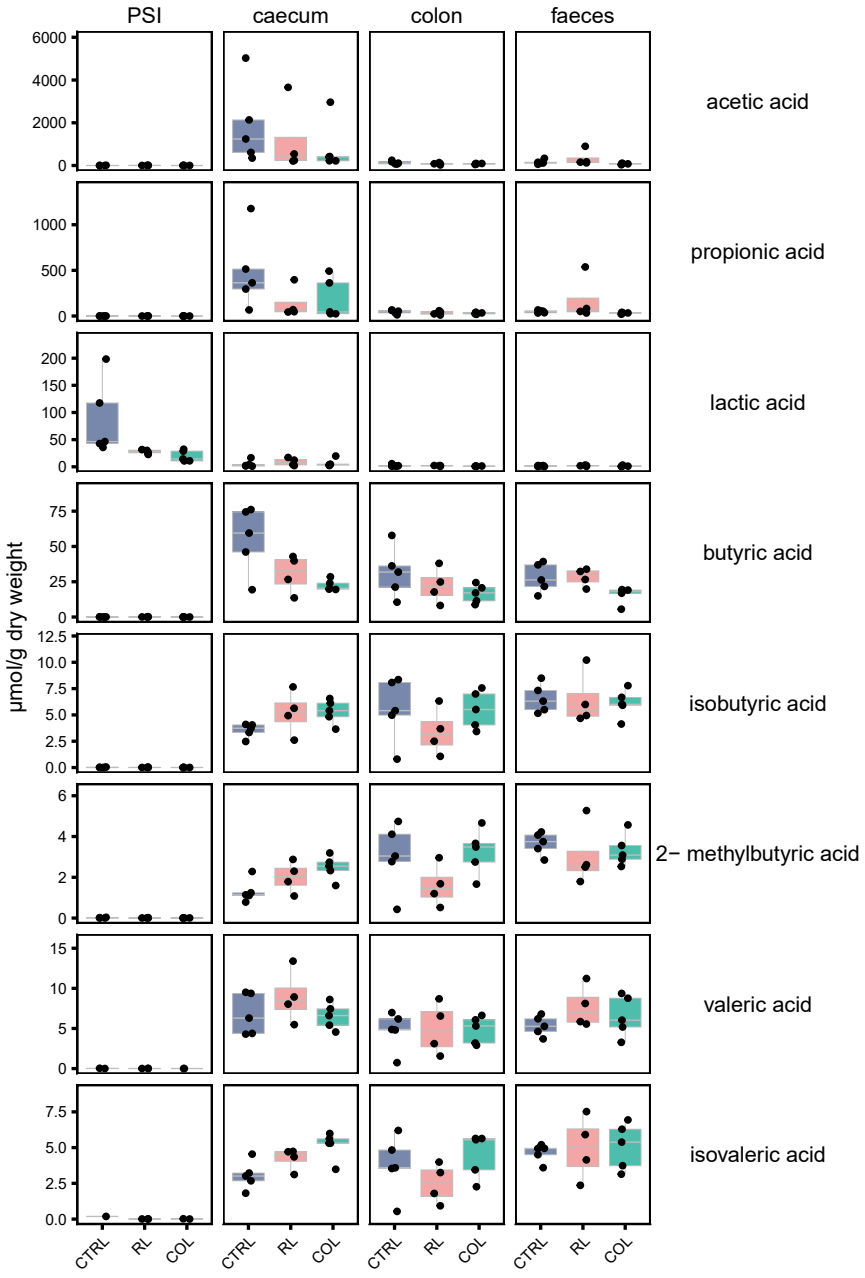

Figure A.17: SCFA in different gut regions (PSI = proximal small intestine). SCFA concentrations were lowest in the proximal small intestine, with the exception of lactic acid in the CTRL group. Highest concentrations were observed in the caecum, with no significant differences between the three groups. Also in the colon and faeces, no significant differences were found. Concentrations of zero or not detected are not plotted.

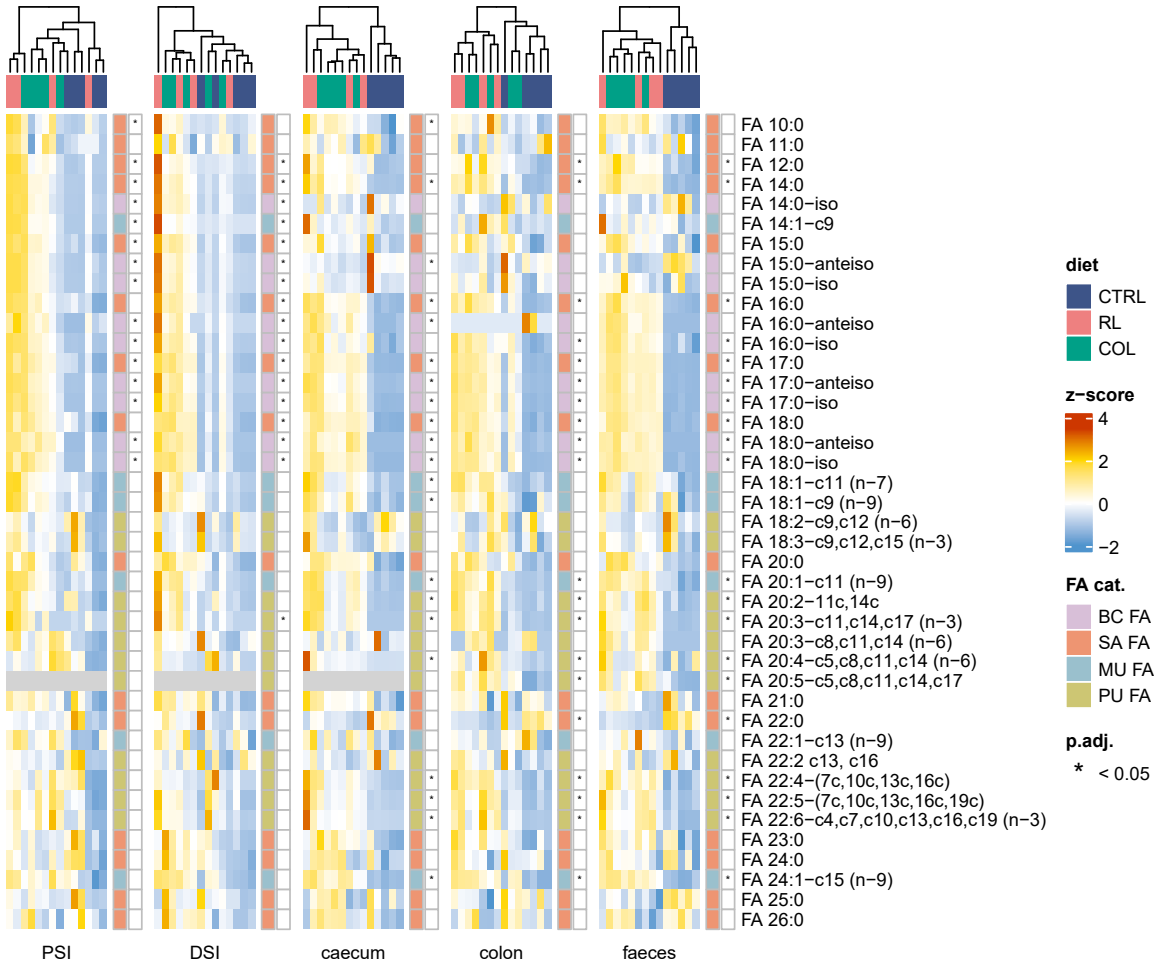

Figure A.18: Heatmaps with euclidean clustering of fatty acids for different intestinal regions (PSI = proximal small intestine, DSI = distal small intestine), displayed as z-scores calculated per gut region. FA categories (branched chain fatty acids (BC FA), saturated (SA FA), mono-unsaturated (MU FA), and poly-unsaturated FA (PU FA) are marked in different colours. Statistics (Kruskal-Wallis with Benjamini-Hochberg adjustment) are shown as stars on the right: * p.adj <0.05.

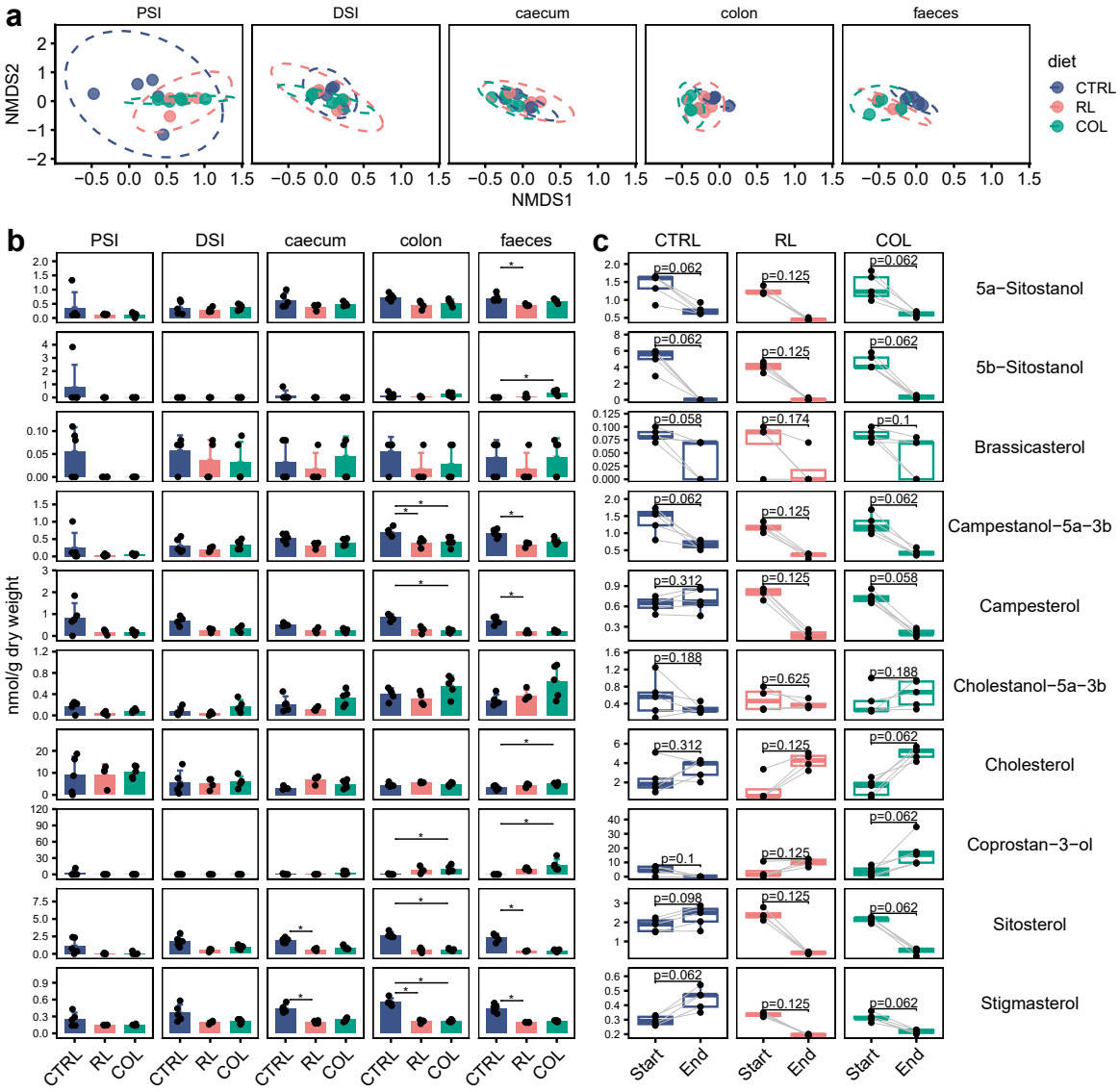

Figure A.19: Sterol and stanol levels at different times and intestinal locations. **a** NMDS plot of sterols/stanols in different gut regions. Stress= 0.17. **b** Instestinal sterol/stanol composition at the end of the feeding period. **c** Levels of sterol/stanols before and after the feeding intervention in faeces. Statistics: **b** Kruskal-Wallis with Dunn's multiple comparisons and Benjamini-Hochberg adjustment, * p.adj <0.05; **c** paired Wilcoxon signed-rank test. Zeroes are not plotted, but were included for statistical analysis.

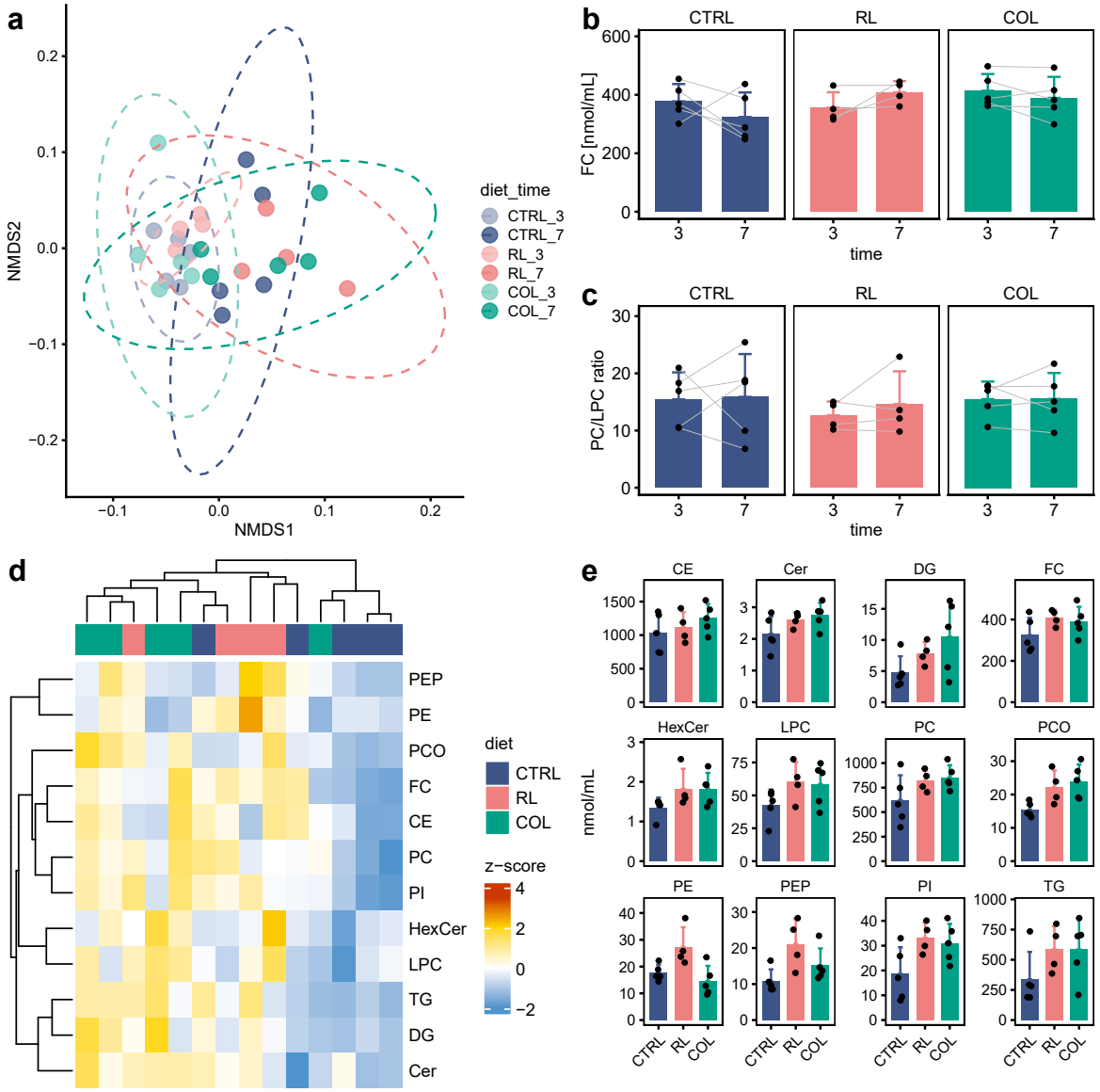

Figure A.20: Plasma lipidomic profiles. **a**, NMDS plots of plasma lipidomic profiles before (month 3) and after (month 7) the feeding period. **b** Free cholesterol levels, compared by paired Wilcoxon test. **c** Ratio of PC to LPC over time. **d** Heatmap of normalised lipid levels, clustering calculated with euclidian distance. **e**, lipid class levels at the end of the feeding period (no significant differences). CE: cholesteryl ester, Cer: ceramide, DG: diglyceride, FC: free cholesterol, HexCer: hexosylceramide, LPC: lysophosphatidylcholine, PC: phosphatidylcholine, PCO: phosphatidylcholine-ether, PE: Phosphatidylethanolamine, PEP: PE based plasmalogens.

Table A.3: Composition of feed used for the dietary intervention in *Apc*$^{1311/+}$ pigs.

Ingredient	**Unit**	**CTRL**	**RL**	**COL**
Product Nr.		*S5745-S084*	*S5745-S086*	*S5745-S088*
Casein	%	3.000	-	-
Soybean concentrate	%	10.000	-	-
Lamb meal (with bones)	%	-	32.000	32.000
Wheat (∼11 % protein)	%	24.000	20.000	20.000
Corn starch, pre-gelatinized	%	9.000	5.700	5.700
Potato starch, raw	%	3.000	-	-
Maltodextrin	%	6.000	7.000	7.000
Colestyramin / Additives	%	2.850	2.850	2.850
Sucrose	%	9.500	9.500	9.500
Lignocellulose	%	3.350	3.350	3.350
Wheat bran	%	8.000	5.000	5.000
Sugar beet pulp	%	3.000	3.000	3.000
L-Lysine HCl	%	0.110	-	-
L-Threonine	%	0.030	-	-
L-Tryptophan	%	-	0.030	0.030
Vitamin premix w/o choline	%	1.000	1.000	1.000
Mineral & trace element mix	%	11.900	4.000	4.000
Choline Cl	%	0.250	0.250	0.250
Butylated hydroxytoluene	%	0.010	0.010	0.010
Cholesterol	%	-	0.010	0.010
Pork lard	%	-	6.300	6.300
Soybean oil	%	5.000	-	-
Energy				
Total	MJ/kg	12.7	14.2	14.2
Protein	kcal%	22	30	30
Fat	kcal%	15	27	27
Carbohydrates	kcal%	63	43	43
Approximate contents				
Crude protein	%	13.3	20.0	20.0
Crude fat	%	5.5	11.6	11.6
Crude fibre	%	5.8	5.2	5.2
Crude ash	%	10.1	10.2	10.2
Starch	%	27.1	18.2	18.2
Sugar	%	15.8	15.2	14.5
Dextrin	%	5.9	6.9	6.9
Calcium	%	2.00	2.68	2.68
Phosphorus	%	1.25	1.53	1.53
Sodium	%	0.25	0.38	0.38
Lysine	%	0.86	1.05	1.05
Met+Cys	%	0.54	0.68	0.68
Threonine	%	0.56	0.74	0.74
Tryptophan	%	0.17	0.20	0.20

Ingredient	**Unit**	**CTRL**	**RL**	**COL**
Fatty acids, % in the diet				
C14:0	%	0.01	0.33	0.33
C16:0	%	0.69	2.65	2.65
C18:0	%	0.18	1.69	1.69
C16:1	%	0.01	0.32	0.32
C18:1	%	1.35	4.52	4.52
C18:2	%	3.02	1.03	1.03
C18:3	%	0.34	0.24	0.24
Cholesterol	mg/kg	∼1	∼175	∼175
Colestyramine / Additives				
Colestyramine	g/kg	-	-	12
Cellulose	g/kg	12	12	-
Carmellose-Na (Na CMC)	g/kg	1.17	1.17	1.17
Siliciumdioxid	g/kg	1.2	1.2	1.2
Citronensäure H2O	g/kg	0.9	0.9	0.9
Vanillin	g/kg	0.3	0.3	0.3
Riboflavin	g/kg	0.03	0.03	0.03
Orangen-Aroma	g/kg	0.9	0.9	0.9
Saccharose	g/kg	12	12	12
Total	g/kg	28.5	28.5	28.5
Mineral & trace element premix				
Potassium phosphate, dibasic	g/kg	6.4000	6.4000	6.4000
Potassium citrate monohydrate	g/kg	4.8000	4.8000	4.8000
Potassium sulphate	g/kg	3.2000	3.2000	3.2000
Natriumchlorid	g/kg	1.6000	1.6000	1.6000
Magnesium oxide	g/kg	0.9600	0.9600	0.9600
Iron(III) citrate monohydrate g	g/kg	0.3280	0.3280	0.3280
Zinc hydroxide carbonate	g/kg	0.1108	0.1108	0.1108
Manganese(II) chloride	g/kg	0.0840	0.0840	0.0840
Copper(II) sulphate pentahydrate	g/kg	0.0640	0.0640	0.0640
Potassium iodide	g/kg	0.0004	0.0004	0.0004
Sodium selenite pentahydrate	g/kg	0.0004	0.0004	0.0004
Sodium molybdate dihydrate	g/kg	0.0004	0.0004	0.0004
Sucrose (ad 40 g)	g/kg	22.4520	22.4520	22.4520
Calcium carbonate	g/kg	-	-	34.0000
Calcium phosphate	g/kg	-	-	40.0000
NaCl	g/kg	-	-	4.0000
Magnesium oxide	g/kg	-	-	1.0000
Vitamin premix (10 g/kg diet) provides per kg diet (dextrose as carrier):				
15000 IU vitamine A; 1500 IU vitamine D3; 150 mg vitamine E (all-rac-alpha-tocopherylacetate);20 mg vitamine K3; 30 mg vitamine C; 25 mg vitamine B1; 16 mg vitamine B2; 16 mg vitamine B6; 30 μg vitamine B12; 50 mg niacin; 55 mg pantothenicacid; 16 mg folic acid; 300 μg biotin;1 g DL-methionine				